Permeability, Porosity, and Grain-Size Distribution of Selected Pliocene and Quaternary Sediments in the Albuquerque Basin, Central New Mexico

by

Daniel M. Detmer

Submitted in partial fulfillment

of the requirements for the degree of

Master of Science in Geology

New Mexico Institute of Mining and Technology

Department of Earth and Environmental Science

Socorro, New Mexico

June, 1995

ABSTRACT: As part of an investigation of natural artificial recharge in the northern Albuquerque basin, ten outcrops of aquifer-related sediments were studied in the Albuquerque municipal area. Three outcrops of upper Santa Fe Group were selected, along with proximal and medial Tijeras Arroyo facies, a recent outcrop in Bear Canyon Arroyo, and distal Embudo fan facies. Late Pleistocene river-terrace deposits, the Los Duranes and Edith Gravel type sections, and young Rio Grande channel deposits were also sampled. A range of permeability was determined for most exposures, and relationships among facies, continuity of facies, scale of bedding, and sedimentary structures were recorded at each exposure. Permeability of surface exposures were measured with a lightweight syringe-based air-minipermeameter. Permeability was measured in-situ, porosity of the deposit was determined, and a soil sample taken from the point of measurement. Grain-size distributions of sediment samples were determined by mechanical sieving. Permeability was correlated with porosity, lithification, and a number of grain-size distribution parameters of the outcrop samples. A weak correlation was found with porosity and permeability, explained in part by cementation and sorting of the samples. Relatively minor amounts of cementation are found to reduce the permeability of sandy sediments. A strong correlation is observed with measured permeability and mean grain size. Correlation of permeability with the 10 and 20 percent passing sieve diameters is also high. Grain distribution parameters generally correlate better with measured permeability if grains larger than 2 mm in diameter are excluded from the samples before calculating distribution parameters. Multiple regression analysis was used to formulate predictive permeability equations based on grain-size distribution parameters. A regression based on d_{10} and mean grain size explains 78 percent of the variability in the permeability values of the outcrop samples. Several commonly used published permeability equations based on porosity and grain-size distribution correlate poorly with measured permeability. Samples were classified by the following bedding types: crossbeds, channels, horizontal beds, scour and fill structures, and structureless deposits. Moment measurements were

used to calculate sorting coefficients, and the bedding types were found to have characteristic grain-size distributions. Log-log plots were used as an effective way to graphically represent and compare grain-size distributions. Well cuttings from three wells in the basin where found to have grain-size distributions similar to the outcrop samples. The permeability of well core and cuttings from shallow wells can be estimated from the grain-size distribution of the samples, and can be used to supplement or calibrate permeability estimates based on geophysical well log analysis.

ACKNOWLEDGMENTS

This research was funded by the U.S Bureau of Reclamation through the U.S. Bureau of Reclamation - New Mexico Bureau of Mines and Mineral Resources Cooperative Agreement No. 3-FC-40-14120. Additional funding was contributed by the New Mexico Geological Society, the Roswell Geological Society, the Antonius Budding Award from the Geoscience Department at New Mexico Tech and the Matuszeski Award from the Graduate Student Association at New Mexico Tech. I wish to express my gratitude to all contributors who made this research possible.

I would like to thank Dr. John Hawley for getting me involved with the Bureau of Reclamation project and helping in the conception of this study. I am indebted to Dr. Bill Haneberg, whose many valuable suggestions helped define the scope of my work and bring it to a presentable form. Dr. Haneberg's analysis of geophysical well logs related to the sediments I studied in outcrop is also appreciated. Dr. Dave Love helped me in the field and with the analysis of grain-size distributions, for which I am grateful. I would like to thank Dr. Peter Mozley and Dr. Bruce Harrison for serving on my committee and their advice regarding my research.

I extend thanks to the Hydrology Program at New Mexico Tech for allowing me to use the air-minipermeameter. I thank the City of Albuquerque and the Public Service Company of New Mexico for releasing geophysical well logs for analysis. I also thank the many employees of the Bureau of Mines and the Department of Earth and Environmental Science who have helped me over the past several years.

TABLE OF CONTENTS

List of Tables vi

List of Figures. vii

Chapter 1: Introduction 1

Chapter 2: Geologic Setting 6

Chapter 3: Methods 17

3.1 Field Methods 17
3.2 Laboratory Methods 22
3.3 Permeability and Grain-Size Distribution of Outcrop Samples . .28

Chapter 4: Results 33

4.1 Outcrop Descriptions and Permeability Profiles 33
4.2 Permeability and Porosity of Outcrop Samples 44
4.3 Comparison of Bedding Types 63
4.4 Grain-Size Distributions of Well Cuttings 76
4.5 Geophysical Well Logs 78

Chapter 5: Discussion 87

5.1 Permeability, Porosity and Grain-Size Distribution of Sediments . .87
5.2 Permeability Equations 95
5.3 Comparison of Bedding Types. 99
5.4 Outcrop Permeability Profiles 101
5.5 Comparison of Outcrop Samples and Well Cuttings 103
5.6 Geophysical Well Logs 104

Chapter 6: Conclusions 106

References 109

Appendix A: Log-Log Plots, Cumulative Percent Plots, and Grain-Size Distribution Parameters of Outcrop Samples

Appendix B: Comparison of Measured Permeability Values to Published Permeability Equations, Multiple Regression Permeability Equations

Appendix C: Measured Permeability Plotted with Grain Distribution Parameters of Outcrop Samples

Appendix D: Comparison of Porosity, Permeability and Grain-Size Distribution Parameters of Outcrop Samples Grouped by Bedding Type

Appendix E: Grain-Size Distributions of Well Cuttings

Appendix F: Outcrop Mosaics and Permeability Profile Measurements

LIST OF TABLES

Table 1: Parameters for Cementation Values 26

Table 2: Sieve Sizes Used in Mechanical Size Analysis of Sediments 27

Table 3: Outcrop Permeability Profile Data Summary 35

Table 4: Pearson Correlation Coefficients for Measured Permeability and Grain Distribution Parameters. 47

Table 5: Pearson Correlation Coefficients for Log_{10} of Measured Permeability and Grain Distribution Parameters 48

Table 6: Correlation Coefficients for Measured Permeability and Published Permeability Equation Values. 59

Table 7: Regression Analysis with Measured Permeability 60

Table 8: Regression analysis with Log_{10} of Measured Permeability 61

Table 9: Distribution of Grain-Size Parameters by Bedding Type 65

Table 10: Permeability Distribution by Bedding Type 75

LIST OF FIGURES

Figure 1: Index Map of the Rio Grande Rift and Albuquerque Basin 10
Figure 2: Upper Santa Fe Group Contributing Drainages 11
Figure 3: Geologic Map of the Albuquerque Basin 12
Figure 4: Schematic Hydrogeologic Cross-Section of Albuquerque Basin . . .14
Figure 5: Outcrop Locations 16
Figure 6: Measured Permeability Profile Values by Outcrop 34
Figure 7: Scatter Plot of Porosity vs. Permeability 49
Figure 8: Influence of Cementation on Permeability 50
Figure 9: Influence of d_{10} Grain Size on Permeability 51
Figure 10: Influence of d_{20} Grain Size on Permeability 52
Figure 11: Influence of Mean Grain Size on Permeability 53
Figure 12: Influence of Kruger Diameter on Permeability 54
Figure 13: Mean, Standard Deviation and Skewness of Sieved Outcrop Samples, Complete Samples 66
Figure 14: Mean, Standard Deviation and Skewness of Sieved Outcrop Samples, Cut Samples 67
Figure 15: Scatter Plot of Mean and Standard Deviation of Outcrop Samples. . .68
Figure 16: Scatter Plot of Mean and Skewness of Outcrop Samples 69
Figure 17: Permeability by Bedding Type, Unsieved Permeability Profile Measurements 71
Figure 18: Permeability Ranges for Bedding Subgroups Based on Log-Log Plots .72
Figure 19: Permeability by Bedding Type, Sieved Outcrop Samples. 73
Figure 20: Porosity by Bedding Type, Sieved Outcrop Samples 74
Figure 21: Mean, Standard Deviation and Skewness of Well Cuttings 80
Figure 22: Scatter Plot of Mean and Standard Deviation of Well Cuttings . . .81
Figure 23: Scatter Plot of Mean and Skewness of Well Cuttings 82
Figure 24: Scatter Plot of Mean and Standard Deviation of Well Cuttings and Outcrop Samples 83
Figure 25: Scatter Plot of Mean and Skewness of Well Cuttings and Outcrop Samples 84
Figure 26: Geophysical Well Logs and Estimated Permeability for Well PSMW-19 85
Figure 27: Geophysical Well Logs and Estimated Permeability for Well Coronado 2 86

CHAPTER 1: INTRODUCTION

The northern Albuquerque Basin is experiencing rapid population growth, and there is increasing concern about the quantity and quality of groundwater in the area. Recent geologic studies emphasize the hydrogeologic framework of the basin, mapping the basin by hydrostratigraphic units and lithofacies (Hawley and Haase, 1992; Hawley et al., 1995). A knowledge of hydrologic and geologic properties of the hydrostratigraphic units of the northern Albuquerque Basin is required to constrain numerical models of ground-water flow and transport. Outcrop studies allow detailed investigation of the range of permeability, types of bedding, continuity of bedding and grain-size distribution of sediments common to hydrostratigraphic units of the northern Albuquerque Basin. The research presented herein was completed as part of cooperative investigations of the northern Albuquerque Basin, emphasizing natural and artificial groundwater recharge in the basin, that were jointly funded the U.S. Bureau of Reclamation, the New Mexico Bureau of Mines and Mineral Resources, and the City of Albuquerque.

Ten outcrops in the Albuquerque municipal area were selected for study. Three exposures of fluvial facies of the upper Santa Fe Group were investigated, as was river alluvium from recent deposits of the Rio Grande. Three deposits of valley alluvium were studied, as were three outcrops of piedmont alluvium . Several of these units are in hydrologic contact with the Rio Grande river or are located in natural recharge areas, and others are related to productive aquifer units.

Outcrop permeability studies allow direct measurement of the permeability of aquifer-related sediments that crop out at the surface. Recent advances in the design of portable permeameters allow rapid in-situ permeability measurements of undisturbed deposits (Stalkup, 1986; Goggin et al., 1988b; Chandler et. al., 1989; Dreyer et. al., 1990; Davis, 1990; Hartkamp et. al., 1993). In this study, the permeability of surface exposures were measured with an air-minipermeameter, and sediment samples taken at the

point of measurement. Permeability was then related to the porosity, lithification and grain-size distribution of the samples. Samples were classified by bedding type, and a range of measured permeability was determined for crossbeds, channels, horizontal beds, scour and fill structures and structureless deposits.

A number of published permeability equations based on grain-size distribution and porosity of sandy sediments are used by researchers to estimate the permeability of well core. It is important to determine which permeability equations are appropriate for use in the northern Albuquerque Basin. In this study, measured permeability was compared to permeability values derived from a number of commonly used permeability equations. In addition, new permeability equations were generated from a set of outcrop samples of known permeability. By determining the grain-size distribution of sediments of known permeability, it was possible to determine which sample parameters have the highest correlation with measured permeability. Multiple regression analysis was applied to the data set to generate predictive permeability equations for use on sediments common to the study area.

A knowledge of the grain-size distribution and permeability of aquifer-related sediments determined from outcrop can be used to predict the permeability of sediments in the subsurface. Cores of aquifer material or samples of well cuttings are commonly collected when a well is drilled. If well core is available, permeability can be estimated at small vertical increments, which is useful in detailed subsurface investigations. Uncertainty as to the quality of sediment samples is introduced if well cuttings instead of well core is available. The cuttings from wells Coronado 2, PSMW-19 and MW1 were sieved in this study, and the grain-size distributions of the cuttings are found to be similar to those of the outcrop samples. It appears that well cuttings can be used to approximate the permeability of sediments at depth, but additional studies are necessary to verify the reliability of these techniques. Geophysical well logs are commonly used to estimated the porosity and relative permeability of aquifer units. Geophysical logs do not measure permeability

directly, and permeability equations based on grain-size distribution may be used to calibrate permeability estimations from geophysical logs.

In addition to geophysical well logs, pump tests are commonly used to estimate aquifer transmissivity. Pump tests are subject to a number of limitations. Pump tests are inappropriate in areas with a history of groundwater withdrawal, due to intersecting cones of depression and highly perturbed natural gradients (Kruseman and de Ridder, 1990). Even in a suitable setting, the estimation of aquifer transmissivity by pump tests is somewhat subjective. Assumptions are required to define the extent and properties of the aquifer, including specific assumptions as to the location and extent of aquicludes, whether the aquifer is confined or unconfined, the thickness, extent, and homogeneity of aquifer units, and the location and shape of the water table (Kruseman and Ridder, 1990). Permeability estimations from pump tests are also influenced by the placement of the well screen, and the gravel pack (Driscoll, 1986). Permeability estimations based on the grain-size distribution of well core requires few assumptions, and provides data of higher resolution.

The hydrostratigraphic units of the northern Albuquerque Basin are large and variable. Outcrop studies detailing types of bedding, and the influence bedding has on permeability distribution, are useful when evaluating related sediments in the subsurface. The combined use of permeability estimations from the grain-size distribution of sediments, geophysical well log analysis, and a knowledge of the styles of sedimentation of aquifer-related sediments that crop out at the surface allow a better understanding of the recharge areas and aquifers of the northern Albuquerque Basin.

Previous Work and Related Studies

A number of researchers have conducted outcrop studies addressing the relationships between permeability, porosity and styles of sedimentation. An early study by Pryor (1973) found a weak correlation between porosity and permeability among

uncompacted beach and river sands. He concluded that different styles of natural grain packing influence sample permeability, obscuring relationships between grain sorting and permeability that have been demonstrated in the laboratory. A recent study by Hartkamp et al. (1993) also found a poor correlation between permeability and total porosity. However, permeability was found to decrease with a reduction in the average pore size of the samples.

Several studies have investigated the relationship between permeability and sedimentary structures. Hurst and Rosvoll (1991) used a laboratory permeameter to measure the permeability of lightly consolidated marine sandstones. They found that the permeability of laminae of some lithofacies tend to group together, while in other instances a 1:3 contrast in permeability was observed between laminae of the same lithofacies. Goggin et al. (1988a) completed an investigation of the Jurassic eolian Page sandstone in Arizona and found distinct permeability ranges for grainflow, grainfall and wind-ripple deposits. A secondary study by the same group of researchers (Chandler et al., 1989) found extra-erg and interdune deposits to form extensive bounding surfaces that restrict fluid flow and tend to compartmentalize the reservoir.

Recent studies by a number of researchers employ geostatistics to quantify relationships between permeability and sedimentary features. Dreyer et al. (1990) used semivariogram analysis to demonstrate good correlation with the permeability values associated with five depositional facies in delta-plain distributary channel sand bodies in the Jurassic Ness Formation in Yorkshire, England. It was concluded that clay content, grain size, and stratification type were the main factors influencing permeability. Davis, (1993, 1994) completed a comprehensive study on fluvial deposits of the ancestral Rio Grande (upper Santa Fe Group) west of Belen, New Mexico. An extensive outcrop was mapped by lithofacies and architectural elements, the architectural elements being divided into high- and low-energy channel deposits, fine overbank deposits and paleosols. Approximately 2000 permeability measurements were obtained from the mapped and surveyed outcrop,

and variograms were used to interpret spatial correlation scales from the permeability data. At the lithofacies scale the correlation function was found to coincide with the character of the internal fluvial bounding surfaces, and at the architectural element scale the correlation structure appears to coincide with the axis of deposition.

CHAPTER 2: GEOLOGIC SETTING

The Albuquerque Basin, in the Mexican Highland section of the Basin and Range province, is one of the largest basins of the Rio Grande rift, covering an area of approximately 6000 square kilometers (Hawley, 1986; Hawley et al., 1995). The northern and central portions of the Rio Grande rift consist primarily of four north-trending axial basins, including, from north to south, the Upper Arkansas, San Luis, Española and Albuquerque Basins (Figure 1). South of the Albuquerque Basin, the rift bifurcates and widens into a series of parallel basins (Chapin and Cather, 1994). The Rio Grande rift is a major break in the continental lithosphere, separating the Colorado Plateau to the west from the interior of the craton to the east (Chapin and Cather, 1994). The extensional processes that characterize continental rifting began approximately 30 million years ago, resulting in the formation of the basins of the Rio Grande rift as large crustal segments tilted and sank relative to adjacent elevated mountain blocks (Cather, 1992). The eastern border of the Albuquerque Basin is formed by uplifted blocks of crystalline Precambrian basement rocks, forming the Sandia, Manzanita, Manzano, and Los Pinos Mountains from north to south. The Colorado Plateau lies on the western boundary of the basin, and the western basin margin is poorly defined when compared to the impressive uplifts to the east. The Rio Puerco fault zone marks the western boundary of the Albuquerque Basin, with the Jemez volcanic center and Nacimiento Mountains forming the northwestern margin of the basin. The Ladron Mountains and Lucero uplift form the southwestern boundary of the basin (Hawley et al., 1995).

Current understanding of the structural framework of the Albuquerque Basin is based on recent reports on deep test drilling, surface and subsurface geophysical surveys, and geologic mapping by several major oil companies (primarily Shell, Exxon and ARCO) who were involved in natural gas exploration between 1960 and 1985. According to Russell and Snelson (1990, 1994) the basin is composed of two tilted-fault-block sub-

basins or half-grabens. The northern half graben is controlled by the Rio Grande fault, and the older beds of the northern portion of the basin tilt to the east. The southern half graben is principally controlled by the Santa Fe-Coyote fault, and the tilt of this block is towards the west . Most of the major basin-bounding faults are listric, and offset along the faults is normal. The northern and southern basins are separated by a structurally complex accommodation zone, trending southwest as an extension of the Tijeras fault zone between Los Lunas and Isleta (Cather, 1992; Chapin and Cather, 1994; Russell and Snelson, 1994).

The Neogene and Lower Pleistocene sediments of the Santa Fe Group form the primary fill of the Albuquerque Basin. At least one additional depositional basin predates the rifting that formed what is now known as the Albuquerque Basin. The Eocene Galisteo-Baca Formations and the late Eocene to late Oligocene un-named unit of Isleta #2 underlies the sediments of the Santa Fe Group, but exposures of these units are limited to only a few areas along the margins of the basin (Lozinsky and Tedford, 1991; Cather, 1992). The Santa Fe Group is divided into lower, middle, and upper units based on age and depositional environment. The thickness of the sedimentary fill in the Albuquerque Basin ranges from approximately 900 to 1200 m along the basin margins, to more than 4500 m in the deepest portions of the central basin (Lozinsky, 1988, 1994; Hawley and Haase, 1992).

The sediments of the lower Santa Fe Group range in age from approximately 25 to 15 million years (Hawley et al., 1995). This unit is characterized by interbedded fine-grained sand and clay, indicating a low to moderate-energy environment (Lozinsky and Tedford, 1991). Deposits are primarily intertonguing eolian, piedmont-slope, and basin-floor deposits. This type of deposition is indicative of an internally drained basin that existed before significant subsidence and surrounding uplift of mountain blocks occurred in the young Rio Grande rift. With the exception of the thick eolian deposits of the Zia sands, the sediments of this unit do not produce significant quantities of quality groundwater (Hawley et al., 1995).

The middle Santa Fe unit was deposited from approximately 15 to 5 million years ago. Tectonism was most active in the basin during these times, and thick sequences of piedmont-slope deposits formed along the basin margins. By this time additional sediment was being transported into the basin from the north, northeast and southwest by major fluvial systems. During this time the northern and southern half-basins filled to form a single topographic basin ((Lozinsky, 1988, 1994). However, the basin as a whole was still internally drained, and it appears that the fluvial systems terminated in playa lakes in the southern reaches of the basin (Lozinsky and Tedford, 1991). The sediments of the middle Santa Fe are locally well indurated, contain abundant fine material, and generally make poor aquifers.

Approximately 5 million years ago, the ancestral Rio Grande established a through-flowing fluvial system through the basin, marking what is now considered to be the base of the upper Santa Fe Group. The ancestral Rio Puerco and Rio San Jose also flowed into the basin, forming a large aggradational plain in the central basin (Lozinsky et al., 1991). Fluvial basin floor deposits are characterized by thick sequences of clean river sands and gravels, and fine-grained overbank deposits. The basin floor deposits intertongue with poorly to well sorted piedmont deposits. Figure 2 illustrates the various sources of sediment for deposits of the upper Santa Fe. The deposits of the upper Santa Fe Group form the major aquifer units of the northern Albuquerque Basin (Hawley and Haase, 1992; Thorn et al., 1993; Kernodle et al., 1995; Hawley et al., 1995).

Between approximately 1 and 0.5 million years ago the Rio Grande and Rio Puerco started to cut their present valleys, forming the first major incision of the Rio Grande and associated fluvial systems in the basin, marking the end of what is considered to be the deposits of the upper Santa Fe Group. Tectonism has been relatively less active in the last 0.5 million years, and aggradation and subsequent incision of the river valleys appears to correspond with drier and wetter interglacial and glacial periods (Lozinsky et al., 1991). Thus, most inner valley post-Santa Fe units were deposited as a series of river terraces,

followed by renewed incision by the river systems (Lambert, 1968). Piedmont surfaces along the basin margins have continued to aggrade during post-Santa Fe times, particularly in the Holocene when the tributary arroyo systems have been delivering more sediment than the axial fluvial system can remove (Lozinsky et al., 1991). The river terraces and floodplain deposits deposited in the last 1 million years are commonly coarse-grained and highly permeable, forming shallow aquifer units as well as major recharge and discharge areas for groundwater in the northern Albuquerque Basin (Hawley et al., 1995). Figure 3 is a map of the geology and major faults of the Albuquerque Basin, and Figure 4 is a cross-section of basin geology, extending through the northern portion of the city of Albuquerque. Figure 5 shows the locations of the outcrops and wells used in this study.

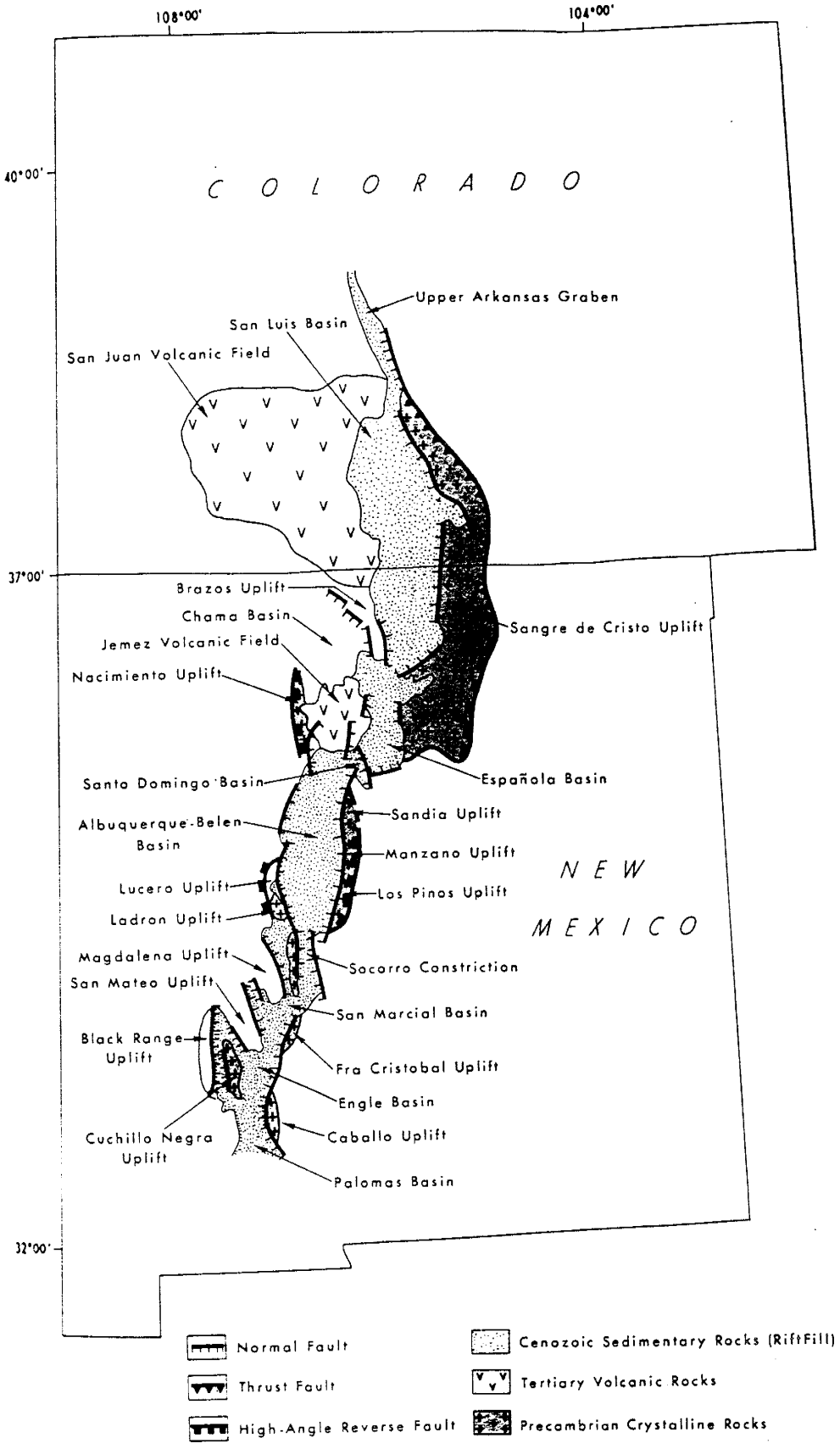

Figure 1. Index map showing the Rio Grande Rift and Albuquerque Basin (Russel and Snelson, 1994)

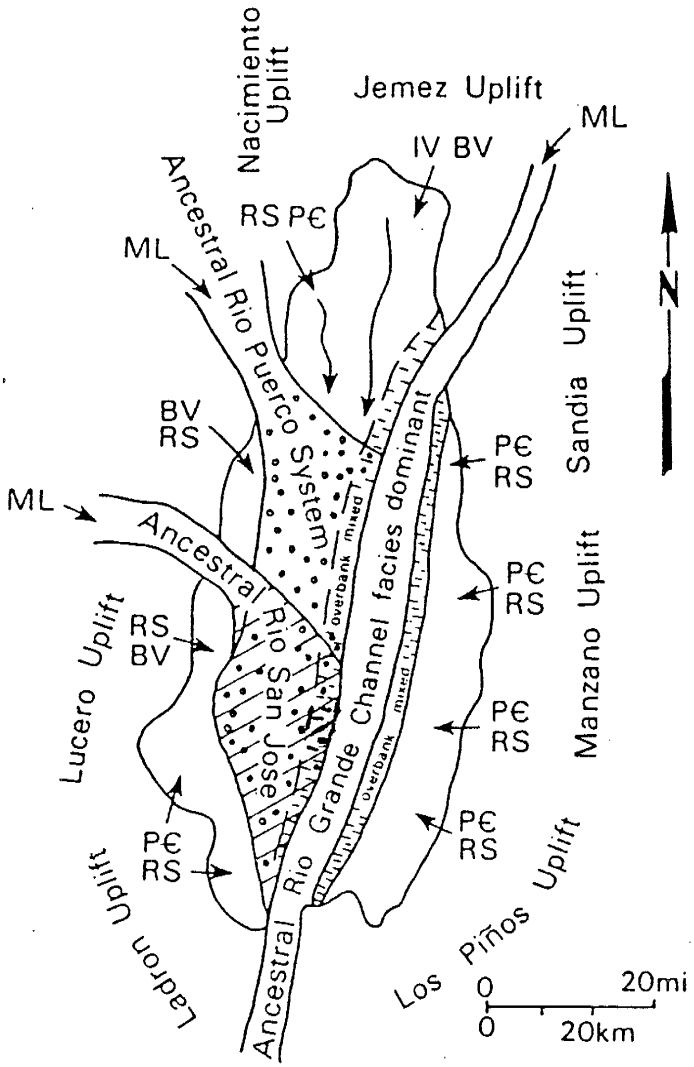

Figure 2. Schematic drawing of contributing drainage systems during the deposition of the upper Santa Fe Group (Lozinsky et al., 1991). Arrows indicate source areas and clast types derived from those areas. PC=Precambrian igneous and metamorphic rocks, RS=party reworked sedimentary rocks, IV=intermediate volcanic rocks, BV=mafic volcanic rocks, ML=mixed lithologies

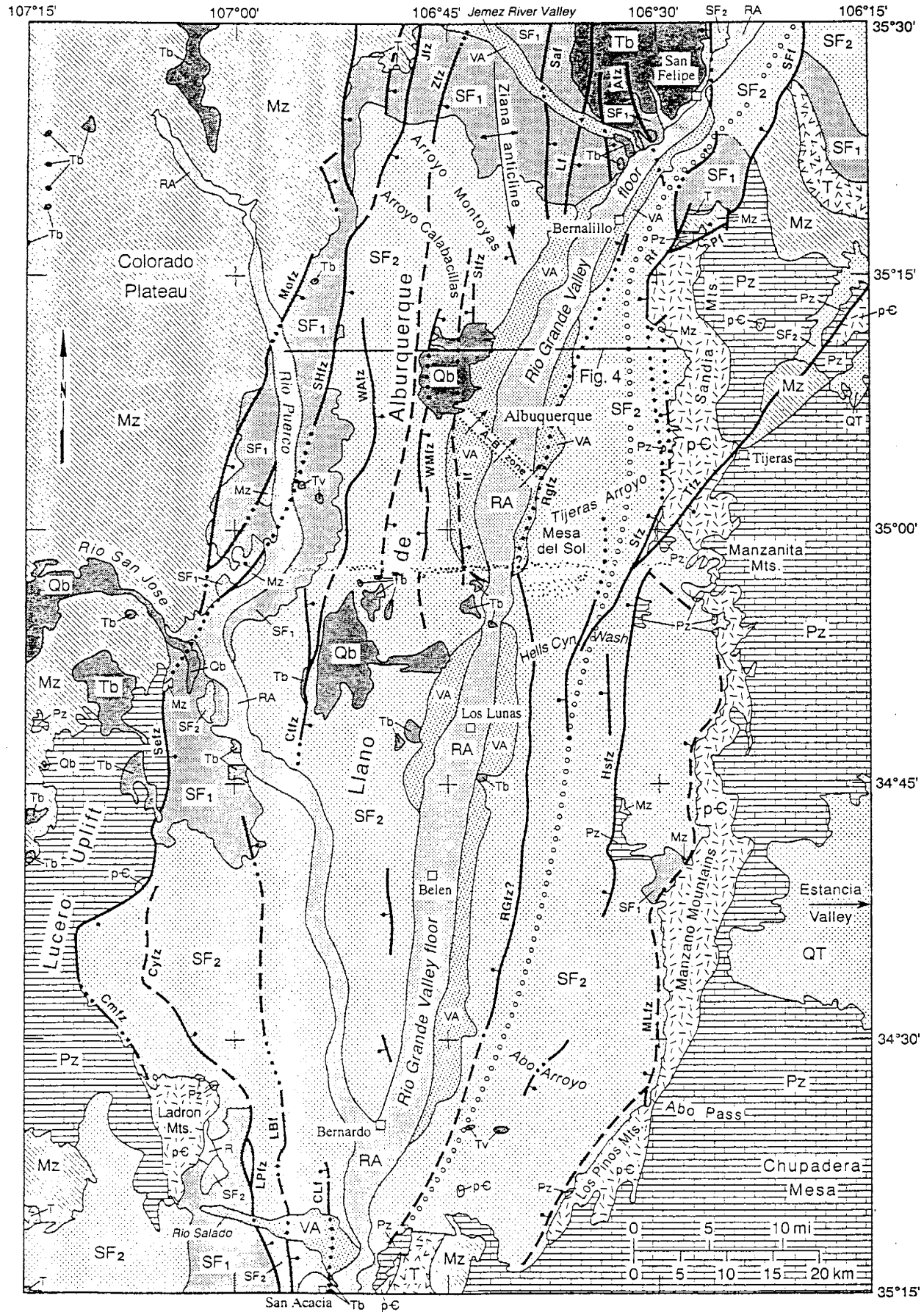

Figure 3. Simplified geologic map of the Albuquerque Basin (Hawley et al., 1995)

Key on following page.

Explanation of Rocks Units

RA Rio Grande and Rio Puerco fluvial deposits defined in Table 1

VA Alluvial fill of the lower Jemez River and Rio Salado Valley and valley–border alluvium defined in Table 1

Qb Younger basaltic volcanics fields; extensive lava flows, with localized vent units such as cinder cones and lava domes, and possible feeder dikes and sills in subsurface; late middle Pleistocene

QT Older alluvium, equivalent to USF–1 defined in Table 1

SF_2 Upper and Middle Santa Fe Group, primarily USF and MSF units defined in Table 1 (including discontinuous veneer of units VA and PA)

Tb Older basaltic volcanics of the Wind Mesa and Isleta fields, extensive lava flows, with localized vent units; include possible sills and/or buried flows west of the Albuquerque volcanoes; Pliocene and Miocene

SF_1 Lower and Middle Santa Fe Group, primarily LSF and MSF units defined in Table 1 (including discontinuous veneer of units PA and VA)

Tv Silicic to basaltic intrusive and volcanic rocks; Miocene and late Oligocene (?)

T Lower and middle Tertiary sedimentary rocks undivided; primarily sandstone and mudstone; includes "unit of Isleta #2" of Lozinsky (1988), and Galisteo and Espinosa Formation correlatives

Mz Mesozoic rocks–undivided; pimarily upper Cretaceous sandstone and mudstone, and local Jurassic clastic rocks, and Triassic sandstone and mudstone

Pz Paleozoic rocks–undivided; including 1) sandstone, mudstone, and limestone of the Permian Abo, Yeso, Glorieta, and San Andres Formation; and 2) limestone, sandstone, and shale of the Pennsylvanian Madera Group and Sandia Formation

p-€ Proterozic rocks–undivided; Precambrian igneous and metamorphic rocks

R Undifferentiated pre-Santa Fe bedrock units

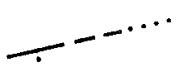
Normal fault, bar & ball on downthrown side; dashed where approximate; dotted where concealed

Eastern edge of axial Rio Grande deposits (USF–2)

FAULT ZONE ABBREVIATIONS: A-B= Atrisco-Barelas fault zone, Afz= Algodones fault zone, CLF=Cliff fault, Cmfz=Comanche-Saiz zone, Ctfz=Cat Meas zone, Cyfz=Coyote zone, HSfz=Hubbel springs zone, Jfz=Jemez zone, LBf=Loma Blanca fault, LPfz=Loma Pelada zone, LF=Luce fault, Mofz=Moquino zone, MLfz= Manzano-Los Pinos zone, Pf=Placitas fault, Rf=Rincon-Rancho fault, RGfz=Rio Grande zone, Sefz=Santa Fe zone, SFf=San Francisco fault, SHfz=Sand Hills zone, Stfz=Star Heights zone, Tfz=Tijeras zone, WAfz=West Atrisco zone, WMfz=West Mesa zone, Zfz=Zia zone.

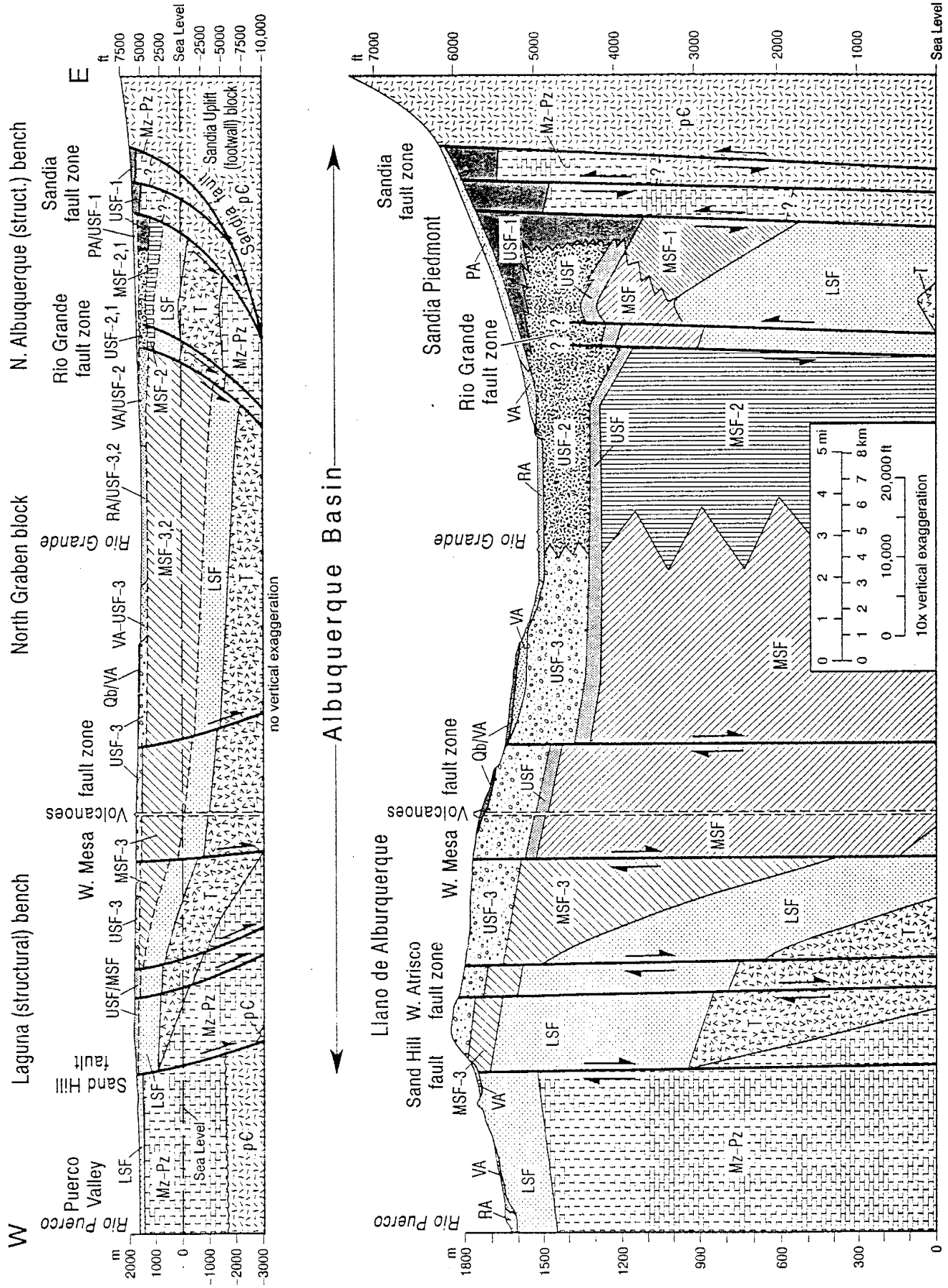

Figure 4. Schematic hydrogeologic cross-section along Paseo del Norte Blvd (Hawley et al., 1995). Key on following page.

POST SANTA FE UNITS

RA River Alluvium

VA Valley–Border Alluvium

PA Piedmont Alluvium

SANTA FE GROUP HYDROSTRATIGRAPHIC UNITS

UPPER UNITS

USF–1 Eastern Piedmont Facies

USF–2 Rio Grande Facies

USF–3 Western Basin Facies

USF Transition Zone Facies (1–2, 2–3)

MIDDLE UNITS

MSF–1 Eastern Piedmont Facies

MSF–2 Basin–Floor Facies

MSF–3 Northwestern Basin Facies

MSF Transition Zone Facies (1–2, 2–3)

LOWER UNIT

LSF Piedmont & Basin–Floor Facies

PRE–SANTA FE UNITS

T Older Tertiary Rocks

Mz–Pz Mesozoic & Paleozoic Rocks

p€ Precambrian Crystalline Rocks

Figure 5. Outcrop locations in the Albuquerque municipal area.
Location abbreviations included in text.

CHAPTER 3: METHODS

FIELD METHODS

Outcrop Selection, Sampling and Permeability Measurements

The outcrops chosen for study were selected on the basis of location and quality of exposure. Outcrops of river alluvium, valley-border alluvium, piedmont-slope alluvium, and upper Santa Fe Group hydrostratigraphic units were sampled (Hawley and Haase, 1992). Whenever possible, outcrops were selected near known natural recharge areas. If several outcrops exist in the same vicinity, the outcrop with the greatest variability in styles of sedimentation and greatest area of exposure was selected for sampling.

Samples were collected from every major sedimentary structure or bed occurring in each outcrop. Outcrop sampling included an in situ measurement of permeability, and collection of sediment samples for grain size analysis and calculation of porosity. The bedding style and degree of cementation of the samples were also recorded. Sampling was limited to deposits with permeabilities within the range measurable by the air-minipermeameter, approximately 0.8 to 270 darcys.

The air-minipermeameter (AMP) used in this study is a lightweight device that is considerably more portable than compressed-gas type permeameters. It weighs approximately 2 kilograms and measures 13x15x23 cm, and is supported by a neck strap when in use. Its primary components are a 100 cm^3 ground glass syringe, timing circuit, and tip seal to direct air flow through the soil matrix. Permeability measurements are obtained by orienting the permeameter vertically, raising the syringe piston, applying the tip seal to the outcrop, and releasing the piston. The glass piston falls at a steady rate under its own gravitational force, applying a small constant pressure through the tip seal. A bubble level mounted on the top of the permeameter allows leveling of the permeameter before measurement. This assures that friction between the piston and syringe body is constant for each measurement. A stopwatch wired to optical switches measures the time required for a

known volume of air to diffuse through the outcrop material. This design allows rapid, non-destructive in situ measurement of outcrop permeability. Davis et al. (1994) discuss the operating principles and calibration of the AMP.

The sampling range of the air-minipermeameter is approximately 0.8 to 270 darcys (approximately 0.5 to 165 m/day for water at 10 degrees Celsius). This range corresponds with permeabilities common to poorly to moderately lithified sands and silty sand deposits in the Albuquerque Basin. Silt, clay and well indurated sand beds generally have permeabilities lower than those measurable by the AMP. Coarse sands and gravels typically have permeabilities exceeding 270 darcys. This permeameter cannot sample unconsolidated fine sands, as a seal cannot be attained between the tip seal and the sediments because the soil matrix is compressed or destroyed when pressure is applied. Sampling of gravel beds is also problematic because it is difficult to seat the tip seal against irregular surfaces. The permeameter was calibrated to a set of epoxy-cemented sand standards prepared in the lab, for which permeability was determined with a constant flow device.

When necessary, outcrop surfaces were prepared prior to sampling. A smooth surface is required to form a tight seal between the outcrop and the tip seal of the permeameter. A small trowel was used to scrape a smooth vertical surface on the deposit. This produced a glazing of some of the surfaces of the finer deposits, which was removed with a brush prior to sampling. Three measurements with the AMP were taken for each sample, and the median value recorded. Obvious outliers among the three measurements, such as would occur if leakage took place, were resampled.

Horizontal permeability was measured parallel to bedding and perpendicular to the outcrop surface, because most outcrop surfaces are vertical or nearly vertical. Vertical permeability measurements would require the excavation of a bench on the outcrop surface. It is difficult to construct such a bench in coarse deposits without disturbing the matrix of the sediments. In stratified rocks and sediments horizontal permeability is generally greater than vertical permeability (Domenico and Schwartz, 1990). Permeability measurements

were made only from air-dry sediments, as soil moisture causes an underestimation of permeability (Davis et al., 1994). Standards were taken into the field to assure the accuracy and consistency of permeability measurements.

A plug of sediment was cored from the outcrop at the point where permeability was measured, allowing comparison of permeability and grain-size distribution parameters. A small cordless electric drill fitted with a 35 mm diameter hole saw was used for sampling. Samples were cored horizontally, corresponding to the orientation of the permeability measurement. Coring in the horizontal direction minimizes the sampling of grains of slightly different sedimentary structure or depositional environment, as fluvial structures are generally more uniform laterally than vertically (Collinson and Thompson, 1982). The permeameter measures the permeability of several cubic centimeters of sediment. The volume of the sample collected for grain size analysis is significantly larger than the volume of material sampled by the permeameter, as a larger sample was necessary for grain size analysis. Approximately 60 to 80 grams of sediment was collected at each sampling point, and retained in manila envelopes. Outcrops and sampling points were photographed for later reference.

A second set of permeability values was compiled from outcrop permeability profile measurements. The permeability, location and bedding type of the sampling points were recorded, but no sediment sample was taken. Prior to sampling, outcrops were sectioned into 15 m horizontal increments for photographing and the construction of photo mosaics. These same points, spaced every 15 m along the base of the outcrops, were used locate vertical sections along which permeability was measured every 15 cm in the vertical direction. Most beds or assemblages of similar sedimentary structures found in the outcrops are at least 15 cm thick. By using a sampling spacing smaller than the thickness of most beds, it is likely that most beds are sampled in the vertical profiles. Likewise, the lateral continuity of many beds exceeds 15 m, so this horizontal resolution is considered appropriate. Care was taken to make permeability measurements along a vertical column at exactly 15

cm increments. Despite this intent, the design of the tip seal of the air-minipermeameter did not always allow strict adherence to this sampling scheme. Some of the coarser deposits found at the outcrops, commonly coarse channels and scour and fill deposits, contain enough pebble and gravel sized clasts to prevent a good seal between the tip seal of the permeameter and the surface of the deposit. In this case a measurement was taken as near as possible to the left or right, where a smooth enough surface could be found or prepared with a trowel. Care was taken that the sediments sampled had a matrix similar to the adjacent point on the vertical transect. If sampling points along the vertical profiles were located on beds more or less permeable than the measurement range of the permeameter, no permeability measurement was recorded. It was noted if the deposit was too permeable or impermeable to be sampled by the permeameter.

Photo mosaics of the outcrops were constructed. Individual photographs cover a horizontal distance of approximately 15 m, and were pieced together to portray the outcrop surface in two dimensions. Scaling of some of the photographs is imprecise because most outcrop surfaces are neither vertical or planar. The azimuth of the individual photographs was recorded. Overlays detailing the contacts between major beds were drawn from the photo mosaics. Overlays and brief geologic descriptions are included in Appendix F.

Collection of Porosity Samples

Sediment samples were collected adjacent to the point where permeability was measured, for the purpose of determining sample porosity. The porosity of fine-grained, poorly consolidated deposits were determined from a relatively undisturbed sample obtained from outcrop. A level horizontal surface was prepared along the bed to be sampled, and a small cylindrical sampling tin was pushed down through the matrix, isolating a relatively undisturbed core. A shovel blade was then driven under the sampling tin, allowing it to be turned upright without the loss of sandy material. The soil matrix is disturbed near the edges of the tin, but most of the sample retains its original packing.

The porosity of coarse-grained or moderately cemented samples was determined by an alternative method. It is impossible to drive the rim of a sampling tin through sediments containing particles larger than coarse sand without greatly disturbing the original matrix. For coarse or moderately cemented samples a horizontal surface was prepared on the bed to be sampled, and a small pit was made with a drill, trowel or spoon, and the excavated material retained in a sample bag. The depression was then filled with fine sand poured from a graduated cylinder. The volume of sand required to fill the depression was then easily determined from the volume measurements on the graduated cylinder. Knowing the bulk volume, weight and average grain density of the sample, the porosity can be determined.

Classification of Outcrop Samples

Samples were classified on the basis of style of bedding and sedimentary structures, and grouped into five categories. Classifications were designed to differentiate between several types of sedimentation on the outcrop scale. This appears to be the most appropriate way to classify deposits, considering the disparity in scale between sediment samples used for grain size analysis and the size and variability of beds occurring in the outcrops.

Crossbeds are the first bedding classification, and are most common in the river facies. This classification includes trough crossbeds, tabular crossbeds, and foresets. This style of bedding includes the sediments of most accretionary bar deposits.

Channels include larger scours and associated lateral accretion deposits. They commonly cut into underlying beds, and have a concave base in cross-section. Most channels observed in outcrop are composed of coarse sand, pebbles and gravel. They may occur as part of a channel-fill sequence, as described by Picard and High (1973). Channels typically consist of material coarser than the beds they cut into or overlie.

Horizontal beds are commonly fine-grained deposits, but may be of medium to coarse sand. They are tabular and laterally continuous. Horizontal beds greater than one centimeter thick are relatively uncommon, and the majority of the sediments of this grouping are actually horizontal laminations (less than 1 cm thick). Fine-grained low angle ripples are included in this bedding type.

Scour and fill deposits commonly form crude horizontal beds of limited lateral continuity, typically extending no more than one meter along the outcrop surface. Sorting of the sediments is generally poor. This type of deposit is common to the piedmont fan facies, and it is likely that they are formed in accretionary lobes. This bedding classification is applied only to the fan facies.

Structureless deposits exhibit no primary sedimentary structures. Silts of the river facies sometimes lack primary sedimentary structures. Structureless beds contained in the fan deposits may be eolian in origin. Several deposits classified as structureless are buried paleosols.

The degree of cementation was recorded for each outcrop sample. The relative amount of cementation was evaluated in the field, and no rigorous measurement of lithification was determined. Phreatic and pedogenic cementation was not differentiated. Table 1 list the criteria used in ranking cementation.

LABORATORY METHODS

Calibration of the Air-Minipermeameter

The air-minipermeameter was calibrated to standards prepared in the laboratory. Standards were constructed by filling stainless steel cylindrical rings with a mixture of sands and low viscosity epoxy. The one-dimensional permeability of the samples was determined with a compressed gas source, rotameters and pressure transducer, following the ASTM D4525 method. These procedures are detailed in a publication by Davis et al. (1994), who were responsible for the design, construction and calibration of the perm-

eameter used in this study. The original standards prepared by Davis were used to recalibrate the permeameter. The dimensions of the tip seal were changed since the original calibration of the instrument, and recalibration found that a geometric factor of 5.2 provided the best fit with the prepared standards, instead of 4.5 as used earlier by Davis, based on the investigations of Goggin et al. (1988).

Sensitivity of calculated permeability values to changes in atmospheric pressure and air temperature was evaluated by the author. A change in air temperature from 45 to 90 degrees Fahrenheit in the permeability equation increases the value of measured permeability by 6.8 percent. Standards were not measured at these temperature extremes, so it was not determined how readings vary due to changes in air viscosity. An average temperature of 55 degrees, or air viscosity of 0.0000178 Pascal·seconds, was used in all calculations. Permeability values are considerably less sensitive to changes in atmospheric pressure. A pressure change from 82.5 kPa to 87.5 kPa Pascals results in a 0.015 percent decrease in permeability values. An average pressure of 85.153 kPa was used in all calculations.

The air-minipermeameter is extremely sensitive to measurement times for highly permeable sediments. The free-fall time of the piston averages 0.72 seconds. The smallest times recorded at the outcrops were 0.78 seconds, indicating a permeability of 271 darcys. A measurement time of 0.83 seconds indicates a permeability of 200 darcys, demonstrating the sensitivity of measurements in this range. The most permeable laboratory standard has a permeability of 250 darcys, so permeability measurements in this range can be used with confidence. Readings for sediments with fall times less than 1 second were recorded only if good agreement was attained between consecutive measurements. Otherwise the deposit was recorded as too permeable for measurement with the air-minipermeameter in the current configuration. The weight of the piston and dimensions of the tip seal may be adjusted to allow sampling of sediments of higher or lower permeability.

The air-minipermeameter was used by another researcher between the time permeability measurements for the sieved outcrop samples and the outcrop permeability

profiles were taken. He was negligent in his use of the instrument, drawing fine particles through the in-line filter and into the glass syringe. Slight scoring occurred near the top of the syringe body. The damage is in the uppermost range of piston travel, and it is not felt that this has an influence on the permeability readings. The upper microswitch is located approximately one third of the length of the syringe body from the top, and the piston falls freely well before it reaches this point. This upper piston travel allows steady state conditions to be established before the timing of air flow through the soil matrix begins.

Porosity Measurements

The porosity of outcrop samples was estimated by two methods. The first method requires a petrographic determination of the average particle mass density of the sample. Most of the samples are predominantly quartz and feldspar, and a density of 2.65 g/cm^3 is assumed for these samples. Porosity is calculated by subtracting the quantity of the bulk mass density divided by the particle mass density from one, as shown in Equation 3.1 (Lambe, 1951).

$$n = 1 - \frac{\rho_{bulk}}{\rho_{grain}} \qquad \text{(Equation 3.1)}$$

It is difficult to apply this method to samples containing clasts of widely varied density, most notably pumice, common to some samples from the upper Santa Fe Group and the Edith Gravels.

Porosity was estimated by an additional method for sample cores obtained with the sampling tins. Distilled water was poured from a graduated cylinder into the undisturbed material, allowing the volume of water required to saturate the pore spaces of the sample to be accurately determined. The water was poured along one side of the tin to minimize the volume of air trapped in the matrix. The sample was then probed with a narrow blade to release air bubbles trapped in the matrix. By subtracting the volume of water added from

the total volume of the tin, and dividing by the dry weight of the sample, an estimation of the average particle mass density was obtained. The porosity of the sample was then determined using Equation 3.1. See the Discussion section for the limitations and use of this method.

Grain Size Analysis

Outcrop samples were prepared for particle size analysis in the laboratory. A sample splitter was used to reduce samples to the desired weight for sieving. Between 40 and 43 grams of material were used for most samples, but up to 50 grams were used for the coarsest samples. Samples were oven dried at approximately 90° Celsius for at least 24 hours. After drying, samples were allowed to cool to room temperature and weighed. Samples were inspected for aggregates prior to mechanical sieving. Samples containing aggregates were ground with a mortar and pestle to break up all aggregates. Most samples required no disaggregation beyond that which occurred in sampling and handling.

A set of 21 sieves were used for grain size analysis. Sieves diameters are listed in Table 2. Sieves with mesh diameters of 0.600 mm and larger are 8 inch diameter Soiltest brass sieves. Sieves 0.500 mm and smaller are 3 inch diameter nickel mesh sieves manufactured by the Buckbee Mears Co. The large-diameter sieves were placed on a Rotap sieve shaker for 15 minutes. The small-diameter sieves were placed on a separate shaker that shakes the sieves more violently than the Rotap machine, but does not have a tapping arm. Most of the outcrop samples have only minor percentages of silt and clay, and therefore no wet-sieving was necessary.

In contrast to the outcrop samples, many of the well cuttings from PSMW-19 required wet sieving prior to dry sieving. Nested sieves with meshes of 0.074 and 0.045 mm were used to remove silt and clay-sized particles from the sand-sized fractions. The runnings from the wet sieving were dried and weighed. The sand fractions were then oven-dried, and dry-sieved as described above. The cuttings from Coronado 2 contain

TABLE 1. Parameters for Cementation Values

Degree of Cementation	Description
1	Unlithified to very poorly consolidated. Deposit is easily disaggregated, but matrix has sufficient integrity to allow sampling with the permeameter.
2	Poorly consolidated. Outcrop material breaks off in clumps that are easily crushed between the fingers.
3	Weakly to moderately consolidated. Outcrop material resists probing with trowel or hammer.

TABLE 2. Sieve Sizes Used in Mechanical Size Analysis Of Sediments.

Millimeters	ϕ unit ($-\log_2$ mm)
2.00	-1.00
1.70	-0.77
1.40	-0.49
1.18	-0.24
1.00	0.00
0.850	0.23
0.710	0.49
0.600	0.74
0.500	1.00
0.400	1.32
0.300	1.74
0.250	2.00
0.225	2.15
0.200	2.32
0.175	2.51
0.150	2.74
0.125	3.00
0.100	3.32
0.090	3.47
0.060	4.06
0.045	4.47

fines in very small percentages, and no wet-sieving was required. Approximately half of the samples from MW1 required wet sieving.

PERMEABILITY AND GRAIN-SIZE DISTRIBUTION OF OUTCROP SAMPLES

Graphical Representation of Grain-Size Distributions

Two separate methods were used to plot particle size distributions. The first is the common cumulative percent graph. These plots are easily generated from the raw sieve data. Sieve opening sizes in millimeters are plotted on the x-axis, and weight percent smaller than the sieve size from 0 to 100 is plotted along the y-axis. From these curves the general grain-size distribution is observed in a familiar format, and the percentage of the sample passing through each sieve size is easily determined. Effective diameters are used in many published empirical permeability equations. The effective diameter d_{10} is simply the sieve diameter through which only the smallest 10 percent of the sample by weight will pass. Values for d_{10}, d_{15}, d_{17}, d_{20}, d_{50} and d_{60} were interpolated from the smoothed cumulative frequency curve of each sieved outcrop sample. An effective diameter based on the entire grain distribution was also computed for each sample. This effective diameter d_e is proposed by Kruger, and is calculated as:

$$\frac{1}{d_e} = \sum_{i=1}^{N} \frac{\Delta g_i}{d_i} \qquad \text{(Equaton 3.2)}$$

where g_i is the fractional percent weight retained on individual sieves, and d_i is the mean grain diameter in millimeters of the corresponding fraction (Vukovic and Soro, 1992).

Effective diameters were determined in millimeters, then converted to ϕ units for subsequent correlations with permeability. Phi units are the grade scale commonly used by geologists to describe particle size distributions, calulated as $\phi = -\log_2 d$, where d is grain diameter in millimeters. The negative sign is added for convenience, giving all grains

smaller than 1 mm in diameter (very coarse sand) a positive value (Krumbein, 1934). Sieve diameters listed in Table 2 are converted to ϕ units for comparison.

The plotting style used in this study for the comparison of sample particle size distributions is the log-log plot, proposed by R.A. Bagnold (1941). This style of plot may also be referred to as log-hyperbolic plots or Bagnold plots, and is constructed as

$$N = \frac{\delta p}{\delta R} \qquad \text{(Equation 3.3)}$$

where δp is the weight percent of the sample retained on a sieve, and

$$\delta R = \log \frac{d_1}{d_2} \qquad \text{(Equation 3.4)}$$

where d_2 is the sieve aperature in millimeters of the sieve retaining the percentage of the sample, and d_1 is the aperature of the next larger sieve. Plotting the log of N on the linear y-axis and sieve diameter d_2 on the logarithmic x-axis forms the log-log plot. By plotting the log of N on the y-axis, all intervals are given equal prominence (Bagnold, 1941). Plots of this type effectively display the relative abundance of fine-grained material, which has a large influence on permeability. Cumulative percent and log-log plots are displayed for comparison in Appendix A.

Grain-Size Distribution Statistics

Particle size distribution statistics and representative diameters were calculated for two sets of data. The first group includes the entire particle size distribution of the sample, while the second excludes all grains greater than 2 millimeters in intermediate diameter. For the complete sample no sieves larger than 2 mm were used, but the maximum intermediate diameter of the largest clast of the sample was measured and recorded. The weight

of clasts retained on the 2 mm sieve and the maximum intermediate diameter of the largest clast were used to determine the moment measurement of the pebble-sized fraction of the sample.

Moment calculations, as opposed to graphical methods, were used to calculate the mean, standard deviation, skewness, and mean-cubed deviation for each sieved outcrop samples. The following formulas were used for the computation of moment statistics. Grain size is reported in ϕ units, so a log normal distribution is implied. The mean is defined as

$$\bar{x} = \sum_{i=1}^{N} f_i \cdot m_i \qquad \text{(Equation 3.5)}$$

where N is the number of sieves, f is the fractional percent by weight retained on each sieve, and m is the midpoint for that sieve interval. Standard deviation is calculated as

$$\sigma = \sqrt{\sum_{i=1}^{N} f_i \cdot (m_i - \bar{x})^2} \qquad \text{(Equation 3.6)}$$

The standard deviation is a measure of sorting, reflecting the spread of the distribution on either side of the mean. Skewness, also termed the third moment about the mean, describes the symmetry of the curve, and defines how far the curve deviates from a symmetric form. Skewness is computed as

$$\alpha = \sum_{i=1}^{N} \frac{f_i \cdot (m_i - \bar{x})^3}{\sigma^3} \qquad \text{(Equation 3.7)}$$

(Friedman, 1962). The mean-cubed deviation is calculated as

$$\sum_{i=1}^{N} fi \cdot (mi - \bar{x})^3 \qquad \text{(Equation 3.8)}$$

and has been found to be a useful parameter for distinguishing between different depositional environments in other studies (Friedman, 1967). Kurtosis, the fourth moment, is not used in this study. A spreadsheet was created to compute statistical parameters for the outcrop samples and the well cuttings.

Comparison of Bedding Types

Outcrop samples were grouped by bedding type. Box and scatter plots were generated to compare separation between bedding style, based on permeability, porosity and grain-size distribution parameters. Comparative statistics were generated for grain-size distribution parameters grouped by bedding type. Some 1314 permeability measurements from the outcrop permeability profiles were grouped by bedding type, allowing comparison of permeability among bedding types. Box and scatter plots were used to compare grain-size distribution parameters of cuttings from wells Coronado 2, MW1, and PSMW-19 to the outcrop samples.

Comparison of Measured Permeability to Published Permeability Equations

Scatter plots contrasting measured permeability values and permeability values estimated by a number of published permeability equations are included in Appendix B. Permeability is plotted on logarithmic axis for ease of comparison. The published equations, detailed in the Results chapter, yield values for hydraulic conductivity, which are converted to darcys for comparison with measured permeability values. A water temperature of 10 degrees Celsius (50 degrees Fahrenheit) is used for all conversions to intrinsic permeability. SYSTAT statistical software, version 5.2, was used to calculate Pearson correlation coefficients for measured and predicted permeability values.

Predictive Permeability Equations

The SYSTAT statistical software package was used to determine Pearson correlation coefficients for measured permeability and a number of grain distribution and outcrop parameters. The same software was used to formulate predictive permeability equations for use on well cuttings in the Albuquerque Basin. Stepwise multiple regression analysis was applied to various parameters found to have high correlation with the measured permeability of the outcrop samples. Sample parameters were correlated with both measured permeability and the $\log_{10}$ of measured permeability.

CHAPTER 4: RESULTS

OUTCROP DESCRIPTIONS AND PERMEABILITY PROFILES

Ten representative outcrops in the northern Albuquerque Basin were selected for the characterization of aquifer-related units. They were selected based on the size, quality and location of the exposures. Sediment samples and permeability measurements were obtained from these ten outcrops to determine the range of permeabilities and associated particle size distributions common to several of the different hydrostratigraphic units known to be recharge areas. Ten outcrops are not sufficient to characterize the heterogeneity of lithofacies found in the Albuquerque Basin. This study is limited by the availability of quality outcrops, the sampling range of the permeameter, and the time frame of this project. Outcrops are limited in the Albuquerque urban area, but enough exposures do exist to gain valuable information on the nature of these sediments. Figure 6 is a box plot showing the range of permeability values measured at each outcrop. Boxes in the box plots enclose 50 percent of the values of each parameter, and the solid line within the boxes denotes the median value. Lines extend beyond the boxes to the maximum and minimum values, or to a distance of 1.5 times the length of the inner box (whichever is the lesser value). Values plotting beyond 1.5 times the length of the inner box are considered outliers by the graphing program and marked by small circles. The range of permeability values displayed in Figure 6 are based on the 1314 permeability profile measurements, and do not include data for the sieved outcrop samples. Table 3 is a statistical summary of the same permeability profile measurements. Photo mosaics of the outcrops, along with generalized geologic overlays and the locations of sampling points, are included in Appendix F.

Three outcrops of the upper Santa Fe Group were selected for study. Approximately 5 million years ago the through-flowing ancestral Rio Grande was established, marking a change in sedimentation from the fine-grained valley floor sediments common to the middle Santa Fe, to the sand-dominated river deposits of the upper Santa Fe

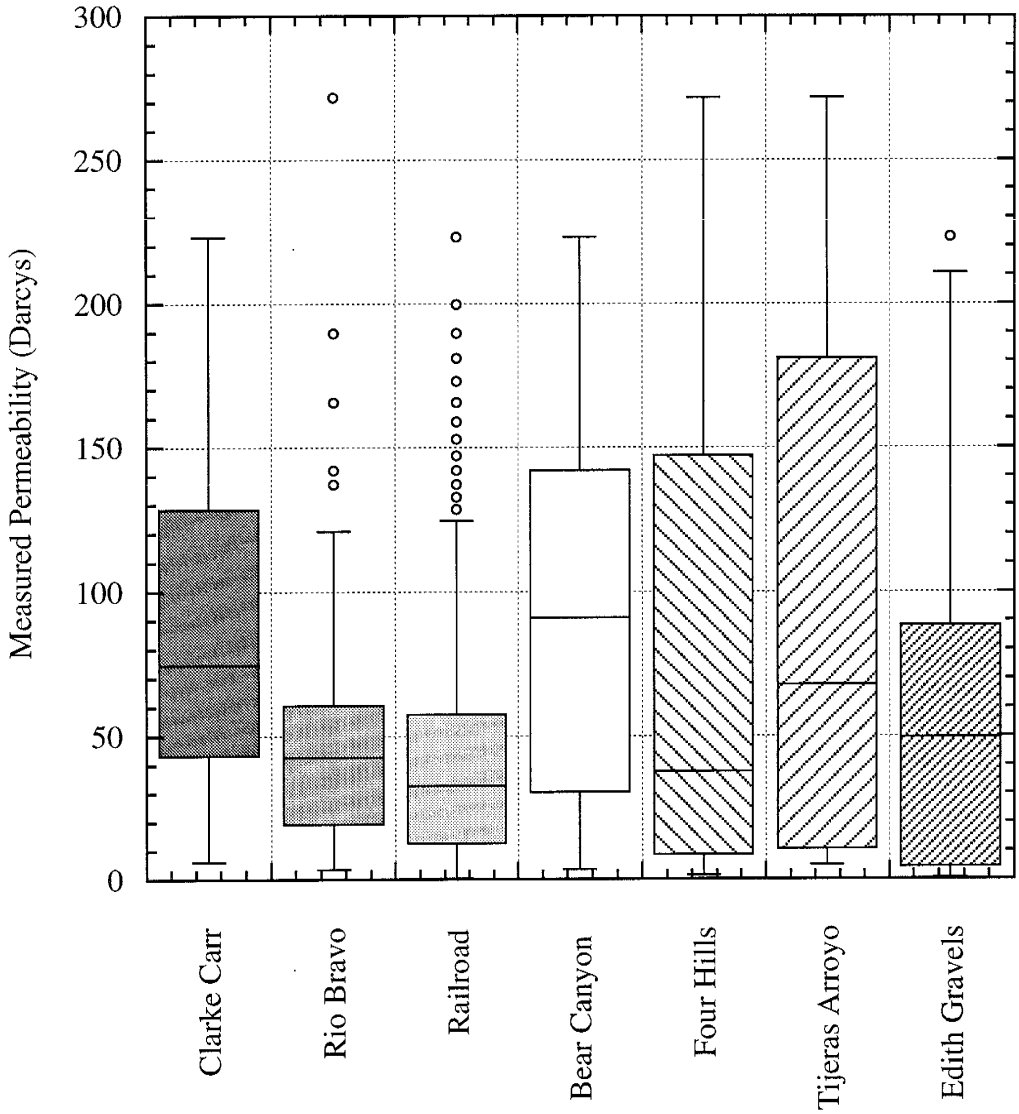

Figure 6. Measured permeability values by outcrop. Permeability profile measurements, unsieved samples. Circles are data points considered outliers by the graphing program.

TABLE 3. Outcrop Permeability Profile Data Summary

Outcrop	Median	Mean	Std. Dev.	Skewness
USF-2, Clarke Carr	74.67	88.89	56.55	0.664
USF-2, Rio Bravo	42.59	50.20	43.14	1.977
USF-2, Railroad	32.86	42.13	40.51	1.636
VAs, Los Duranes (sands)	66.90	71.25	29.76	0.497
VAg, Edith Gravels	49.42	55.76	52.54	1.029
PA, Bear Canyon	90.94	91.00	63.22	0.386
PAt, Four Hills	37.63	83.37	89.52	0.915
PAt, Tijeras Arroyo	67.89	98.10	90.00	0.407

Group (Lozinsky and Tedford, 1991). This unit has been divided further by various authors, and the hydrostratigraphic units and lithofacies of Hawley and Haase (1992) are used to classify the outcrops studied here. The three outcrops of upper Santa Fe Group sediments investigated in this study all belong to the USF-2 hydrostrati-graphic unit, which includes river deposits of the ancestral Rio Grande and associated fine-grained deposits in the river-valley area. Large channels, gravel beds, and thick tabular beds are exposed in the three outcrops, and beds and structures of this scale could only have been deposited by a major through-flowing river system (Lambert, 1968). The presence of trough cross-bedding, a poorly defined main channel, and high sand-to-clay ratios suggest a braided-river style of deposition (Lozinsky and Tedford, 1991). Thin clay drapes and horizontally laminated silt beds are present but uncommon, deposited in backwater environments and as overbank deposits.

The first outcrop of USF-2 deposits is located approximately 100 m southeast of the corner of University Boulevard and Clarke Carr Road. In reference to more familiar landmarks, this is 1 km east of Interstate 25, between the University of New Mexico Golf Course and the Albuquerque International Airport. This outcrop, referred to as CC, consists of high-energy axial river deposits of the ancestral Rio Grande, and is classified as Lithofacies I (Hawley and Haase, 1992). Approximately 7 m of vertical section is exposed. Deposits consist of alternating sand and gravel beds. Sandy deposits vary from well sorted fine to medium sands, to poorly sorted medium to coarse sands with alternating sand and pumice laminations, to beds composed nearly entirely of pumice clasts. Large foresets, trough crossbeds, minor channels, and horizontal beds and laminations are common among the sandy beds. Cements are uncommon, with small moderately cemented concretions occurring in one of the fine sand beds. Gravels and coarse sand with abundant gravel-sized clasts form approximately 30 percent of the exposure, both as continuous beds and as channels cut in the sand beds.

Seventy four permeability measurements were obtained at the Clarke Carr location. The minimum permeability measured was 6 darcys, and the maximum 223 darcys. Near the top of the outcrop thick gravel beds are exposed, and have permeabilities greater than those measurable by the air-minipermeameter. Of the measured samples, the mean permeability value is 89 darcys, and the standard deviation is 57. The median recorded value is 75 darcys. Most permeability measurements were taken from the sandy beds, so the average permeability of this outcrop would increase by an undetermined amount if the permeability of the gravels beds were included.

The second outcrop of USF-2 fluvial facies, referred to as RB, is located immediately east of Interstate 25 at the University/Rio Bravo Boulevard underpass. Beds were deposited by high discharge flows of the ancestral Rio Grande, and best classified as lithofacies I or Ib (Hawley and Haase, 1992). Beds are tabular and very continuous, some being continuous across the entire length of the exposure, a distance of over 200 m. Sandy beds form the majority of the deposit, ranging from well sorted fine sands to poorly sorted coarse sands and pebbles. Horizontal beds and laminations are common, with crossbeds and minor channels also present. A bed of large foresets, composed of gravel with a coarse sand matrix, is continuous across the outcrop. Broad gravel scours less than 20 cm thick are found between two of the sandy beds. A moderately cemented fine sand bed of low permeability, with local well-developed cementation, is found near the top of this exposure. Approximately 10 m of vertical section was sampled. Well PSMW-19 is located several hundred meters northwest of this outcrop.

A total of 116 permeability measurements were obtained at the Rio Bravo outcrop. The lowest measured permeability is 4 darcys, and the maximum is 271 darcys. The mean permeability value is 50 darcys, and the median is 43. The standard deviation of the permeability measurements is 43.

The third Upper Santa Fe (USF-2) outcrop from which samples were gathered is located approximately 1.4 km south of the Rio Bravo outcrop, where railroad tracks pass

under Interstate 25, north of Tijeras Arroyo. This location is referred to as RR, and exposures were formed by the excavation of the railroad underpass and an adjacent sand and gravel quarry, just west of Interstate 25. This outcrop is dominated by sandy deposits, and classified as lithofacies II. The lower beds exposed at this location are medium to coarse-grained river sands forming trough crossbeds, horizontal beds and minor channel structures of coarse sands and pebbles. One gravel channel approximately 1 m deep and 3 m wide cuts through the lower sand beds. This style of sedimentation is common to braided channels. A slightly to moderately cemented bed of horizontally laminated fine to very fine sand, 1.5 to 2.5 m thick, overlies the lower coarse sands. This bed extends the length of the outcrop, some 60 m. Well-indurated laminae are found near the top of this bed, and angle or diverge up into the overlying bed. The upper sand bed at this location is a well sorted medium sand, containing large scale convoluted bedding. The convolutions do not appear to be depositional in origin, and may be due to soft sediment deformation. The origin of this bed is not readily apparent, but may be eolian. Capping the outcrop are discontinuous gravel deposits; poor exposure obscures the nature of these deposits. A second exposure two hundred meters to the north consists primarily of low angle crossbeds and horizontal beds of medium to coarse sands and pebbles.

For the 496 measurements taken at the RR outcrop, the maximum value was 223 darcys, and the minimum .8 darcys. The mean permeability is 42 darcys, and the standard deviation 41 darcys. The median measurement value is 33 darcys. This outcrop is located approximately 1.6 km south of the well PSMW-19.

Three younger inner valley deposits were sampled. They include the Los Duranes and Edith gravel type sections of Lambert (1968), and a section of clean river sands exposed 10 m below the present floodplain of the Rio Grande. The Edith terrace was deposited during interglacial periods, following valley cutting events during wet glacial episodes. The Los Duranes terrace is believed to deposited by the waning flows of one of these events. (Lambert, 1968; J.W. Hawley, personal comm.) The Los Duranes unit is in

direct hydraulic contact with the present-day channel of the Rio Grande. The other two units appear to be disconnected from the river by the lowering of the water table below the modern flood plain.

The Los Duranes (LD) type-section forms the prominent bluffs along the west bank of the Rio Grande, approximately 1.5 km north of Interstate 40. Access is possible from Crown Point Court, east of Coors Blvd. This valley-border alluvial terrace deposit is representative of the VAs hydrostratigraphic unit, lithofacies III, and is comprised of interbedded sand and silt/clay beds (Hawley and Haase, 1992). Fine-grained overbank beds in this aggradation sequence of floodplain deposits grade downward into river-channel sands. Overbank sediments consist of thin interbeds clay, silt, and sandy silt and clay, in stacked sequences that are 3 to 9 m thick. Sandy channel deposits range from 2 to 6 m in thickness. Beds are tabular and lateral continuity is on the order of hundreds of meters. Horizontal laminations, low angle crossbeds and foresets, and minor channels of coarse sand and pebble gravel are the most common structures of the sandy beds. Sand beds are typified by minor percentages of silt and clay, are unconsolidated to very poorly consolidated, and of moderate permeability. This deposit is described in greater detail as part of Lambert's (1968) Adobe Cliffs Section.

The sandy beds of the Los Duranes section are moderately permeable. Permeability measurements were difficult to obtain at this location, as many of the sandy beds are unconsolidated and crumble under the pressure of the tip seal of the air-minipermeameter. Twenty permeability measurements were obtained from the sandy beds, with a mean value of 71 darcys, a standard deviation of 30, and a median value of 67 darcys. The minimum recorded permeability for the sandy beds was 25 darcys, and the maximum was 137. These values reflect the lower ranges of permeability of the sandy deposits. The maximum permeability recorded for the silty beds at this location was 5 darcys. The permeability of clay beds interbedded with the silts is considerably lower, but the range of these values was not determined.

The Edith gravels (EG) of Lambert (1968) are exposed at a number of locations along the inner valley of the Rio Grande. The Edith Gravels are an axial river terrace deposit, being of the VAg hydrostratigraphic unit, and lithofacies Iv of Hawley and Haase (1992). Excellent outcrops can be found along Edith Blvd., approximately 0.5 km north of Paseo Del Norte in the north valley. This outcrop is adjacent to the site of well MW1, drilled by the Bureau of Reclamation in the summer of 1993. A thick sequence of medium to very coarse sands with abundant pumice forms the lower 4 m of the deposit, with trough crossbedding and small channels the most common sedimentary features. Large convoluted beds are also present. A laterally extensive bed of white silt forms the upper rim of the outcrop, lying over the lower convoluted and channeled sands. Gravel beds of undetermined thickness cap the exposure. The gravels have a matrix of coarse sand, and it was not poosible to measure the permeability of these beds with the air-minipermeameter.

A total of 134 permeability measurements were taken at this location, ranging from 0.8 to 223 darcys. The mean value is 56 darcys, standard deviation 53, and the median permeability value is 49 darcys. Permeability of the sandy beds is relatively high, and the presence of extensive gravel beds makes the overall permeability of these deposits very high.

The third inner valley deposit sampled is young river alluvium from the ancestral Rio Grande (hydrostratigraphic unit RAr, lithofacies Iv). The exposure is located approximately 200 m south of Claremont Avenue, between Broadway Blvd. and the AT&SF railroad tracks. This exposure is 4 km east of the present channel of the Rio Grande, and referred to as the Claremont outcrop (MS). A large trench was excavated to construct a flood control structure, exposing the sediments of the floodplain. The deposit consists of clean channel sands deposited by the ancestral Rio Grande. Bedding continuity is on the order of hundreds of meters. Channels and trough crossbeds are the major sedimentary features. A few very fine sand lenses are present, but the deposits are primarily medium to very coarse sand and pebbles. Measured permeabilities were near the upper

range of the air-minipermeameter. The sediments are unconsolidated, prohibiting extensive sampling.

Distal Embudo Fan (EF) (Lambert, 1968) facies were exposed at the southern end of the above mentioned excavation, exposing the Claremont river alluvium. This deposit is classified as Valley Alluvium, VA, lithofacies V (Hawley and Haase, 1992). Crude horizontal beds are common, and scour and fills are the most common sedimentary structures. Individual thin depositional lobes can generally be traced for less than 1 to 2 m along the outcrop surface. This is typical of alluvial fan deposits, where sediment is abundant and channel avulsion and lobate deposition is common (Collinson, 1986). Poorly sorted coarse-grained beds are prevalent, with abundant fines resulting in low to moderate permeability values. Fine-grained structureless beds are also present. The more permeable deposits appear to be poorly connected. Permeability profiles were not sampled at this location, due to the poor quality and limited extent of the exposure.

Piedmont-slope alluvium is the fourth hydrostratigraphic unit studied in outcrop. Medial fan facies of the Bear Canyon Arroyo were sampled in two locations, and proximal and medial Tijeras Fan facies were sampled. Sediment is derived mainly from the Sandia Mountains. Feldspar and quartz are the most common minerals, weathered from the Sandia Granite. Many samples from these deposits are poorly sorted and have a large percentage of clasts greater than 2 mm in intermediate diameter. These exposures contain beds of high porosity and permeability, but are often separated by beds of low permeability. Detailed studies of the architecture and hydrogeologic properties of an alluvial fans in the region were completed by Bowman and Stevens (1991) and Neton et al. (1994), and provide more thorough documentation of fan heterogeneity.

The Tijeras Arroyo (TA) outcrop is located approximately 3 km west of the point where Tijeras Arroyo crosses the Tijeras fault at the mouth of Tijeras Canyon. It is most easily reached by traveling south on Eubank Blvd., past the entrance to Sandia National Laboratories, then east to the point where power lines cross the arroyo. A sequence of fan

deposits approximately 12 m thick is exposed in a gully on the north side of Tijeras Arroyo. The sediments are classified as PAt, Tijeras piedmont-slope alluvium, lithofacies VI. The outcrop is characterized as a sequence of alternating coarse and fine beds. Coarse beds are poorly sorted gravely sands and silts with crude horizontal bedding. Scour and fill structures are common. Coarse channels are contained in these beds, with boulders up to 30 cm in diameter. Channels are locally coarse and lacking in fines, resulting in high porosity and very high permeability. Fine silty sand beds are largely structureless, with occasional horizontal laminations. The laminations appear to be overbank deposits, while the majority of the sediments may be eolian. The lack of sedimentary structures suggests they may be buried paleosols. Horizontal exposure is limited, and it is difficult to define the lateral extent of these beds.

The instability of the upper portions of this outcrop, and angled surfaces at the base prevented the acquisition of complete vertical permeability profiles. As an alternative, measurements were staggered up the exposure in 1.5 m segments, forming the equivalent to one vertical profile sampling the complete section. A total of 91 permeability measurements were gathered, with a mean of 98 darcys, standard deviation of 90, and median of 68 darcys. The highest permeability sampled was 271 darcys, and the lowest 5.

Proximal Tijeras fan deposits were sampled at an exposure along Four Hills Road, south of the intersection of Interstate 40 and Tramway Blvd. The exposure is located several hundred meters north of the point where Tijeras Arroyo crosses the Tijeras fault zone, forming the head of the Tijeras fan. This location is referred to as the Four Hills (FH) outcrop. Deposits are similar to those found further down the arroyo at the TA outcrop, and are also classified as PAt deposits of lithofacies VI. Coarse channel deposits with clasts as large as 40 cm in diameter extend across the outcrop. One thick structureless bed of low permeability is present, composed of very fine sands and silts. Poorly sorted pebbly coarse to fine sands, in discontinuous horizontal beds and scour and fill structures,

are common at this outcrop. Approximately 8 m of section is exposed here, but float covers much of the upper exposure.

A total of 211 permeability measurements were taken at the Four Hills outcrop. The mean recorded value was 83 darcys, with a standard deviation of 90. The median value was 38 darcys, with a maximum of 270 and minimum of 1 darcy. Sampling of the upper portions of the outcrop was limited by the abundance of float.

The final two outcrops sampled in this study are located in Bear Canyon Arroyo (BC). Deposits are modern in age, as evidenced by canvas and metal debris embedded in the outcrops. Samples BC1 - BC5 were collected from a small outcrop along the northern cutbank of the arroyo, approximately 0.5 km west of where Tramway Blvd. crosses Bear Canyon Arroyo. These deposits consist of scour and fill structures, are poorly sorted, and have moderate permeabilities. Outcrop exposure is limited, and the continuity of bedding is not evident. These beds have localized moderate cementation. A second exposure exists several kilometers down the arroyo, west of Wyoming Blvd., adjacent to the Arroyo Del Oso Soccer Fields. This exposure is also modern, and contains scour and fill structures, large channel deposits, and structureless beds. These deposits are classified as Piedmont Alluvium (PA), and are of lithofacies V (Hawley and Haase, 1992). Poorly sorted pebbles to fine sands form the lower beds of this exposure. Discontinuous horizontal beds and scour and fill structures are common. Channels of pebbles and granules form much of the upper portion of the exposure. The channel deposits are locally well sorted with an open matrix, and have high porosity and permeability values. Channels at this outcrop do not contain clasts larger than approximately 2 cm in diameter, unlike the deposits found in Tijeras Arroyo. A buried paleosol of limited extent is exposed in the upper right corner of the outcrop.

Sixty eight permeability measurements were obtained from the lower Bear Canyon exposure. The mean permeability was 100 darcys, the standard deviation 63, and the

median 91 darcys. The greatest recorded permeability was 223 darcys, and the smallest 4 darcys.

PERMEABILITY AND POROSITY OF OUTCROP SAMPLES

Permeability, Porosity and Cementation

A notable finding among the sieved outcrop samples is a poor correlation between porosity and permeability. Inspection of sample data indicates that the degree of cementation, sorting and packing influences the relationship between porosity and permeability. Figure 7 is a scatter plot showing the association between porosity and permeability. Most outcrop samples having high porosity values and low measured permeability are moderately cemented, and samples with high permeability and low porosity values tend to be coarse and poorly sorted. Figure 8 displays the observed relationship between permeability and cementation of the outcrop samples, with permeability tending to decrease with higher degrees of cementation.

Correlation of Permeability with Grain-Size Distribution Parameters

Measured permeability was correlated with a number of particle size parameters for the sieved outcrop samples. Scatter plots were generated to compare measured permeability with a number of effective diameters and particle size distribution parameters. A strong correlation is observed between permeability and the finer portion of the sediment samples. Listwise Pearson product moment correlation coefficients for permeability correlated with sample parameters are listed in Table 4. Complete sample values were derived from the entire sediment sample, and cut sample values were calculated with clasts larger than 2 mm in diameter excluded. Scatter plots comparing measured permeability to d_{10}, d_{15}, d_{17}, d_{20} and d_{50} grain size, the Kruger effective diameter (Vukovic and Soro, 1992), grain distribution statistics, porosity and sample cementation are included in Appendix C. In the following tables d_{10} is the sieve size through which the finest 10

percent of the sample by weight will pass. The uniformity coefficient d_{60}/d_{10} is also correlated with permeability.

Visual comparison of the effective diameter plots reveal a more constrained grouping of data points for the cut samples than for the complete distributions. An abundance of large grains in a sample of average sorting will result in a larger value for the effective diameter in the complete sample than in the cut sample. The measured permeability is constant, and the result is that the large grains in the complete sample influence the effective diameter without changing the measured permeability. It is expected that the cut sample would correlate better with permeability, as the smaller grains of a deposit that have the greatest influence on permeability, not the size and abundance of larger clasts surrounded by matrix material.

Comparison of effective diameters in ϕ units to measured permeability shows a reversal of the trends noted above. Correlation of d_{10}, d_{15} and d_{17} ϕ with measured permeability is better for the complete sample distribution. The effective diameter d_{20} correlates slightly better with the cut distribution, but the values are very similar. Correlation of the effective diameters of the complete distribution in ϕ units have values similar to the correlation of the cut sample in millimeters. Figures 9 and 10 are scatter plots of d_{10} and d_{20} of the complete samples plotted with measured permeability. The d_{10} diameter in millimeters has a correlation of r=0.803 with measured permeability, while d_{10} in ϕ units has a correlation coefficient of r=0.836. Squaring the correlation coefficients reveals how much of the variance in the permeability values is explained by the d_{10} particle size, being 64.5 percent by d_{10} in millimeters and 69.9 percent in ϕ units.

The correlation of d_{10}^2, d_{17}^2 and d_{20}^2 terms with permeability for the complete sample is considerably worse than correlation with unsquared effective diameters. The diameter term d_{10}^2 is a common parameter in published permeability equations, and is found to have a correlation coefficient of just r=0.654 with measured permeability.

Correlation is slightly better with squared diameters taken from the cut distribution. However, none of the empirical formulas recommend using a cut distribution.

A number of grain-size distribution parameters are compared with permeability. The mean grain size is the only parameter with meaningful correlation with permeability. Notice that this correlation is not as good as correlations with effective diameters. Figure 11 is a scatter plot of mean grain size and permeability for the outcrop samples. Skewness, percent fines and lithification have correlation coefficients near r=0.5.

Effective diameters and distribution parameters were also correlated with the $\log_{10}$ of measured permeability in darcys. As shown in Table 5, correlation is slightly better with the effective diameters in ϕ units than in millimeters. A correlation coefficient of r=0.851 exists between d_{10} and permeability for the complete sample, and r=0.846 for the cut sample. Correlation for d_{20} and the complete sample is r=0.834, and is r=0.863 with the cut sample.

The effective diameter with the best correlation with the log of measured permeability is the diameter used in the Kruger empirical permeability equation. This diameter is calculated as shown in Equation 3.2. If converted to ϕ units, the Kruger diameter correlates better with permeability than mean grain size of the sample. Figure 12 is a scatter plot of Kruger diameters and measured permeability.

The mean grain diameter of the cut sample correlates well with the $\log_{10}$ of measured permeability, having a coefficient of r=0.872. Squaring this term shows that 76 percent of the variability in the measured permeability values can be explained by the mean grain size of the sample. Calculation of the mean and other grain-size distribution parameters is detailed in the Methods section of this chapter. A correlation of r=0.634 is observed with the weight percentage of fines in both the complete and cut samples. Correlation of permeability with the standard deviation, skewness, mean-cubed deviation, percent pebbles and maximum intermediate diameter of the largest clast are poor.

TABLE 4. Pearson Correlation Coefficients for Measured Permeability and Grain Distribution Parameters

VARIABLE	COMPLETE SAMPLE	CUT SAMPLE
d_{10}, mm	0.803	0.819
d_{15}, mm	0.794	0.837
d_{17}, mm	0.789	0.839
d_{20}, mm	0.782	0.842
d_{50}, mm	0.571	0.812
Kruger, mm	0.821	0.844
d_{60}/d_{10}, mm	-0.049	0.154
d_{10}^2, mm	0.654	0.754
d_{17}^2, mm	0.636	0.765
d_{20}^2, mm	0.633	0.762
d_{10}, phi	-0.836	-0.796
d_{15}, phi	-0.833	-0.815
d_{17}, phi	-0.827	-0.818
d_{20}, phi	-0.818	-0.823
d_{50}, phi	-0.680	-0.782
Kruger, phi	-0.801	-0.791
d_{60}/d_{10}, phi	-0.509	-0.714
Mean	-0.718	-0.785
Standard Deviation	-0.034	-0.102
Skewness	0.321	0.505
Mean-Cubed Deviation	0.299	0.494
Percent Fines	-0.407	-0.405
Percent Pebbles	0.478	--
Max. Clast Diameter, phi	-0.402	--
Porosity	-0.198	-0.198
Lithification	-0.444	-0.444

TABLE 5. Pearson Correlation Coefficients for Log_{10} of Measured Permeability and Grain Distribution Parameters

VARIABLE	COMPLETE SAMPLE	CUT SAMPLE
d_{10}, mm	0.669	0.749
d_{15}, mm	0.659	0.747
d_{17}, mm	0.655	0.746
d_{20}, mm	0.649	0.746
d_{50}, mm	0.524	0.734
Kruger, mm	0.723	0.813
d_{60}/d_{10}, mm	0.000	0.218
d_{10}, phi	-0.851	-0.846
d_{15}, phi	-0.842	-0.856
d_{17}, phi	-0.848	-0.861
d_{20}, phi	-0.834	-0.863
d_{50}, phi	-0.741	-0.852
Kruger, phi	-0.858	-0.885
d_{60}/d_{10}, phi	-0.396	-0.668
Mean	-0.776	-0.872
Standard Deviation	-0.018	-0.117
Skewness	0.261	0.439
Mean-Cubed Deviation	0.310	0.458
Percent Fines	-0.634	-0.634
Percent Pebbles	0.397	--
Max. Clast Diameter, phi	-0.430	--
Porosity	-0.161	-0.161
Lithification	-0.611	-0.611

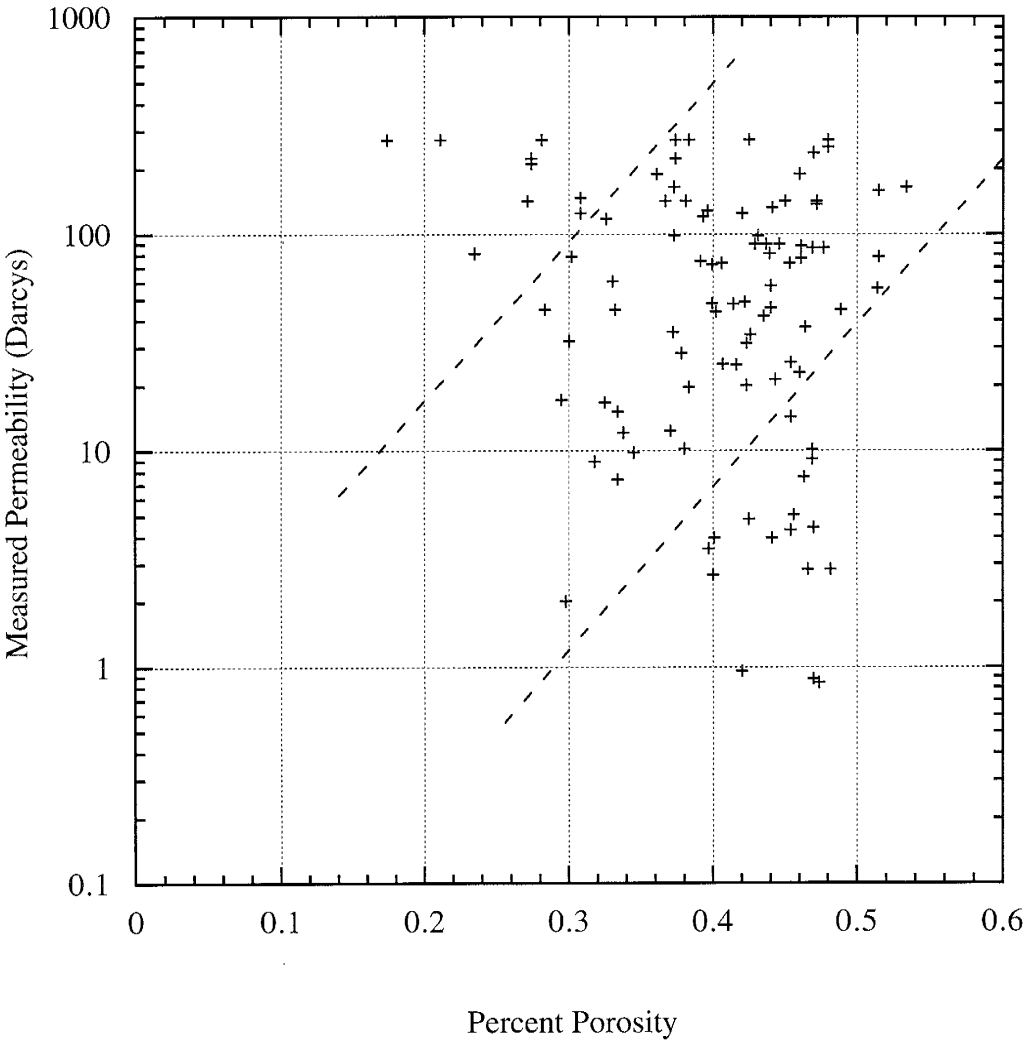

Figure 7. Scatter plot of porosity vs. permeability. Dashed lines separate moderately cemented samples to the lower right, and coarse, poorly sorted samples to the upper left.

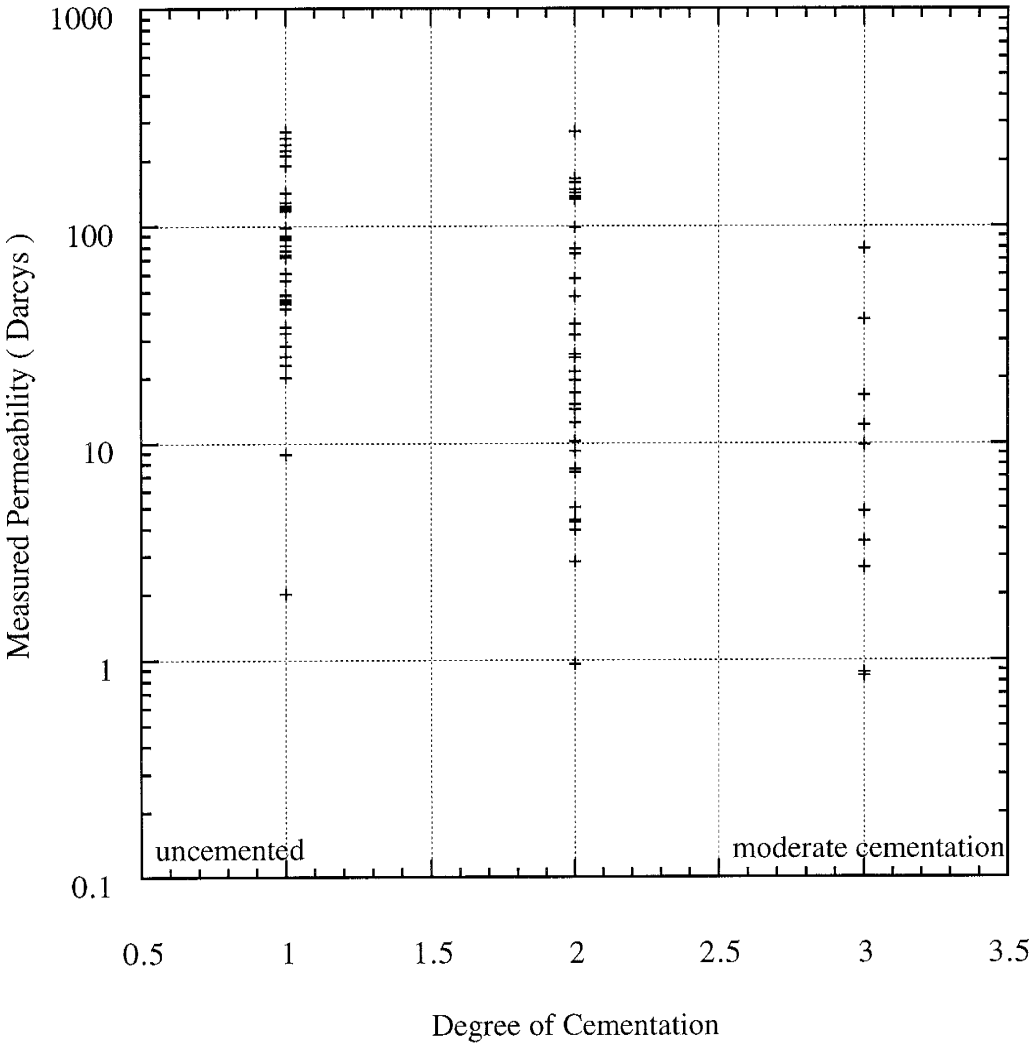

Figure 8. Influence of cementation on permeability.

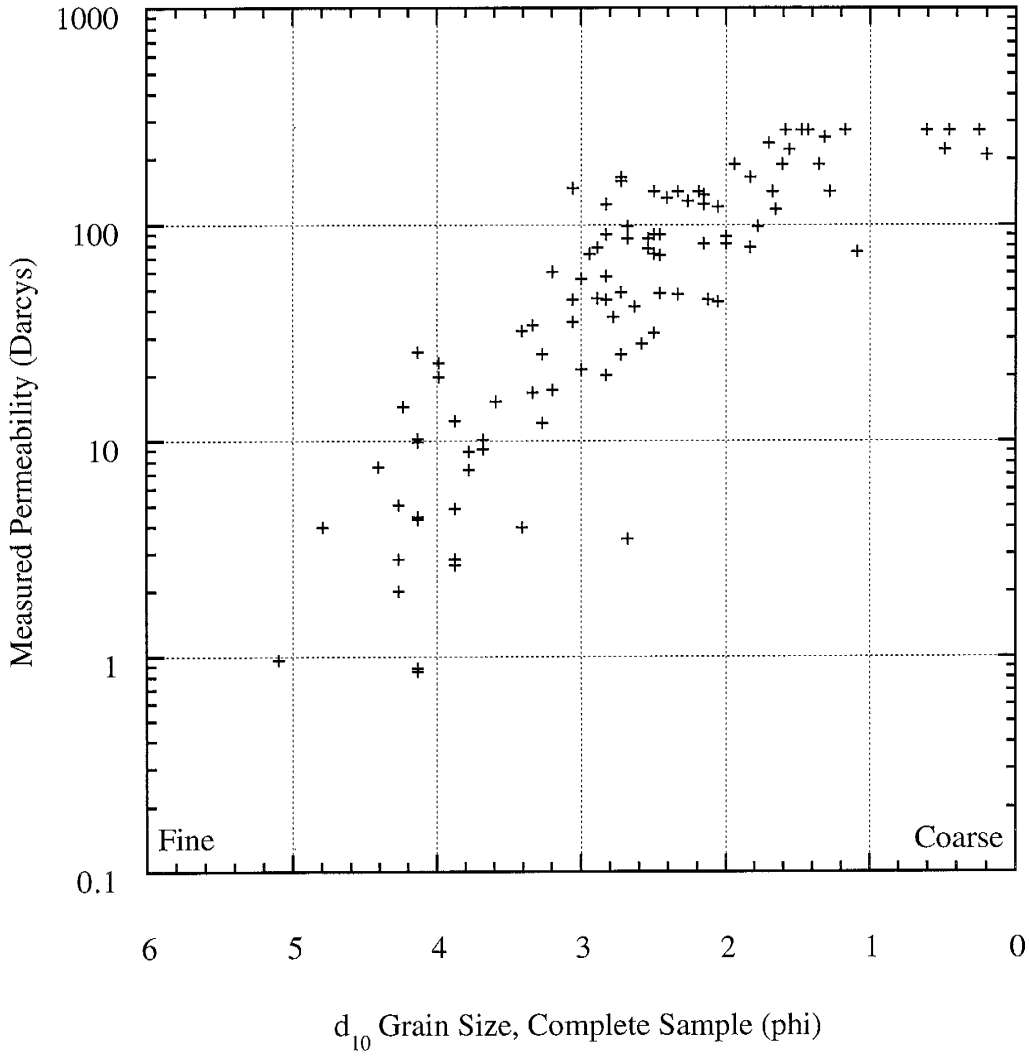

Figure 9. Influence of d_{10} grain size on permeability.

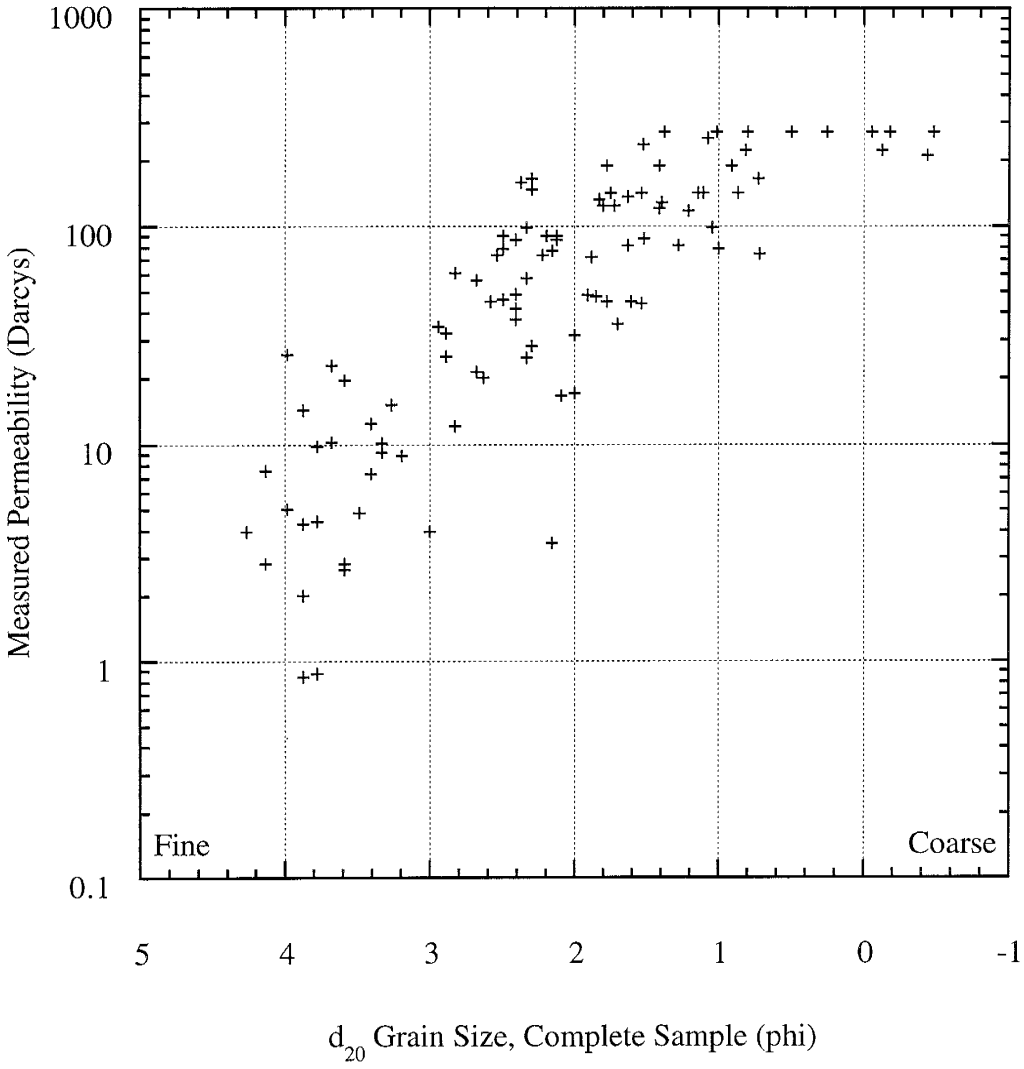

Figure 10. Influence of d_{20} grain size on permeability.

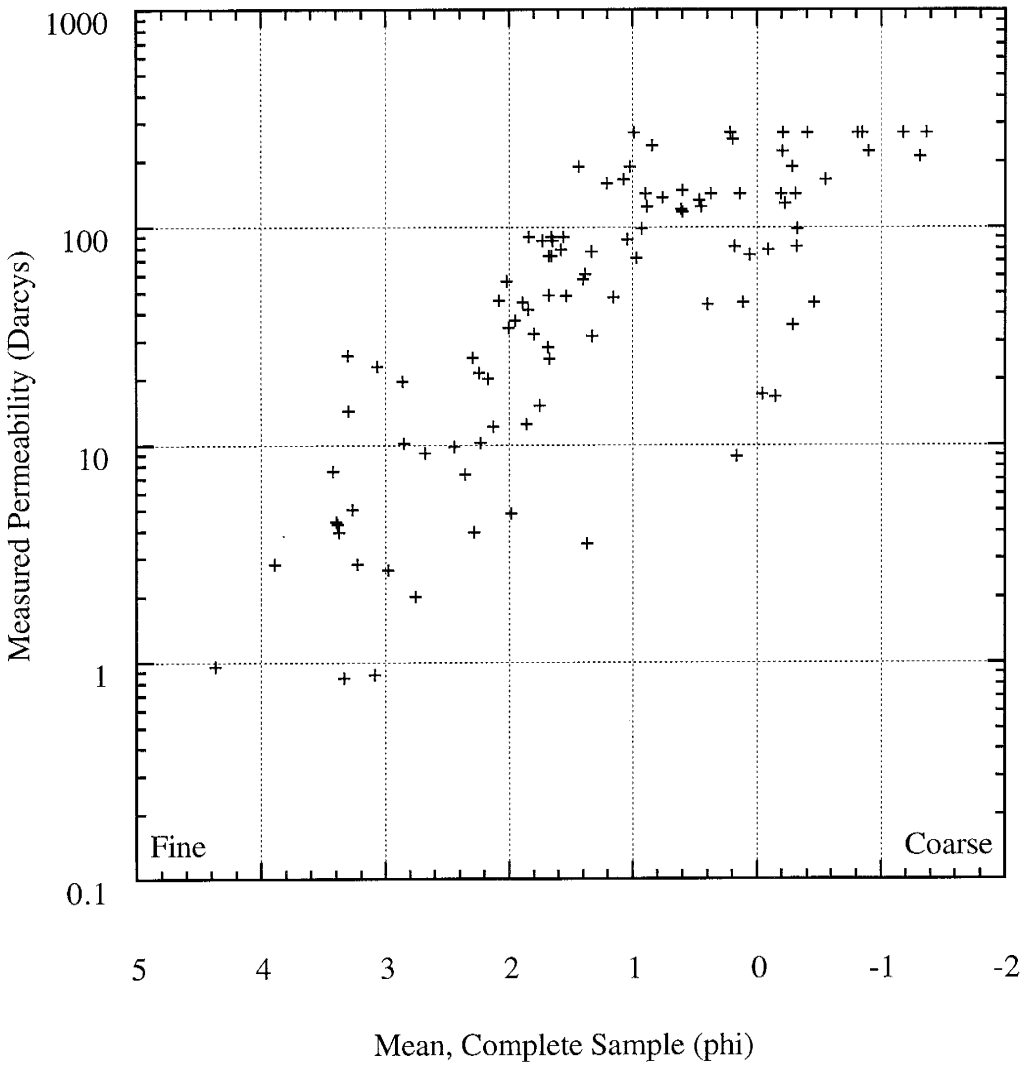

Figure 11. Influence of mean grain size on permeability.

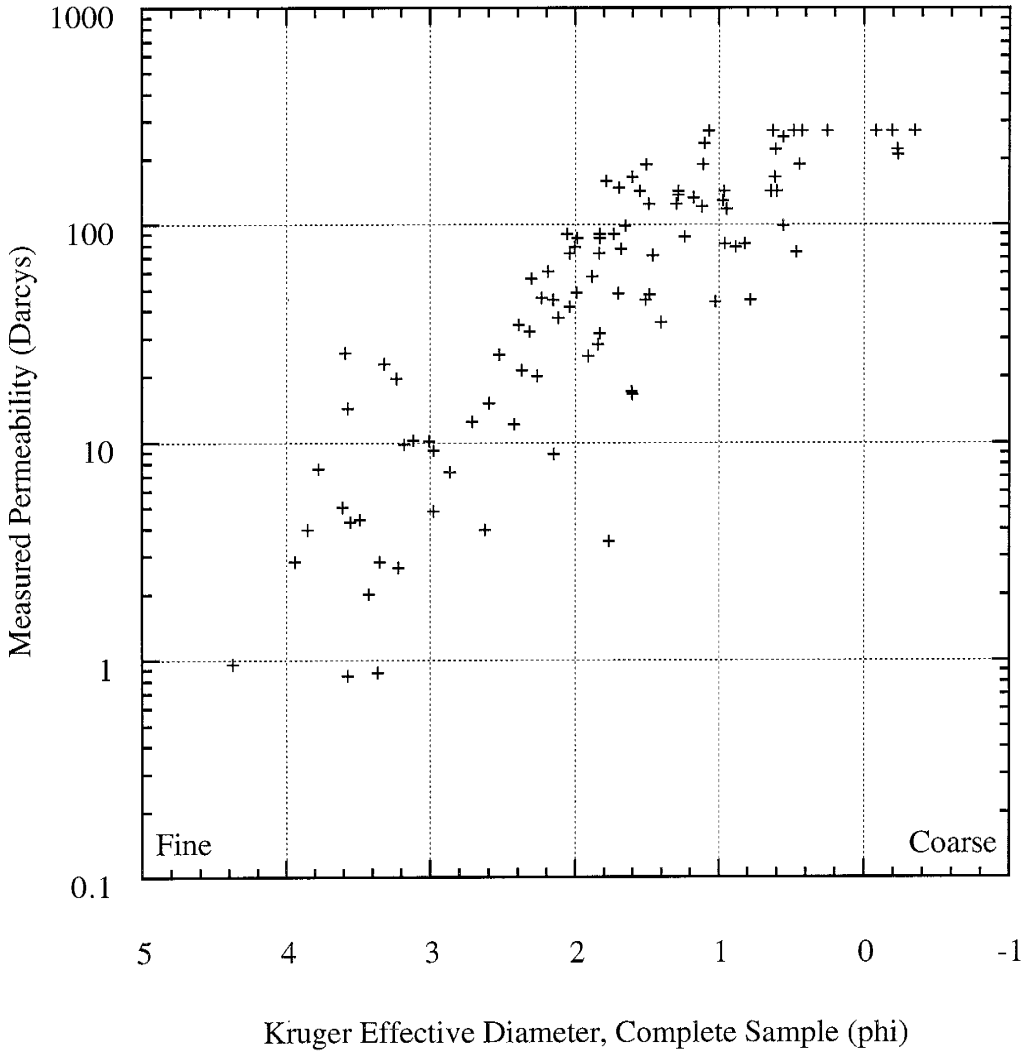

Figure 12. Influence of Kruger diameter on permeability.

Comparison of Measured Permeability with Published Permeability Equations

Table 6 presents listwise Pearson correlation coefficients for measured permeability values compared to values predicted by a number of published rational and empirical permeability equations. Comparisons are based on 100 outcrop samples, representing the most common beds of the outcrops studied in this report, having permeabilities within the measurement range of the air-minipermeameter. The Beyer, Hazen, Kozeney, Kruger, Sauerbrei, Schlichter, USBR and Zamarin equations were applied to the outcrop samples. All formulas are taken from a publication by Vukovic and Soro (1992). The original formulas calculate hydraulic conductivity, which is converted to darcys for comparison with measured permeability values. One Darcy is equivalent to a hydraulic conductivity of approximately 0.6 meters per day, for a water temperature of 10 degrees Celsius. Scatter plots comparing measured and predicted permeability are included in Appendix B. It is important to refer to the scatter plots when evaluating the effectiveness of the individual methods. A given method may have a high correlation with measured permeability values, but the equation may consistently overestimate or underestimate the permeability of the samples.

The Beyer formula has the form

$$K = C \cdot de^2 \qquad \text{(Equation 4.1)}$$

where the empirical C term is $4.5\text{x}10^{-3} \cdot \log^{500}/_{U}$. The effective diameter is d_{10} in mm, U is the uniformity coefficient $^{d_{60}}/_{d_{10}}$, and K is hydraulic conductivity in meters per second. The Beyer equation is the only equation using the coefficient of uniformity instead of a porosity term, common to most of the other formulas applied here. The Beyer formula has a correlation of r=0.713 with the measured permeability of the cut samples, providing one of the best fits of the models applied here.

The Hazen formula has the form

$$K = A \cdot C \cdot t \cdot d_{10}^2 \qquad \text{(Equation 4.2)}$$

The term A determines the dimensions of hydraulic conductivity, being 1 for K in meters per day, and 0.00116 for K in centimeters per second. C is a function of porosity, approximated by $C = 400+40(n-26)$, where n is percent porosity. The t term is a correction for water viscosity, being $0.70+0.03\cdot(^{\circ}C)$, and d_{10} is reported in millimeters. Measured permeability values correlate well with Hazen values for the complete sample, with a correlation coefficient of r=0.697. Hazen values for the complete sample tend to underestimate permeability.

Two forms of the Kozeney equation appear in the literature, and the form found to correlates best with measured permeability is expressed as

$$K = 5400 \cdot \frac{n^3}{(1-n)^2} \cdot d_{10}^2 \qquad \text{(Equation 4.3)}$$

where n is the fractional porosity of the sample, and d_{10} is reported in millimeters. This equation significantly underestimates permeability for the cut samples. A correlation coefficient of r=0.654 exists with the complete samples, but permeability is also underestimated.

The Kruger formula assumes the form:

$$K = 240 \cdot \frac{n}{(1-n)^2} \cdot d_e^2 \qquad \text{(Equation 4.4)}$$

The effective diameter is calculated as

$$\frac{1}{d_e} = \sum_{i=1}^{N} \frac{\Delta g_i}{d_i} \qquad \text{(Equation 4.5)}$$

where g_i is the weight percentage retained on each sieve, and d_i is the mean grain diameter for the sieve interval. N is the fractional percent porosity, and the effective grain diameter is reported in millimeters. K is reported in meters per day. This formula provides the best correlation with permeability for both the complete and cut samples, with correlation coefficients of r=0.783 and r=0.723 respectively.

The Sauerbrei formula predicts hydraulic conductivity in centimeters per second, and has the form

$$K = 3.49 \cdot \frac{n^3}{(1-n)^2} \cdot t \cdot d17^2 \qquad \text{(Equation 4.6)}$$

Fractional porosity is the n term, and$t$ is dependent on water temperature, equaling 1.05×10^{-6} divided by the kinematic viscosity of water in meters per second. This formula has a relatively poor correlation with measured permeability and tends to underestimate permeability of the samples, sometimes by more than an order of magnitude.

The Schlichter formula has the form

$$K = 4960 \cdot n^{3.287} \cdot d10^2 \qquad \text{(Equation 4.7)}$$

The effective diameter d_{10} is in millimeters, n is fractional porosity, and K is reported in meters per day. This formula correlates rather poorly with the measured permeability values, and significantly underestimates the permeability of most of the samples.

The USBR formula has the form

$$K = 0.36 \cdot d20^{2.3} \qquad \text{(Equation 4.8)}$$

The effective diameter d_{20} is reported in millimeters, and hydraulic conductivity in centimeters per second. Permeabilities values calculated by this equation underestimate permeability fairly significantly, yet the correlation with the cut samples is an acceptable r=0.712. Correlation is poor with the complete sample.

The Zamarin formula has the form

$$K = 8.07 \cdot \frac{n^3}{(1-n)^2} \cdot C \cdot t \cdot de^2 \qquad \text{(Equation 4.9)}$$

The C term is a function of porosity, equaling $(1.275\text{-}1.5 \cdot n)^2$, with n as a fractional percent. The value for$t$ is 0.807 for a water temperature of 10 degrees Celsius. The variable d_e is approximated by an equation similar to the Kruger effective diameter term, which is substituted here. Hydraulic conductivity is reported in meters per day. Correlation with measured permeability for the complete sample is r=0.753. Correlation with the cut sample is r=0.690, and permeability values are fairly accurate in general.

Multiple Regression Analysis

Multiple regression analysis was applied to sample parameters to generate a number of predictive permeability equations. Several equations use an effective diameter as the sole input parameter. Correlation of these simple regressions compare favorably to several of the more complex published permeability equations that require an estimation of porosity. In the tables detailing the equations a name for each model is listed in quotation marks, and input parameters are listed in parenthesis. The equations were correlated to measured permeability in darcys, and the $\log_{10}$ of permeability in darcys. Table 7 lists regressions with measured permeability, and Table 8 list correlations with the $\log_{10}$ of permeability. The tables list the parameters used in the regressions, listwise Pearson correlation

TABLE 6. Pearson Correlation Coefficients for Measured Permeability and Published Permeability Equation Values

Equation	Complete sample	Cut sample
Beyer	0.629	0.713
Hazen	0.697	0.653
Kozeney	0.654	0.566
Kruger	0.783	0.723
Sauerbrei	0.658	0.621
Schlichter	0.688	0.602
USBR	0.584	0.712
Zamarin	0.753	0.690

TABLE 7. Regression Analysis with Measured Permeability

	Pearson Correlation r	r^2
Measured permeability vs. grain size in mm:		
402.42(d_{10} mm complete) + 5.58	0.806	0.650
245.07(d_{20} mm complete) + 14.06	0.785	0.616
650.69(d_{10} mm cut) - 23.69	0.819	0.671
425.80(d_{20} mm cut) - 15.88	0.842	0.709
Measured permeability vs. phi grain size:		
-65.87(d_{10} phi complete) + 264.55	0.836	0.699
-71.76(d_{10} phi cut) + 290.23	0.798	0.637
-60.30(d_{20} phi complete) + 219.31	0.816	0.666
-68.13(d_{20} phi cut) + 249.18	0.825	0.681
Measured permeability vs. entire distribution parameters:		
"MSP1 COM"		
267.39(Kruger mm complete) + 4.91(mean complete) - 2.24(% fines complete) -13.31	0.824	0.679
"MSP1 CUT"		
372.36(Kruger mm cut) - 16.57(mean cut) + 3.32(% fines cut) + 0.58	0.849	0.721
"MSP2 COM"		
258.34(Kruger mm complete) + 0.235(mean complete) - 7.54	0.821	0.674
"MSP2 CUT"		
396.93(Kruger mm cut) - 6.31(mean cut) - 17.85	0.844	0.712

TABLE 8. Regression Analysis with Log_{10} of Measured Permeability

	Pearson correlation r	r^2
Log_{10} of measured permeability vs. phi grain size:		
-0.519(d_{10} phi complete) + 3.026	0.851	0.724
-0.462(d_{20} phi complete) + 2.651	0.842	0.709
-0.590(d_{10} phi cut) + 3.298	0.844	0.712
-0.553(d_{20} phi cut) + 2.943	0.854	0.729
Log_{10} of measured permeability vs. entire distribution parameters:		
"LMSP1 COM"		
-0.752(Kruger phi complete) + 0.231(mean complete) - 0.014(% fines complete) + 2.731	0.872	0.760
"LMSP1 CUT"		
-0.456(Kruger phi cut) - 0.145(mean cut) - 0.003(% fines cut) + 2.802	0.887	0.787
"LMSP2 COM"		
-0.799(Kruger phi complete) + 0.249(mean complete) + 2.773	0.871	0.759
"LMSP2 CUT"		
-0.469(Kruger phi cut) - 0.140(mean cut) + 2.815	0.887	0.787
"LMSP3 COM"		
-0.389(d_{10} phi complete) - 0.076(mean complete) - 0.026(% fines complete) + 2.811	0.861	0.741
"LMSP3 CUT"		
-0.202(d_{10} phi cut) - 0.369(mean cut) - 0.010(% fines cut) + 2.820	0.883	0.780
"LMSP4 COM"		
-0.432(d_{10} phi complete) - 0.082(mean complete) + 2.894	0.856	0.733
"LMSP4 CUT"		
-0.221(d_{10} phi cut) - 0.374(mean cut) + 2.865	0.882	0.778

coefficients, and squared correlation coefficients which reveal the percentage of the variability of the permeability explained by the regressions.

Effective diameters d_{10} and d_{20} in millimeters are used as input parameters for regression fits with measured permeability. Regressions with the effective diameters of the complete samples tend to overestimate permeability for the finer samples, and overestimate permeability for the more permeable coarse samples. Fits with cut samples are considerably better: the fit for the d_{20} diameter regression has a correlation of r=0.842 with the measured permeability. This model slightly overestimates permeability in the lower ranges, but the fit over the entire range of permeabilities is good.

The regressions of d_{10} and d_{20} diameters in ϕ units also overestimate permeability in the lower ranges. Of this group of models, the d_{10} ϕ complete and d_{20} ϕ cut regressions yield the best results, with correlations of r=0.836 and r=0.825, respectively. These models have a more pronounced overestimation of permeability in the lower ranges than the models based on effective diameters recorded in millimeters.

The final four regressions with measured permeability include parameters from the entire grain-size distribution. Parameters include the Kruger effective diameter in millimeters, the mean grain size in ϕ units, and the weight percentage of silt and clay in the sample. Like the models based on effective diameters alone, permeability in the lower ranges of the complete samples is overestimated. Models "MSP1 Cut" and "MSP2 Cut" make accurate predictions over the entire range of permeabilities, with correlation coefficients of r=0.849 and r=0.844, respectively.

Regression analysis was repeated with the $\log_{10}$ of measured permeability for the same parameters as discussed above. In each case the correlation with the log of permeability is better than correlation with permeability in darcys. This indicates that permeability tends to be log-normally distributed, as suggested by a number of researchers (Nelson, 1994). As listed in Table 5, effective diameters in millimeters do not correlate well with the log of permeability, and diameters in millimeters are not used in regressions.

Regressions using d_{10} and d_{20} with the complete and cut distributions all yield similar results. The best fit is found with d_{20} of the cut distribution, with a correlation coefficient of r=0.854 Overestimation of the lowest permeability values is still present, but to a lesser degree than with the correlations to permeability. This trend is addressed in the Discussion section of this report.

Regressions LMSP1 and LMSP2 show good correlation with the log of measured permeability for both the complete and cut distributions. The models with the cut samples are slightly better than the complete samples, but all models have correlation coefficients between r=0.871 and r=0.887. Models LMSP3 and LMSP4 substitute d_{10} diameters in ϕ units for the Kruger diameters used in the LMSP1 and LMSP2 models. Examination of the scatter plots of the data, included in Appendix B, show that permeability is overestimated for several samples in the higher ranges when the complete sample is used, but this over-estimation is reduced when the cut sample is used. Correlations are slightly less accurate if the Kruger diameter is used in place of d_{10}, with correlations ranging from r=0.856 to r=0.883.

COMPARISON OF BEDDING TYPES

Comparison of Bedding Types Based on Particle Size Distribution Parameters

One hundred sixteen sediment samples, representing the most common beds from twelve outcrops in the Albuquerque municipal area, were sieved to allow comparison of grain-size distributions. From the raw sieve data, statistical moment measurements were used to calculate the mean, standard deviation, skewness and mean-cubed deviation of the samples. Sample data, grouped by bedding type, is included in Appendix A. The formulas used to calculate the grain distribution parameters are included in the Methods section. Phi units are used in the following comparisons.

Box plots allow rapid comparison of grain-size distribution parameters. Figures 13 and 14 show the mean, standard deviation, and skewness of the outcrop samples grouped by bedding type (crossbeds, channels, horizontal beds and laminations, scour and fills, and structureless), for the complete and cut samples, respectively. Inspection of Figure 13 shows good separation between the mean grain sizes of the various bedding types, and less separation between the standard deviation and skewness of the bedding types. Relationships among grain distribution parameters are similar for the cut samples shown in Figure 14, but there is less separation between groups. Table 9 lists the mean, standard deviation and skewness of samples grouped by bedding type, and how grain distribution parameters vary between the groups. A more complete list of grouped parameter statistics, along with additional box plots relating percent fines, percent pebbles and maximum intermediate diameter to measured permeability, is included in Appendix D.

An alternative method for comparing grain-size distribution parameters by bedding type is by scatter plot. An advantage of scatter plots over box plots is that all data points are displayed. Figure 15 plots mean grain size against the standard deviation of the samples, and shows fair separation between the bedding types. Crossbeds show considerable overlap of both standard deviation and mean grain size with channels and horizontal beds. Mean grain sizes of -1 to 0 ϕ and standard deviations of 1.1 to 1.5 are common to channels and scour and fill structures. Separation between cut sample distributions is considerably worse.

Figure 16 is a scatter plot of mean grain size versus skewness of samples grouped by bedding type. Crossbeds overlap with all other bedding types, most severely with horizontal and structureless beds. There is little overlap among the other four bedding types in this plot. There is much less separation between bedding types if the mean and skewness of cut sample distributions are plotted. Scatter plots for cut distributions appear in Appendix E. Scatter plots of standard deviation versus skewness were also prepared, but separation between bedding types is poor. These plots are included in Appendix E.

TABLE 9. Distribution of Grain-Size Parameters by Bedding Type, Complete Samples

Bedding Type, Parameter	Mean Value	Standard Deviation	Skewness
Crossbeds, mean grain size	1.323	0.677	0.390
Channels, mean grain size	-0.490	0.830	0.096
Horizontal, mean grain size	2.204	0.880	0.743
Scour and fill, mean grain size	-0.072	0.743	2.250
Structureless, mean grain size	2.467	0.886	-0.759
Crossbeds, standard deviations	0.902	0.314	0.629
Channels, standard deviations	1.304	0.303	1.006
Horizontal, standard deviations	0.969	0.233	0.122
Scour and fill, standard deviations	1.722	0.347	0.410
Structureless, standard deviations	1.535	0.402	-0.015
Crossbeds, skewness	-0.051	0.779	-0.236
Channels, skewness	0.968	1.550	1.377
Horizontal, skewness	0.090	0.664	0.281
Scour and fill, skewness	0.638	0.639	0.429
Structureless, skewness	-0.460	0.441	-0.125
Crossbeds, percent fines	0.316	0.552	3.002
Channels, percent fines	0.154	0.138	1.547
Horizontal, percent fines	1.983	3.721	3.668
Scour and fill, percent fines	0.858	1.546	3.968
Structureless, percent fines	4.707	4.159	1.526

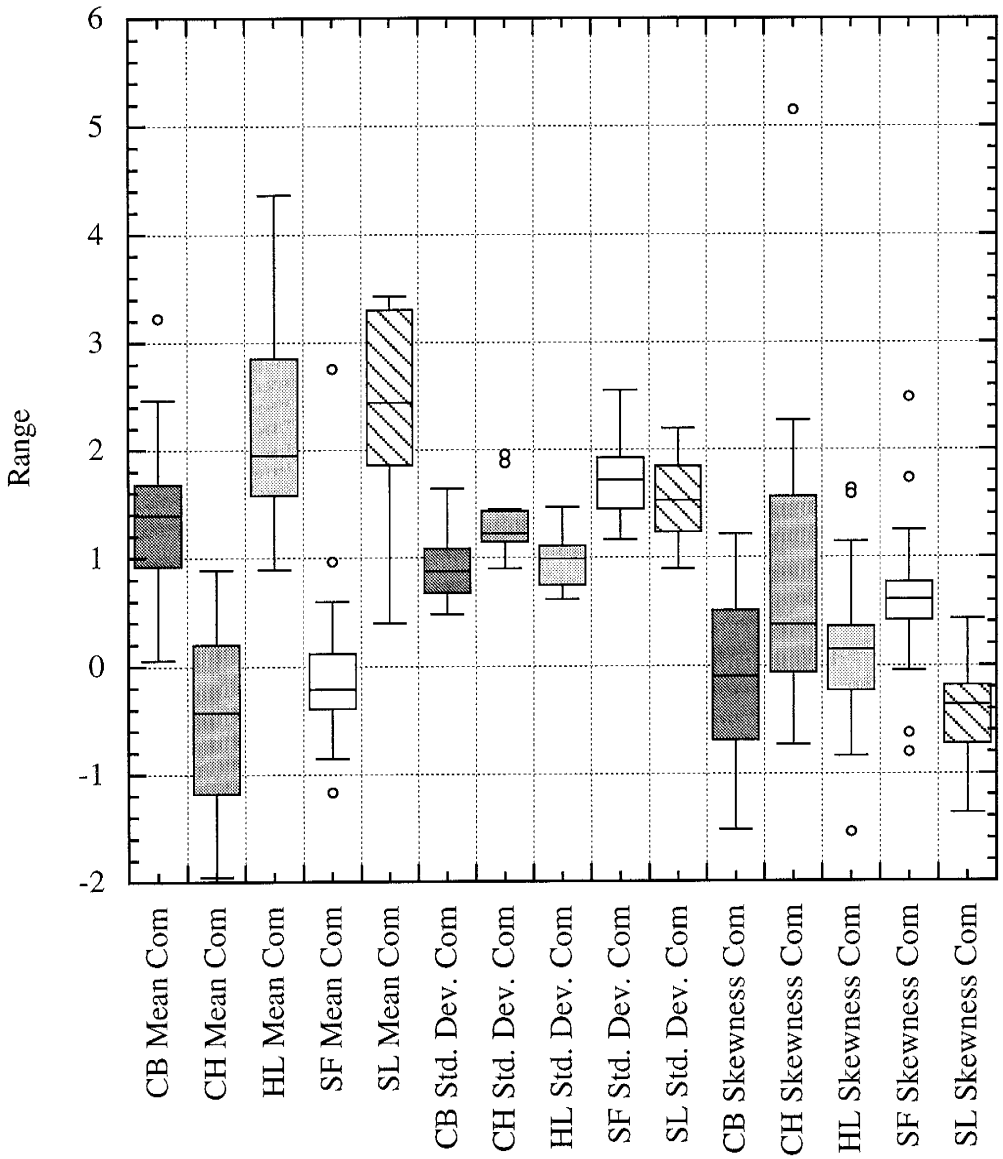

Figure 13. Mean, standard deviation and skewness of sieved outcrop samples. Complete samples, grouped by bedding type. Circles are data points considered outliers by the graphing program.

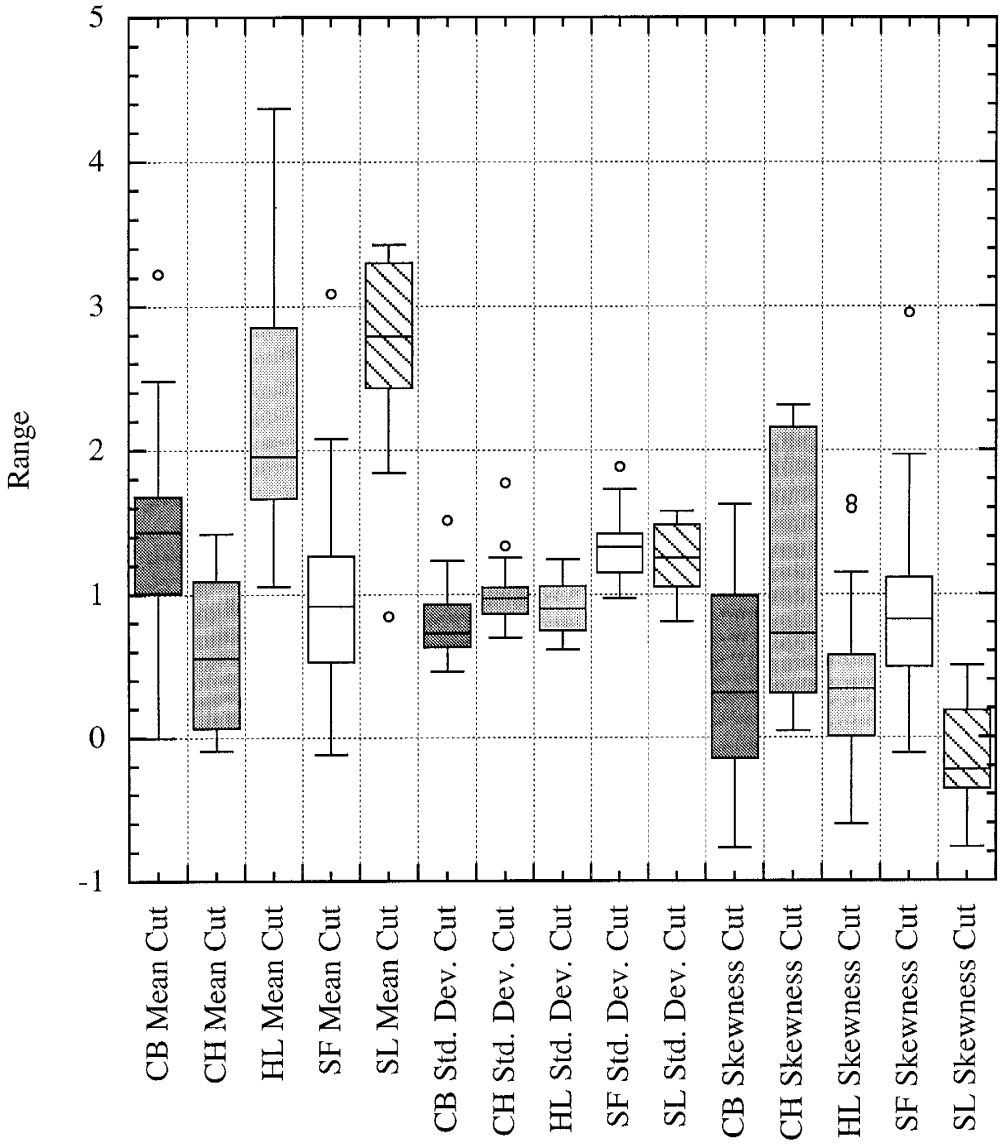

Figure 14. Mean, standard deviation and skewness of sieved outcrop samples. Cut samples, grouped by bedding type. Circles are data points considered outliers by the graphing program.

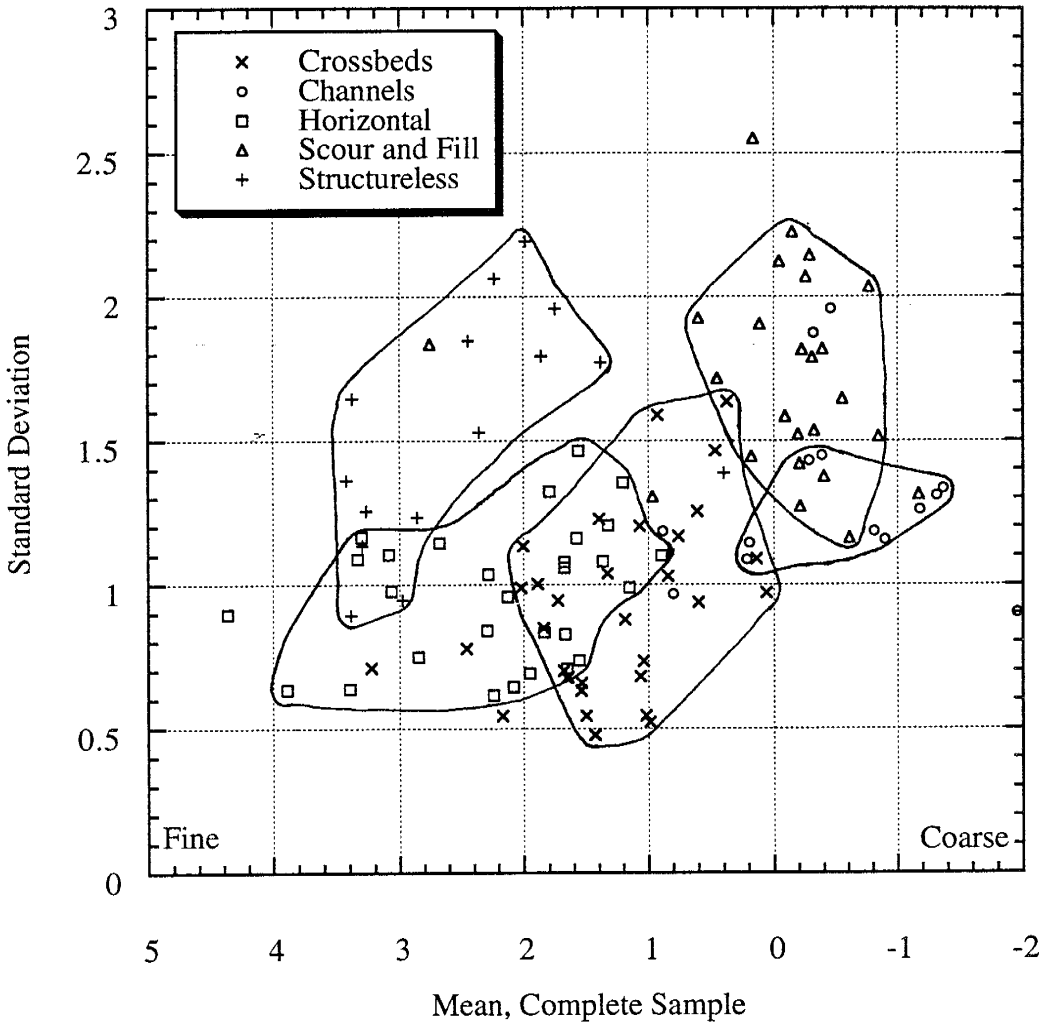

Figure 15. Scatter plot of mean and standard deviation of complete outcrop samples. Ranges of bedding types circled based on visual comparison.

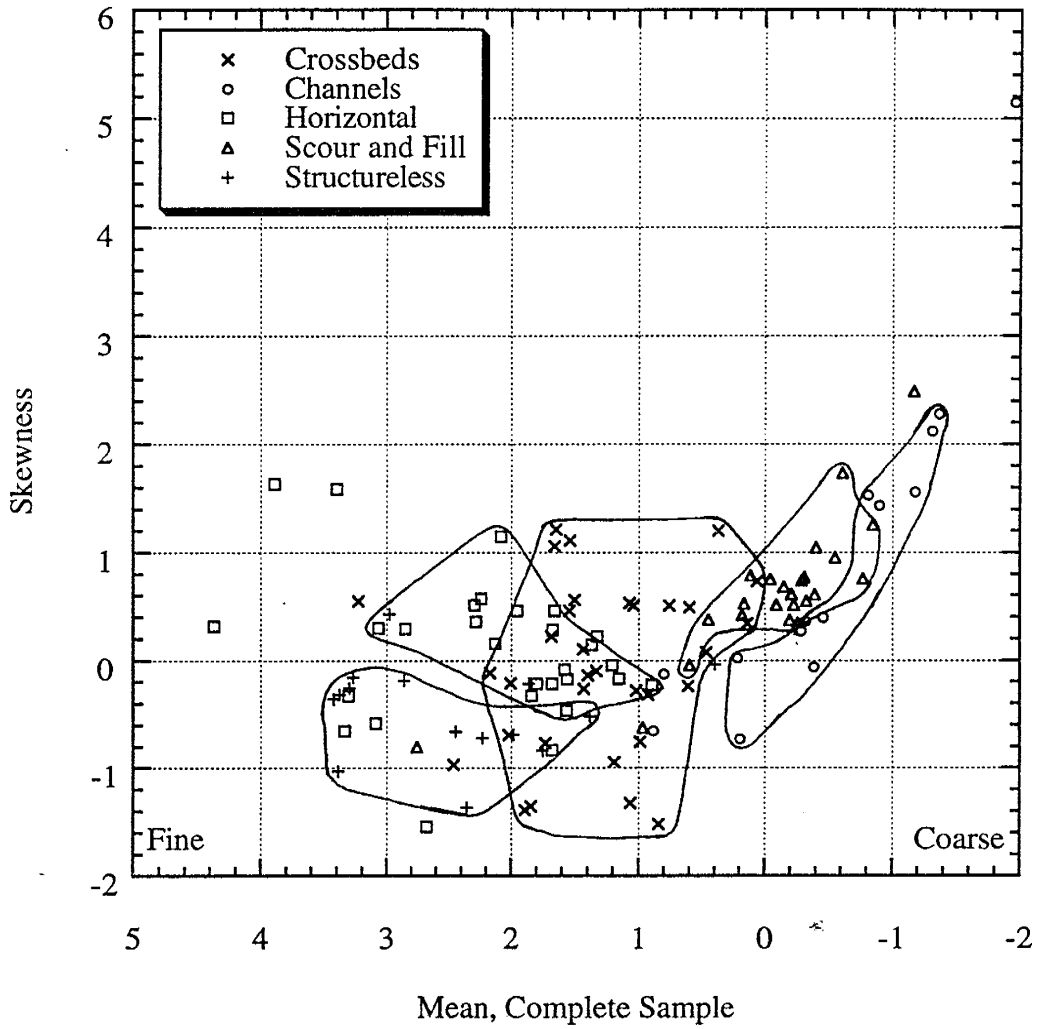

Figure 16. Scatter plot of mean and skewness of complete outcrop samples. Ranges of bedding types circled based on visual comparison.

Comparison of Bedding Types by Log-Log Plots

Log-log plots, described in the Methods section, were used to display grain-size distributions graphically. The log-log plots reveal the relative abundance of grain sizes within the sample, with the peak of the curve occurring near the mean grain size as calculated by moment measurements. Grains larger than 2 mm in diameter are not included in the log-log plots. Outcrop samples were classified by bedding type, then samples of the same bedding type were divided into groups of similar grain distributions based on log-log plots. Log-log plots and cumulative percent plots, grouped by bedding type, are included in Appendix A. Also included in Appendix A are values of porosity, measured permeability, lithification and particle size distribution parameters for all sieved outcrop samples.

Figure 17 is a box plot summarizing the range of permeability for each bedding type, compiled from outcrop permeability profile measurements. Considerable spread in the permeability values exists for several of the bedding types, but others have a fairly constrained permeability range. Figure 18 is a box plot showing permeability values of the bedding subgroups. There is considerable separation between groups, demonstrating the influence of particle size distribution on permeability. Half of the bedding subgroups contain 6 or fewer samples, so this analysis is intended for casual comparison only.

Comparison of Permeability and Porosity by Bedding Type

Rapid comparison of permeability and porosity by bedding type is possible with box plots. Figures 19 and 20 show measured permeability and porosity of the sieved outcrop samples. Note the poor correlation between porosity and permeability, especially among the horizontal and structureless beds. Figure 17 is a box plot of the 1314 permeability measurements from the outcrop permeability profiles. The range of measured permeability of each bedding type is similar for both data sets, as expected. A complete listing of permeability distributions by bedding type is included in Appendix D. Table 10 is an abbreviated list of permeability distribution by bedding type.

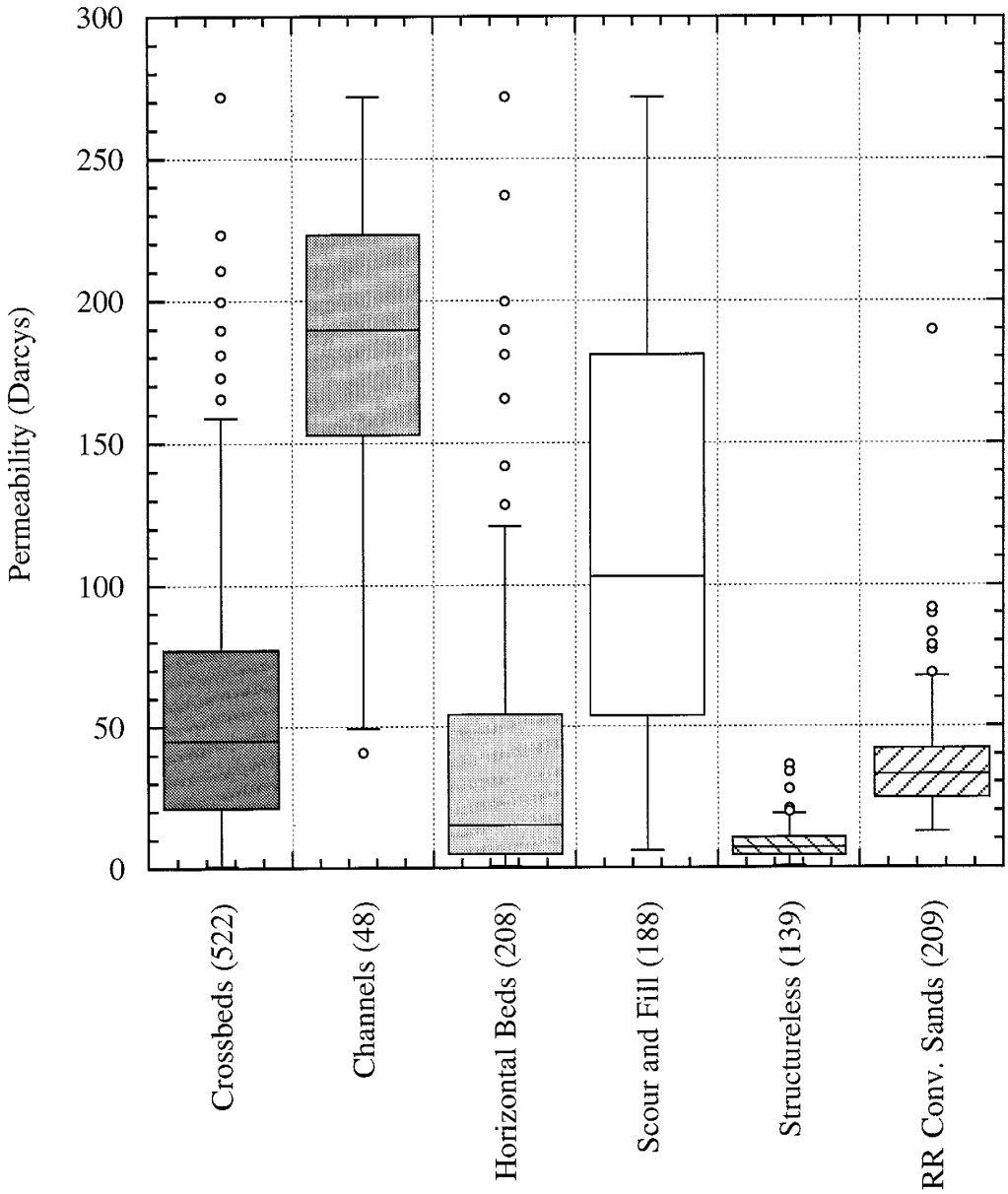

Figure 17. Permeability by bedding type, unsieved permeability profile measurements. Numbers in parentheses indicate number of samples. Circles are data points considered outliers by the graphing program.

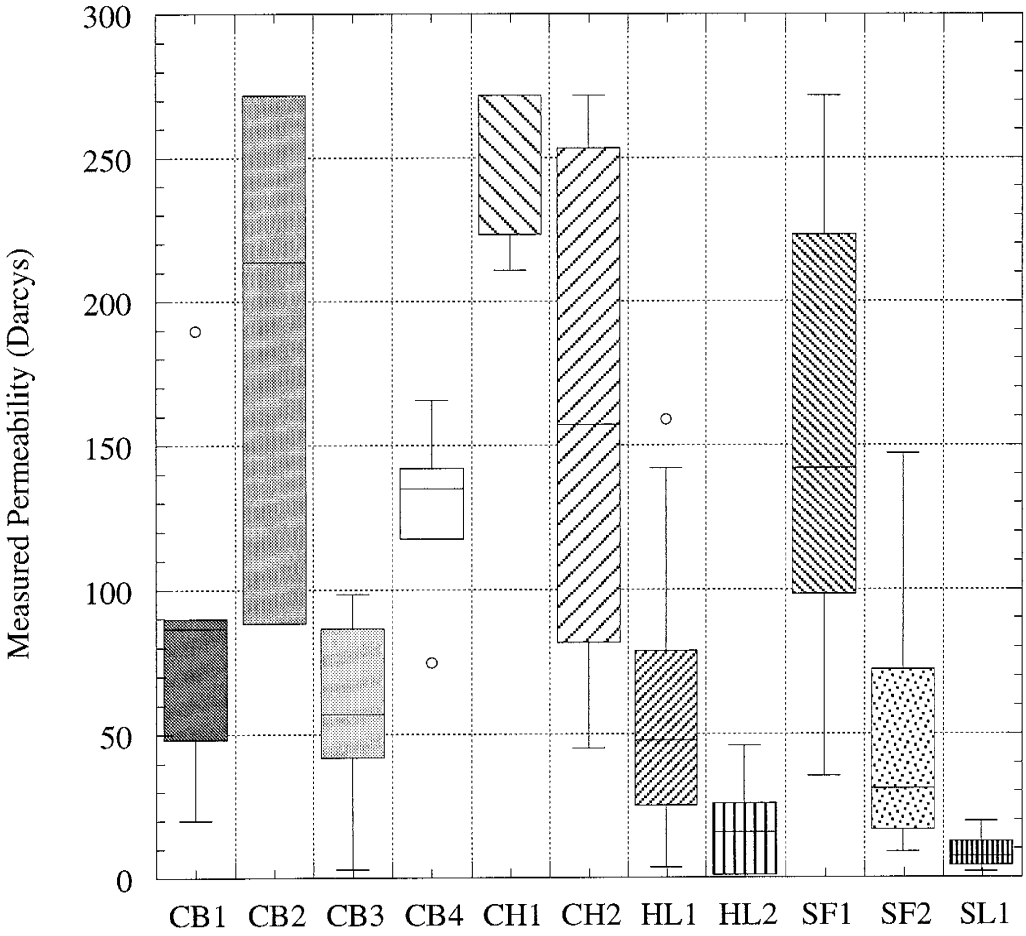

Figure 18. Permeability ranges for bedding subgroups by grain size distribution. Subgroups determined from log-log plots. Circles are data points considered outliers by the graphing program.

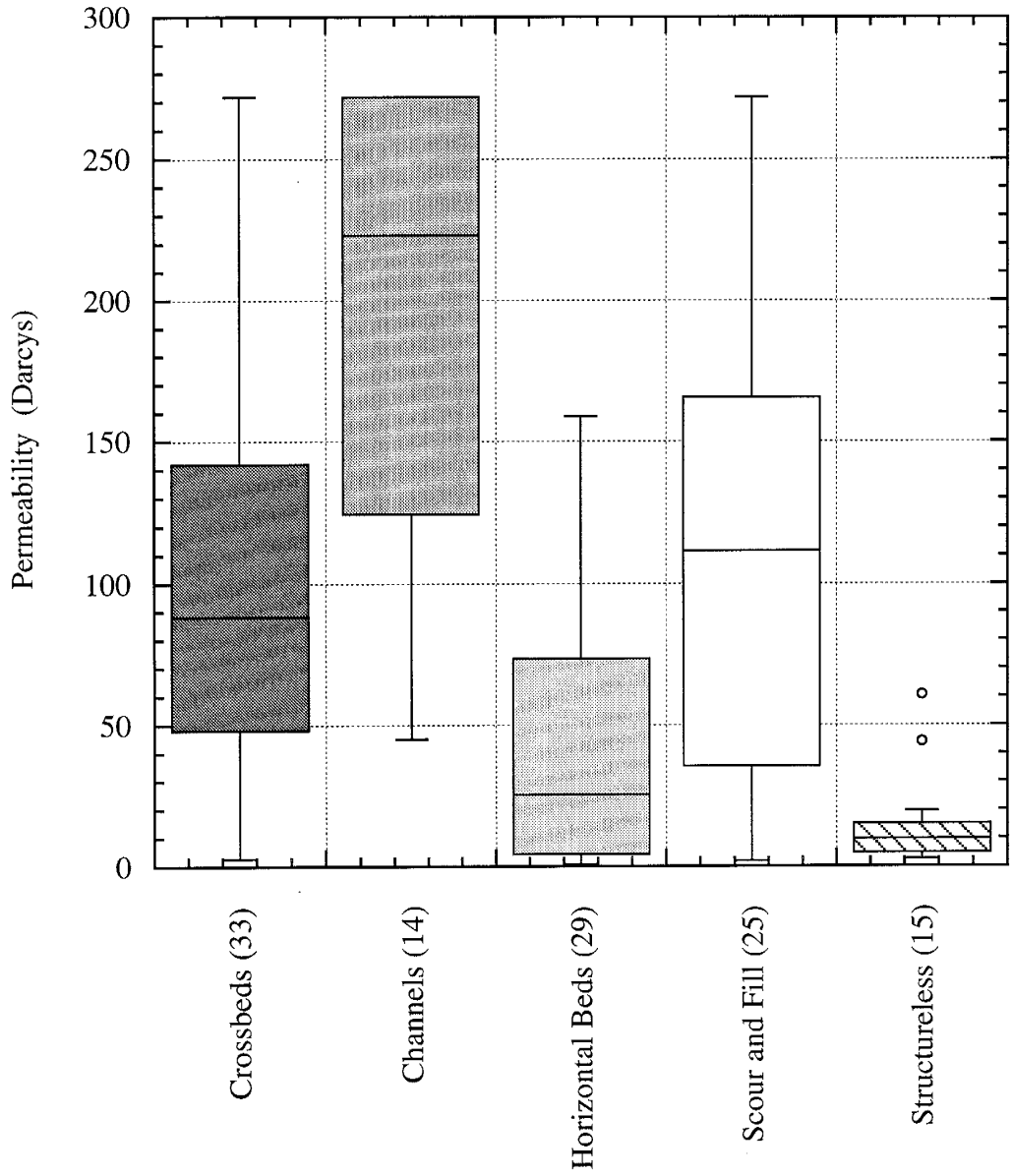

Figure 19. Permeability by bedding type, sieved outcrop samples. Number in parentheses indicates number of samples for each bedding type. Circles are data points considered outliers by the graphing program.

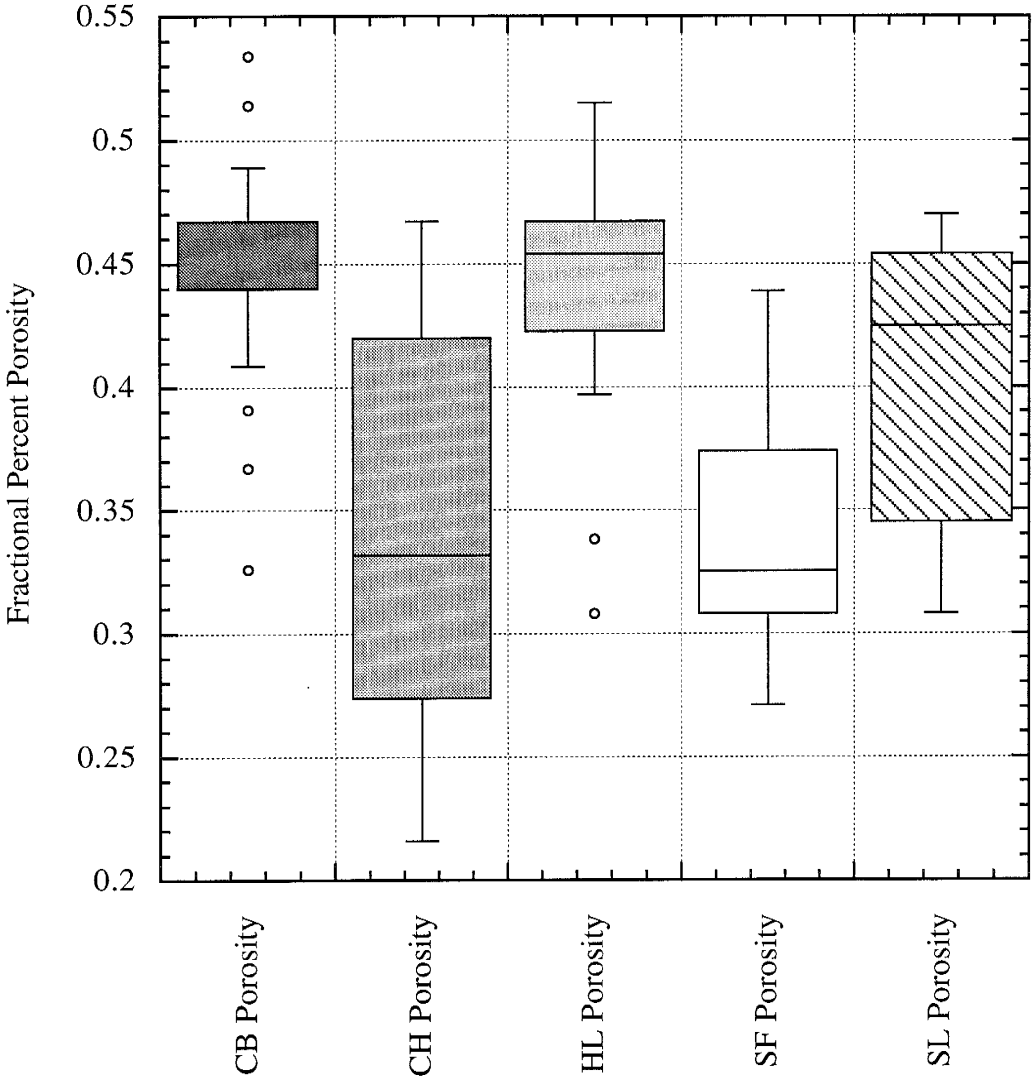

Figure 20. Porosity by bedding type, sieved outcrop samples. Circles are data points considered outliers by the graphing program.

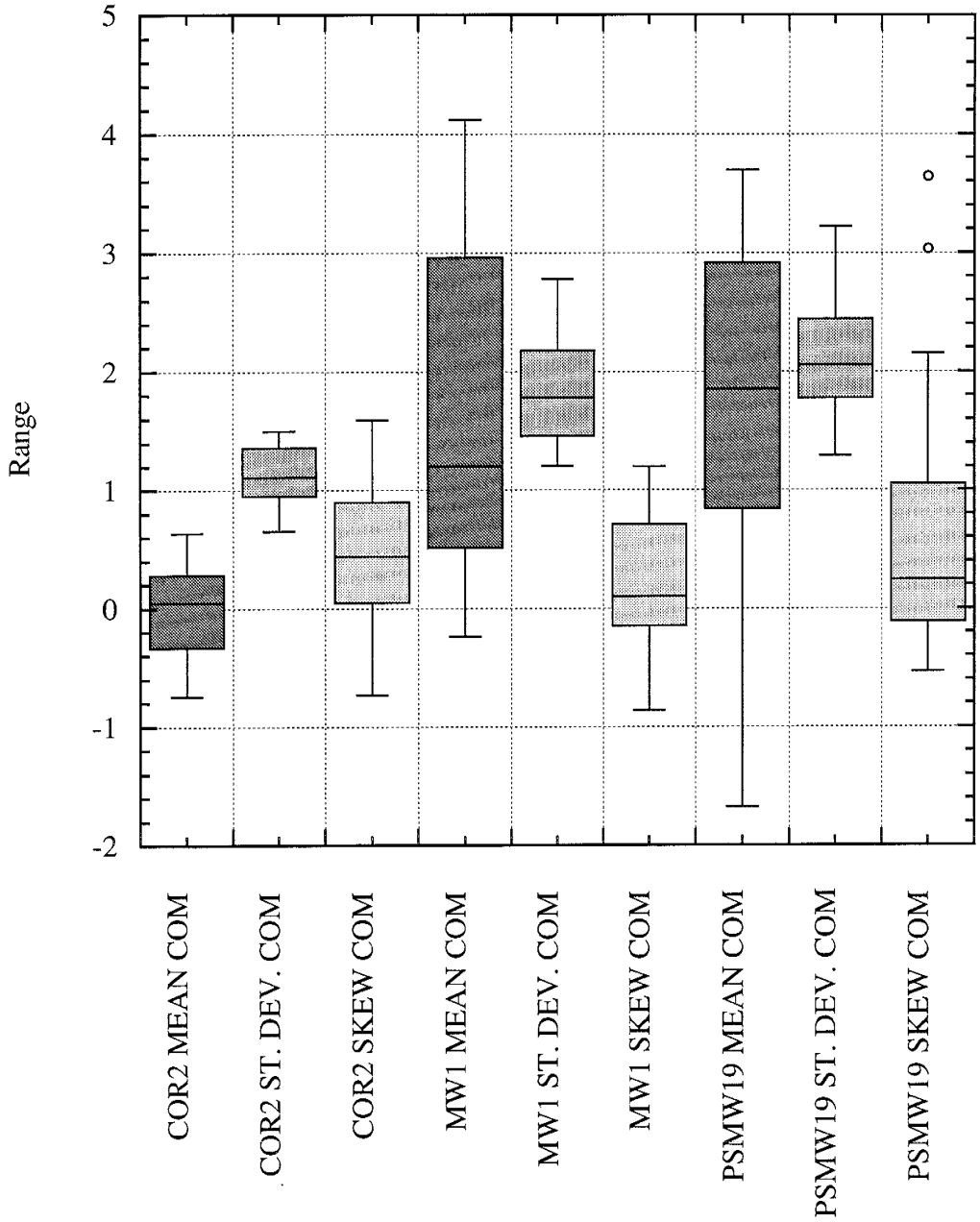

Figure 21. Mean, standard deviation and skewness of well cuttings, complete samples. Circles are data points considered outliers by the graphing program.

TABLE 10. Permeability Distribution by Bedding Type, Permeability Profile Measurements. Permeability in Darcys.

Bedding Type	Mean	Standard Deviation	Skewness
Crossbeds (522 samples)	55.7	47.3	1.358
Channels (48)	178.1	57.3	-0.826
Horizontal (208)	38.6	49.3	2.058
Scour and Fill (188)	119.8	75.3	0.474
Structureless (139)	8.2	6.3	2.115
RR Conv. Sand (209)	36.0	17.9	3.732

GRAIN-SIZE DISTRIBUTIONS OF WELL CUTTINGS

Grain size analysis was completed on the cuttings of 3 wells in the Albuquerque municipal area. The first well is Coronado 2, a water supply well for the City of Albuquerque. It is located approximately 1 km southwest of the corner of Paseo Del Norte and Wyoming Blvd., penetrating a thick sequence of piedmont alluvium. This location is approximately 2 miles north-northwest of the lower Bear Canyon Arroyo outcrop. The well was drilled with a mud rotary rig, and the sampling interval was 10 feet. Twenty five samples from the uppermost 900 feet of this well were sieved. The mean value of the mean grain sizes of all the cuttings is -0.022 ϕ, with a minimum mean diameter of 0.639 and maximum of -0.742 ϕ. The range in the standard deviation values of the samples is also relatively small, the mean value being 1.129, with a maximum of 1.503 and minimum of 0.652. Thus a high degree of uniformity is observed among the cuttings of this well. The range of skewness values for this well is similar to those of the other two wells. Figure 21 is a box plot of the mean grain size, standard deviation and skewness of the cuttings of Coronado 2, along with wells PSMW-19 and MW1. Inclusive grain distribution statistics for all of the well cuttings are included in Appendix D.

The second well for which cuttings were analyzed is well MW1, drilled by the Bureau of Reclamation in the summer of 1993. It was drilled on the floodplain of the Rio Grande, just west of the Edith Gravels outcrop from which samples were obtained. The well is located just north of Paseo Del Norte, and west of Edith Blvd. This well penetrates 105 feet of river sands and gravel, with minor clay lenses. Core was obtained in lengths of up to 3 feet, and samples used for grain size analysis were skimmed from the entire length of the core. Unfortunately samples were not gathered from distinct depths in the core barrel. The mean grain size of the sediments of this well are considerably smaller than those of Coronado 2, with a mean over the entire depth being 1.617 ϕ, ranging from -0.236 to 4.121. The standard deviation of the grain distributions ranges from 1.204 to 2.782.

The third well from which cuttings were obtained and sieved is well PSMW-19. This well is located several hundred meters north of Rio Bravo Blvd. on the west side of Interstate 25. It was drilled as a monitoring well for the Public Service Company of New Mexico. The well penetrates upper Santa Fe Group sediments, from which the uppermost 815 feet of cuttings were sieved. The well was drilled with a reverse-rotary drill rig, and samples were collected at 5 foot intervals. The mean of the values for mean grain size for the cuttings of this well is 1.652, ranging from -1.672 to 3.695. The standard deviation ranges from 1.293 to 3.221. Grain distribution parameters from the cuttings of this well are similar to those of well MW1.

Scatter plots were generated to allow a graphical representation of the grain-size distribution parameters of the well cuttings. Figure 22 is a plot of mean grain size versus the standard deviation of the individual well cuttings. Weak trends are apparent in the samples from each of the 3 wells, with standard deviation increasing as the mean grain size increases. This trend is not evident if clasts greater than 2 mm in diameter are excluded from the samples. Additional scatter plots of grain distribution parameters are included in Appendix E.

Inspection of Figure 23, a scatter plot comparing mean grain size with skewness, shows skewness increasing as mean grain size increases. For the PSMW-19 samples, most skewness values are slightly negative or near zero for mean grain sizes smaller than 2 ϕ, and skewness values steadily increase as mean grain diameters become larger. The same trend is observed for the samples from Coronado 2, but the range of mean grain size is considerably smaller. Samples from well MW1 exhibit similar behavior. These trends are more pronounced among the cut sample distributions.

Plots comparing sample standard deviation to skewness reveal no striking trends. The samples from Coronado 2, however, are isolated from the samples from the other two wells due to low standard deviation values. An expected relationship is observed between mean grain size and percent fines. Silt and clay-sized particles become more abundant as

the mean grain size of the sample decreases. Note that none of the cuttings from Coronado 2 contain more than 2 percent fines. This may be due to excessive washing of the samples prior to bagging.

Scatter plots were generated comparing the grain-size distributions of all the outcrop samples to the well cuttings. Figure 24 shows mean grain size plotted with the standard deviation of each sample. Comparison of Figure 24 to Figure 22 shows that standard deviation values for a number of the cuttings from PSMW-19 are larger than the standard deviations of the outcrop samples. Outcrop samples with small mean grain diameters have smaller standard deviations than the well cuttings, but the trend is influenced by the cuttings from PSMW-19.

Figure 25 compares mean grain size to skewness for the outcrop samples and the well cuttings. There is good agreement between the mean and skewness of the outcrop samples and well cuttings.

GEOPHYSICAL WELL LOGS

Figures 26 and 27 show the geophysical logs for wells PSMW19 and Coronado 2, along with permeability predicted by several of the multiple regression equations detailed in this manuscript. Inspection of these figures allows comparison of permeability as calculated from grain-size distribution to several common geophysical logs. Predicted permeability values range from less than 10 to 1000 darcys. The accuracy of the higher permeability values has not been established, as the regressions are based on sediments with permeability of 270 darcys or less, the upper measurement range of the air-minipermeameter. Similar permeability estimates are obtained from all four of the regression equations.

The high permeability zones of well PSMW19 are characterized by high electrical resistivity, good separation of the medium and deep resistivity curves, and lower than average porosity values. The high permeability zone around the 800 foot depth of the well

is also marked by a negative SP kick, but this signature could not be established in the shallow regions of high permeability due to excessive drift in the SP log.

The permeability estimations based on the cuttings of well Coronado 2 show considerably less variability than the cuttings of PSMW19. The cuttings of this well were collected at 10 foot intervals, in contrast to the 5 foot sampling interval for PSMW19. The similarity of the permeability estimates makes it difficult to distinguish how log signatures are related to permeability in this well. However, the few lower than average permeability estimates in this well are characterized by low resistivity values, no separation between the resistivity curves, variably porosity values, and lower than average SP values.

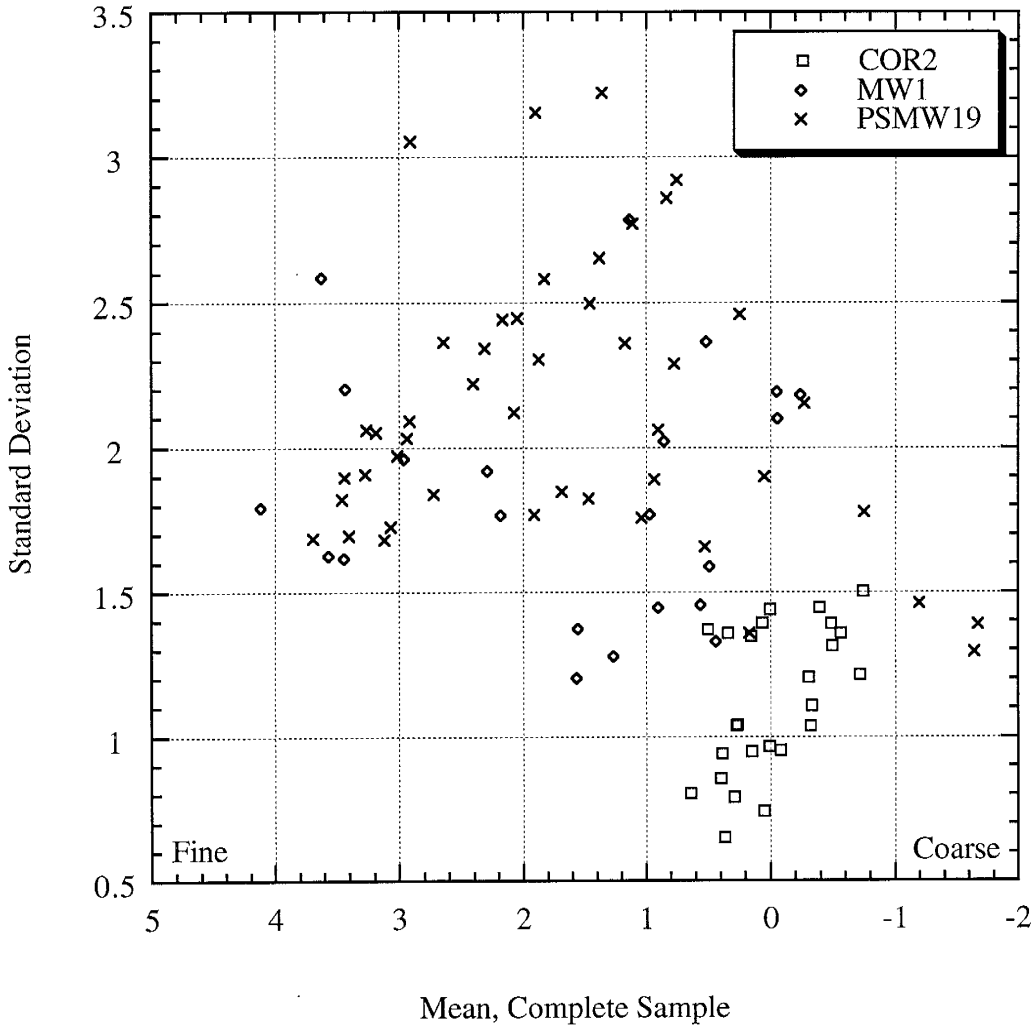

Figure 22. Scatter plot of mean and standard deviation of well cuttings, complete sample.

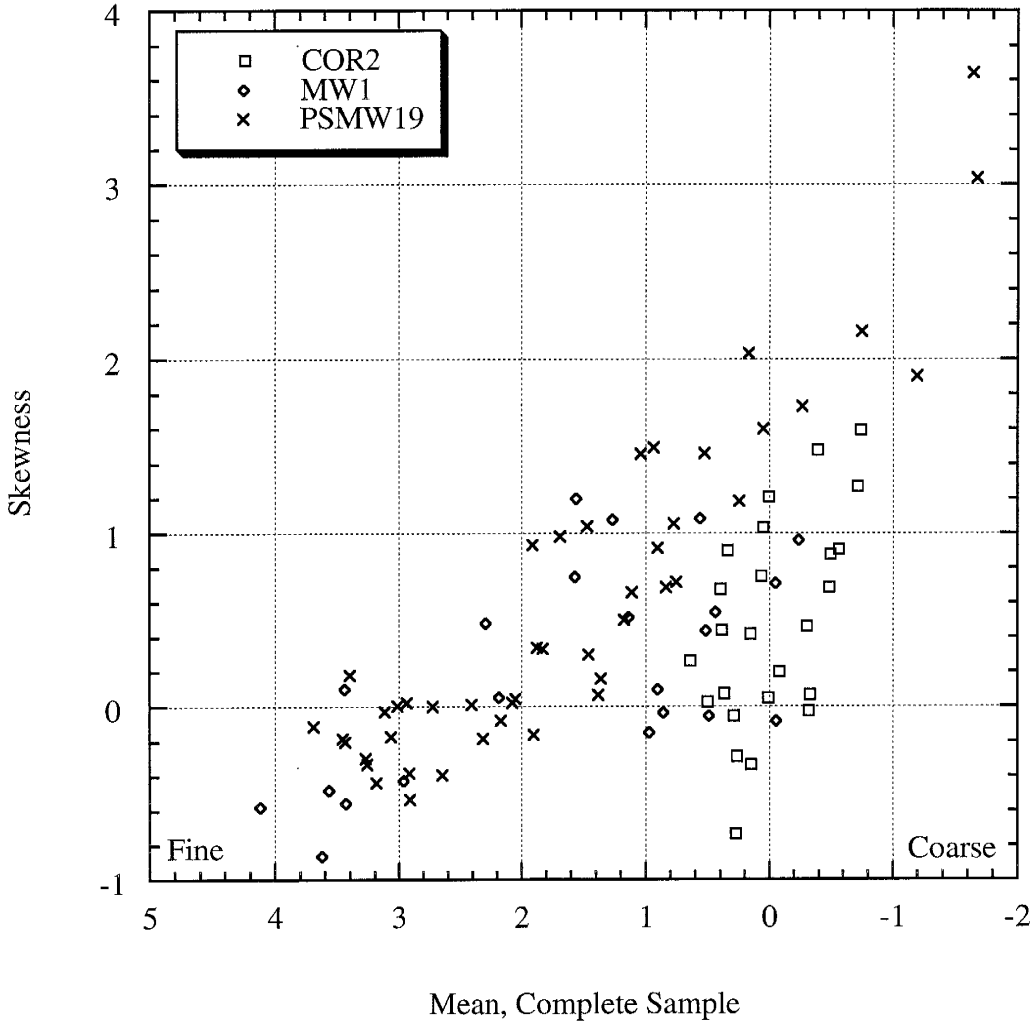

Figure 23. Scatter plot of mean and skewness of well cuttings, complete sample.

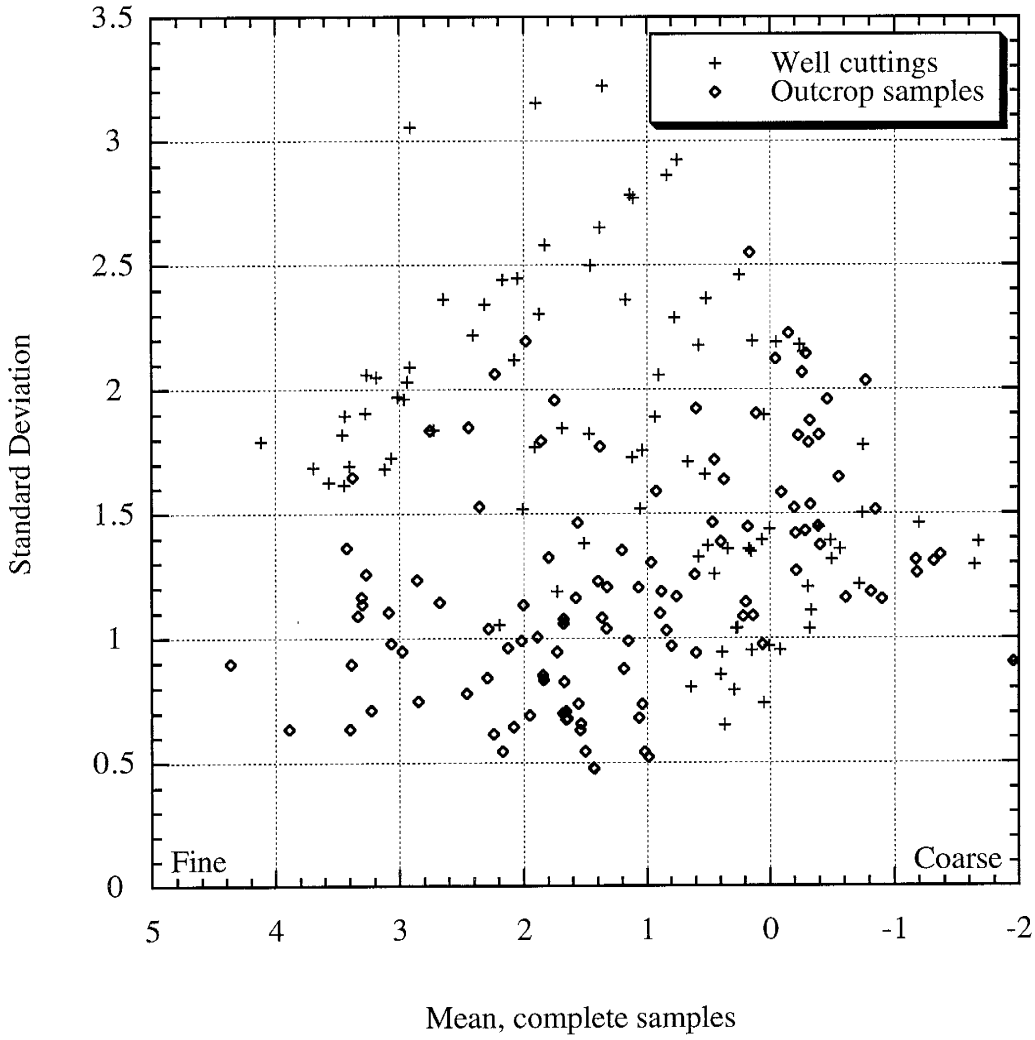

Figure 24. Scatter plot of mean and standard deviation of well cuttings and outcrop samples.

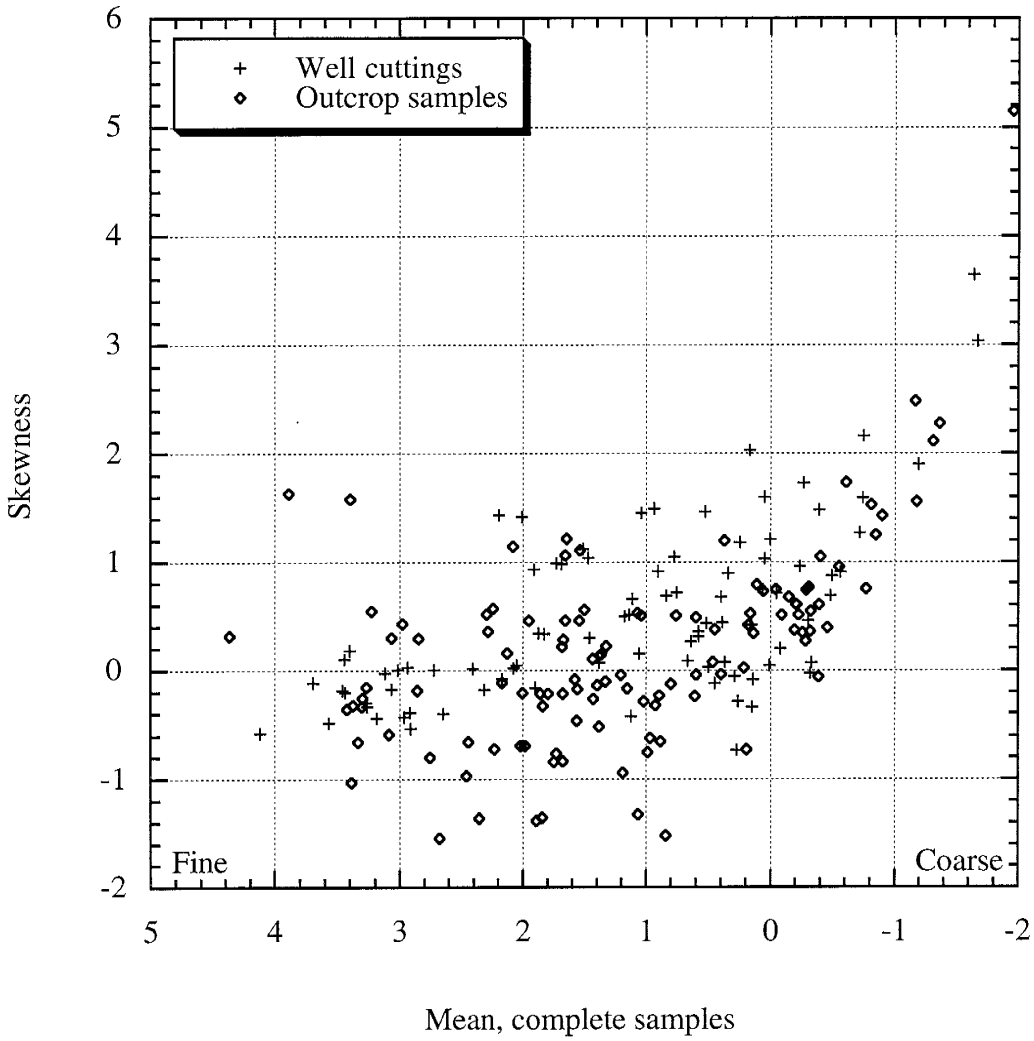

Figure 25. Scatter plot of mean and skewness of well cuttings and outcrop samples.

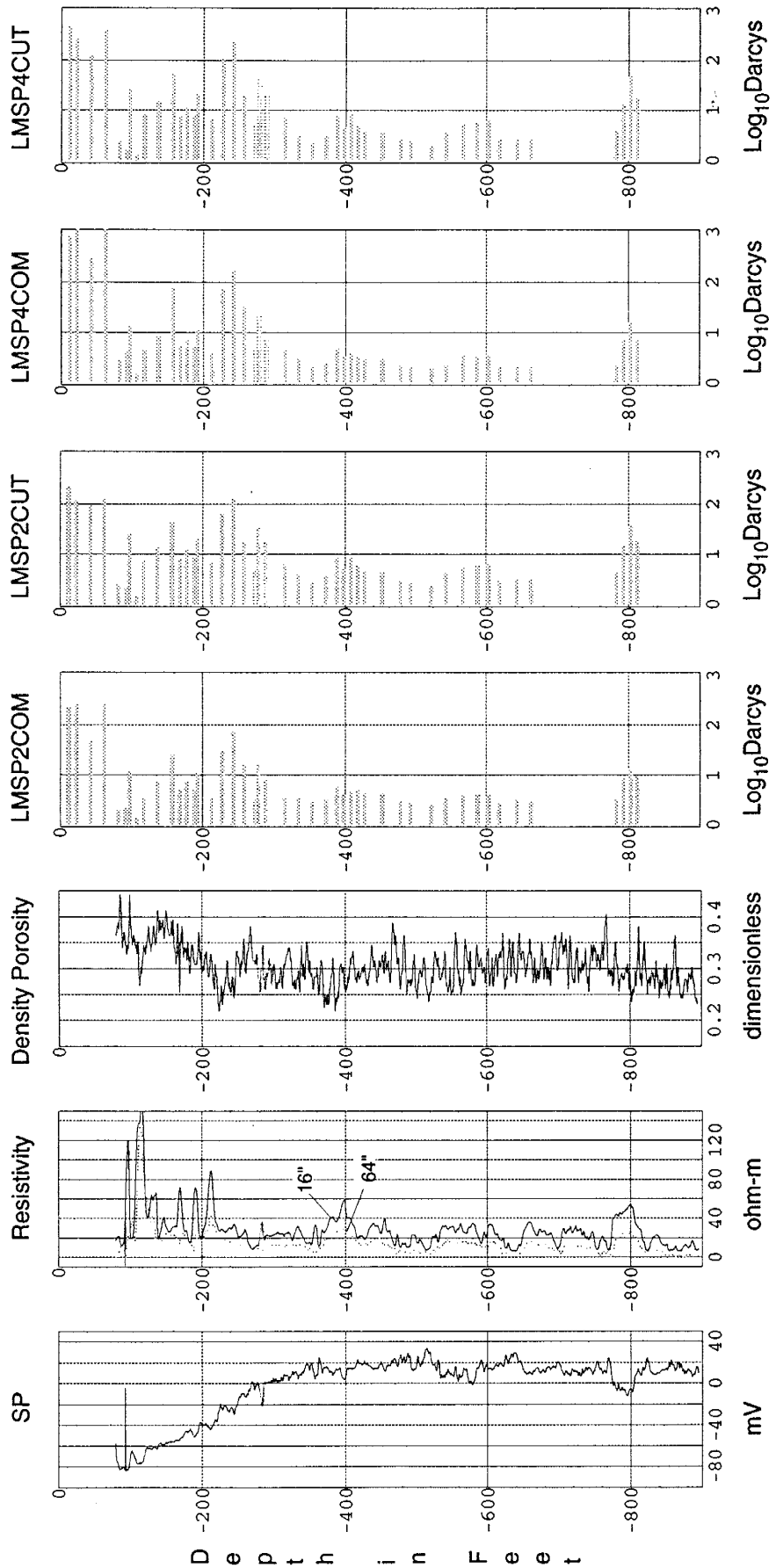

Figure 26. Geophysical logs from well PSMW-19, with permeability values based on grain size distribution of well cuttings. Regression equations described in text.

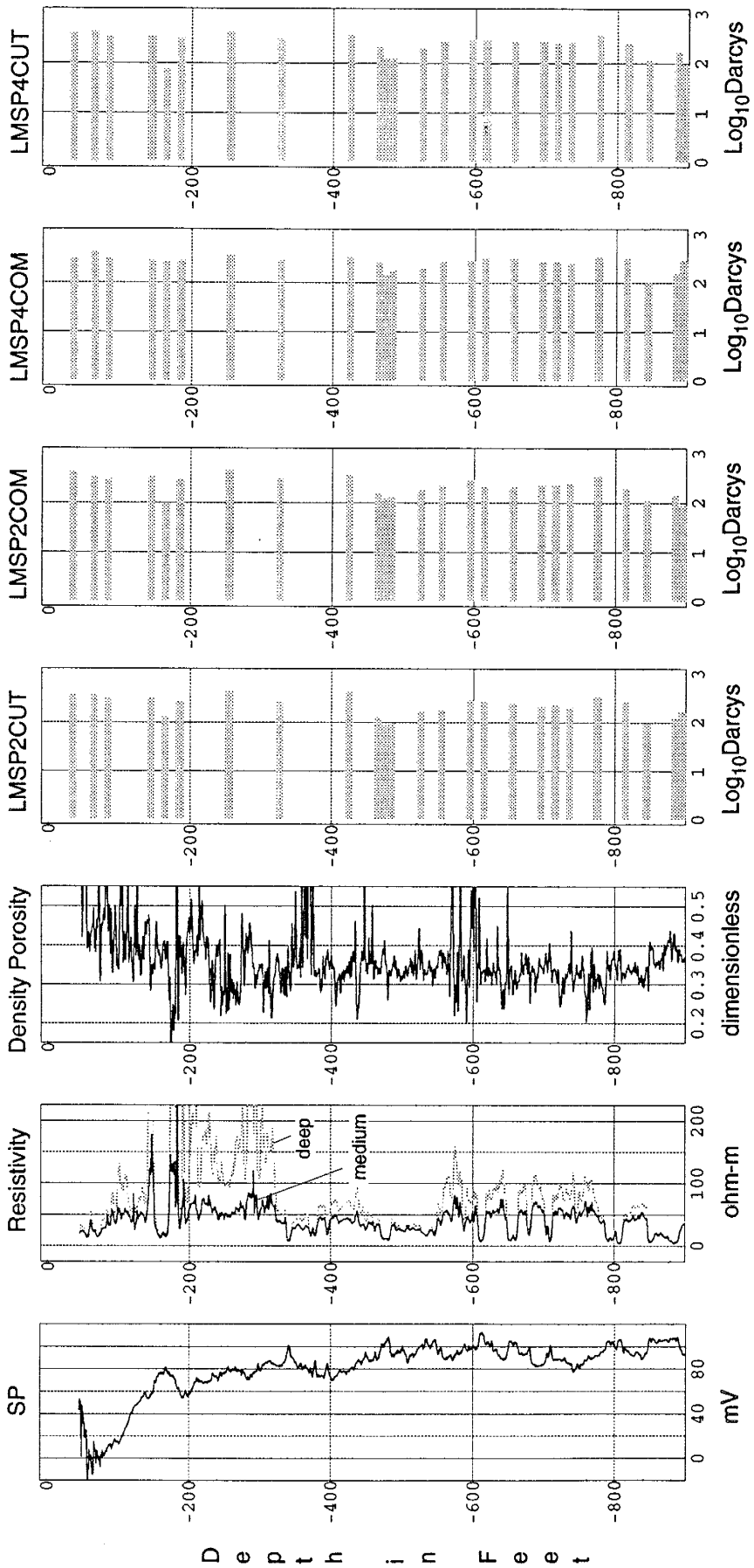

Figure 27. Geophysical logs from well Coronado 2, with permeability values based on grain size distribution of well cuttings. Regression equations described in text.

CHAPTER 5: DISCUSSION

PERMEABILITY, POROSITY AND GRAIN-SIZE DISTRIBUTION OF SEDIMENTS

Permeability, Porosity and Cementation

Figure 7 in the Results section displays the observed relationship between permeability and porosity for the sieved outcrop samples. A slight negative correlation is observed between porosity and permeability, contrary to what might be expected. If the sorting and cementation of the samples is considered, the negative correlation is partially explained. It is found that samples with relatively high porosities and low measured permeabilities are all moderately consolidated (cementation rank of 3). This demonstrates that relatively minor amounts of cementation have an appreciable influence on permeability. Cemented samples were not examined in detail, but it is likely that cementation is sufficiently developed to close pore throats (meniscus cements), but is not so prevalent as to cause a large reduction in porosity. The cluster of samples with low porosity and high permeability values can also be explained. Samples in this region of the plot are primarily scour and fill structures, have an abundance of coarse grains, and are poorly sorted. A high percentage of large grains (having zero porosity) surrounded by fine matrix material increases the bulk density of the sample, resulting in a lowered porosity value (Pryor, 1973). Despite accommodations for the extreme values for sorting and cementation among the samples, the correlation of porosity with permeability is poor.

It is possible that sampling error contributes to the poor correlation of porosity and measured permeability. Quartz and feldspars are the most abundant minerals in the majority of the samples. The average density of these two minerals, 2.65 g/cm^3, was used for the grain density value of these samples. Most other minerals contained in the samples have similar densities, so density was not considered to be a significant source of error. Plug samples obtained with the sampling tins are felt to provide accurate volume

measurements, but there is a greater possibility for error among the coarse samples for which a small pit was excavated and refilled with sand. The uncertainty lies in the packing and volume of sand poured back into the pit from which the sediments were excavated and retained for weighing. Disturbance of the sediments around the rim of the pit, and the difficulty of replacing the removed volume by exactly the same amount of sand, may result in errors in the measurement of the volume of sediment removed. Slight differences in the packing of the sand poured into the pit and that remaining in the graduated cylinder may also produce minor inaccuracies in volume measurements.

Pumice grains occur in large quantities in some of the samples, most notably at the Clarke Carr and Edith Gravels outcrops, creating difficulties for estimating porosity by grain density methods. The density of individual pumice clasts is variable due to differences in the internal porosity of the clasts. Grains with no internal porosity have a density similar to quartz, while those with high intragrain porosity may have a density of less than 1 gram per cubic centimeter (they float on water). Due to the variable grain density in pumice-rich samples, porosity was estimated by measuring the volume of water required to saturate these samples. By comparing porosities obtained by the saturation method to porosity values obtained by the bulk density method, it was determined that the saturation method underestimates porosity by an average of 8.8 percent. It may be faster, simpler and more accurate to determine a saturation correction factor and apply it, than to determine varying grain densities and proportions in samples containing grains of widely varied densities.

A number of researchers have documented a strong positive relationship between porosity and permeability (Archie, 1950; Fuchtbauer, 1967; Thompson, 1978; Bloch, 1991; Luffel et al, 1991; Nelson, 1994). The motivation for most of these studies was the evaluation and prediction of the quality of reservoir rocks for oil and gas recovery. Consequently, studies have dealt primarily with sandstones that have been buried to significant depths and compacted by overburden forces. Diagenesis is common at depth,

and pore-filling cements cause further reductions in porosity and permeability. Inspection of plots relating permeability to porosity in many of these studies reveals that permeabilities seldom exceed 1 darcy, and porosity values ranging from 2 to 30 percent. Considering the fact that the sediments examined in this study were never buried to significant depths, it is not surprising that porosity-permeability trends are less defined in the outcrops examined in this study.

In one of the few comprehensive studies of the relationship between porosity and permeability of modern uncompacted sediments, Pryor (1973) measured the porosity and permeability of 348 cores from point bar deposits of the Wabash, Whitewater and Mississippi Rivers. Permeability of samples was found to be highly variable, ranging from 4 millidarcys to more than 500 darcys. Porosity values varied from 17 to 52 percent, with an average value of 41 percent. Pryor found no clear relationship between porosity and permeability of modern uncompacted sands. In another study of Holocene river deposits, Atkins and McBride (1992) cited porosity values ranging from 40 to 58 percent for point bars and braided bars from five rivers. Thus the poor correlation of porosity and permeability, and the range of porosity values found to exist among the outcrop sample examined in this study are not without precedent.

Figure 8 illustrates the observed relationship between cementation and permeability for the sieved outcrop samples. No attempts were made to measure the permeability of moderately to well-indurated samples. Most cementation at the outcrops studied here is discontinuous, and does not form major barriers to groundwater flow. No attempts were made to differentiate between phreatic and pedogenic cements. One necessary consideration when viewing cementation in outcrop is whether it is buried caliche or originated as groundwater cementation, or if cements formed more recently at the outcrop surface. If an outcrop is down-gradient of a surface water catchment, it is possible for shallow groundwater to flow along a horizontal bed of low-permeability and evaporate at the outcrop exposure, precipitating carbonate. In situations such as this dating of cements would be

necessary to differentiate modern vadose deposits from older calcretes. Cementation in the northern Albuquerque Basin is often variable and discontinuous, and it is not possible to accurately predict the prevalence of cements in the subsurface based on the investigation of a limited number of surface exposures.

Correlation of Permeability with Grain-Size Distribution Parameters

Few comprehensive studies of the relationship between grain-size distribution parameters and permeability have been published. The most commonly cited investigation was conducted by Beard and Weyl (1973). In this study sands from two Texas rivers were sieved and recombined to form 48 samples. Eight size classes of varying mean grain size were constituted, with six subgroups of varied sorting for each size class. It was determined that porosity is independent of grain size for the extremely well sorted samples, but among poorly sorted samples porosity decreases and permeability increases as coarse grains were added. It was also demonstrated that permeability is proportional to the square of mean grain size. If theoretical models of flow being proportional to the square of the radius of a pore opening are accepted, this data demonstrates that pore size is proportional to grain size (Nelson, 1994). An additional finding of Beard and Weyl is that low sphericity and high angularity of grains increases the permeability and porosity of unconsolidated sands. A second study relating mean grain size and sorting to permeability is that of Krumbein and Monk (1942). Glacial outwash sands were sieved and recombined to make 30 samples with systematic changes in mean grain size and sorting (standard deviation). In the first set of samples the standard deviation was fixed at 0.21, and the mean grain size varied from -0.75 to 1.25 ϕ. The second set of sands were mixed with the mean grain size fixed at zero ϕ, and the standard deviation values ranging from 0.15 to 0.80. A constant-head permeameter was used to measure the permeability of the sand samples. Excellent correlation with measured permeability was observed with changes in mean grain size and standard deviation of the samples. It was found that variations in

permeability can be expressed as the product of a power function of the mean grain size and an exponential function of the standard deviation. Another study involving repacked grain distributions and permeability was published by Masch and Denny (1966). Permeability was found to increase as d_{50} grain size increases and standard deviation decreases. However, the permeability of samples with d_{50} values larger than 3.5 ϕ (fine sands) are practically independent of standard deviation. Permeability values were also found to increase with increased skewness values. Shepherd (1989) wrote a brief summary and review of theoretical and empirical studies relating permeability and grain-size distribution.

Measured permeability values and the $\log_{10}$ of measured permeability were correlated with a number of effective diameters and grain distribution parameters for the sieved outcrop samples. The listwise Pearson correlation coefficients for these comparisons are listed in Tables 4 and 5 in the Results section of this chapter. Scatter plots of measured permeability and all effective diameters and distribution parameters are included in Appendix C. In agreement with the studies mentioned above, permeability is found to correlate well with mean grain size and the d_{50} grain diameter. However, correlation of measured permeability with standard deviation is very poor. Skewness of the grain distributions have a slight influence on sample permeability, but correlation values are low.

Comparison of correlation coefficients listed in Tables 4 and 5 reveals some interesting trends. For nearly every effective diameter and distribution parameter, correlation with permeability is better with the cut samples than with the complete sample distributions. An abundance of large grains in a sample of average sorting will increase the mean grain size, but if smaller grains fill the spaces between the larger grains, the permeability of the sample will not be highly dependent on mean grain size. Excluding grains larger than 2 millimeters in diameter from the samples results in a better correlation of mean grain size and permeability. A correlation coefficient of r=0.872 is found between mean grain size of the cut sample and the $\log_{10}$ of measured permeability. Squaring the correlation coefficient shows that mean grain size explains 76 percent of the variability in this

relationship. The Kruger effective diameter is another sample parameter that correlates well with measured permeability. Like mean grain size, it is calculated from the percent weight retained on each sieve. The Kruger diameter of the cut samples and the log of measured permeability have a correlation coefficient of r=0.885, the highest of all correlations made for permeability and grain distribution parameters. This term explains 78.3 percent of permeability variability among the samples.

Most of the effective diameters calculated for the outcrop samples correlate well with measured permeability. If effective diameters are recorded in millimeters, the best correlations are with measured permeability and the cut samples. Higher correlation coefficients are found to exist between effective diameters from the cut distribution converted to ϕ units, and the $\log_{10}$ of measured permeability. The effective diameter d_{20} ϕ cut yields the best fit, with a R value of 0.863, explaining 74.5 percent of the variability in permeability among the samples. Correlations for some effective diameters approach the goodness of fit of the Kruger diameter and mean grain diameter. Much less sieving is required to determine effective diameters of d_{20} and smaller, compared to mean grain size and Kruger diameter. Determining mean grain size requires sieves covering the entire range of grain diameters, while d_{10} and d_{20} can be accurately determined with half as many sieves.

Grain-Size Distribution Statistics

A number of researchers have demonstrated that the grain-size distribution of many sediments approach lognormality. A brief review of some of these studies may be found in Pettijohn (1957). Due to the wide range of particle sizes found in many natural sediments, it is convenient to use a grade scale, or a series of class intervals that have a constant relationship to one another. The grade scale most commonly used by sedimentologists is the ϕ scale, proposed by Krumbein (1934). Departures from lognormality among samples is generally a function of the material available for sedimentation and the natural processes

of sedimentation, but may also be influenced by sampling procedures (Friedman, 1962). It is assumed that most outcrop samples sieved in this study do not deviate significantly from a lognormal distribution, but no rigorous validation of this assumption was made.

Moment measurements were used to calculate the grain distribution parameters of the sieved outcrop samples (calculations are described in the Methods section). Distribution parameters may also be calculated from size frequency histograms, but moment calculations generally yield more accurate results (Koldijk, 1968). The mean grain size, or first moment, represents the center of gravity of the distribution (size frequency histogram). Higher moments are calculated about this mean size. The second moment, or standard deviation, measures the dispersion of the distribution. The third moment is the skewness of the sample, and describes the symmetry of the sample (Friedman, 1962). The fourth moment measures the peakedness of the sample, but was not considered in this study. Moment measurements provide a useful method for describing the grain-size distribution of a sediment sample, but do not define a unique distribution function (Middleton, 1962).

The frequency distributions of some of the outcrop samples are bimodal. If a sample is bimodal, the peak from the coarser grains is often formed by clasts larger than 2 mm in diameter. The exclusion of the grains larger than 2 mm generally eliminates or greatly reduces bimodality among the samples. Griffiths (1967) questions the appropriateness of using moment calculations on open-ended grain distributions. This is addressed in this study by assuming a minimum grain diameter of 7.5 ϕ (0.0055 mm) for the finest grains of each sample. Among the cut sample distributions the frequency curve does not return to zero if the sample contained grains larger than 2 mm. These assumptions are not believed to produce large inaccuracies in the computation of grain-size distribution parameters for the cut samples.

Log-Log Plots

Several researchers have conducted detailed studies on the size distributions of natural sediments, and found a log-histogram the best way to display grain distributions. It was found that grain distributions of natural sands are most closely approximated by a hyperbola when weight percent retained on each sieve is normalized relative to sieve interval, and plotted on a log-log plot (Bagnold, 1941; Bagnold and Barndorff-Nielsen, 1980; Barndorff-Nielsen et al., 1982; Sutherland and Lee, 1994). Grain distribution parameters may be defined using hyperbolic parameters, but in this study the plots are used only for visual comparison. Log-log plots are useful as a graphical method because they require no assumption about the nature of grain distributions (D.W. Love, personal comm., 1994).

Log-log plots were generated for each of the sieved outcrop samples. Samples were classified by bedding type at the outcrop. Based on visual comparison of log-log plots, each bedding type was divided into subgroups. Plots of bedding subgroups are included in Appendix A, along with the particle size distribution parameters of each sample, arranged by log-log plot subgroups. By comparing the plots to the data files listing grain-size distribution parameters, one can quickly become proficient at interpreting the log-log plots. The mean grain size, as computed by moment measurements, is approximated by the peak on the log-log plot (grain size is plotted by millimeters, mean reported in ϕ units). The relative abundance of fine and coarse grains is also displayed; The y-value of the plot is influenced by the percent weight of the sample retained on each sieve, and larger y-values indicate a greater percentage of the total sample weight.

Figure 18 is a box plot of sample permeability divided by bedding subgroups. The good separation between the various subgroups demonstrates the effectiveness of the log-log in making rough approximations of sample permeability. The mean grain size, and relative abundance of coarse and fine grains is known to affect sample permeability, and these characteristic are easily approximated from the plots. The median grain diameter is

displayed on cumulative percent plots, but this parameter does not correlate as well with permeability. The relative abundance of coarse and fine grains is more difficult to interpret from cumulative percent plots. Log-log plots are useful in grouping sediment samples by bedding type and displaying grain distribution parameters that influence permeability.

PERMEABILITY EQUATIONS

Published Permeability Equations

A number of rational and empirical equations relating permeability to porosity and grain-size parameters exist. Many of these models are based on a relationship developed by Kozeny, and later modified by Carmen, known as the Kozeny-Carmen equation (Carmen, 1956). This equation represents the porous media as a bundle of capillary tubes of differing radii, where laminar flow is maintained in each tube. The two basic components of the equation are a particle size term related to the specific surface with respect to a unit volume of the solid, and a porosity term. The porosity term was found to equal $n^3/(1-n)2$, where n is fractional porosity (Bear, 1972). The idea that permeability varies with the square of grain diameter was proposed by Hazen (1892) and Schlichter (1899), and later experimentally verified (Krumbein and Monk, 1943; Burmister, 1954). Kozeney and Carmen also employed a squared diameter term, but the term was derived as an expression of specific surface area with respect to a unit volume of porous medium (Bear, 1972).

The empirical permeability equations applied to the outcrop samples are described in the Results section of this paper. Table 6 lists Pearson correlation coefficients for values predicted by the various equations compared to measured permeability values. Scatter plots comparing measured to predicted permeability are included in Appendix B. The Kruger and Zamarin equations yield the highest correlations with measured permeability, with the complete samples yielding better results than the cut samples. The Beyer and USBR equations correlate equally well with measured permeability when applied to the cut

samples, but the Beyer equation slightly underestimates permeability, and the USBR equation significantly underestimates permeability. The other equations generally underestimate permeability, and correlation with measured values is poor.

Inspection of scatter plots in Appendix C comparing squared effective diameters to measured permeability illustrates one reason why there is a large degree of scatter in the upper range of permeability values predicted by empirical formulas employing a squared diameter term. The squared diameter term generally increases more rapidly than the measured permeability of the outcrop samples. This disparity is tempered by the use of ϕ units, where the log conversion causes the effective diameter to change less rapidly. However, a logarithmic scale is not recommended for use in any of the published permeability equations. While the squared diameter term has a proven theoretical and empirical basis, it is not appropriate to square the effective diameter simply to maintain consistent units, as the data obtained in this study demonstrates that unsquared diameter terms correlate better with measured permeability.

An additional source of error in the empirical equations is the inclusion of a porosity term. Except for the Beyer and USBR equations, all permeability equations applied in this study include a porosity function. The poor correlation of porosity and permeability observed in the outcrop samples contributes to the inaccuracy of the empirical equations. The difficulty of obtaining porosity values, coupled with the poor correlation of porosity and permeability, suggest that it is not worthwhile to collect porosity values for the purpose of estimating the permeability of sediments. A major advantage of the regression equations formulated in this study is the exclusion of a porosity term.

Multiple Regression Analysis

Multiple regression analysis was applied to grain-size distribution parameters to formulate predictive permeability equations for use on sediments common to the northern Albuquerque Basin. The predictive permeability equations and scatter plots comparing

measured permeability to predicted permeability are included in Appendix B. Correlation with measured permeability yields coefficients ranging from r=0.785 to r=0.854 for regressions based on a single effective diameter, and coefficients as high as r=0.887 are attained with regressions including mean grain size, Kruger effective diameter and percent fines. The issue of colinearity, occurring when regression variables are themselves related (Ott, 1988), was not evaluated for the regression equations.

Inspection of the scatter plots of measured permeability and values predicted by regression equations shows that regressions based on a single effective diameter tend to overestimate permeability in the lower ranges. Errors are most pronounced when effective diameters are determined from the complete grain distributions. Overestimation of the low permeability samples is less severe for regressions with the log of permeability. It is worth noting that the outcrop samples with the lowest permeability are typically fine grained and/ or moderately cemented, where correlation of measured permeability with grain distribution parameters becomes more problematic. Overestimation of lower permeability values and low estimates in the higher permeability ranges could also be a result of least-squares fits used by the statistics program in generating the regression models. However, several of the regression equations based on a single effective diameter provide a good estimate of measured permeability over the entire range of measured permeabilities.

Regressions predicting the $\log_{10}$ of measured permeability, based on various parameters including mean grain size, the Kruger effective diameter, d_{10} diameter, and percent fines correlate well with measured permeability values. Regressions LMSP1 through LMSP 4 produce correlations of r=0.856 to r=0.887, explaining 73 to 79 percent of the variability in the data set. Inspection of scatter plots of the regressions reveals that values are centered around the 1:1 line of measured to predicted permeability. This is significant in that there is no systematic overestimation or underestimation of permeability by these equations.

The percentage of silt and clay contained in the majority of the outcrop samples is less than 5 percent, and inclusion of percent fines as an input parameter did not significantly improve any of the regression equations. The application of regression equations including a term for percent fines is not recommended for well cuttings. It is difficult to ascertain what portion of the fines of a sample are drilling mud and what is native to the sediments. Quality core is required to accurately determine the abundance of silt and clay in subsurface deposits .

It is recognized that cementation has a significant influence on permeability, but cementation is difficult to quantify in outcrop, much less in the subsurface. This study does not evaluate how cementation influences the permeability of samples of varied grain distributions, and cementation values are not included in any of the regression equations. If sediments are more than moderately cemented, the influence on permeability is significant, and relationships between grain-size distributions and permeability are obscured.

The regression equations developed here are based on a relatively small data set. Depending on the grain-size distribution of samples to which they are applied, the different regression equations may produce varied permeability values. The regression equations were not applied to an independent data set, and further validation and refinement of these regressions may be necessary before they are widely applied to sediments of the northern Albuquerque Basin.

The prediction of permeability based on grain-size distributions of uncemented sandy sediments are only appropriate for use in the shallow subsurface. Compaction curve studies show that porosity decreases exponentially with depth (Sclater and Christie, 1980; Baldwin and Butler, 1985). An investigation of argillaceous sediments shows porosity reduction of over 50 percent in the first 100 m of burial (Haneberg, 1988). Compaction with depth is probably less pronounced in the sands of the upper Santa Fe Group, but compaction does take place, altering the original packing of the sediments. With progres-

sive compaction there is a reduction in pore volume, and estimation of permeability based on grain-size distribution (and the inferred depositional packing) becomes problematic.

COMPARISON OF BEDDING TYPES

Comparison of Bedding Types by Grain-Size Distribution

A number of researchers have used grain-size distributions to investigate differences in depositional processes and sedimentary environments (Friedman, 1961; 1967; 1979; Bull, 1962; Koldijk, 1968; Visher, 1969; Sutherland and Lee, 1994). Friedman was one of the first researchers to advance to use of scatter plots of grain distribution parameters to differentiate between sands of different origins. He had considerable success isolating dune, beach and river sands by their textural characteristics (Friedman, 1961; 1979). A recent study by Sutherland and Lee (1994) uses moment measurements, log-log plots and non-parametric discriminate analysis to evaluate the textural differences between coastal subenvironments of a beach in Hawaii.

Both box plots and scatter plots were used in this study to compare textural differences between outcrop samples. Box plots effectively show the global characteristics of sorting parameters for each bedding type, but scatter plots have the advantage of displaying paired variables for the individual samples. Box plots do not allow comparison of individual samples. Log-log plots display the entire grain-size distribution, but it is cumbersome to compare a large number of these plots.

Figures 15 and 16 are scatter plots comparing grain distribution parameters of the outcrop samples. Samples are plotted by bedding type, and considerable separation between bedding types is illustrated by this style of plot. Figure 15 is a plot of mean grain size and standard deviation, displaying good separation between the bedding types with the exception of crossbeds, which overlaps with each of the other bedding types. Similar separation exists between bedding styles when mean grain size is plotted against skewness, with crossbeds overlapping each of the four other groups. Appendix D contains scatter plots comparing additional grain distribution parameters. The distribution statistics for each set of parameters shows better separation if complete instead of cut sample distributions are plotted.

Permeability and Porosity by Bedding Type

Figures 17 and 19 are box plots showing permeability measurements grouped by bedding type for the permeability profile measurements and sieved outcrop samples, respectively. Permeability trends among the bedding types are partially explained by comparison to Figure 13, a box plot of the mean, standard deviation and skewness of the samples of each bedding type. Table 9 provides a statistical summary of grain distribution parameters by bedding type. Figure 20 is a box plot of the porosity of the sieved samples, also grouped by bedding type. Comparison of the four plots illustrates the relationship between texture, porosity and permeability of the outcrop samples. Channels are found to have the greatest average permeability. Not surprisingly, they also have the smallest ϕ values of mean grain size (largest grain diameter). However, channels have moderate standard deviations and a large range of positive skewness values, resulting in a wide range of porosity values. Despite the fact that sorting and porosity is widely distributed among the channel samples, average permeability is high due to the coarse grains common to channels.

Crossbeds and horizontal beds have similar porosity, permeability and grain distribution characteristics. The average permeability is greater for crossbeds than for horizontal beds and laminations, which is largely a function of the larger mean grain size of the crossbeds. Both bedding types have average standard deviations of slightly less than one, and skewness values near zero. The consistent sorting of crossbeds and horizontal laminations results in high porosities and a relatively small range of permeability values for these bedding types.

Scour and fill deposits have a wide range of permeability values, with average permeability being relatively high. The average mean grain size of these structures is fairly large, and the samples are poorly sorted. The poor sorting results in low and varied porosity values. Structureless deposits have the lowest average permeability of the various bedding types, and the smallest average mean grain size. Samples have relatively high

standard deviation values, and slightly negative skewness values. Porosity of the structureless deposits is moderate to high. Structureless deposits tend to be more cemented than the other bedding types, which contributes to the low measured permeability values.

OUTCROP PERMEABILITY PROFILES

The first set of permeability measurements was collected when sediment samples were gathered and porosity measurements were made. The sampling criterion was to sample all major beds at each outcrop. This data was used for the generation of predictive permeability equations by regression analysis that can be applied to the wide variety of sedimentary textures found in the northern Albuquerque Basin. A second set of permeability values was compiled from the outcrop permeability profile measurements. The location of sampling points is recorded in Appendix F, allowing variogram analysis or other rigorous geostatistical methods to be applied to the data sets. Variogram analysis is beyond the scope of this study, and no attempts were made to characterize permeability heterogeneity from the permeability profile measurements.

The sediments of the three upper Santa Fe Group outcrops investigated in this study would make excellent aquifer material. Table 3 summarizes the permeability measurements from each outcrop. A more inclusive list of the range of outcrop permeability measurements is included in Appendix F along with geologic outcrop sketches. The outcrops of hydrostratigraphic unit USF-2 (Hawley and Haase, 1992) are dominated by deposits of the ancestral Rio Grande, and are characterized as a braided style of deposition (Lozinsky and Tedford, 1991). Channeling is common, occurring both as coarse gravel and cobble deposits between and within beds, and as coarse sand and pebble scours within sandy beds. Channels tend to be highly permeable, and the sinuosity and avulsion of channels results in a high degree of interconnectedness between beds. Fine grained beds of low permeability are relatively uncommon in the outcrops selected for study. The absence of laterally continuous beds of low permeability and the presence of channels connecting beds

of moderate to high permeability allows for high rates of water movement through these sediments.

Deposits classified as River Alluvium by Hawley and Haase (1992) also contain thick sandy beds of high permeability. However, the Edith and Los Duranes outcrops also contain laterally extensive silt and clay beds of low permeability. Given the limited exposures available for investigation, it is difficult to assess the continuity of the fine beds. The horizontal hydraulic conductivity of the River Alluvium deposits is great, but more work must be completed to determine to what degree vertical flow is impeded by the presence of fine overbank deposits.

Piedmont Alluvium deposits also contain alternating permeable and relatively impermeable beds. Beds and assemblages of beds of alluvial fan deposits are often lobate in shape. Although beds of high porosity and permeability exist within the fan deposits, at times they may be isolated from other permeable deposits. The Bear Canyon, Four Hills and Tijeras Arroyo deposits have some of the highest average permeabilities recorded in this study, but the outcrops also contain beds of relatively low permeability. These beds are generally of fine sand, and have higher permeability than the silt and clay deposits associated with the ancestral Rio Grande.

The hydrostratigraphic units defined by Hawley and Haase (1992) may be hundreds or thousands of meters thick, while the outcrops examined here are generally less than 10 meters high. The variability of sediments observed in outcrop does not necessarily reflect the entire range of deposits occurring within the hydrostratigraphic units. However, it is useful to integrate outcrop studies with the analysis of well cuttings and geophysical well logs when assessing local and regional rates of groundwater recharge and flow.

COMPARISON OF OUTCROP SAMPLES AND WELL CUTTINGS

Box plots and scatter plots are useful in comparing grain-size distributions of outcrop samples to well core and cuttings. One must remember that there is some degree of uncertainly in the comparisons, because cuttings and not core were obtained from wells Coronado 2 and PSMW-19. As cuttings move up the well bore as drilling progresses, some amount of mixing takes place among the sediments. If beds are fairly thick and grain distributions of the sediments are similar, a small sample of the cuttings coming out of the well should have grain distributions similar to the beds at the bottom of the well. If beds in the subsurface are relatively thin and of varied texture, mixing in the well bore may completely obscure the grain-size distributions of the individual beds at depth. Sloughing and caving of the well may also produce samples at the surface that do not reflect the sediments being cut by the bit at the recorded depth of the sample. Well PSMW-19 was drilled with a reverse-rotary drill rig, where drilling mud flows down the outside of the well bore and up through the drill pipe. This style of rig minimizes mixing of the sediments as they are transported to the surface. With mud drilling, an additional complication is the uncertainty of knowing how much of the clay in a sample is native to the sediments and how much is drilling mud. It is important that well cuttings are collected directly from the well bore and not from the silt shaker, as many of the fines of the sample, which have a large influence on permeability, will be removed by the silt shaker. In addition, an accurate estimation of the time required for sediments to travel up the well bore is necessary to determine from what depth samples are cut.

Despite the considerations listed above, comparison between the grain-size distributions of outcrop samples and well cuttings are possible. Figure 24 is a scatter plot comparing the mean and standard deviation of all outcrop samples to all well cuttings from the three wells considered in this investigation. It is demonstrated that there is good agreement between the two data sets. Comparing Figure 24 to Figure 22, it can be seen that most of the high standard deviation values are from the cuttings of well PSMW-19.

Figure 24 also shows that the coarse well cuttings tend to be better sorted than the fine well cuttings. The reason for this trend is not readily apparent, as a weak trend of coarse samples having higher standard deviations is observed among the outcrop samples. One possible explanation is that fine grains were removed from the well cuttings when the samples were washed.

The combined use of the petrography and grain-size distributions of well cuttings and core may allow the investigator to infer the nature and origin of sediments at depth. Comparison of Figures 12 and 21 shows the grain-size distributions of the cuttings of well Coronado 2, penetrating a thick sequence of piedmont fan and fluvial facies, are similar to the scour and fill structures sampled in outcrop. A knowledge of the lithology and textures common to the various hydrostratigraphic units within the basin, as determined in outcrop, can be applied to well core and cuttings to infer the types of bedding and range of permeability values of sediments at depth.

GEOPHYSICAL WELL LOGS

It is beyond the scope of this study to include a detailed analysis of the relationships between geophysical log signatures and permeability as estimated from the grain-size distribution of well cuttings. However, several of the findings of this study warrant discussion. The poor correlation between porosity and permeability observed in the outcrop samples is also observed in the subsurface. The zones of highest permeability in Figures 26 and 27 generally do not correspond with the zones of high density porosity, but in zones of average to below average porosity. A porosity term is common to most equations estimating permeability from wireline geophysical logs (Jorgensen, 1988), and the research presented here suggests that the assumed relationship between porosity and permeability should be used with caution among sediments that have never been buried to significant depths.

From the limited data presented here, it appears that zones of high permeability are associated with a distinct separation of the medium and deep resistivity curves, high resistivity values, and lower than average spontaneous potential values. It is not possible to make broad generalizations on the data from a limited number of cuttings from two wells, but trends are recognizable in the data, and more research is required to substantiate or redefine what is observed here. The author was not present when wells PSMW19 and Coronado 2 were drilled, and the accuracy of the recorded depths of the well cuttings is unknown. The use of well core, as opposed to well cuttings, would be required for a rigorous validation of the findings presented in this manuscript.

CHAPTER 6: CONCLUSIONS

The investigations detailed in this thesis represent preliminary efforts to characterize hydrostratigraphic units of the northern Albuquerque Basin based on permeability measured in outcrop and the grain-size distribution of sediments. Outcrop investigations allow detailed study of the permeability of aquifer-related sediments, styles of bedding and relationships between bedding types. Permeameters allow rapid in-situ measurements of permeability, and the collection of sediment samples allows comparison of permeability to the grain-size distributions of sediments.

A number of grain distribution parameters correlate well with measured permeability. Mean grain size, the Kruger effective diameter, and effective diameters ranging from d_{10} to d_{20} have high correlation coefficients with measured permeability. Correlations are generally better if grains larger than 2 mm in diameter are excluded from the sample before calculating grain distribution parameters.

Cementation in relatively minor amounts has an appreciable influence on the permeability of sandy sediments. Estimation of permeability based on grain-size distribution is not appropriate for sediments having more than moderate cementation. No clear relationship is observed between measured permeability and porosity for outcrop samples from the northern Albuquerque Basin. Permeability estimates based on porosity values obtained from geophysical well logs should be used with caution when applied to sediments of the Albuquerque Basin that have never been buried to significant depths. For deeper sandy sediments in the basin, where original packing has been altered by compaction, it is likely that relationships exist between porosity and permeability.

The use of a portable air-minipermeameter allows evaluation of the accuracy of a number of published permeability equations based on porosity and grain distribution of sandy sediments. The Kruger and Zamarin equations were found to correlate well with measured permeability, but both equations use porosity values, which are difficult to

obtain. Of the equations based on texture alone, the Beyer equation provides the best results. Several of the regression equations generated in this thesis produce permeability values that correlate well with measured permeability, but they were not checked against an independent data set, and the accuracy of predicted permeability values above the measurement range of the air-minipermeameter is uncertain.

Characteristic grain-size distributions and a typical range of permeability was determined for several bedding types common to the sediments of the northern Albuquerque Basin. Channels and scour and fill structures are found to be highly permeable. Channels often have sinuous paths and cut into surrounding beds, resulting in beds connected by permeable pathways, which is conducive to groundwater flow and recharge.

Recent mapping of hydrostratigraphic units in the subsurface has been based largely on the analysis of well cuttings. Comparison of the texture and petrography of outcrop samples and well cuttings, combined with a knowledge of associated bedding types and common associations between beds determined in outcrop, allows the hydrogeologist to infer the hydrologic quality of subsurface deposits. The accurate estimation of the permeability and bedding type of subsurface deposits based on grain-size distributions requires well core, as opposed to well cuttings.

Estimation of permeability from grain distributions can be used to check permeability values obtained by other methods. Slug test and pump test permeability data is influenced by well construction and relies on a number of assumptions, and geophysical well log analysis provides only relative permeability values. If quality core samples are obtained from wells, the resolution of permeability estimations based on sedimentary texture is better than those obtained from slug tests or pump tests, and may be used to calibrate permeability estimates from geophysical well log analysis. Inspection of well logs from two wells in the study area indicates that zones of high permeability, as determined from the grain-size distributions of well cuttings, are characterized by high electrical

resistivity, good separation of the medium and deep resistivity curves, and lower than average porosity values.

The deposits of hydrostratigraphic unit USF-2 evaluated in this study are characterized by highly permeable sand and gravel beds, and generally lack extensive beds of low permeability. The mean measured permeability for the sands of the three USF-2 outcrops studied here ranges from 42 to 89 darcys. Two of the outcrops contain gravel beds of permeability greater than approximately 300 darcys, which were not sampled. The recorded average permeability values for these outcrops underestimates the true average permeability.

Two outcrops of Valley Alluvium were sampled, but average permeability values reported here do not include measurements from all beds occurring in either outcrop. The sands of the Los Duranes exposure are unconsolidated and poorly suited for sampling with the air-miniperm-eameter. From the few readings obtained here, it was determined that the sands have an average permeability of at least 71 darcys. Laterally extensive silt and clay beds form part of this deposit, having undetermined permeability of less than 1 darcy. The sands and silts of the Edith Gravels have an average permeability of 56 darcys, but the highly-permeable gravels of this formation are not included in this average.

Three outcrops of Piedmont Alluvium were sampled and found to have average permeabilities ranging from 83 to 98 darcys. Deposits are characterized by thick interbeds of coarse channels and scour and fill structures, and deposits of fine sands. These outcrops represent some of the more permeable deposits of this hydrostratigraphic unit.

REFERENCES

Archie, G.E., 1950, Introduction to petrophysics of reservoir rocks. Bulletin of the American Association of Petroleum Geologists, Vol. 34, No. 5, pp. 943-961.

Atkins, J.E., and McBride, E.F., 1992, Porosity and packing of Holocene river, dune and beach sands. The American Association of Petroleum Geologists Bulletin, Vol. 76, No. 3, pp. 339-355.

Bagnold, R.A., 1941, The Physics or Blown Sand and Desert Dunes. Chapman and Hall, Ltd., London. 265 pp.

Bagnold, R.A. and Barndorff-Nielsen, O., 1980, The pattern of natural size distributions. Sedimentology, Vol. 27, pp. 199-207.

Baldwin, B. and Butler, C.O., 1985, Compaction Curves. The American Association of Petroleum Geologists Bulletin, Vol. 69, No. 4, pp. 622-626.

Barndorff-Nielsen, O., 1977, Exponentially decreasing distribution for the logarithm of particle size. Proc. Royal Soc. London A. 353, pp. 401-419.

Barndorff-Nielsen, O., Dalsgaard, K., Halgreen, C., Kuhlman, H., Møller, J.T. and Schou, G., 1982, Variation in particle size distribution over a small dune. Sedimentology, Vol. 29, pp. 53-65.

Bear, J., 1972, Dynamics of Fluids in Porous Media. American Elsevier Pub. Co., New York. 764 pp.

Beard, D.C. and Weyl, P.K., 1973, Influence of texture on porosity and permeability of unconsolidated sand. American Association of Petroleum Geologists Bulletin, Vol. 57, No. 2, pp. 349-369.

Bloch, S., 1991, Empirical prediction of porosity and permeability in sandstones. American Association of Petroleum Geologists Bulletin, Vol. 75, No. 7, pp. 1145-1160.

Bowman, R.S. and Stevens, D.B., 1991, Field study of multidimensional flow and transport in the vadose zone. New Mexico Water Resources Research Institute Report No. 262. 132 pp.

Bull, W.B., 1962, Relation of textural (CM) patterns to depositional environment of alluvial-fan deposits. Journal of Sedimentary Petrology, Vol. 32, No. 2, pp. 211-216.

Burmister, D.M., 1954, Principles of permeability testing of soils. Symposium on Permeability of Soils. ASTM Special Pub. 163, pp. 3-20.

Carmen, P.C., 1956, Flow of Gases through Porous Media. Academic Press Inc. 182 pp.

Chandler, M.A., Kocurek, G., Goggin, D.J., and Lake, L., 1989, Effects of Stratigraphic heterogeneity on permeability in eolian sandstone sequence, Page

Sandstone, northern Arizona. The American Association of Petroleum Geologists Bulletin, Vol. 73, No. 5, pp. 658-668.

Cather, S.M., 1992, Suggested revisions to the Tertiary tectonic history of north-central New Mexico. New Mexico Geological Society Guidebook, 43rd Field Conference, San Juan Basin IV, pp. 109-122.

Chapin, C.E. and Cather, S.M., 1994, Tectonic setting of the axial basins of the northern and central Rio Grande rift, *in* Keller, G.R. and Cather, S.M., eds., Basins of the Rio Grande Rift: Structure, Stratigraphy, and Tectonic Setting: Geological Society of America Special Paper 291. Geological Society of America, Boulder. 304 pp.

Collinson, J.D. and Thompson, D.B., 1982, Sedimentary Structures. George Allen and Unwin Ltd., London. 194 pp.

Collinson, J.D., 1986, Alluvial sediments, *in* Sedimentary Facies and Environments, edited by H.G. Reading. Blackwell Scientific Publications, Oxford. 615 pp.

Davis, J.M., 1990, An approach for the characterization of spatial variability of permeability in the Sierra Ladrones Formation, Albuquerque Basin, New Mexico. Unpublished Masters thesis, New Mexico Institute of Mining and Technology. 137 pp.

Davis, J.M., Lohman, R.C., Phillips, F.M, Wilson, J.L. and Love, D.W., 1993, Architecture of the Sierra Ladrones Formation, central New Mexico: depositional controls on the permeability correlation structure. Geological Society of America Bulletin, Vol. 105, pp. 998-1007.

Davis, J.M., 1994, A conceptual sedimentological-geostatistical model of aquifer heterogeneity based on outcrop studies. Unpublished doctorate dissertation, New Mexico Institute of Mining and Technology, 234 pp.

Davis, J.M., Wilson, J.L. and Phillips, F.M., 1994, A portable air-minipermeameter for rapid in situ field measurements. Groundwater, Vol. 32, No. 2, pp. 258-266.

Domenico, P.A. and Schwartz, F.W., 1990, Physical and Chemical Hydrogeology. John Wiley and Sons, New York. 824 pp.

Dreyer, T., Scheie, A., and Walderhaug, O., 1990, Minipermeameter-based study of permeability trends in channel sand bodies. The American Association of Petroleum Geologists Bulletin, Vol. 74, No. 4, pp. 359-374.

Driscoll, F.G., 1986, Groundwater and Wells. Johnson Division, St. Paul. 1089 pp.

Folk, R.L. and Ward, W.C., 1957, Brazos River bar: a study in the significance of grain size parameters. Journal of Sedimentary Petrology, Vol. 27, No. 1, pp. 3-26.

Freeze, R.A. and Cherry, J.A., 1979, Groundwater. Prentice-Hall, Inc., Englewood Cliffs. 604 pp.

Fuchtbauer, H., 1967, Influence of different types of diagenesis on sandstone porosity. Seventh World Petroleum Cong. Proc. Vol. 2, pp. 353-369.

Friedman, G.M., 1961, Distinction between dune, beach, and river sands from their textural characteristics. Journal of Sedimentary Petrology, Vol. 31, No. 4, pp. 514-529.

Friedman, G.M., 1962, On sorting, sorting coefficients, and the lognormality of the grain-size distribution of sandstones. Journal of Geology, Vol. 70, pp. 737-753.

Friedman, G.M., 1967, Dynamic processes and statistical parameters compared for size frequency distribution of beach and river sands. Journal of Sedimentary Petrology, Vol. 37, No. 2, pp. 327-354.

Friedman, G.M., 1979, Address of the retiring president of the International Association of Sedimentologists: differences in size distributions of populations of particles among sand of various origins. Sedimentology Vol. 26, pp. 3-32.

Goggin, D.J., Chandler, M.A., Kocurek, G. and Lake, L.W., 1988a, Patterns of permeability in eolian deposits: Page sandstone (Jurrasic), northeastern Arizona. Society of Petroleum Engineers Formation Evaluation Vol. 3, pp. 297-306.

Goggin, D.J., Thrasher, R. and Lake, L.W., 1988b, A theoretical and experimental analysis of minipermeameter response including gas slippage and high velocity flow effects. In Situ, Vol. 12, pp. 79-116.

Griffiths, J.C., 1967, Scientific Method in the Analysis of Sediments. McGraw-Hill, New York. 508 pp.

Haneberg, W.C., 1988, Some possible effects of consolidation on growth fault geometry. Tectonophysics, Vol. 148, pp. 309-316.

Hartkamp, C.A., Arribas, J. and Tortosa, A., 1993, Griansize, composition, porosity and permeability contrasts within cross-bedded sandstones in Tertuary fluvial deposits, central Spain. Sedimentology, Vol. 40, pp. 787-799.

Hawley, J.W., 1986, Physiographic provinces (and) landforms of New Mexico, *in* Williams, J.L., ed., New Mexico in Maps. The University of New Mexico Press, Albuquerque, pp. 28-31.

Hawley, J.W. and Haase, C.S., compilers, 1992, Hydrogeologic framework of the northern Albuquerque basin. New Mexico Bureau of Mines and Mineral Resources Open-File Report 387. 74 pp., 8 Appendices.

Hawley, J.W., Haase, C.S. and Lozinsky, R.P., 1995, An underground view of the Albuquerque Basin, *in* Ortega-Klett, C.T., ed., Proceedings of the 39th Annual Water Conference, "The Water Future of Albuquerque and the Middle Rio Grande Basin." New Mexico Water Resources Institute (in press).

Hazen, A., 1892, Some physical properties of sands and gravels. Mass. State Board of Health, Annual Report, pp. 539-556.

Hurst, A. and Rosvoll, K.J., 1991, Permeability variations in sandstones and their relationship to sedimentary structures, *in* Lake, L.W., Carroll, H.B. Jr., and Wesson, T.C., eds., Reservoir Characterization II. Academic Press, Inc., San Diego, 726 pp.

Inman, D.L., 1952, Measures for describing the size distributions of sediments. Journal of Sedimentary Petrology, Vol. 22, pp. 125-145.

Jorgensen, D.G., 1988, Using geophysical logs to estimate porosity, water resistivity, and intrinsic permeability. U.S. Geological Survey Water-Supply Paper 2321. 25 pp.

Kernodle, J.M., McAda, D.P., and Thorn, C.R., 1995, Simulation of ground-water flow in the Albuquerque Basin, central New Mexico. U.S. Geological Survey Water-Resources Investigations Report 94-4251, 114 pp.

Koldijk, W.S., 1968, On environment-sensitive grain-size parameters. Sedimentology, Vol. 10, pp. 57-69.

Krumbein, W.C., 1934, Size frequency distribution of sediments. Journal of Sedimentary Petrology, Vol. 4, pp. 65-77.

Krumbein, W.C. and Pettijohn, F.J., 1938, Manual of Sedimentary Petrology. D. Appleton-Century Co., New York. 549 pp.

Krumbein, W.C. and Monk, G.D., 1942, Permeability as a function of the size parameters of unconsolidated sands. Am. Inst. Mining Metall. Engineers. Tech. Pub. 1492.

Kruseman, G.P. and de Ridder, N.A., 1990, Analysis and Evaluation of Pumping Test Data, second edition. International Institute for Land Reclamation and Improvement, The Netherlands. 377 pp.

Lambe, T.W., 1951, Soil Testing for Engineers. John Wiley and Sons, Inc., New York. 165 pp.

Lambert, P.W. 1968, Quaternary stratigraphy of the Albuquerque Area, New Mexico. Unpublished doctorate dissertation, University of New Mexico. 329 pp.

Lozinsky, R.P., 1988, Stratigraphy, sedimentology, and sand petrology of the Santa Fe Group and pre-Santa Fe Tertiary deposits in the Albuquerque Basin, central New Mexico. Unpublished doctorate dissertation, New Mexico Institute of Mining and Technology, 298 pp.

Lozinsky, R.P., Hawley, J.W. and Love, D.W., 1991, Geologic overview and Pliocene-Quaternary history of the Albuquerque basin, central New Mexico. New Mexico Bureau of Mines and Mineral Resources, Bulletin 137, pp. 157-162.

Lozinsky, R.P. and Tedford, R.H., 1991, Geology and Paleotology of the Santa Fe Group, southwestern Albuquerque Basin, Valencia County, New Mexico. New Mexico Bureau of Mines and Mineral Resources, Bulletin 132. 35 pp.

Lozinsky, R.P., 1994, Cenozoic stratigraphy, sandstone petrology, and depositional history of the Albuquerque Basin, central New Mexico, *in* Keller, G.R. and Cather, S.M., eds., Basins of the Rio Grande Rift: Structure, Stratigraphy, and Tectonic Setting: Geological Society of America Special Paper 291. Geological Society of America, Boulder. 304 pp.

Luffel, D.L., Howard, W.E., and Hunt, E.R., 1991, Travis Peak core permeability and porosity relationships at reservoir stress. SPE Formation Evaluation, Vol. 6, No. 3, pp. 310-318.

Masch, F.D. and Denny, K.J., 1966, Grain size distribution and its effect on the permeability of unconsolidated sands. Water Resources Research, Vol. 2, No. 4, pp. 665-677.

Middleton, G.V., 1962, On sorting, sorting coefficients, and the lognormality of the grain-size distribution of sandstones: a discussion. Journal of Geology, Vol. 70, pp.754-756.

Nelson, P.H., 1994, Permeability-porosity relationships in sedimentary rocks. The Log Analyst, Vol 35, No. 3, pp.38-61.

Neton, M.J., Dorsch, J., Olson, C.D. and Young, S.C., 1994, Architecture and directional scales of heterogeneity in alluvial-fan aquifers. Journal of Sedimentary Research, Vol. B64, No. 2, pp. 245-257.

Ott, L., 1988, An Introduction to Statistical Methods and Data Analysis, third edition. PWS-Kent Publishing, Boston. 835 pp.

Pettijohn, F.J., 1957, Sedimentary Rocks, second edition. Harper and Bros., New York. 718 pp.

Pettijohn, F.J., Potter, P.E., and Siever, R., 1972, Sand and Sandstone. Springer-Verlag, New York. 618 pp.

Picard, M.D. and High, L.R. Jr., 1973, Sedimentary Structures of Ephemeral Streams. Elsevier Scientific Publishing Co., Amsterdam. 223 pp.

Pryor, W.A., 1973, Permeability-porosity patterns and variations in some Holocene sand bodies. American Association of Petroleum Geologists Bulletin, Vol. 57, No. 1, pp. 162-189.

Russell, L.R. and Snelson, S., 1990, Structural style and tectonic evolution of the Albuquerque basin segment of the Rio Grande rift, *in* Pinet, B. and Bois, C., eds., The potential for deep seismic profiling for hydrocarbon exploration. Editions Technip, Paris, French Pertoleum Institute Research Conference Proceedings. pp. 175-207.

Russell, L.R. and Snelson, S., 1994, Structure and tectonics of the Albuquerque Basin segment of the Rio Grande rift: Insights from reflection seismic data, *in* Keller, G.R. and Cather, S.M., eds., Basins of the Rio Grande Rift: Structure, Stratigraphy, and Tectonic Setting: Geological Society of America Special Paper 291. Geological Society of America, Boulder. 304 pp.

Schlichter, C.S., 1899, Theretical investigations of the motions of ground waters. U.S. Geological Survey 19th Annual Report, part 2, pp. 295-384.

Sclater, J.G. and Christie, P.A.F., 1980, Continental stretching: an explanation of the post-mid-Cretaceous subsidence of the central North Sea basin. Journal of Geophysical Research, Vol. 85, pp. 3711-3739.

Shepherd, R.G., 1989, Correlations of permeability and grain size. Groundwater, Vol. 27, No. 5, pp. 633-638.

Stalkup, F.I., 1986, Permeability variations observed at the facies of crossbedded sandstone outcrops *in* Reservoir Characterization, Lake L.W. and Carrol, H.B. Jr., editors. Academic Press, Orlando, 1986.

Sutherland, R.A. and Lee, C.T., 1994, Discrimination between coastal subenvironments using textural characteristics. Sedimentology, Vol. 41, pp. 1133-1145.

Thomson, A., 1978, Petrography and diagenesis of the Houston sandstone reservoirs at Bassfield, Jefferson Davis County, Mississippi. Transactions, Gulf Coast Association of Geological Societies, Vol. 28, pp. 651-664.

Thorn, C.R., McAda, D.P., and Kernodle, J.M., 1993, Geohydrologic framework and hydrologic conditions in the Albuquerque Basin, central New Mexico. U.S. Geological Survey Water-Resources Investigations Report 93-4149, 106 pp.

Visher, G.S., 1969, Grain size distributions and depositional processes. Journal of Sedimentary Petrology, Vol. 39, No. 3, pp. 1074-1106.

Vukovic, M. and Soro, A., 1992, Determination of Hydraulic Conductivity of Porous Media from Grain-Size Composition. Water Resources Publications, Littleton, CO. 83 pp.

APPENDIX A

Log-hyperbolic plots, cumulative percent plots, and grain size distribution parameters of outcrop samples

Log-Hyperbolic Distribution - Crossbeds, Group 1

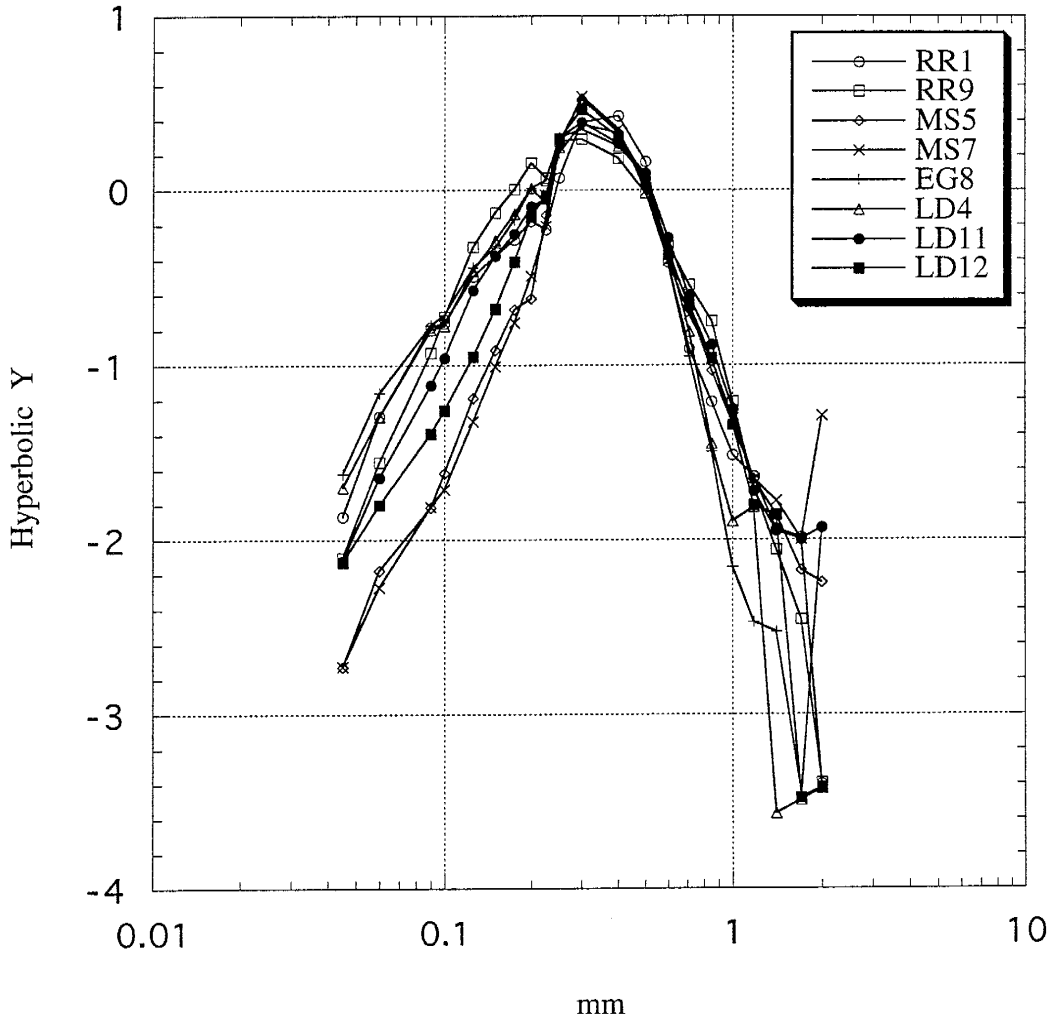

Log-Hyperbolic Distribution - Crossbeds, Group 2

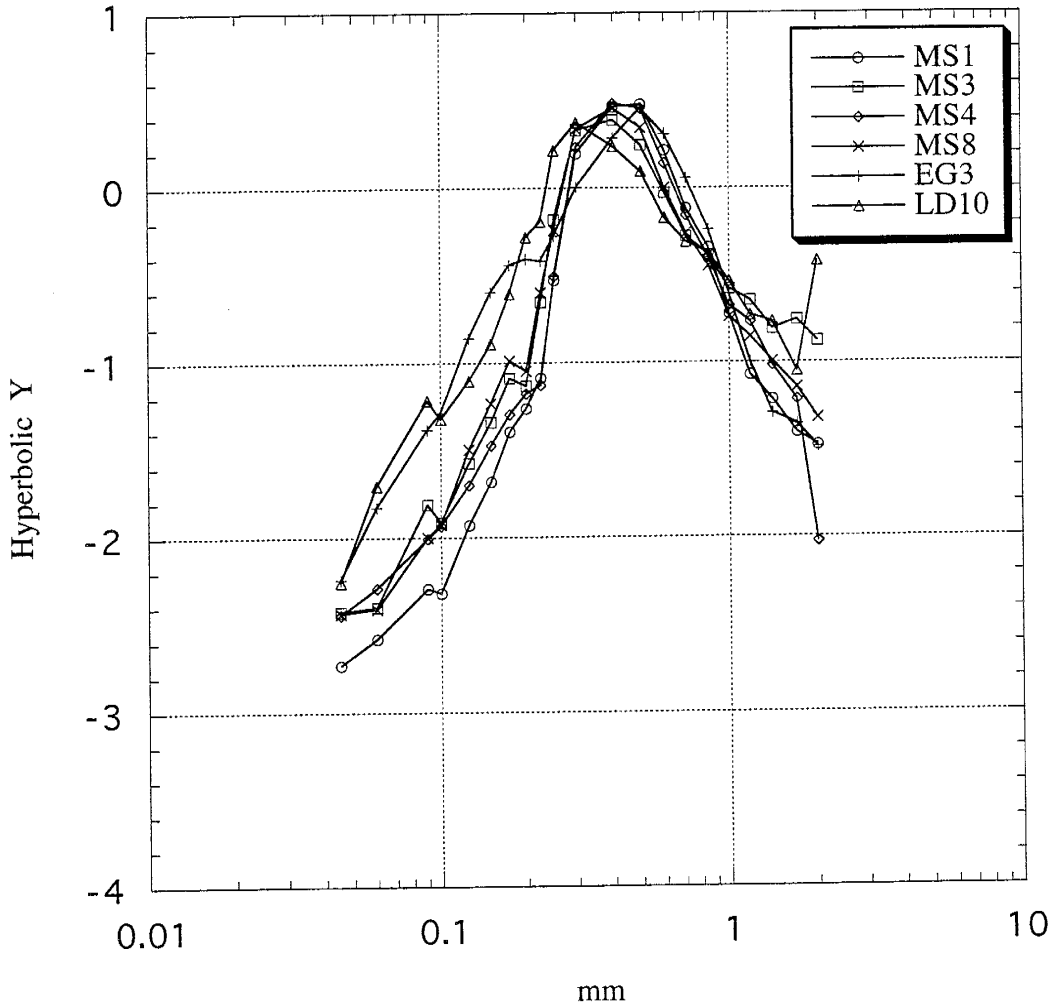

Log-Hyperbolic Distribution - Crossbeds, Group 3

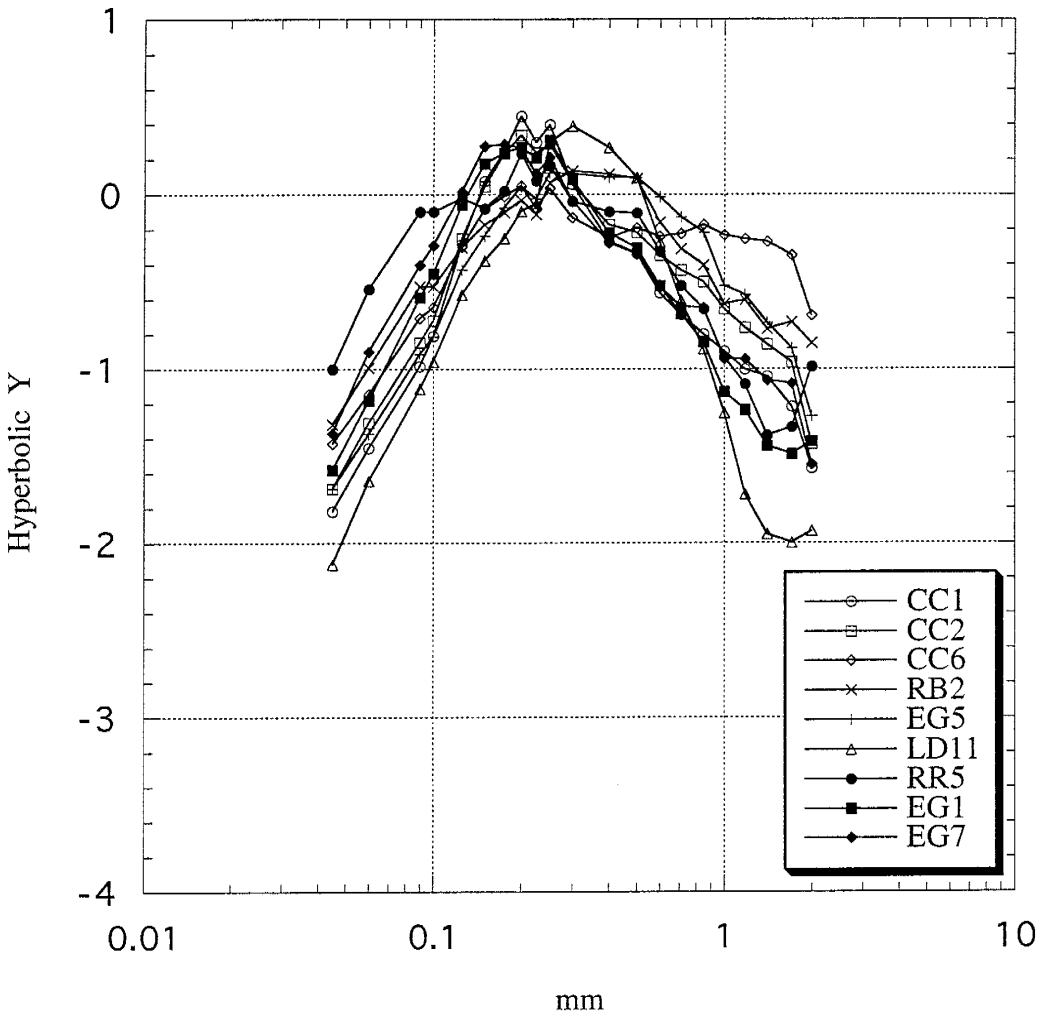

Log-Hyperbolic Distribution - Crossbeds, Group 4

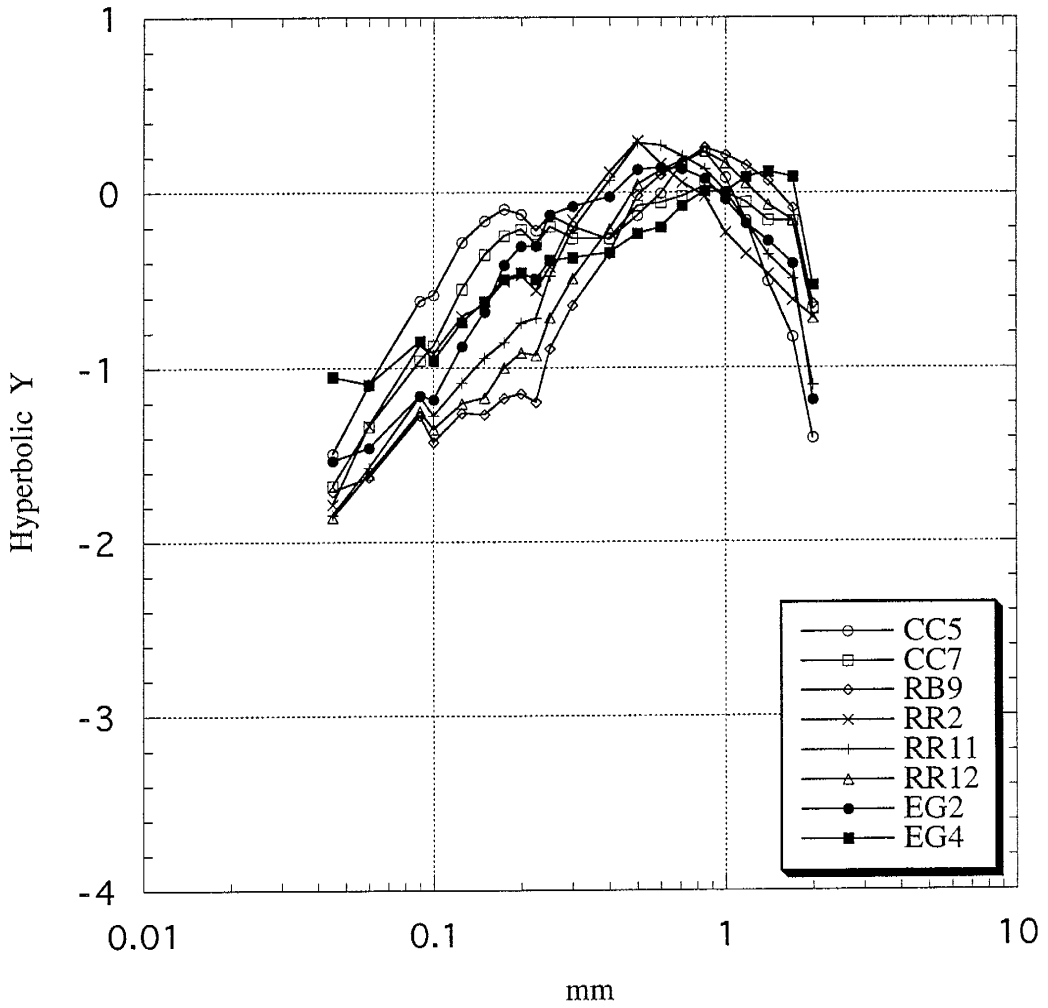

Log-Hyperbolic Distribution - Crossbeds, outliers

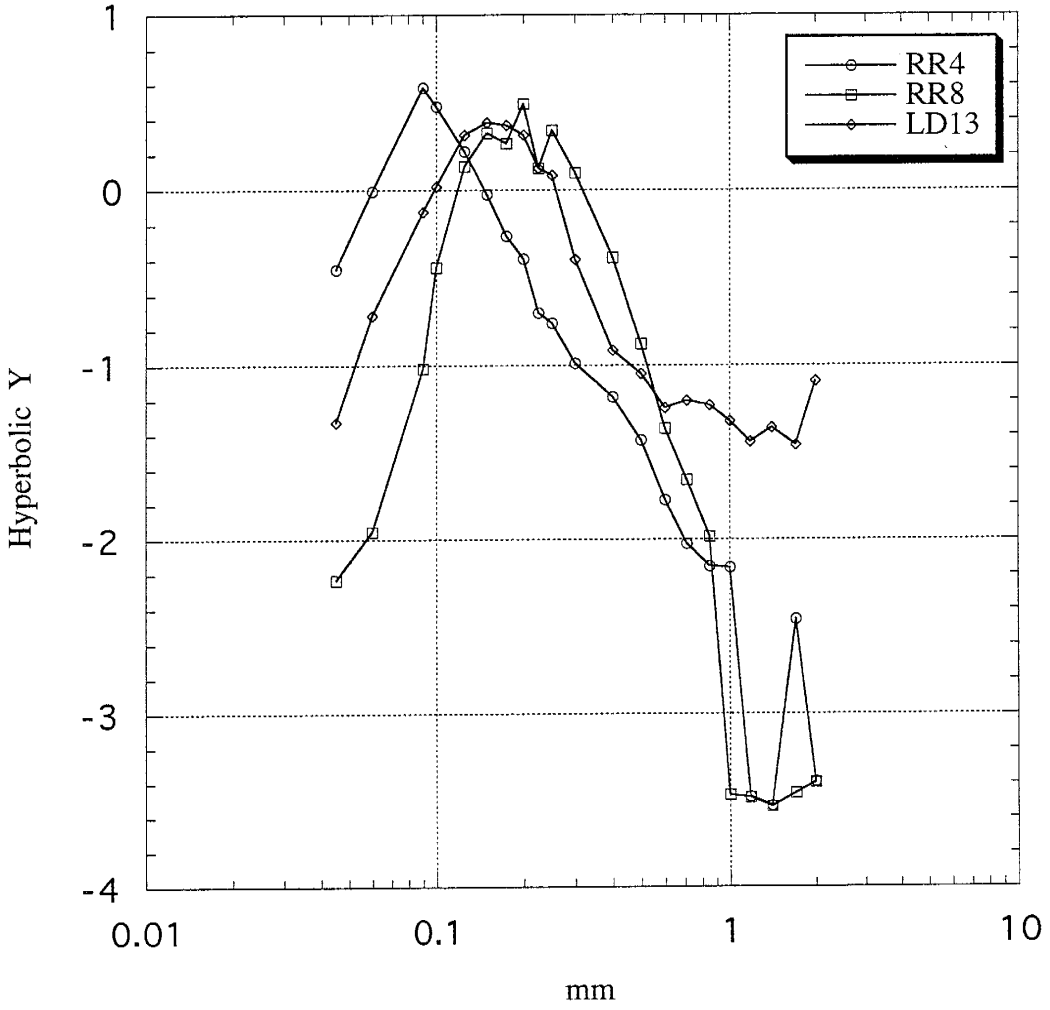

Log-Hyperbolic Distribution - Channels, Group 1

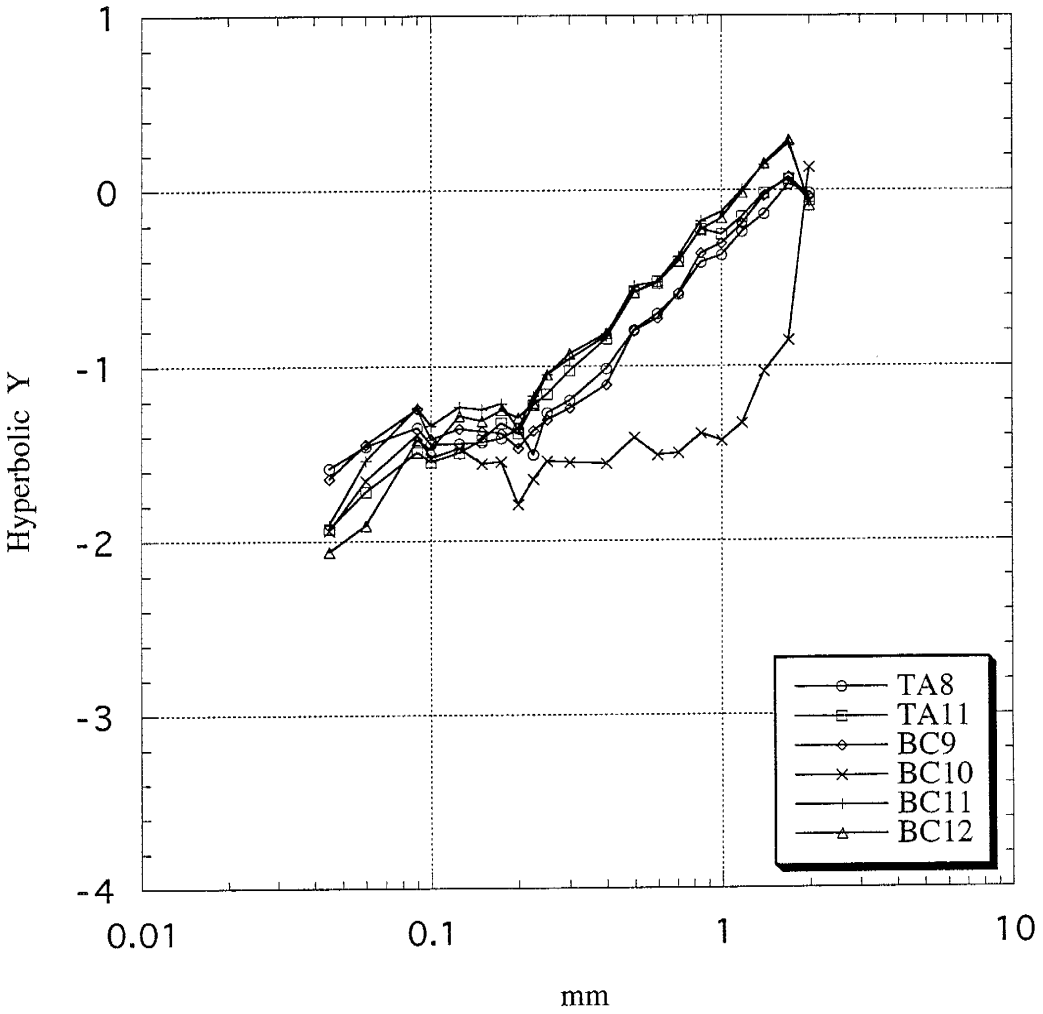

Log-Hyperbolic Distribution - Channels, Group 2

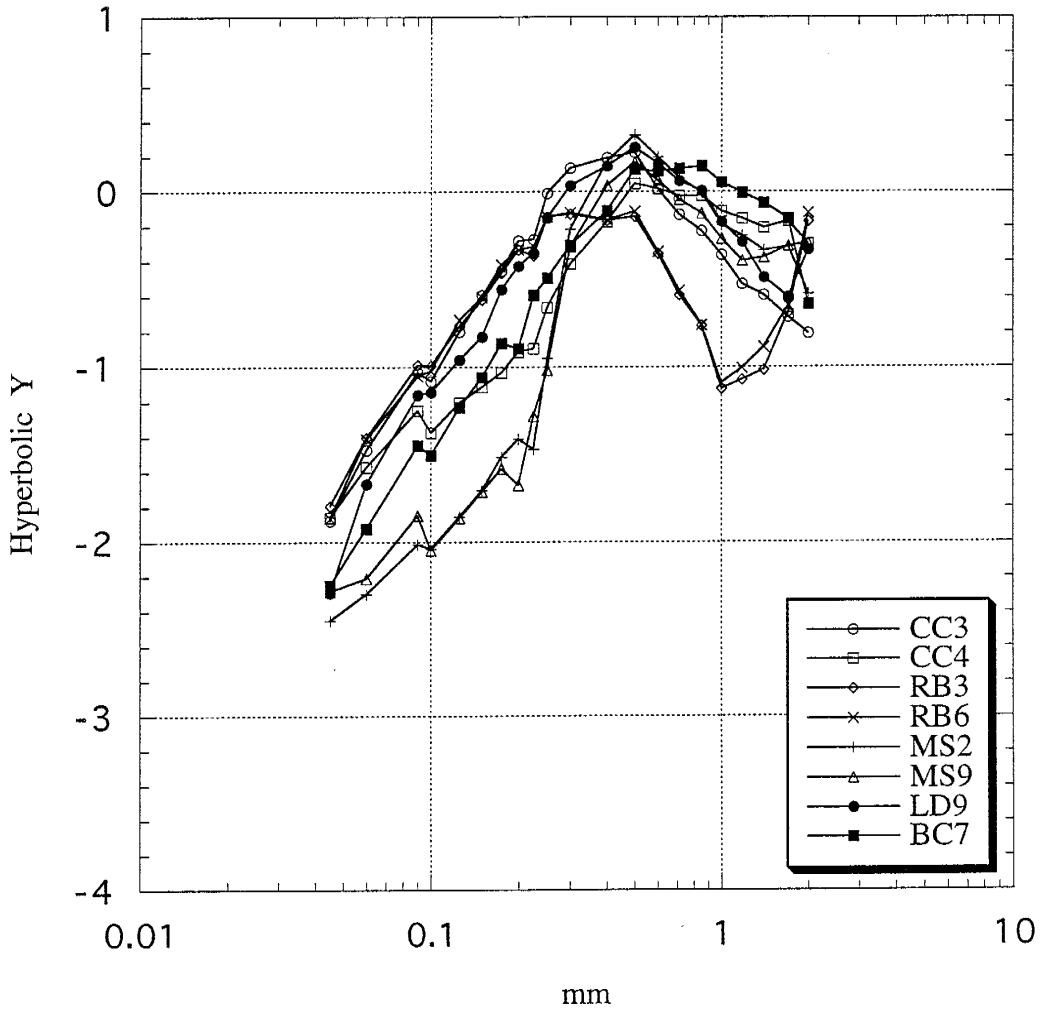

Log-Hyperbolic Distribution - Horizontal Laminations, Group 1

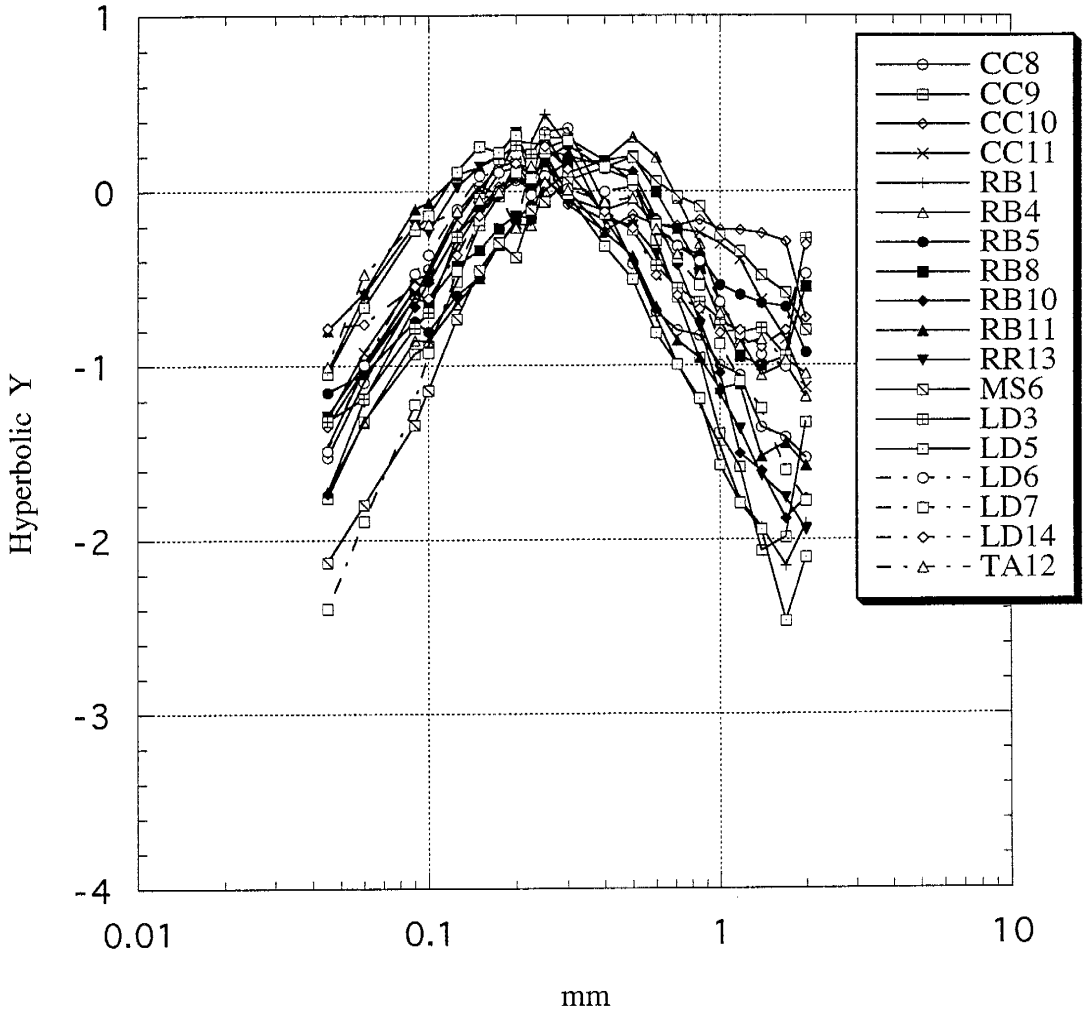

Log-Hyperbolic Distribution - Horizontal Laminations, Group 2

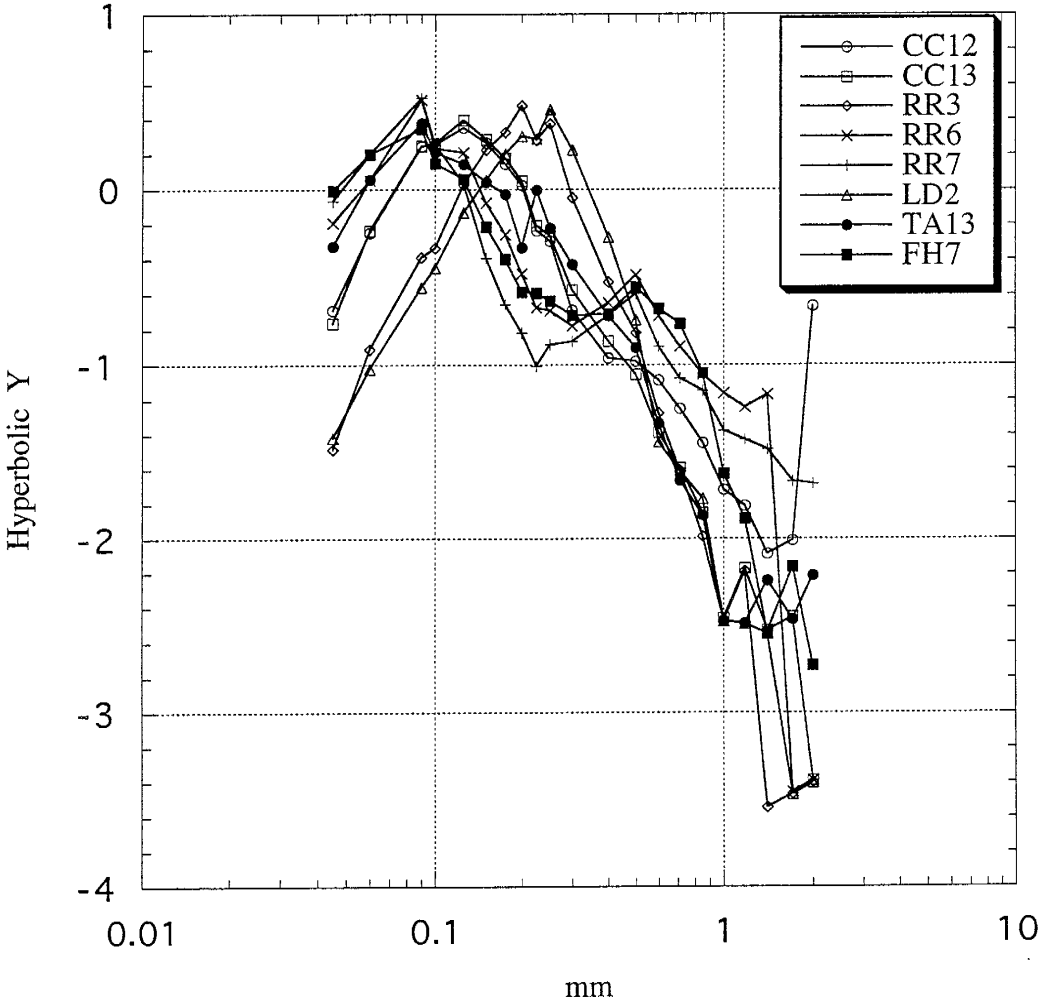

Log-Hyperbolic Distribution - Horizontal Laminations, Group 3

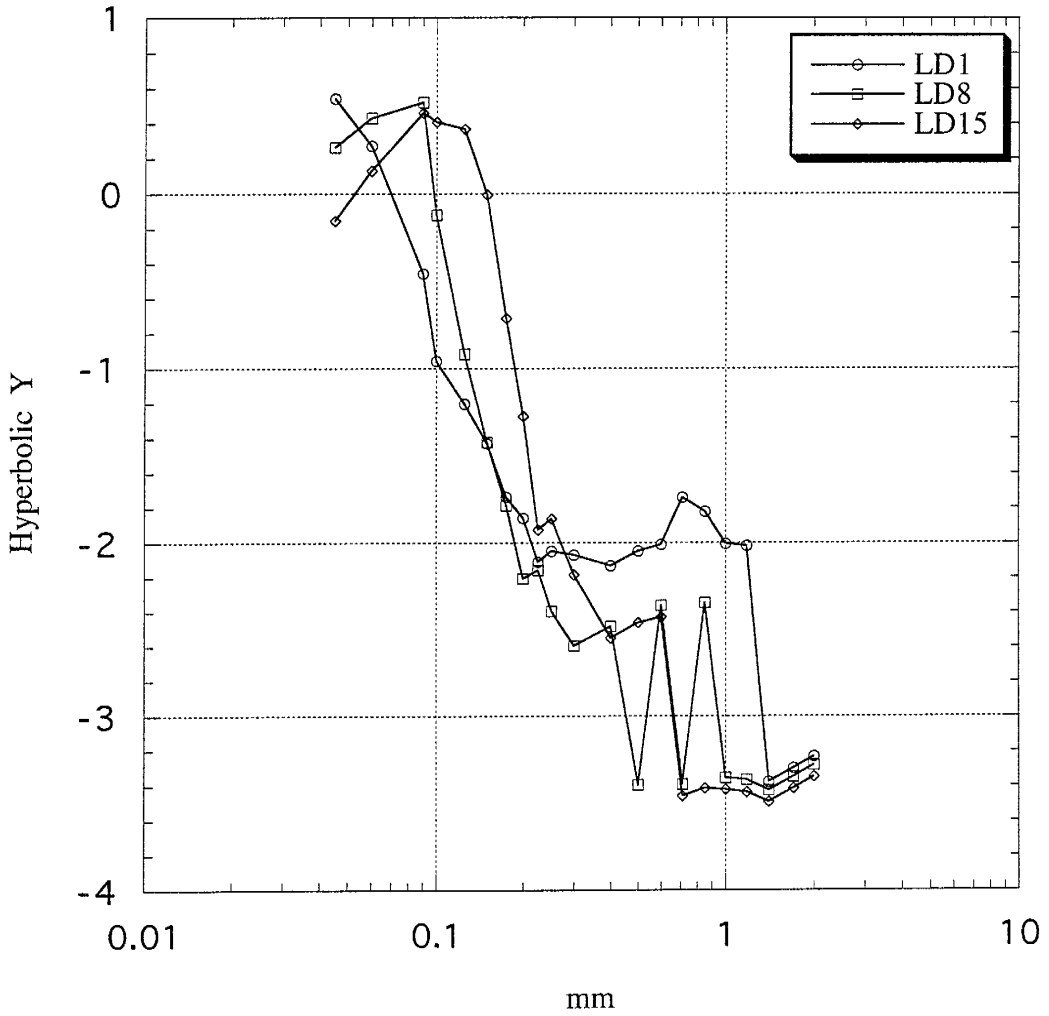

Log-Hyperbolic Distribution - Scour and Fill, Group 1

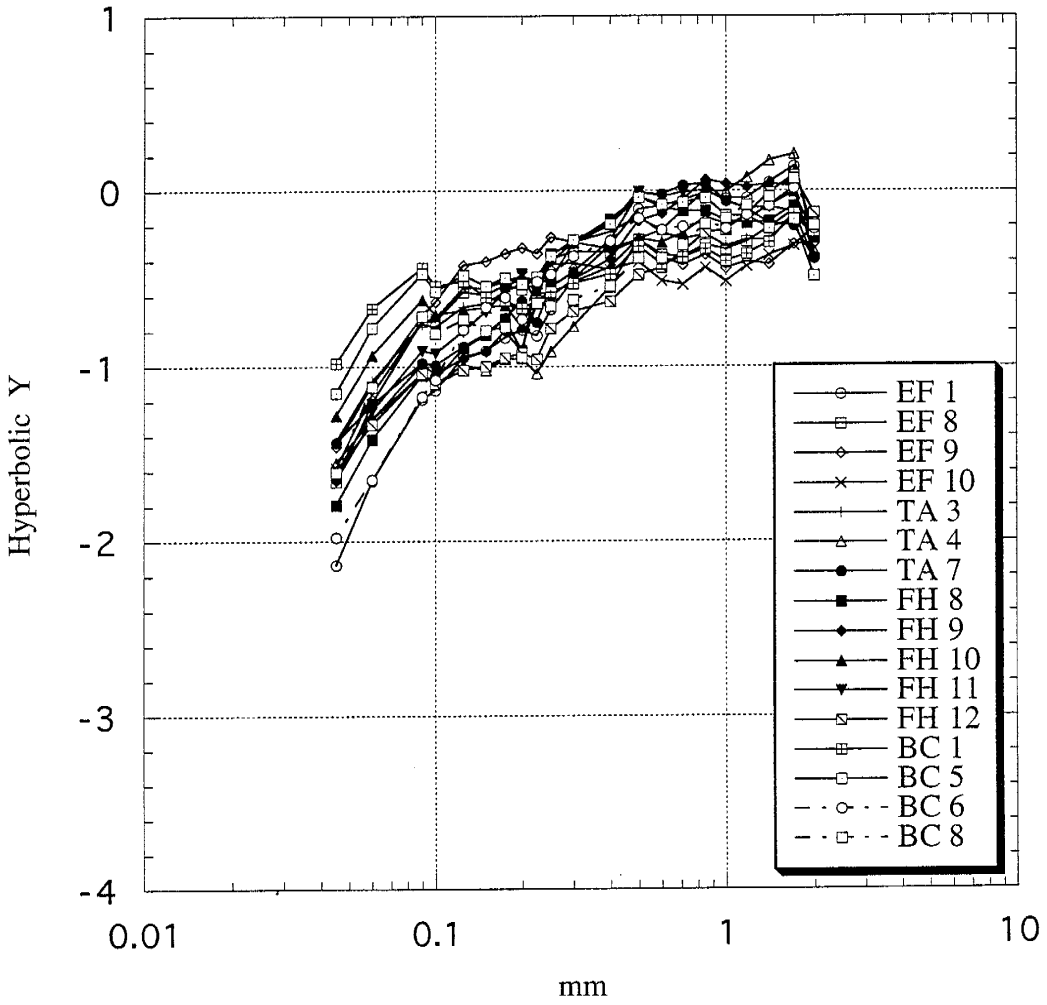

Log-Hyperbolic Distribution - Scour and Fill, Group 2

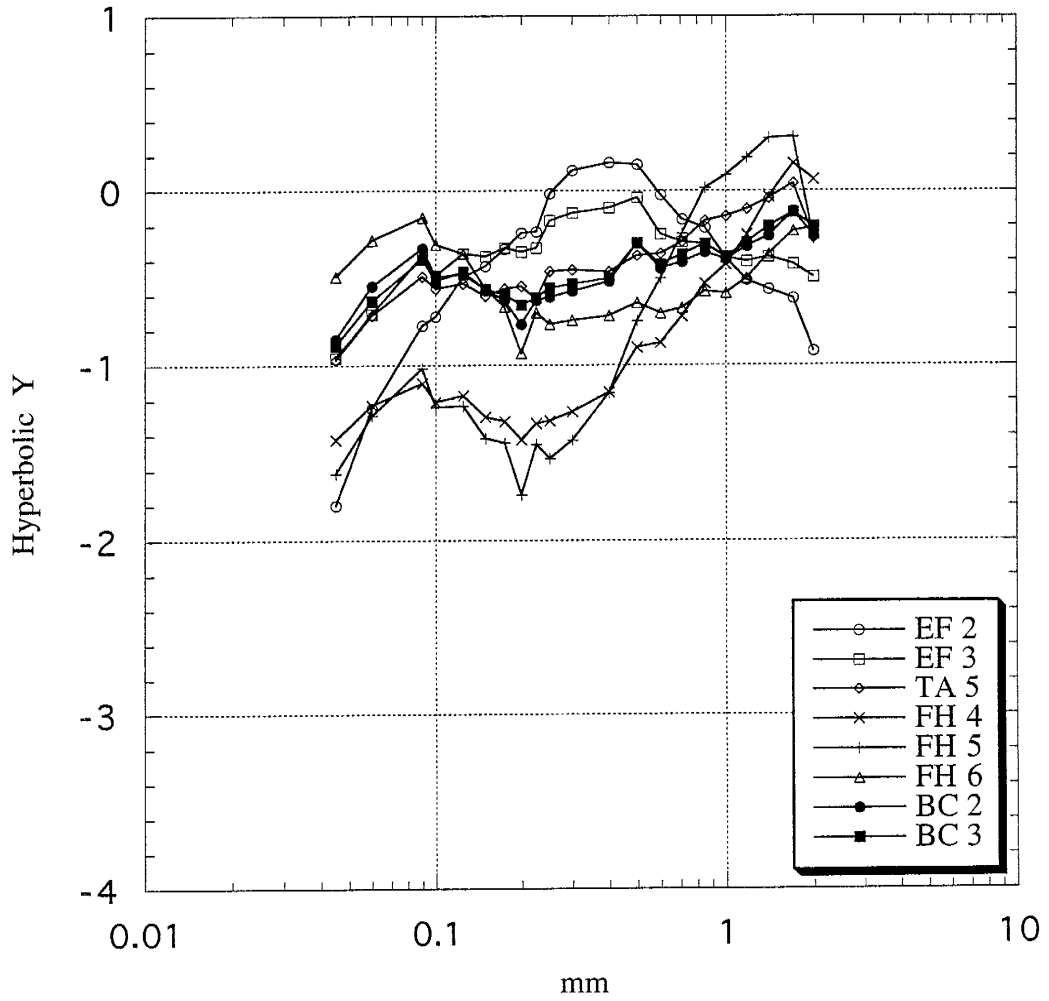

Log-Hyperbolic Distribution - Structureless, Group 1

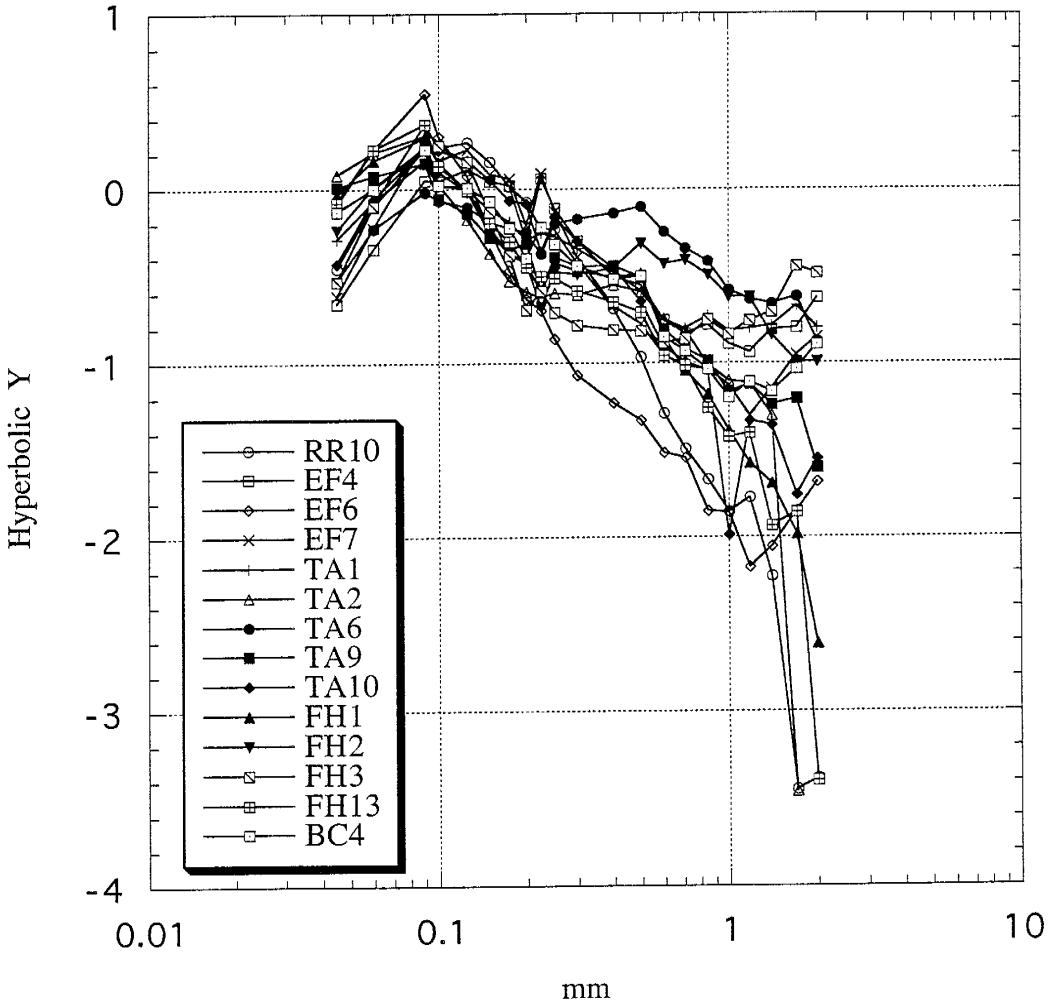

Log-Hyperbolic Distribution - Structureless, Outliers

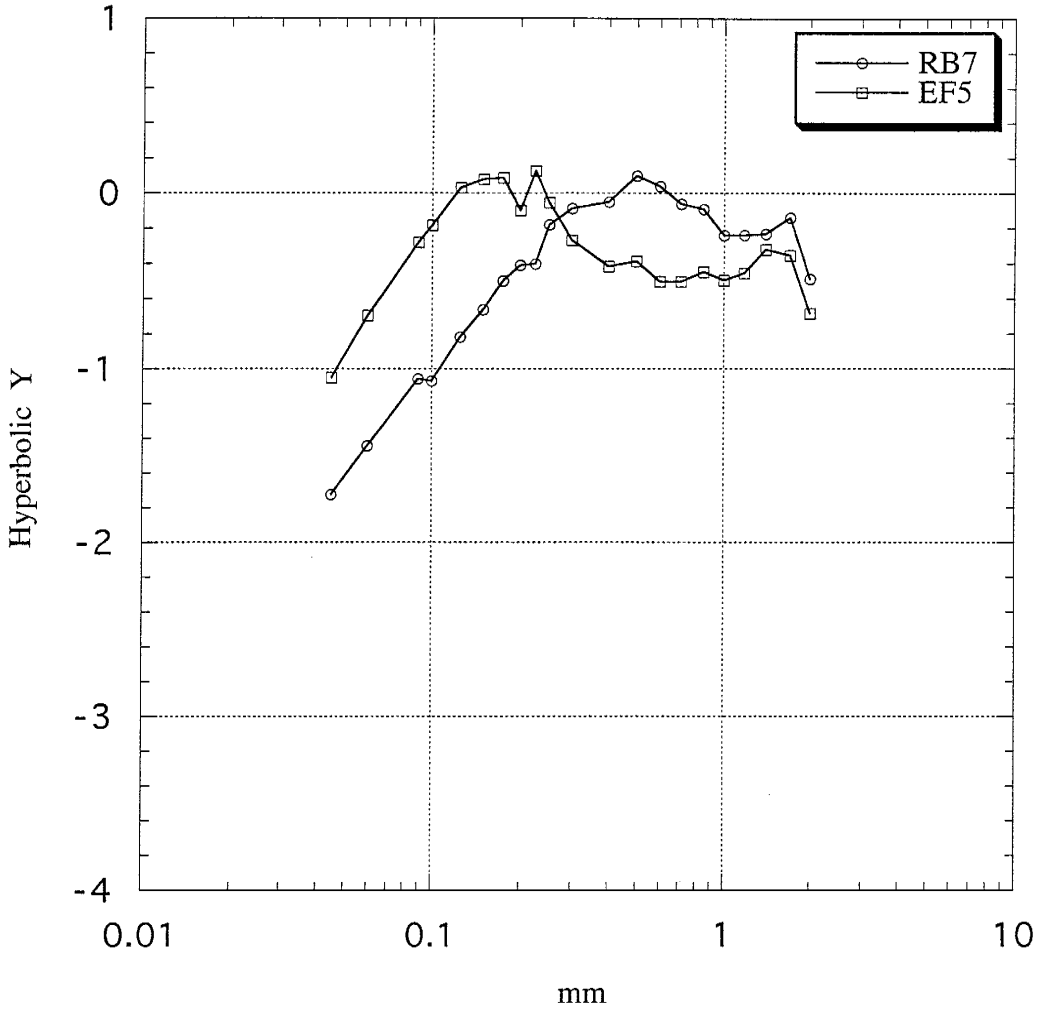

Cumulative Percent Plot - Crossbeds, Group 1

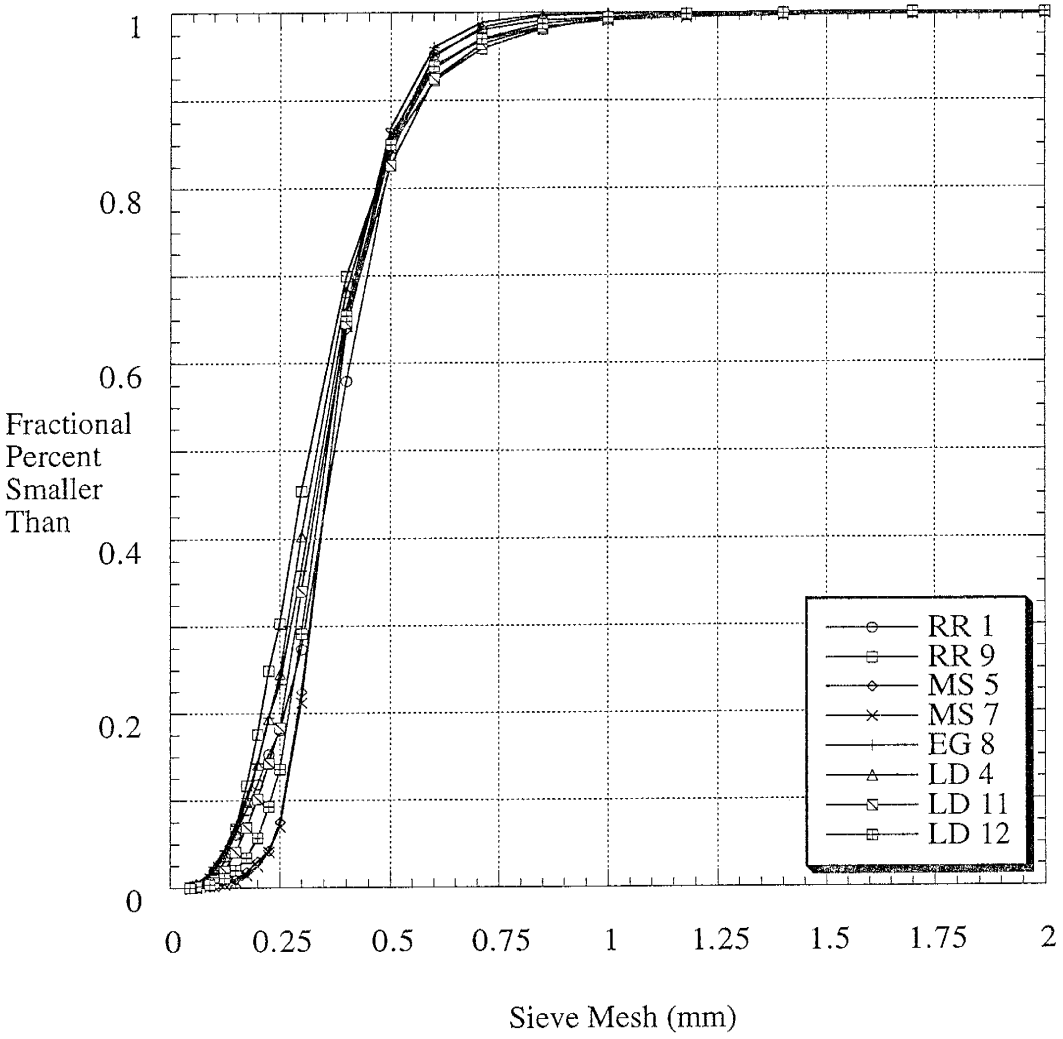

Cumulative Percent Plot - Crossbeds, Group 2

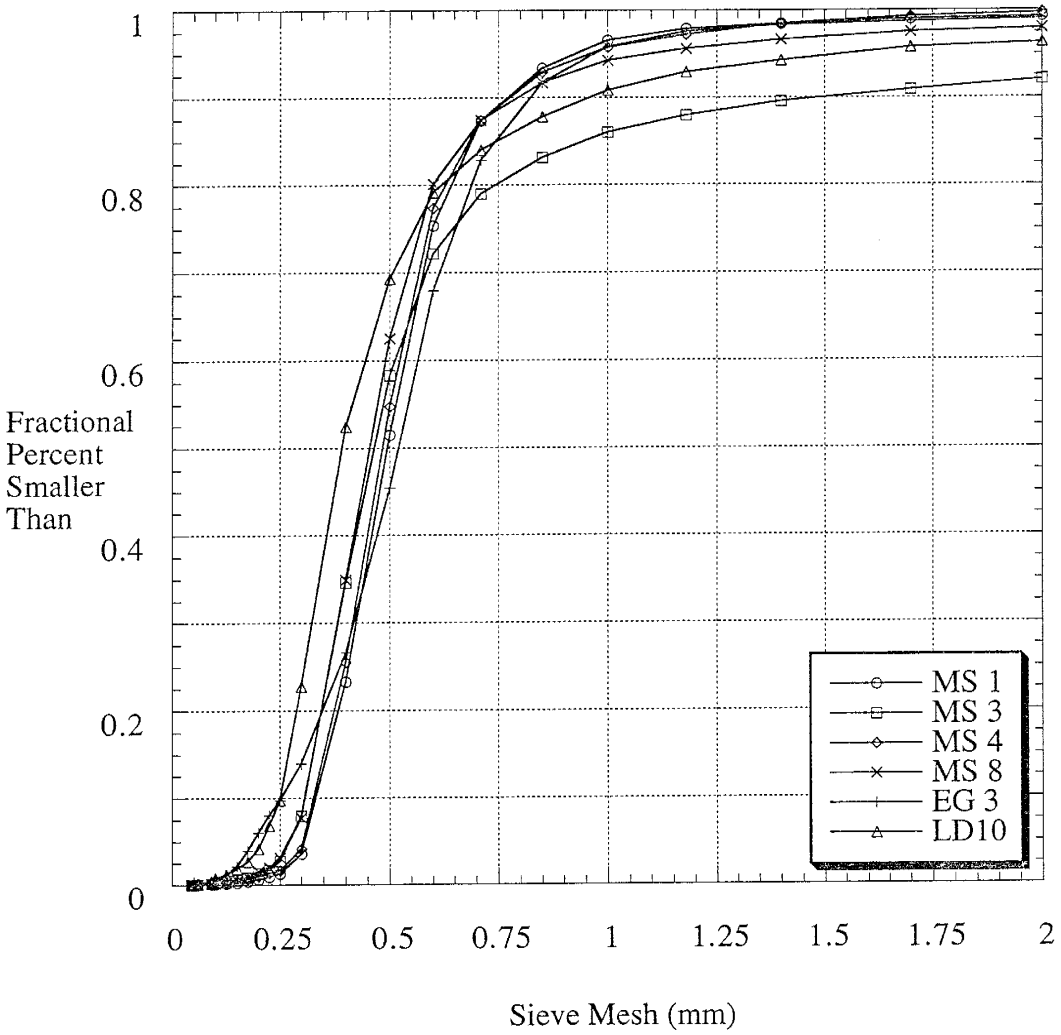

Cumulative Percent Plot - Crossbeds, Group 3

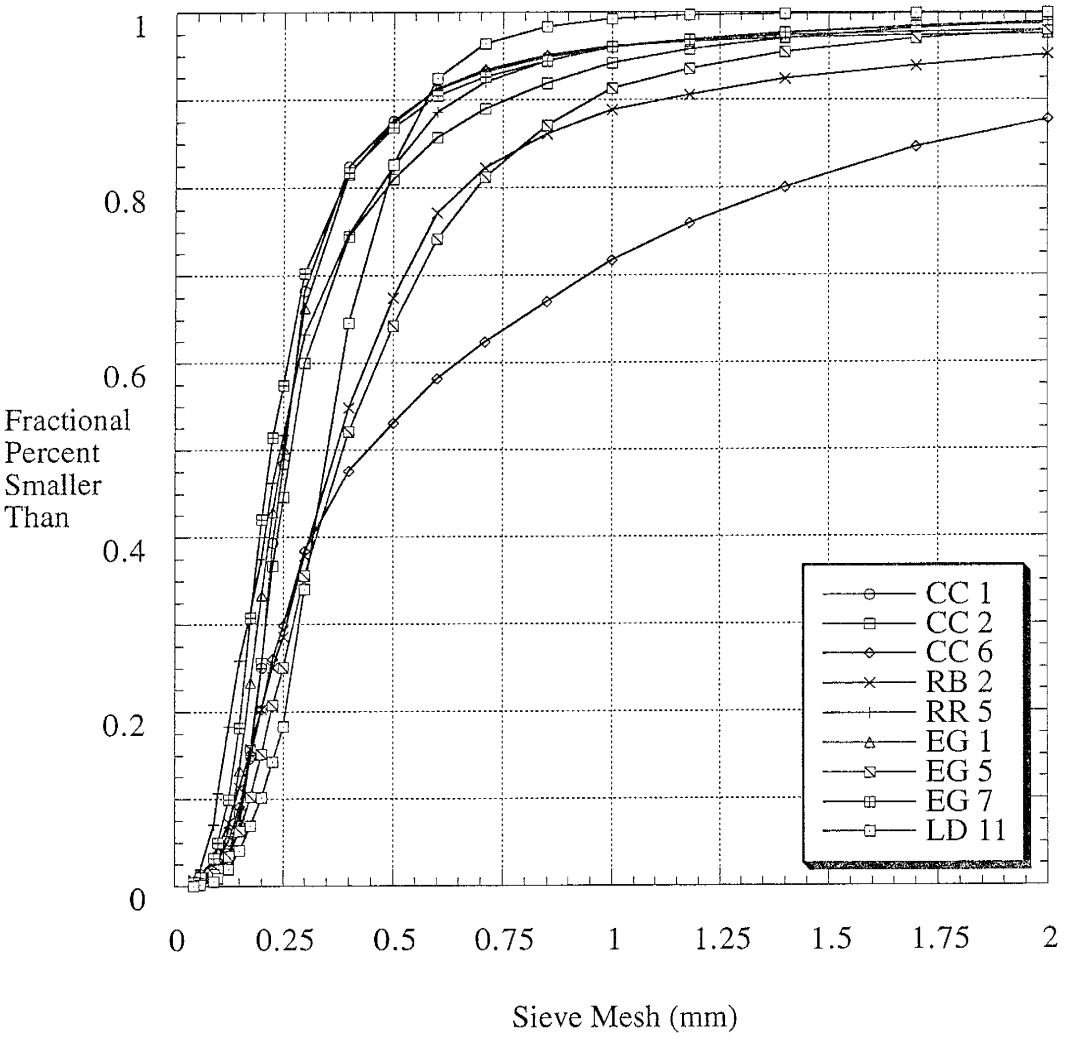

Cumulative Percent Plot - Crossbeds, Group 4

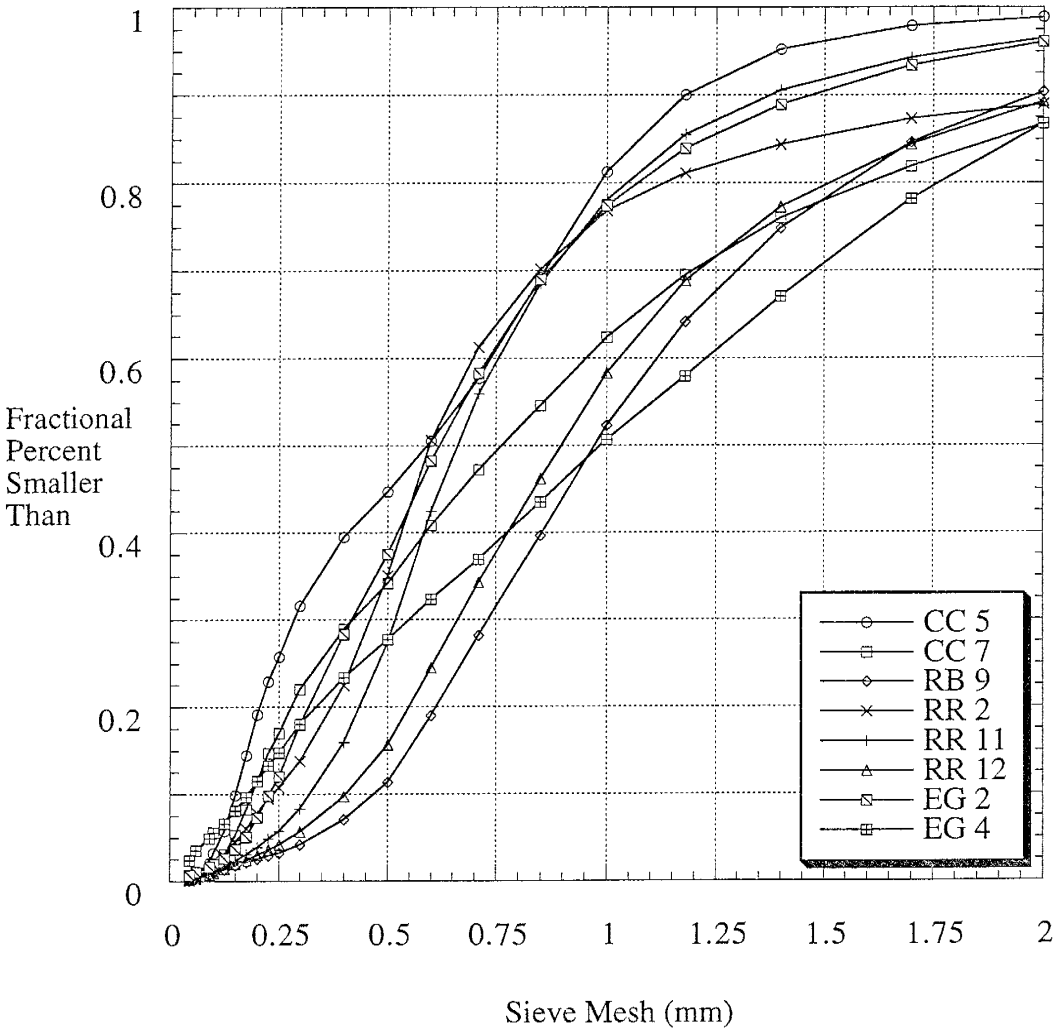

Cumulative Percent Plot - Crossbeds, outliers

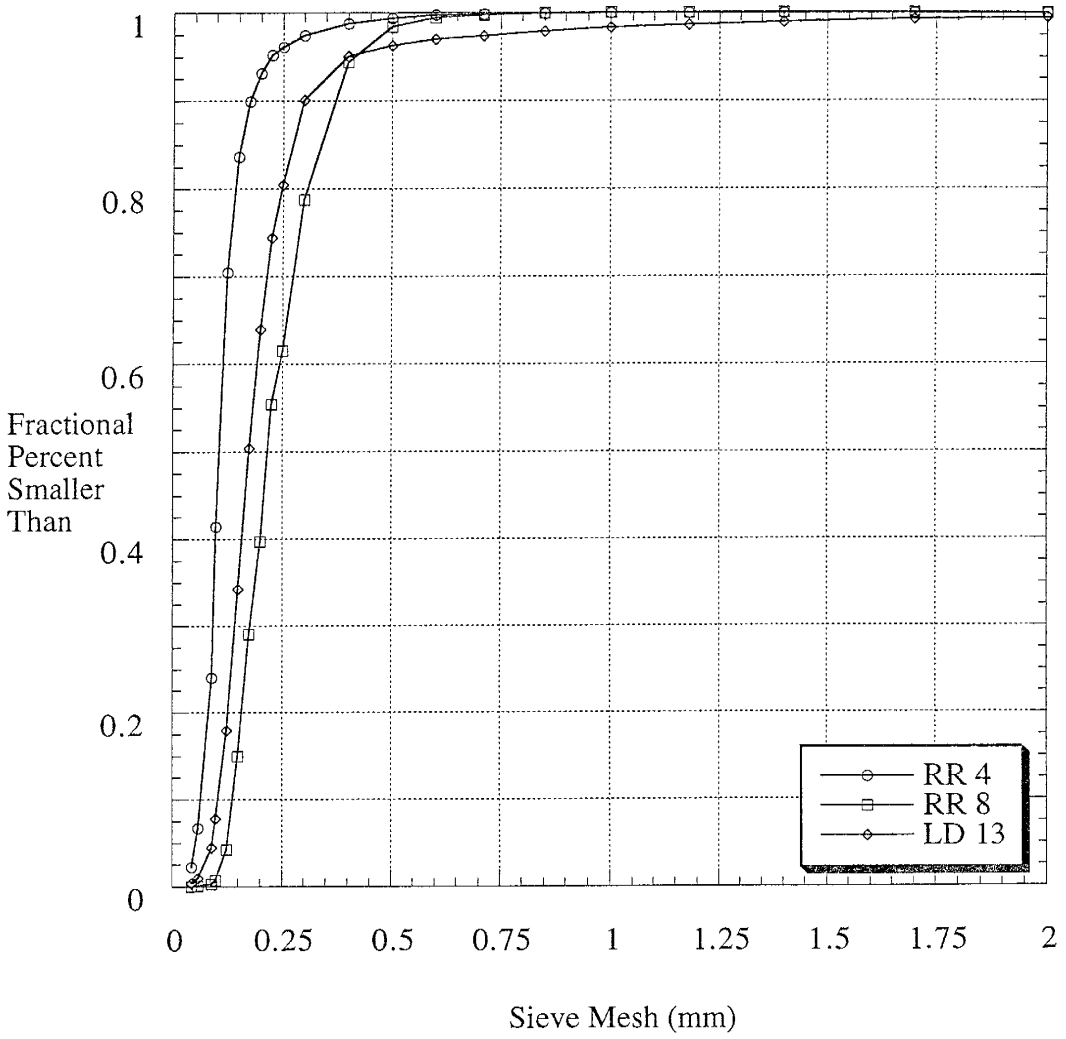

Cumulative Percent Plot - Channels, Group 1

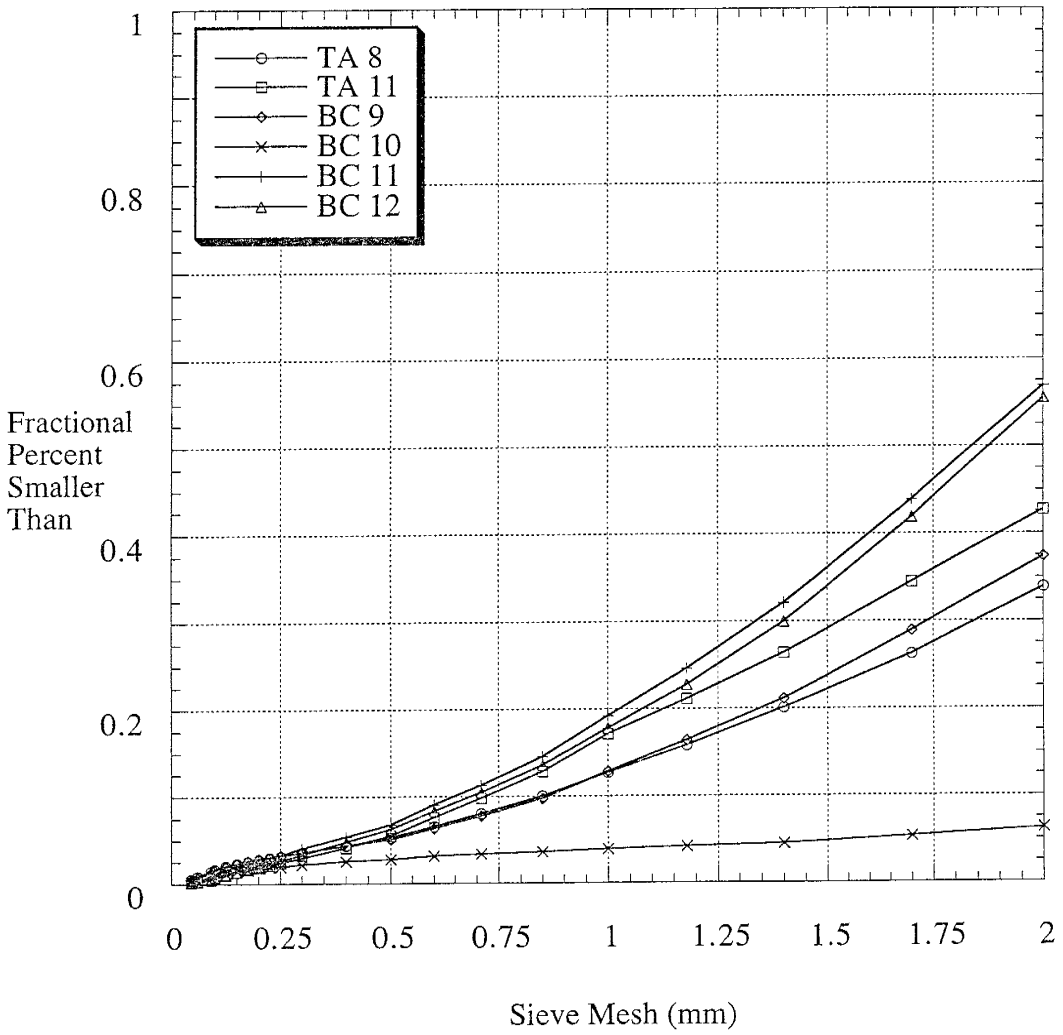

Cumulative Percent Plot - Channels, Group 2

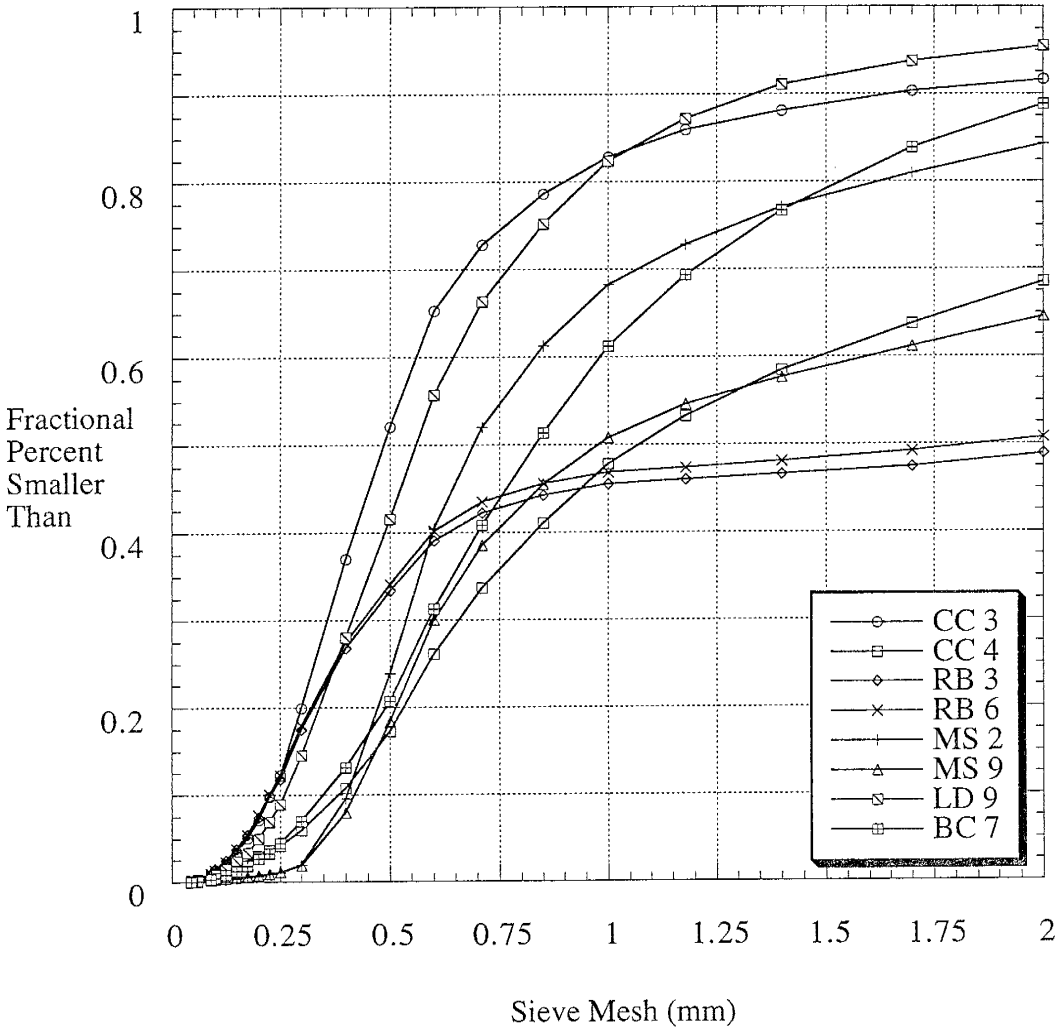

Cumulative Percent Plot - Horizontal Laminations, Group 1

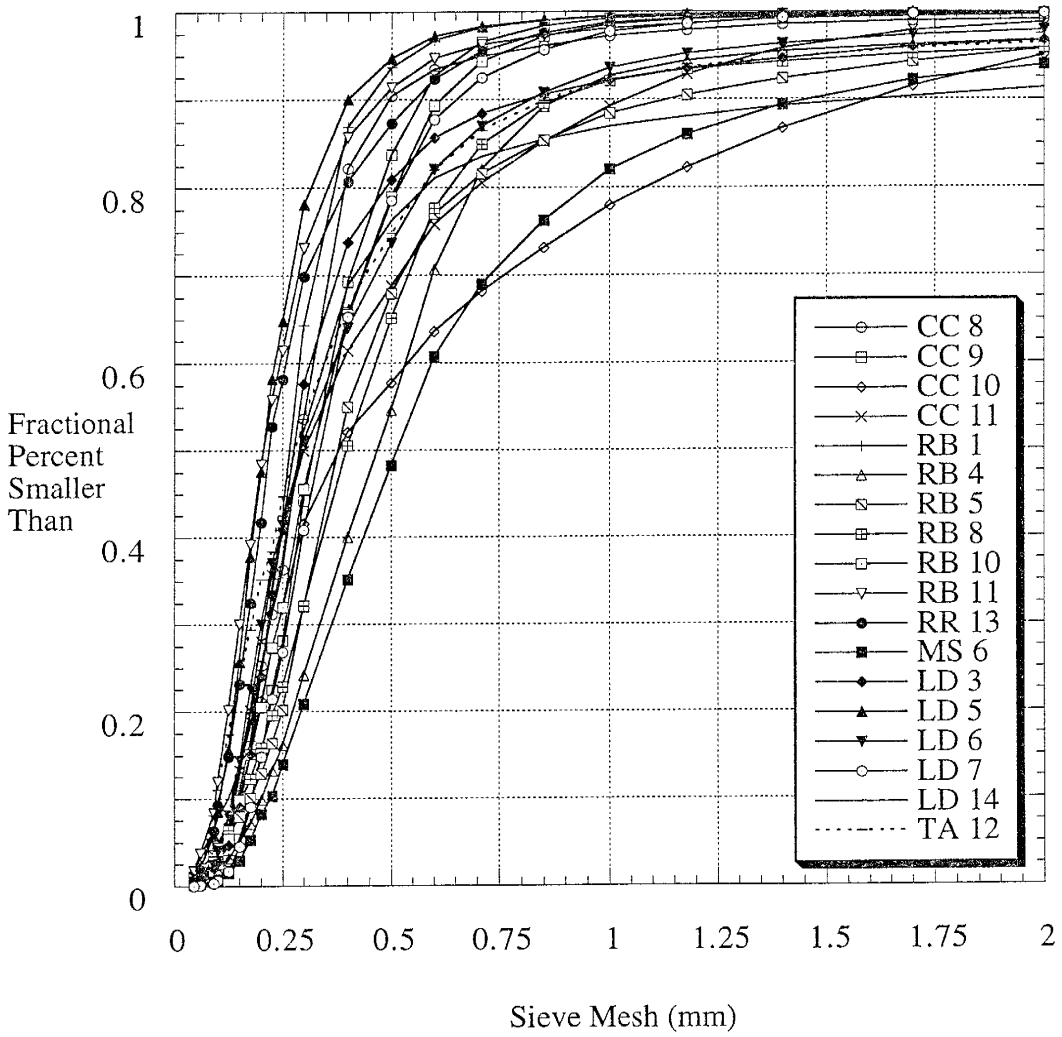

Cumulative Percent Plot - Horizontal Laminations, Group 2

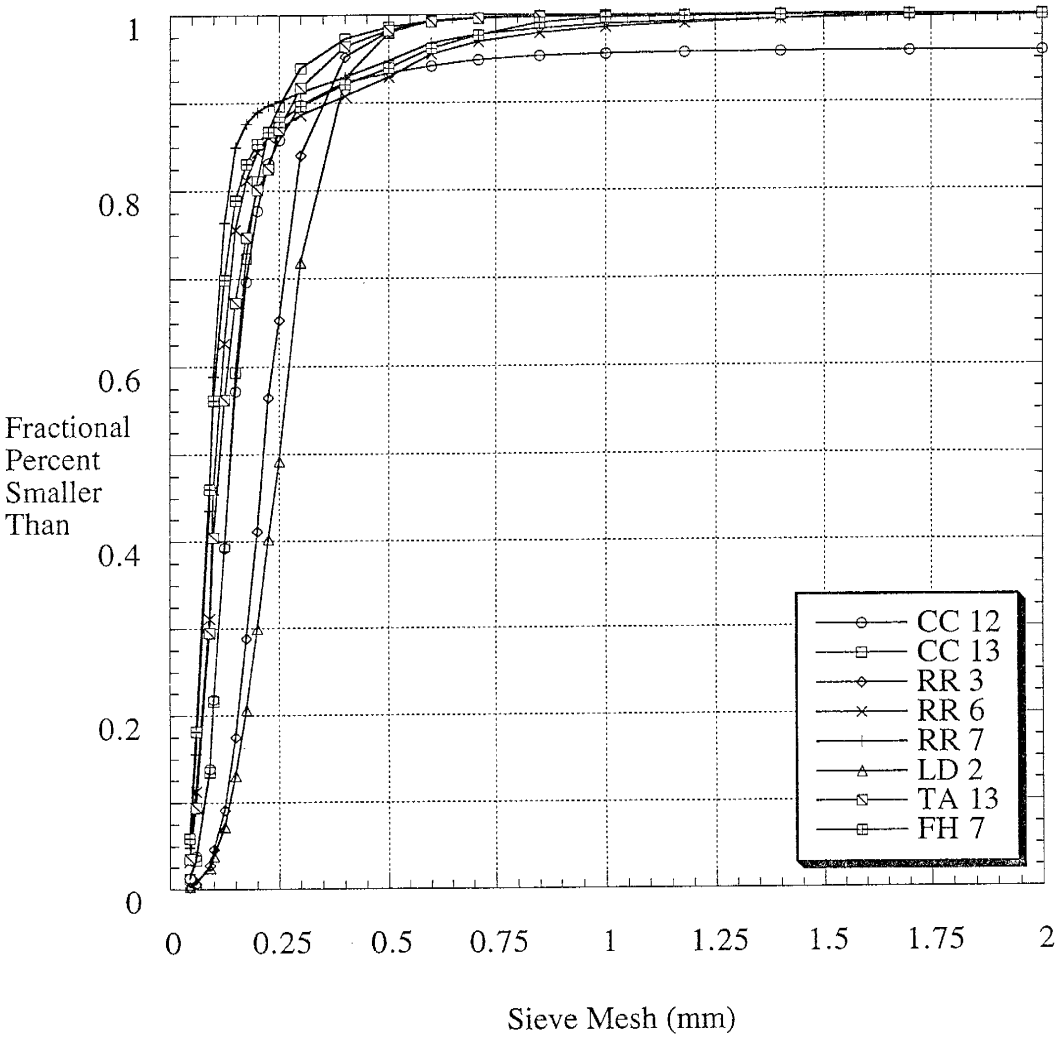

Cumulative Percent Plot - Horizontal Laminations, Group 3

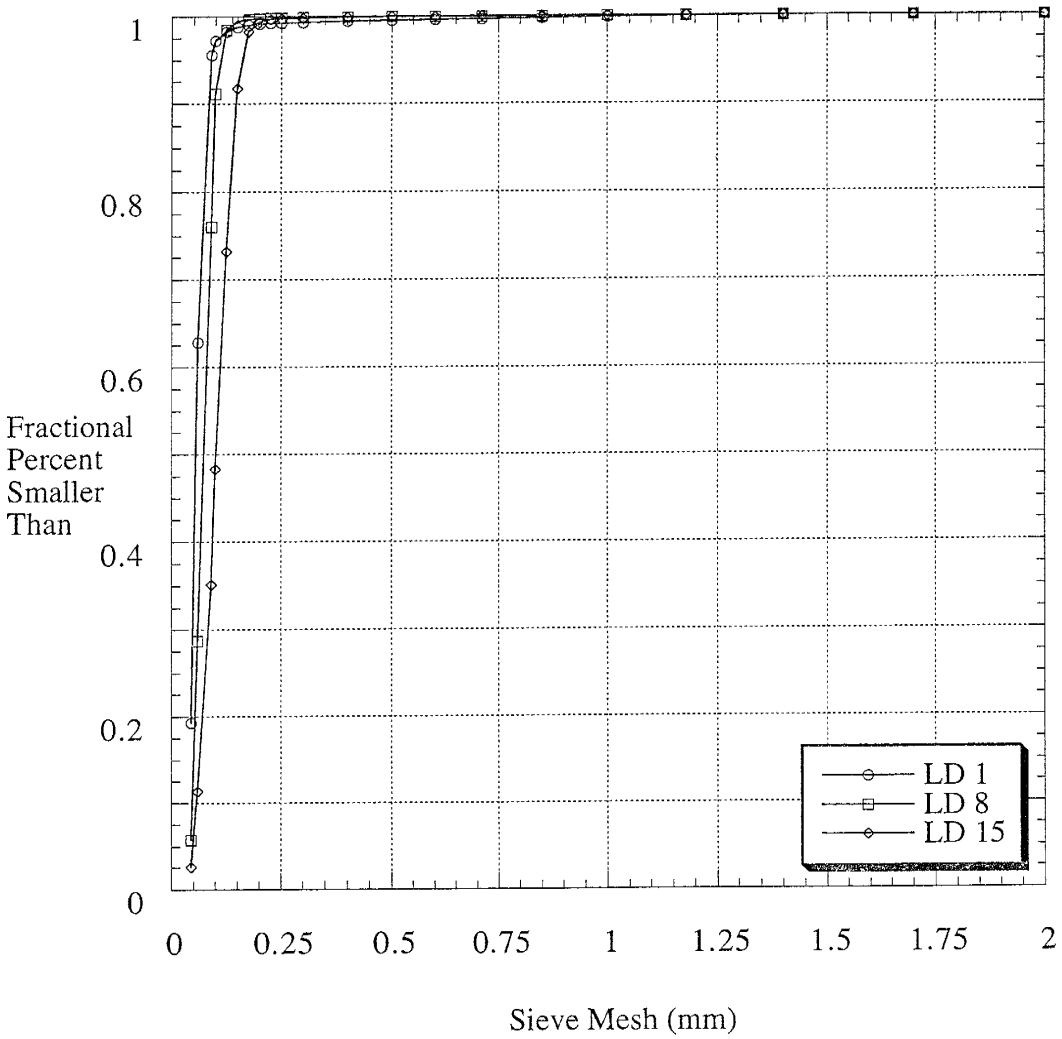

Cumulative Percent Plot - Scour and Fill, Group 1

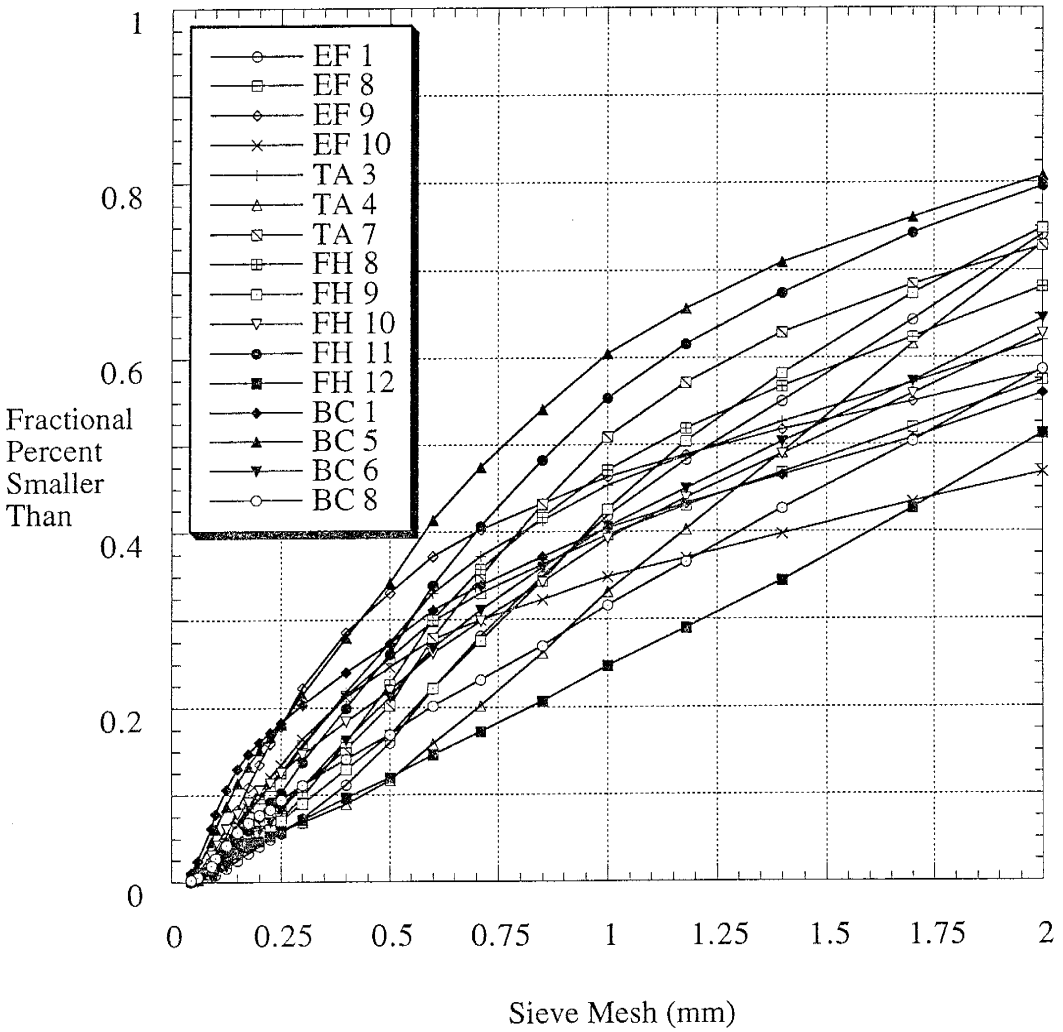

Cumulative Percent Plot - Scour and Fill, Group 2

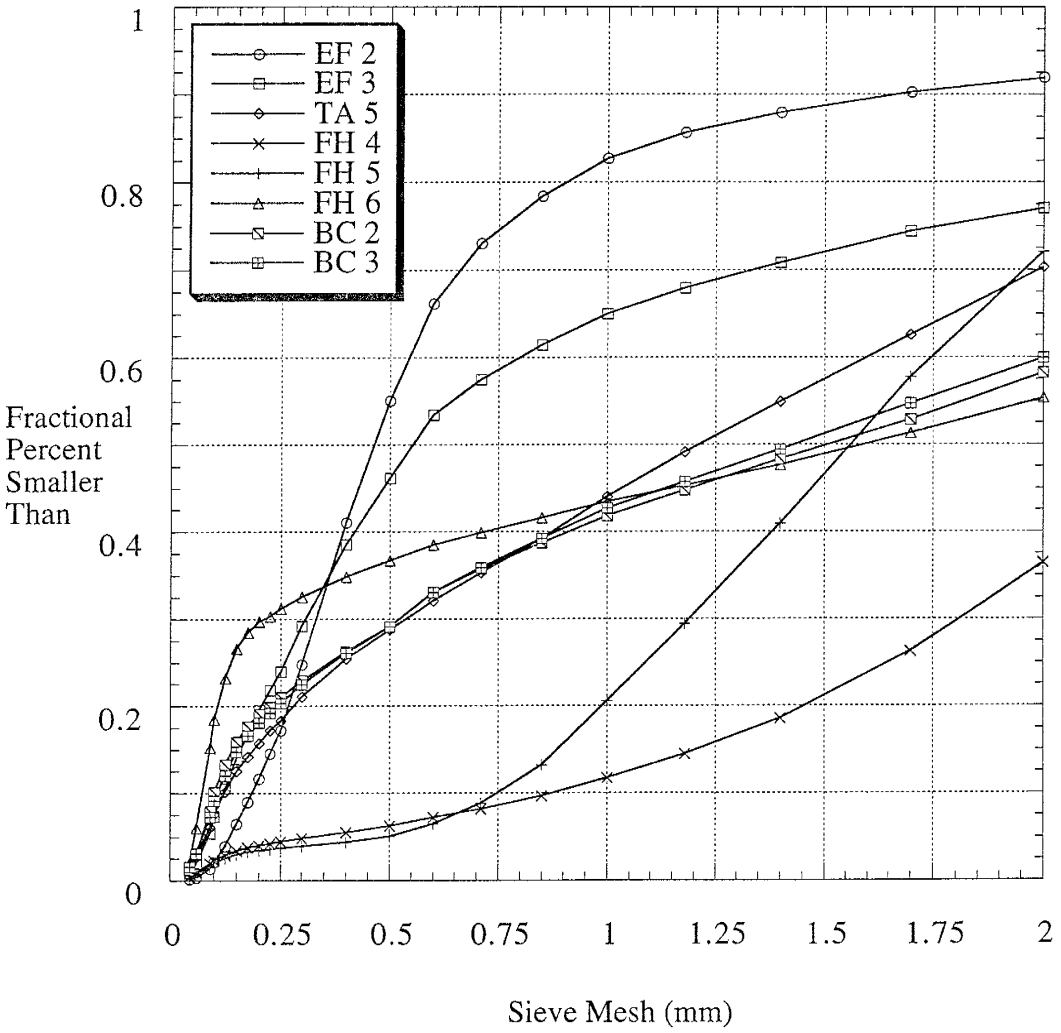

Cumulative Percent Plot - Structureless, Group 1

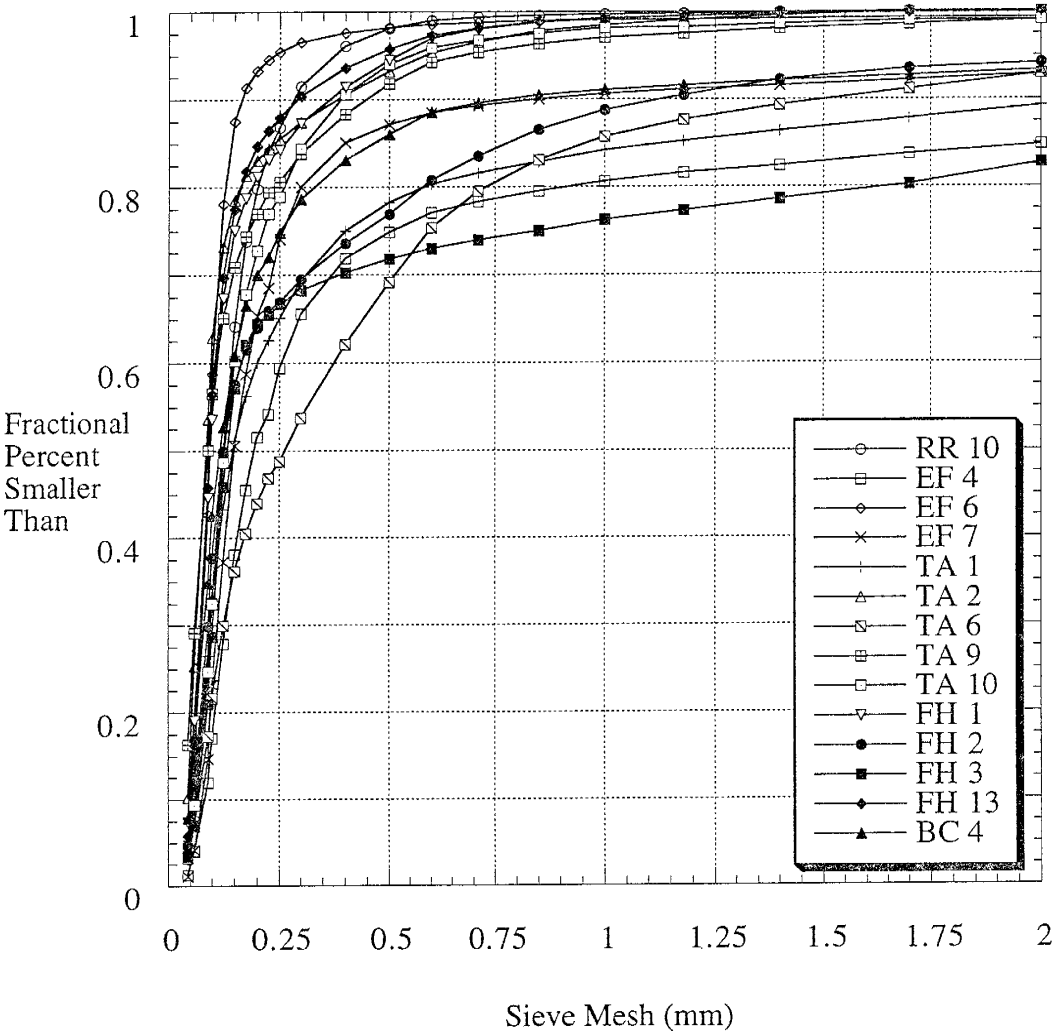

Cumulative Percent Plot - Structureless, Outliers

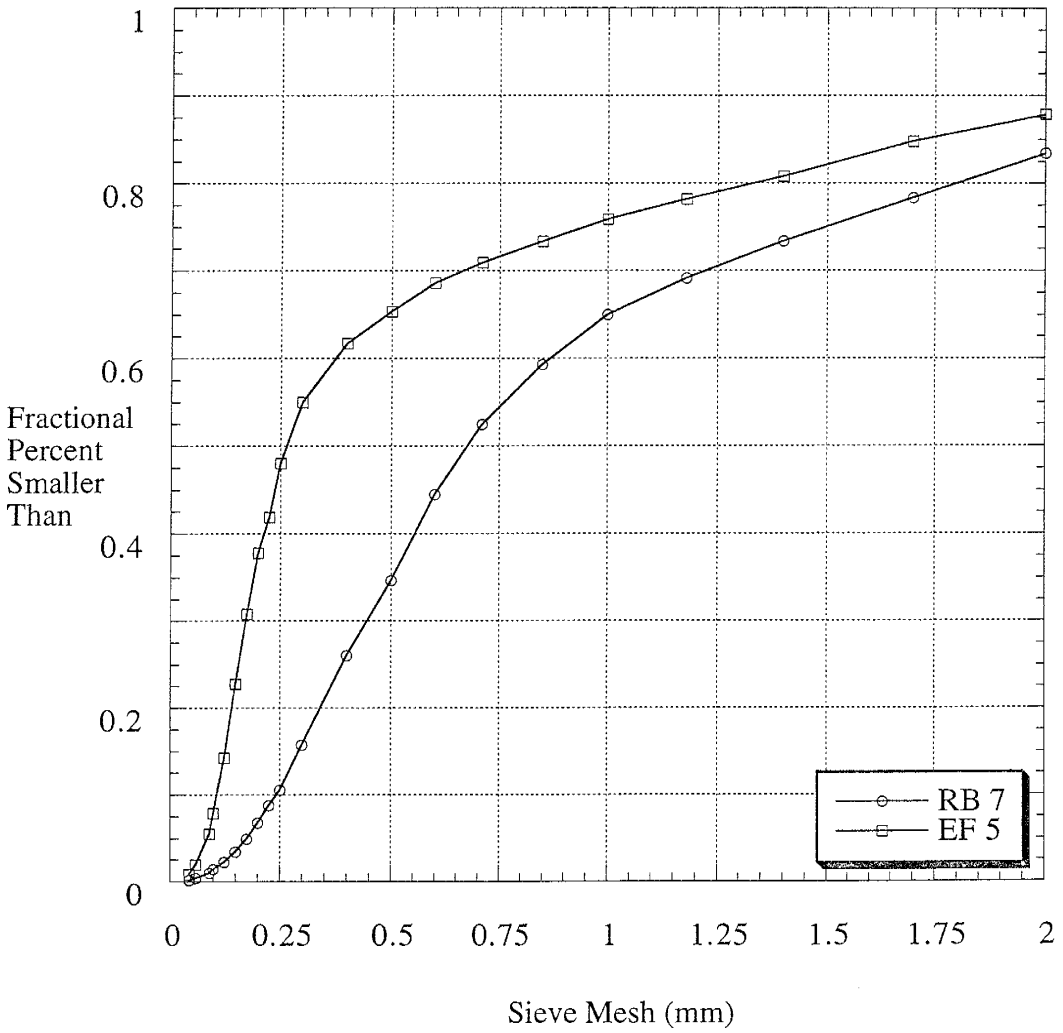

Sample	Structure	MeasPerm	Cement	Porosity	Complete Mean	Std. Dev.	Skewness	M^3 Dev	%>4.5phi	%<-1phi	Max.Diam.
Crossbeds Group 1											
RR1	CB	48.162	1	0.409	1.535	0.658	1.109	0.316	0.073	0.002	-1.007
RR9	CB	20.145	1	0.438	1.681	0.700	0.220	0.075	0.049	0.002	-1.007
MS5	CB	189.818	1	0.467	1.435	0.479	0.107	0.012	0.023	0.023	-1.138
MS7	CB	.	1	.	1.428	0.478	-0.262	-0.029	0.024	0.212	-1.138
EG8	CB	86.397	1	0.477	1.649	0.678	1.214	0.379	0.150	0.002	-1.007
LD4	CB	89.984	1	0.467	1.657	0.676	1.061	0.328	0.182	0.002	-1.007
LD11	CB	.	1	.	1.542	0.632	0.460	0.116	0.047	0.071	-1.070
LD12	CB	.	1	.	1.501	0.546	0.559	0.091	0.047	0.002	-1.007
Crossbeds Group 2											
MS1	CB	271.680	1	0.467	0.990	0.523	-0.751	-0.107	0.000	0.723	-1.722
MS3	CB	237.104	1	0.467	0.843	1.030	-1.517	-1.656	0.024	7.907	-3.000
MS4	CB	189.818	1	0.467	1.019	0.544	-0.283	-0.046	0.023	0.271	-1.963
MS8	CB	.	1	.	1.066	0.681	-1.323	-0.418	0.023	2.025	-2.406
EG3	CB	88.151	1	0.461	1.038	0.735	0.509	0.202	0.072	0.980	-2.000
LD10	CB	.	1	.	1.188	0.878	-0.941	-0.637	0.046	3.668	-2.000
Crossbeds Group 3											
CC1	CB	41.848	1	0.435	1.843	0.850	-1.352	-0.830	0.095	1.239	-2.536
CC2	CB	86.397	1	0.469	1.731	0.944	-0.763	-0.643	0.140	1.072	-1.963
CC6	CB	98.224	2	0.458	0.926	1.590	-0.317	-1.275	0.340	12.249	-3.000
RB2	CB	57.630	2	0.455	1.398	1.228	-0.138	-0.255	0.647	4.842	-2.138
RR5	CB	2.828	1	0.441	2.002	1.134	-0.210	-0.306	0.698	1.953	-1.632
EG1	CB	44.981	1	0.489	1.890	1.003	-1.387	-1.398	0.252	2.447	-3.121
EG5	CB	77.270	1	0.461	1.330	1.039	-0.098	-0.110	0.326	2.072	-2.293
EG7	CB	56.233	1	0.514	2.021	0.989	-0.688	-0.665	0.434	1.038	-2.233

Sample	Structure	MeasPerm	Cement	Porosity	Complete Mean	Std. Dev.	Skewness	M^3 Dev	%>4.5phi	%<-1phi	Max.Diam.
Crossbeds Group 4											
CC5	CB	165.608	2	0.534	1.070	1.202	0.532	0.925	0.276	1.104	-1.926
CC7	CB	132.641	2	0.441	0.465	1.464	0.073	0.231	0.191	13.284	-3.036
RB9	CB	74.671	2	0.391	0.060	0.973	0.734	0.676	0.073	9.609	-2.379
RR2	CB	120.884	1	0.409	0.609	1.254	-0.238	-0.470	0.091	11.002	-2.868
RR11	CB	117.447	1	0.326	0.599	0.939	0.490	0.406	0.180	3.482	-2.459
RR12	CB	141.959	1	0.367	0.138	1.088	0.343	0.442	0.151	10.685	-2.848
EG2	CB	137.130	2	0.472	0.758	1.166	0.509	0.806	0.662	3.872	-2.963
EG4	CB	141.959	2	0.472	0.374	1.636	1.201	5.263	2.390	13.202	-2.485
Crossbed Outliers											
RR4	CB	28.209	2	0.474	3.227	0.711	0.552	0.199	2.243	0.002	-1.007
RR8	CB	34.462	1	0.438	2.170	0.546	-0.115	-0.019	0.024	0.002	-1.007
LD13	CB	.	1	.	2.462	0.778	-0.968	-0.456	0.417	0.491	-1.585
Channels Group 1											
TA8	CH	271.680	2	0.302	-1.369	1.335	2.277	5.420	0.509	66.110	-3.293
TA11	CH	271.680	1	0.281	-1.178	1.262	1.560	3.135	0.211	57.318	-3.186
BC9	CH	210.681	1	0.274	-1.312	1.310	2.118	4.763	0.391	62.696	-3.263
BC10	CH	.	1	.	-1.951	0.902	5.149	3.782	0.144	93.744	-3.307
BC11	CH	271.680	1	0.288	-0.812	1.185	1.530	2.548	0.155	43.126	-2.678
BC12	CH	223.067	1	0.274	-0.896	1.157	1.430	2.212	0.151	44.495	-2.807
Channels Group 2											
CC3	CH	124.547	1	0.420	0.886	1.186	-0.653	-1.089	0.095	8.381	-2.807
CC4	CH	189.818	1	0.361	-0.283	1.431	0.271	0.795	0.129	31.488	-3.087
RB3	CH	44.981	1	0.384	-0.459	1.959	0.393	2.957	0.112	51.112	-3.511
RB6	CH	81.559	1	0.235	-0.318	1.874	0.362	2.384	0.107	49.227	-3.170
MS2	CH	253.153	1	0.467	0.197	1.144	-0.729	-1.090	0.022	15.685	-3.000
MS9	CH	.	1	.	-0.387	1.449	-0.059	-0.179	0.065	35.427	-3.322
LD9	CH	.	1	.	0.804	0.968	-0.126	-0.115	0.021	4.511	-2.000
BC7	CH	271.680	1	0.399	0.217	1.087	0.022	0.028	0.047	11.202	-2.632

Sample	Structure	MeasPerm	Cement	Porosity	Complete Mean	Std. Dev.	Skewness	M^3 Dev	%>4.5phi	%<-1phi	Max.Diam.
Horizontal Group 1											
CC8	HL	89.984	1	0.446	1.837	0.834	-0.325	-0.189	0.174	0.819	-1.926
CC9	HL	73.441	1	0.453	1.659	0.707	0.463	0.164	0.145	0.194	-1.138
CC10	HB	158.933	2	0.515	1.206	1.353	-0.042	-0.103	0.477	4.968	-1.888
CC11	HB	78.645	2	0.515	1.578	1.160	-0.086	-0.135	0.408	1.200	-1.536
RB1	HL	37.346	3	0.478	1.952	0.692	0.462	0.153	0.174	0.075	-1.070
RB4	HL	47.679	2	0.430	1.153	0.989	-0.168	-0.162	0.166	3.135	-2.585
RB5	HL	31.601	2	0.423	1.324	1.205	0.221	0.386	1.152	4.244	-2.202
RB8	HB	3.525	3	0.397	1.364	1.081	0.147	0.186	0.405	4.123	-1.485
RB10	HL	24.990	2	0.431	1.673	0.826	0.283	0.159	0.162	0.301	-1.585
RB11	HL	3.957	2	0.417	2.283	1.037	0.359	0.401	1.707	0.301	-1.379
RR13	HL	12.149	3	0.338	2.128	0.959	0.157	0.138	0.686	0.147	-1.433
MS6	HB	141.959	1	0.467	0.895	1.100	-0.229	-0.305	0.186	6.032	-2.263
LD3	HL	48.656	1	0.406	1.676	1.058	-0.833	-0.986	0.258	3.243	-2.000
LD5	HL	25.239	1	0.440	2.293	0.841	0.516	0.307	0.886	0.048	-1.070
LD6	HL	73.441	1	0.406	1.678	1.078	-0.214	-0.268	0.303	2.021	-1.263
LD7	HL	89.984	1	0.467	1.560	0.737	-0.172	-0.069	0.025	0.100	-1.070
LD14	HL	.	1	.	1.561	1.464	-0.463	-1.453	1.304	8.619	-2.536
TA12	HL	32.217	1	0.308	1.796	1.324	-0.213	-0.495	1.006	3.451	-2.293
Horizontal Group 2											
CC12	HL	9.163	2	0.469	2.680	1.144	-1.544	-2.311	1.265	4.118	-1.632
CC13	HL	10.141	2	0.469	2.850	0.749	0.292	0.123	1.171	0.002	-1.007
RR3	HL	21.411	2	0.457	2.245	0.615	0.573	0.133	0.193	0.002	-1.007
RR6	HL	0.882	3	0.474	3.086	1.106	-0.583	-0.789	3.228	0.002	-1.007
RR7	HL	0.848	3	0.474	3.338	1.090	-0.654	-0.846	4.820	0.126	-1.202
LD2	HL	45.843	1	0.440	2.081	0.644	1.146	0.307	0.335	0.002	-1.007
TA13	HL	22.954	1	0.454	3.070	0.978	0.300	0.280	3.470	0.048	-1.263
FH7	HL	25.754	2	0.454	3.306	1.165	-0.329	-0.521	5.832	0.024	-1.433

Horizontal outliers											
LD1	HL	0.962	2	0.466	4.367	0.899	0.318	0.231	19.245	0.004	-1.007
LD8	HL	2.834	2	0.466	3.890	0.637	1.636	0.422	5.724	0.003	-1.007
LD15	HL	4.430	2	0.466	3.401	0.638	1.585	0.412	2.588	0.003	-1.007

Sample	Structure	MeasPerm	Cement	Porosity	Complete Mean	Std. Dev.	Skewness	M^3 Dev	%>4.5phi	%<-1phi	Max.Diam.
Scour and Fill Group 1											
EF1	SF	271.680	1	0.374	-0.209	1.271	0.611	1.253	0.046	25.972	-2.511
EF8	SF	.	1	.	-0.390	1.818	0.605	3.631	0.216	42.658	-3.293
EF9	SF	.	2	.	-0.256	2.069	0.348	3.081	0.359	41.602	-3.787
EF10	SF	.	2	.	-0.769	2.035	0.755	6.367	0.292	53.257	-3.916
TA3	SF	128.457	1	0.396	-0.222	1.816	0.515	3.088	0.420	38.044	-3.263
TA4	SF	271.680	1	0.396	-0.400	1.375	1.049	2.724	0.373	27.028	-3.000
TA7	SF	78.645	3	0.302	-0.091	1.585	0.514	2.050	0.589	27.215	-3.202
FH8	SF	141.959	1	0.271	-0.194	1.524	0.375	1.326	0.135	31.924	-2.982
FH9	SF	223.067	1	0.374	-0.205	1.421	0.615	1.766	0.214	25.241	-3.018
FH10	SF	141.959	1	0.439	-0.309	1.788	0.767	4.385	0.436	37.342	-3.217
FH11	SF	81.559	1	0.439	0.176	1.446	0.419	1.268	0.325	20.442	-2.678
FH12	SF	271.680	1	0.374	-0.849	1.516	1.252	4.358	0.292	48.820	-3.186
BC1	SF	35.455	2	0.372	-0.287	2.145	0.740	7.308	1.049	44.109	-3.524
BC5	SF	124.547	1	0.308	0.449	1.717	0.377	1.909	0.793	19.211	-2.963
BC6	SF	98.224	1	0.373	-0.324	1.536	0.548	1.986	0.132	35.570	-2.945
BC8	SF	165.608	2	0.373	-0.553	1.648	0.954	4.273	0.247	41.404	-3.170
Scour and Fill Group 2											
EF2	SF	72.253	1	0.399	0.965	1.304	-0.622	-1.378	0.132	8.079	-3.233
EF3	SF	147.170	2	0.308	0.599	1.925	-0.044	-0.311	0.609	22.976	-3.379
TA5	SF	44.981	1	0.283	0.113	1.904	0.790	5.451	1.315	29.692	-2.848
FH4	SF	.	1	.	-1.169	1.314	2.489	5.652	0.446	63.629	-2.828
FH5	SF	.	1	.	-0.610	1.163	1.735	2.728	0.325	27.939	-2.766
FH6	SF	8.899	1	0.318	0.165	2.551	0.528	8.773	2.038	44.619	-3.420
BC2	SF	16.735	3	0.325	-0.148	2.228	0.677	7.483	1.249	41.762	-3.536
BC3	SF	17.181	2	0.295	-0.045	2.122	0.752	7.190	1.534	40.076	-3.138

Sample	Structure	MeasPerm	Cement	Porosity	Complete Mean	Std. Dev.	Skewness	M^3 Dev	%>4.5phi	%<-1phi	Max.Diam.
Structureless Group 1											
RR10	SL	2.659	3	0.469	2.979	0.948	0.432	0.368	3.212	0.003	-1.007
EF4	SL	15.209	2	0.334	1.751	1.958	-0.838	-6.292	1.259	15.153	-3.138
EF6	SL	4.296	2	0.454	3.387	0.895	-1.028	-0.737	3.126	0.620	-2.000
EF7	SL	7.361	2	0.334	2.359	1.529	-1.361	-4.864	1.156	7.077	-2.678
TA1	SL	10.241	2	0.370	2.233	2.063	-0.720	-6.314	5.201	10.751	-3.248
TA2	SL	7.562	2	0.463	3.426	1.363	-0.358	-0.908	10.236	0.002	-1.007
TA6	SL	12.409	2	0.370	1.859	1.795	-0.213	-1.230	3.195	7.143	-2.787
TA9	SL	3.957	2	0.441	3.379	1.648	-0.317	-1.418	16.270	0.996	-2.322
TA10	SL	19.681	2	0.441	2.862	1.234	-0.183	-0.344	4.688	0.933	-2.104
FH1	SL	5.057	2	0.470	3.270	1.256	-0.154	-0.306	7.433	0.073	-2.000
FH2	SL	9.836	3	0.345	2.442	1.848	-0.658	-4.153	4.711	5.829	-2.926
FH3	SL	4.838	3	0.425	1.983	2.195	-0.688	-7.281	3.380	17.242	-2.766
FH13	SL	14.365	2	0.454	3.302	1.136	-0.257	-0.377	5.764	0.002	-1.007
BC4	SL	2.010	1	0.298	2.756	1.836	-0.801	-4.954	7.880	6.659	-2.744
Structureless outliers											
RB7	SL	44.152	1	0.418	0.398	1.387	-0.037	-0.099	0.141	16.604	-2.700
EF5	SL	60.662	1	0.308	1.382	1.772	-0.517	-2.878	0.838	12.115	-2.945

Sample	Excluding <-1 phi Mean	Std. Dev.	Skewness	M^3 Dev.	%>4.5phi	Porosity	MeasPerm	Cement
Crossbeds Group 1								
RR1	1.535	0.658	1.111	0.316	0.073	0.409	48.162	1
RR9	1.681	0.700	0.221	0.076	0.049	0.438	20.145	1
MS5	1.435	0.477	0.138	0.015	0.023	0.467	189.818	1
MS7	1.434	0.464	0.010	0.001	0.024	.	.	1
EG8	1.649	0.678	1.216	0.379	0.150	0.477	86.397	1
LD4	1.657	0.676	1.063	0.329	0.182	0.467	89.984	1
LD11	1.544	0.628	0.508	0.126	0.047	.	.	1
LD12	1.501	0.546	0.562	0.091	0.047	.	.	1
Crossbeds Group 2								
MS1	1.008	0.484	-0.223	-0.025	0.000	0.467	271.680	1
MS3	1.087	0.631	-0.520	-0.130	0.026	0.467	237.104	1
MS4	1.025	0.529	-0.060	-0.009	0.023	0.467	189.818	1
MS8	1.123	0.558	-0.238	-0.041	0.023	.	.	1
EG3	1.063	0.694	0.987	0.330	0.072	0.461	88.151	1
LD10	1.290	0.718	-0.221	-0.082	0.048	.	.	1
Crossbeds Group 3								
CC1	1.889	0.752	-0.768	-0.327	0.096	0.435	41.848	1
CC2	1.765	0.888	-0.533	-0.373	0.141	0.469	86.397	1
CC6	1.334	1.232	0.060	0.113	0.388	0.458	98.224	2
RB2	1.549	1.055	0.470	0.552	0.680	0.455	57.630	2
RR5	2.068	1.043	0.176	0.199	0.711	0.441	2.828	1
EG1	1.990	0.793	-0.148	-0.074	0.259	0.489	44.981	1
EG5	1.393	0.955	0.313	0.273	0.333	0.461	77.270	1
EG7	2.059	0.921	-0.339	-0.265	0.439	0.514	56.233	1

Sample	Mean	Std. Dev.	Skewness	M^3 Dev.	%>4.5phi	Porosity	MeasPerm	Cement
Crossbeds Group 4								
CC5		1.179	0.610	0.999	0.279	0.534	165.608	2
CC7	0.845	1.176	0.599	0.976	0.221	0.441	132.641	2
RB9	0.246	0.829	1.626	0.927	0.081	0.391	74.671	2
RR2	0.924	0.932	0.812	0.656	0.103	0.409	120.884	1
RR11	0.683	0.843	1.162	0.697	0.186	0.326	117.447	1
RR12	0.384	0.870	1.471	0.968	0.169	0.367	141.959	1
EG2	0.868	1.049	1.128	1.301	0.688	0.472	137.130	2
EG4	0.696	1.517	1.505	5.252	2.753	0.472	141.959	2
RR4	3.227	0.711	0.557	0.200	2.243	0.474	28.209	2
RR8	2.170	0.546	-0.111	-0.018	0.024	0.438	34.462	1
LD13	2.480	0.733	-0.574	-0.227	0.419	.	.	1

Excluding <-1 phi

Sample	Mean	Std. Dev.	Skewness	M^3 Dev.	%>4.5phi	Porosity	MeasPerm	Cement
Channels Group 1								
TA8	0.146	1.336	2.224	5.306	1.503	0.302	271.680	2
TA11	0.051	1.047	2.157	2.476	0.494	0.281	271.680	1
BC9	0.066	1.255	2.314	4.573	1.049	0.274	210.681	1
BC10	1.090	1.774	0.671	3.746	2.303	.	.	1
BC11	-0.034	1.032	2.134	2.343	0.273	0.288	271.680	1
BC12	-0.088	0.971	2.174	1.992	0.272	0.274	223.067	1
Channels Group 2								
CC3	1.142	0.870	0.306	0.202	0.103	0.420	124.547	1
CC4	0.527	0.953	1.079	0.934	0.189	0.361	189.818	1
RB3	1.420	0.974	0.150	0.139	0.230	0.384	44.981	1
RB6	1.394	0.980	0.086	0.081	0.212	0.235	81.559	1
MS2	0.606	0.698	0.043	0.015	0.026	0.467	253.153	1
MS9	0.586	0.759	0.422	0.184	0.101	.	.	1
LD9	0.913	0.847	0.364	0.222	0.022	.	.	1
BC7	0.473	0.862	0.783	0.502	0.053	0.399	271.680	1

Sample	Excluding <-1 phi Mean	Std. Dev.	Skewness	M^3 Dev.	%>4.5phi	Porosity	MeasPerm	Cement
Horizontal Group 1								
CC8	1.864	0.782	0.119	0.057	0.175	0.446	89.984	1
CC9	1.664	0.697	0.577	0.196	0.145	0.453	73.441	1
CC10	1.344	1.241	0.116	0.221	0.502	0.515	158.933	2
CC11	1.612	1.124	0.009	0.013	0.413	0.515	78.645	2
RB1	1.954	0.688	0.523	0.170	0.174	0.478	37.346	3
RB4	1.249	0.849	0.740	0.453	0.172	0.430	47.679	2
RB5	1.454	1.058	0.907	1.074	1.203	0.423	31.601	2
RB8	1.476	0.956	0.741	0.646	0.423	0.397	3.525	3
RB10	1.682	0.811	0.414	0.221	0.163	0.431	24.990	2
RB11	2.293	1.021	0.466	0.495	1.712	0.417	3.957	2
RR13	2.133	0.951	0.209	0.180	0.687	0.338	12.149	3
MS6	1.057	0.923	0.370	0.291	0.198	0.467	141.959	1
LD3	1.783	0.898	-0.282	-0.204	0.266	0.406	48.656	1
LD5	2.295	0.838	0.546	0.322	0.886	0.440	25.239	1
LD6	1.735	1.009	0.006	0.006	0.309	0.406	73.441	1
LD7	1.563	0.732	-0.141	-0.056	0.025	0.467	89.984	1
LD14	1.875	1.096	0.551	0.726	1.427	.	.	1
TA12	1.920	1.173	0.270	0.436	1.042	0.308	32.217	1
Horizontal Group 2								
CC12	2.852	0.806	-0.018	-0.009	1.320	0.469	9.163	2
CC13	2.850	0.749	0.295	0.124	1.171	0.469	10.141	2
RR3	2.245	0.614	0.577	0.134	0.193	0.457	21.411	2
RR6	3.086	1.106	-0.582	-0.788	3.228	0.474	0.882	3
RR7	3.344	1.079	-0.602	-0.757	4.827	0.474	0.848	3
LD2	2.081	0.644	1.149	0.307	0.335	0.440	45.843	1
TA13	3.072	0.973	0.336	0.310	3.472	0.454	22.954	1
FH7	3.307	1.163	-0.320	-0.503	5.834	0.454	25.754	2

Horizontal outliers								
LD1	4.367	0.898	0.326	0.236	19.246	0.466	0.962	2
LD8	3.890	0.636	1.654	0.426	5.724	0.466	2.834	2
LD15	3.401	0.638	1.596	0.414	2.588	0.466	4.430	2

	Excluding <-1 phi							
Sample	Mean	Std. Dev.	Skewness	M^3 Dev.	%>4.5phi	Porosity	MeasPerm	Cement
Scour and Fill Group 1								
EF1	0.334	1.024	1.049	1.126	0.062	0.374	271.680	1
EF8	0.917	1.326	0.530	1.237	0.377	.	.	1
EF9	1.267	1.327	0.284	0.663	0.615	.	.	2
EF10	1.156	1.380	0.373	0.981	0.625	.	.	2
TA3	0.951	1.308	0.731	1.633	0.677	0.396	128.457	1
TA4	0.193	1.136	1.877	2.749	0.511	0.396	271.680	1
TA7	0.661	1.173	1.438	2.323	0.810	0.302	78.645	3
FH8	0.648	1.090	0.823	1.066	0.198	0.271	141.959	1
FH9	0.405	1.110	1.367	1.868	0.286	0.374	223.067	1
FH10	0.764	1.422	0.950	2.732	0.697	0.439	141.959	1
FH11	0.694	1.148	1.000	1.512	0.409	0.439	81.559	1
FH12	0.339	1.266	1.468	2.977	0.571	0.374	271.680	1
BC1	1.271	1.651	0.583	2.622	1.877	0.372	35.455	2
BC5	1.027	1.382	0.862	2.275	0.982	0.308	124.547	1
BC6	0.587	1.154	0.758	1.166	0.205	0.373	98.224	1
BC8	0.530	1.344	1.113	2.701	0.422	0.373	165.608	2
Scour and Fill Group 2								
EF2	1.236	0.971	0.314	0.287	0.144	0.399	72.253	1
EF3	1.430	1.341	0.413	0.996	0.790	0.308	147.170	2
TA5	0.973	1.632	0.876	3.810	1.871	0.283	44.981	1
FH4	0.134	1.442	1.972	5.917	1.227	.	.	1
FH5	-0.117	1.003	2.955	2.977	0.450	.	.	1
FH6	2.079	1.883	-0.109	-0.731	3.680	0.318	8.899	1
BC2	1.372	1.728	0.493	2.543	2.144	0.325	16.735	3
BC3	1.308	1.716	0.615	3.105	2.559	0.295	17.181	2

Sample	Excluding <-1 phi Mean	Std. Dev.	Skewness	M^3 Dev.	%>4.5phi	Porosity	MeasPerm	Cement
Structureless Group 1								
RR10	2.979	0.947	0.434	0.369	3.212	0.469	2.659	3
EF4	2.433	1.203	-0.425	-0.741	1.484	0.334	15.209	2
EF6	3.417	0.810	-0.138	-0.073	3.145	0.454	4.296	2
EF7	2.679	1.035	-0.594	-0.658	1.244	0.334	7.361	2
TA1	2.757	1.485	-0.223	-0.729	5.827	0.370	10.241	2
TA2	3.426	1.363	-0.358	-0.906	10.236	0.463	7.562	2
TA6	2.148	1.518	0.206	0.721	3.441	0.370	12.409	2
TA9	3.430	1.576	-0.133	-0.523	16.434	0.441	3.957	2
TA10	2.904	1.162	0.187	0.294	4.732	0.441	19.681	2
FH1	3.274	1.250	-0.124	-0.243	7.438	0.470	5.057	2
FH2	2.715	1.533	-0.295	-1.063	5.003	0.345	9.836	3
FH3	2.788	1.435	-0.765	-2.261	4.084	0.425	4.838	3
FH13	3.302	1.136	-0.256	-0.376	5.765	0.454	14.365	2
BC4	3.087	1.405	-0.081	-0.225	8.442	0.298	2.010	1
Structureless outliers								
RB7	0.846	1.049	0.501	0.578	0.169	0.418	44.152	1
EF5	1.845	1.345	-0.279	-0.678	0.953	0.308	60.662	1

APPENDIX B

Scatter plots of measured permeability compared to permeability values predicted by published empirical permeability equations and multiple regression permeability equations

Listwise Pearson correlation of measured permeability with published empirical permeability equations

Equation	Complete sample	Cut sample
Beyer	0.629	0.713
Hazen	0.697	0.653
Kozeney	0.654	0.566
Kruger	0.783	0.723
Sauerbrei	0.658	0.621
Slichter	0.688	0.602
USBR	0.584	0.712
Zamarin	0.753	0.690

Beyer vs. Measured Permeability Values

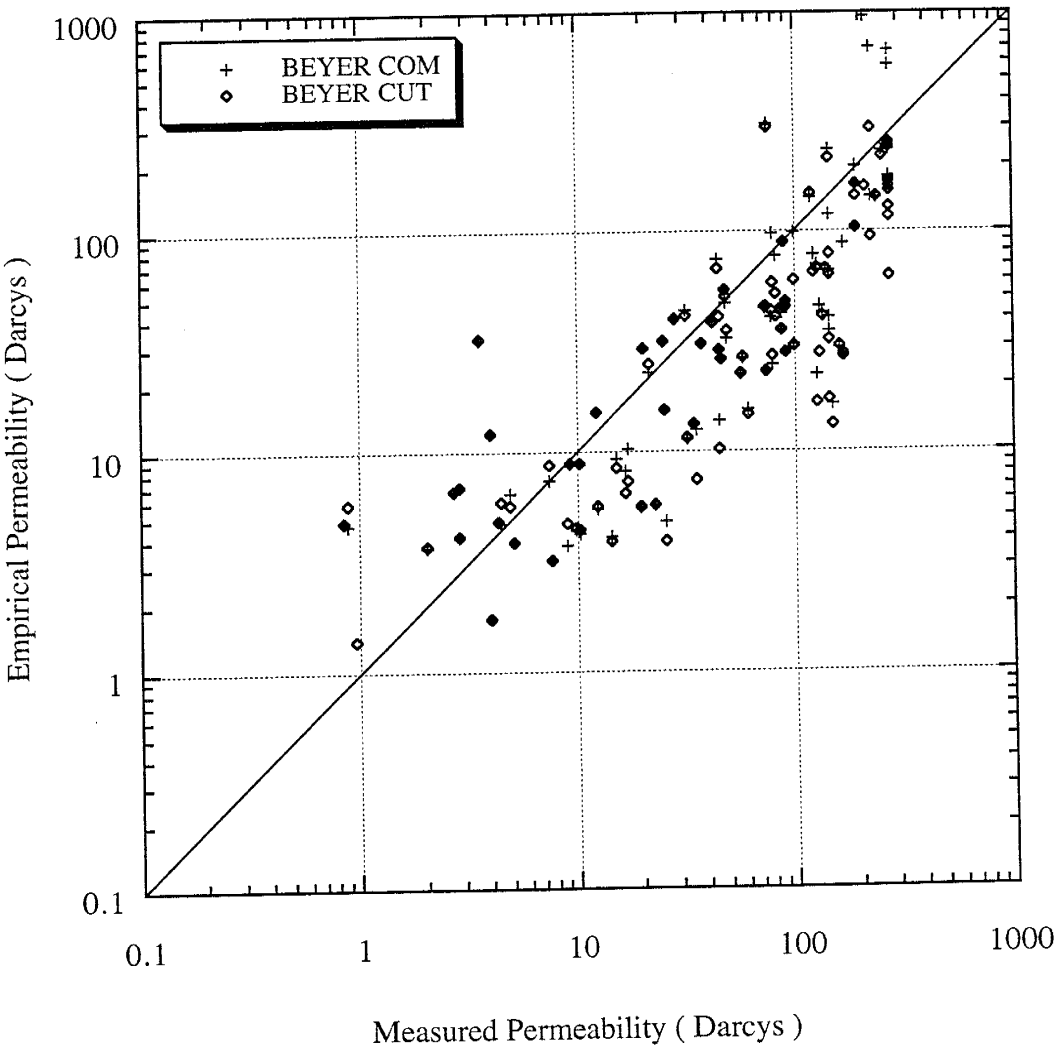

Hazen vs. Measured Permeability Values

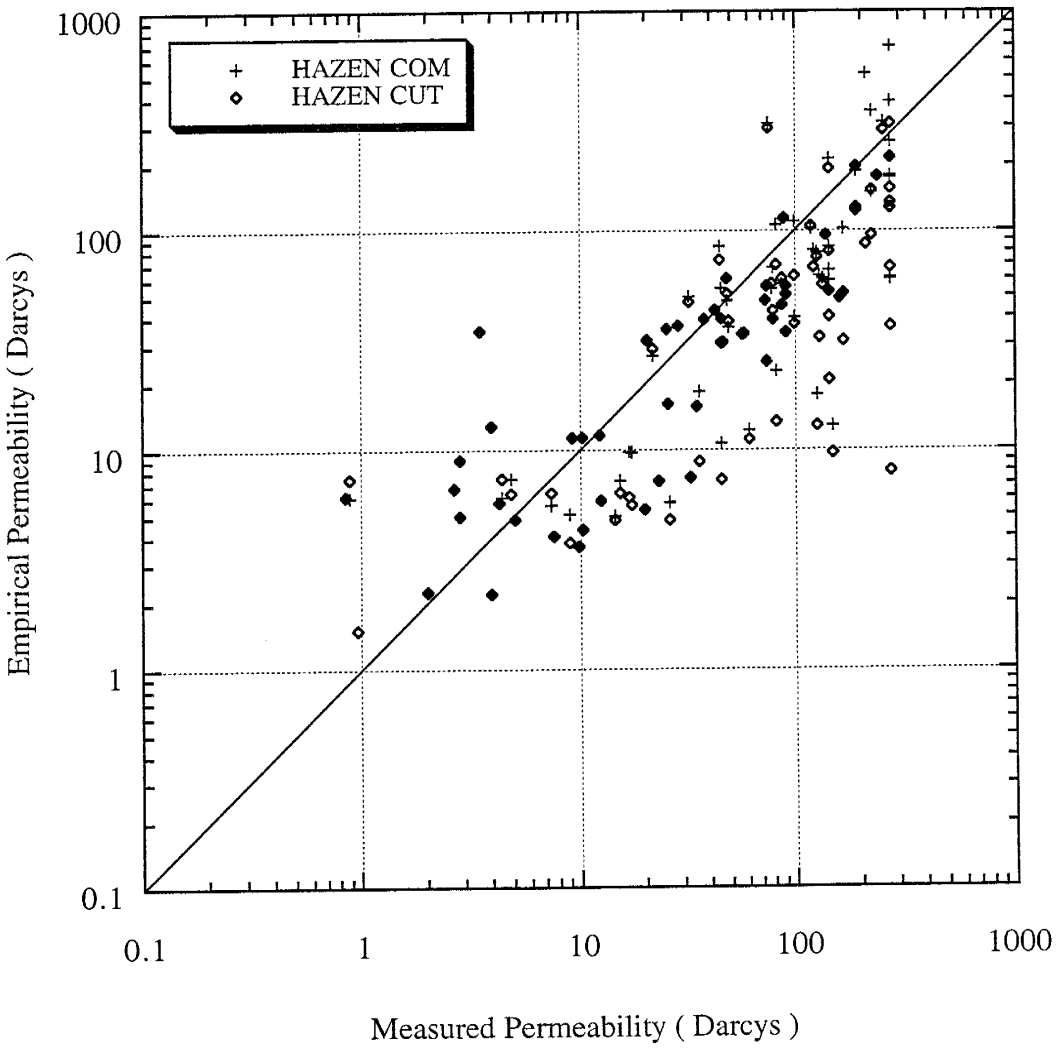

Kozeney vs. Measured Permeability Values

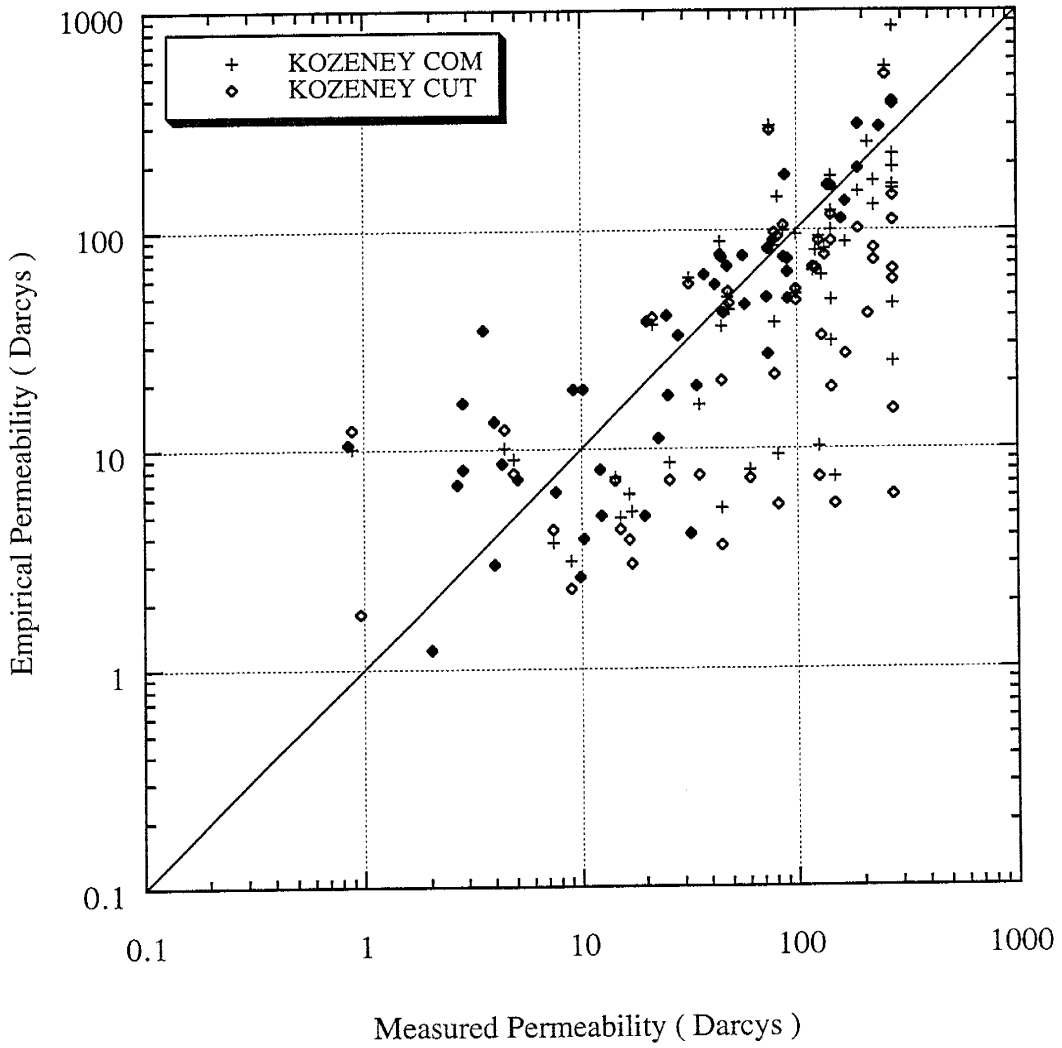

Kruger vs. Measured Permeability Values

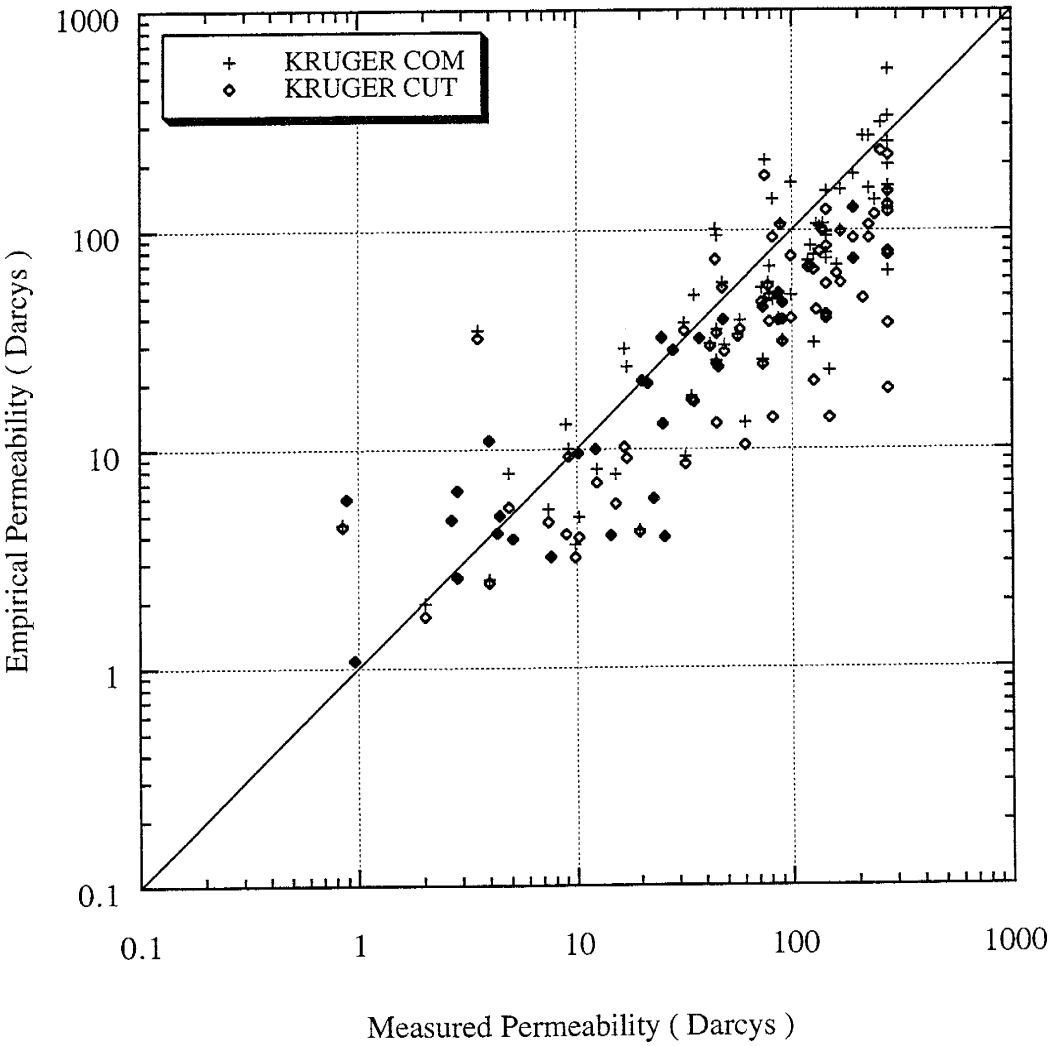

Sauerbrei vs. Measured Permeability Values

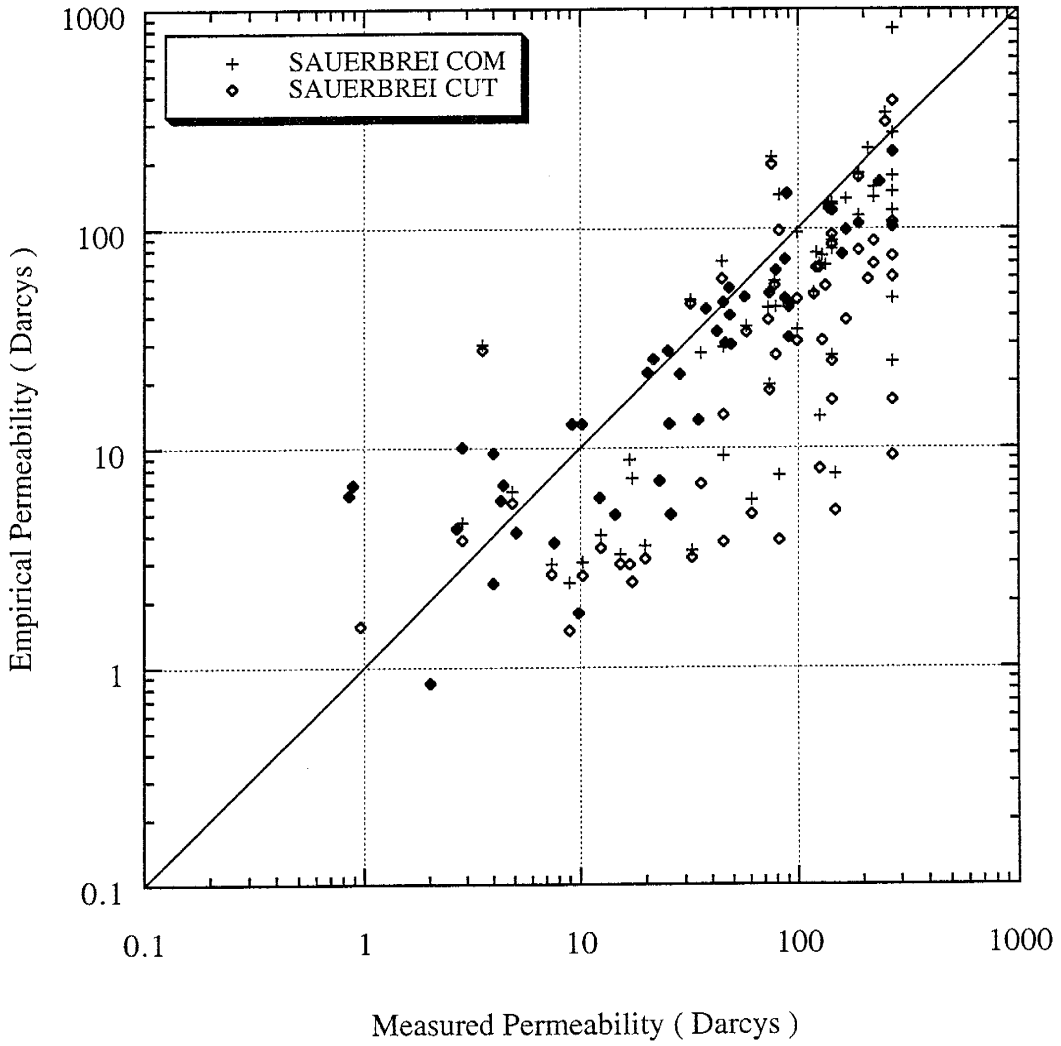

Slichter vs. Measured Permeability Values

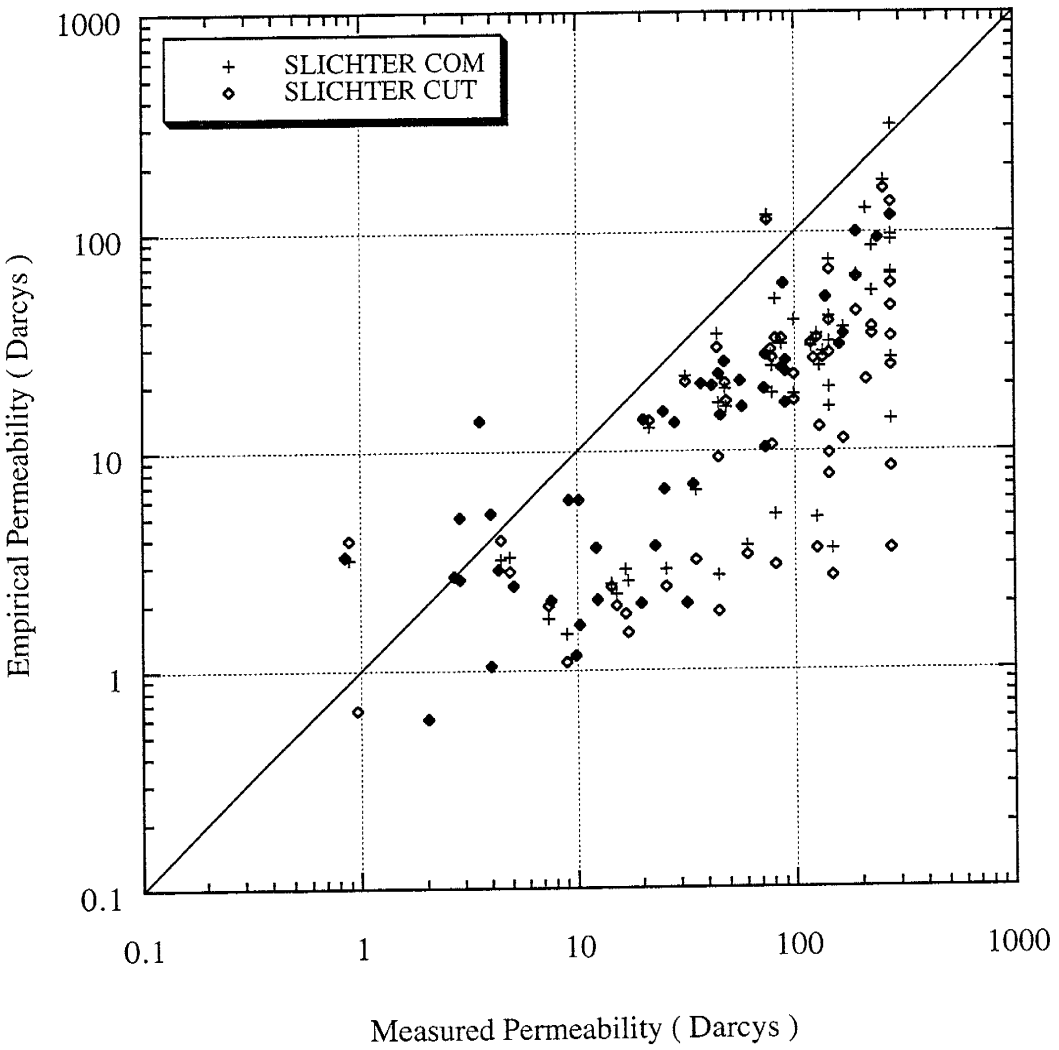

USBR vs. Measured Permeability Values

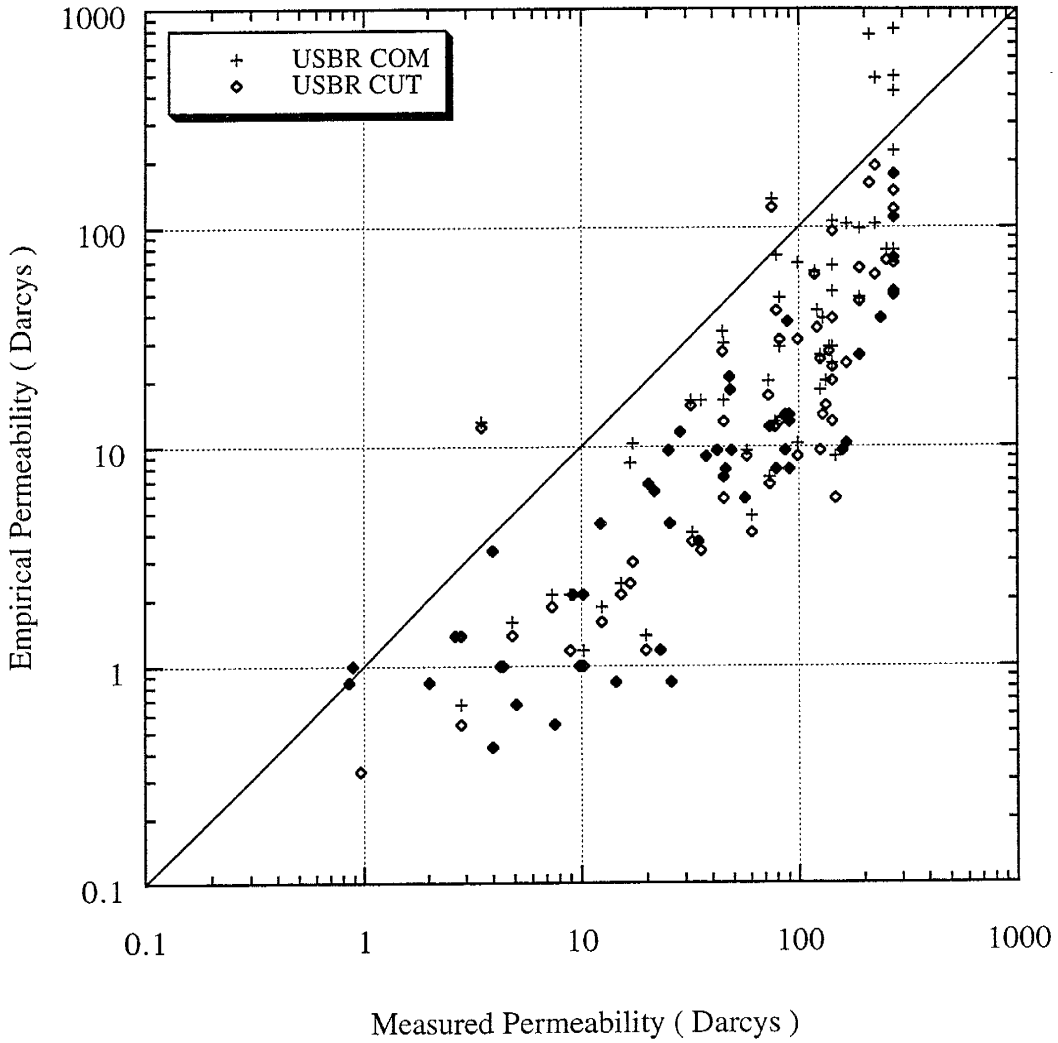

Zamarin vs. Measured Permeability Values

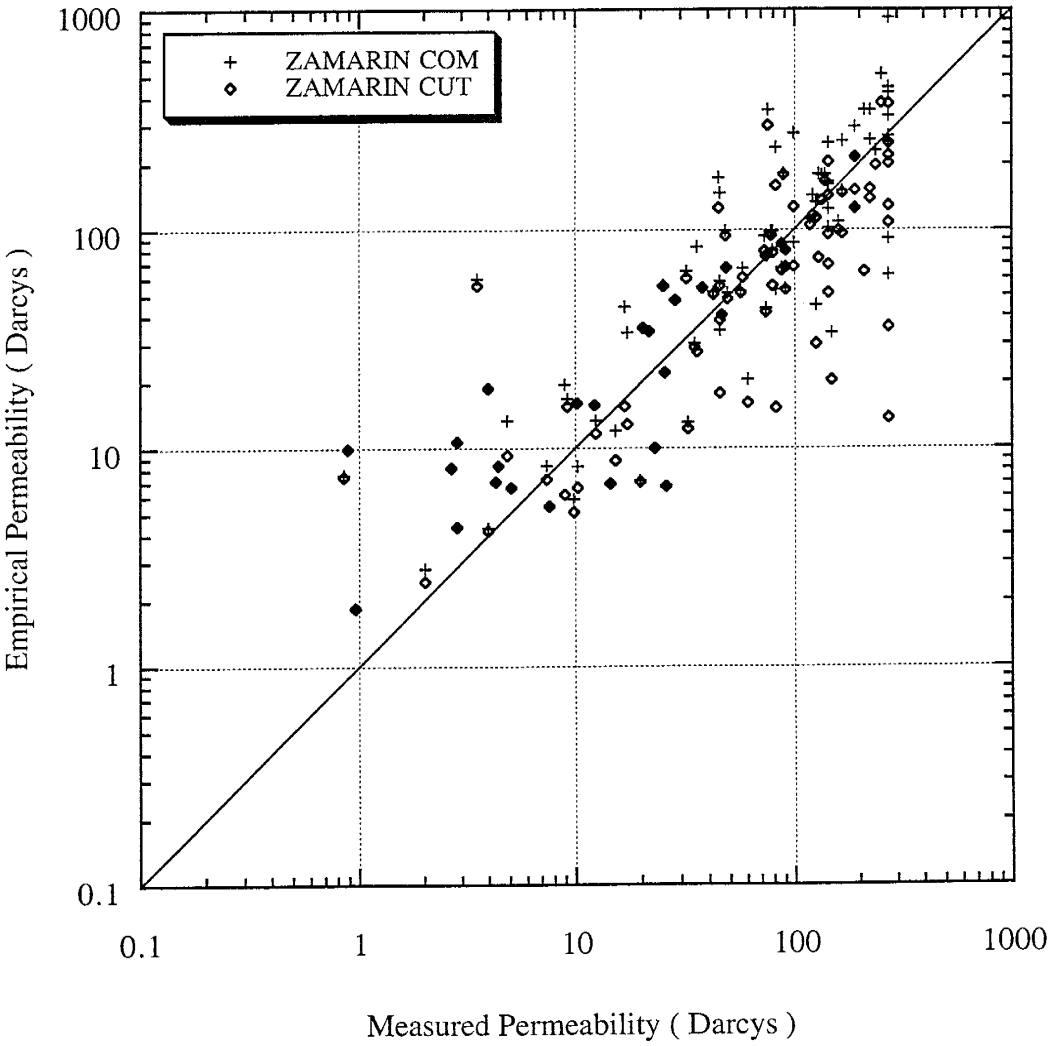

Regression analysis with measured permeability

	Pearson correlation R	R^2
Measured permeability vs. grain size in mm:		
402.42(d_{10} mm complete) + 5.58	0.806	0.650
245.07(d_{20} mm complete) + 14.06	0.785	0.616
650.69(d_{10} mm cut) - 23.69	0.819	0.671
425.80(d_{20} mm cut) - 15.88	0.842	0.709
Measured permeability vs. phi grain size:		
-65.87(d_{10} phi complete) + 264.55	0.836	0.699
-71.76(d_{10} phi cut) + 290.23	0.798	0.637
-60.30(d_{20} phi complete) + 219.31	0.816	0.666
-68.13(d_{20} phi cut) + 249.18	0.825	0.681
Measured permeability vs. entire distribution parameters:		
"MSP1 COM"		
267.39(Kruger mm complete) + 4.91(mean complete) - 2.24(% fines complete) -13.31	0.824	0.679
"MSP1 CUT"		
372.36(Kruger mm cut) - 16.57(mean cut) + 3.32(% fines cut) + 0.58	0.849	0.721
"MSP2 COM"		
258.34(Kruger mm complete) + 0.235(mean complete) - 7.54	0.821	0.674
"MSP2 CUT"		
396.93(Kruger mm cut) - 6.31(mean cut) - 17.85	0.844	0.712

Regression d_{10} mm, complete distribution

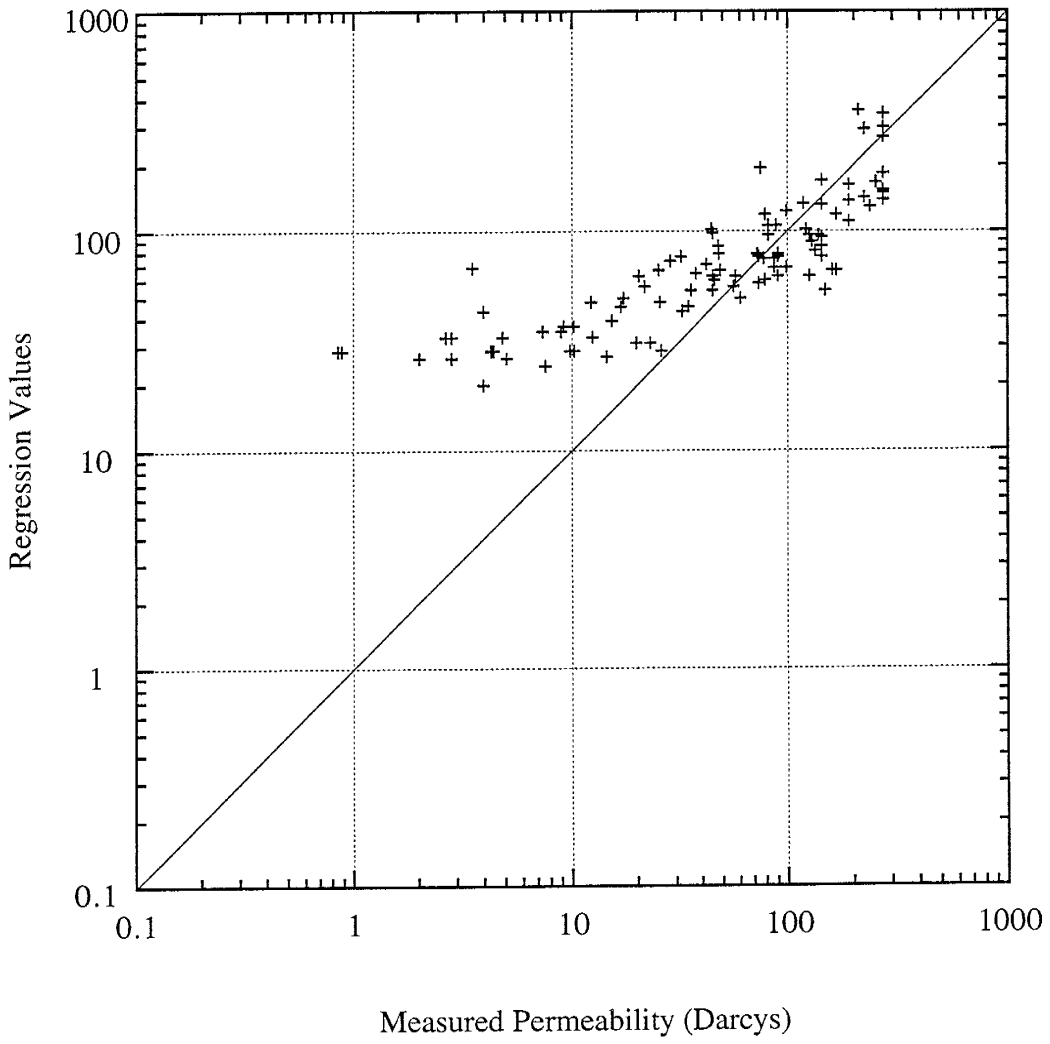

Regression d_{10} mm, cut distribution

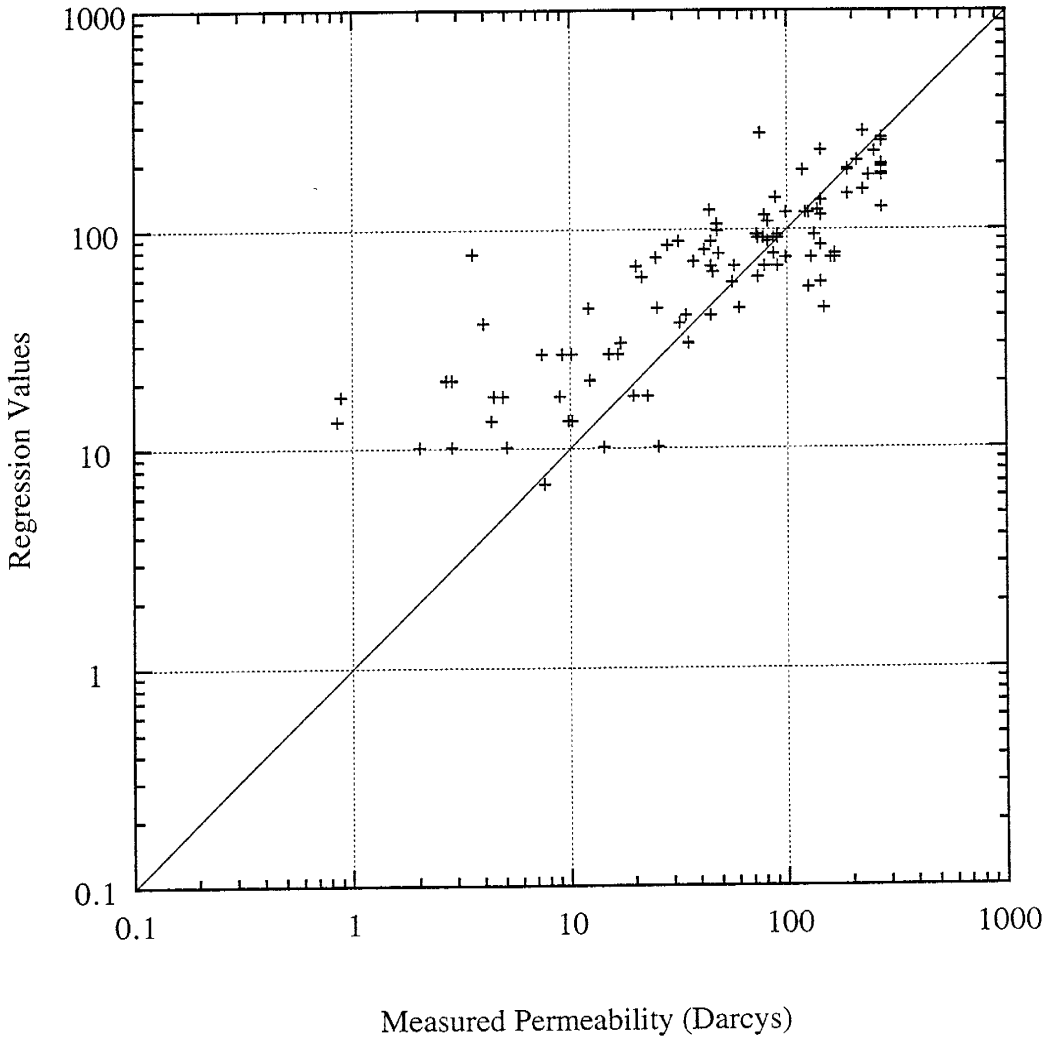

Regression d_{20} mm, complete distribution

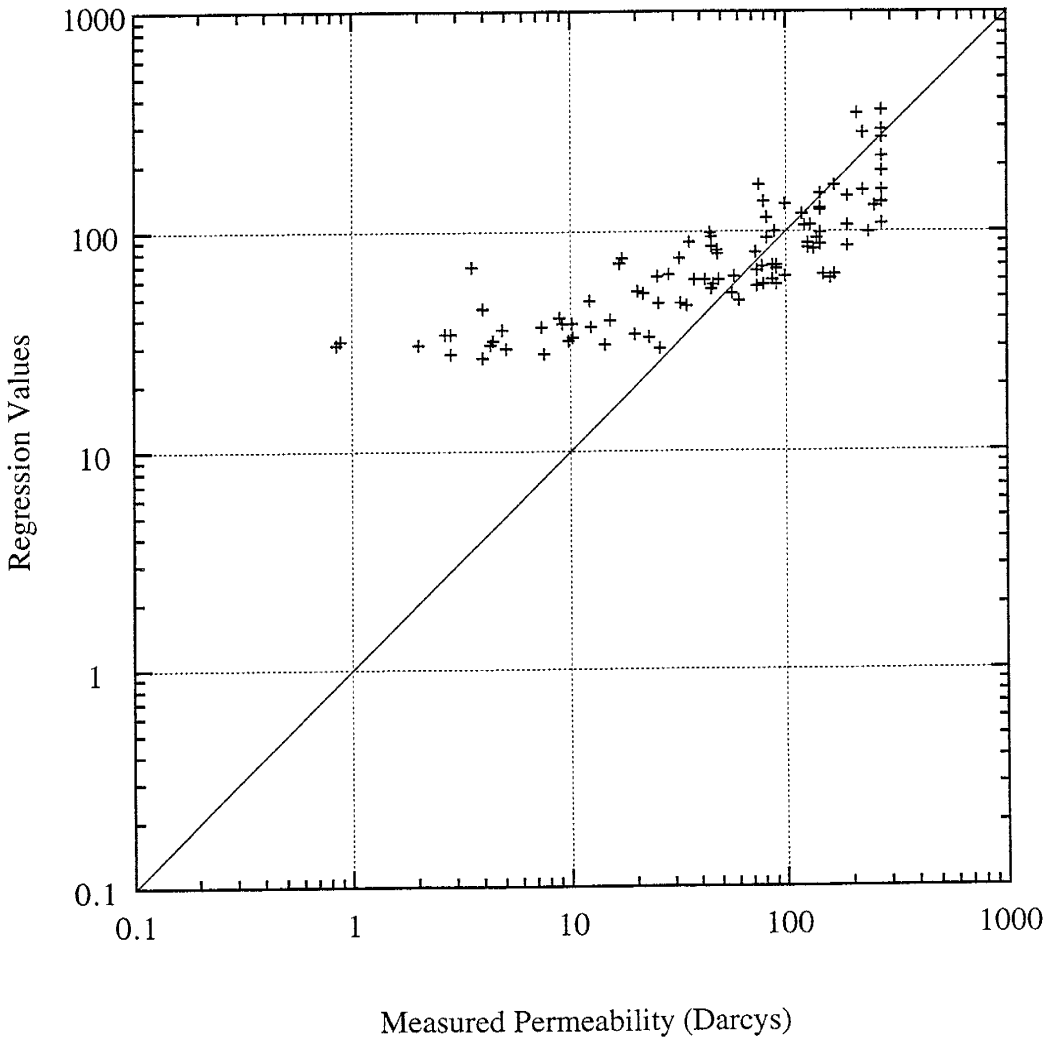

Regression d_{20} mm, cut distribution

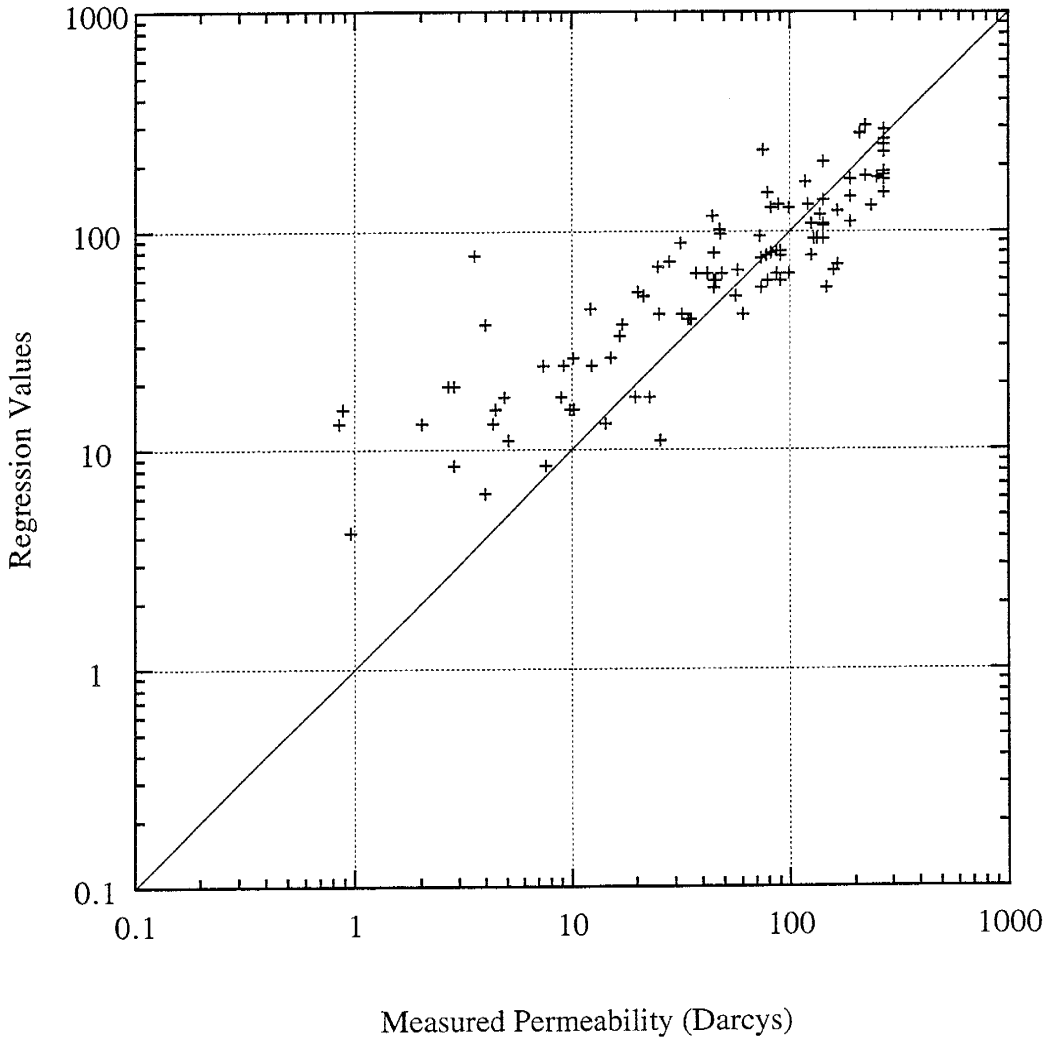

Regression d_{10} phi, complete distribution

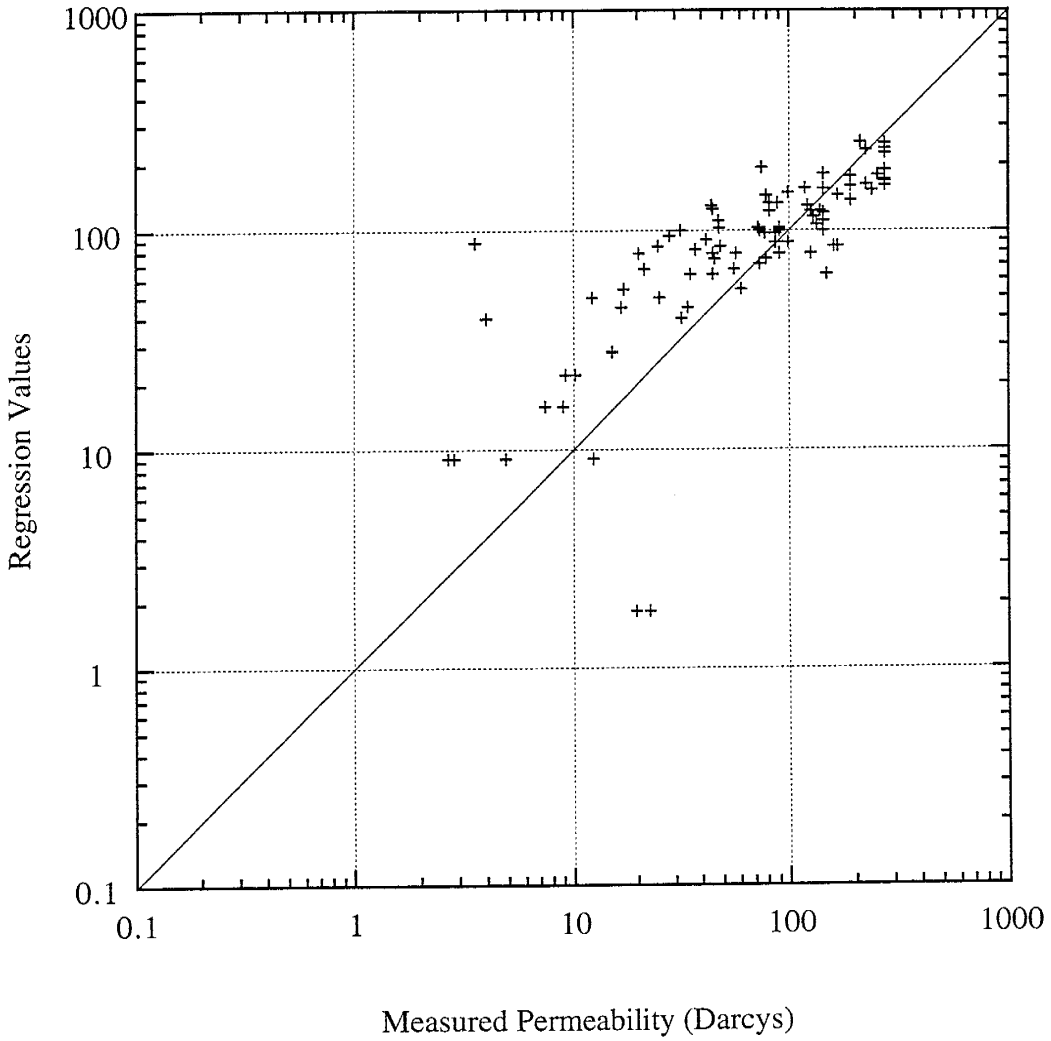

Regression d_{10} phi, cut distribution

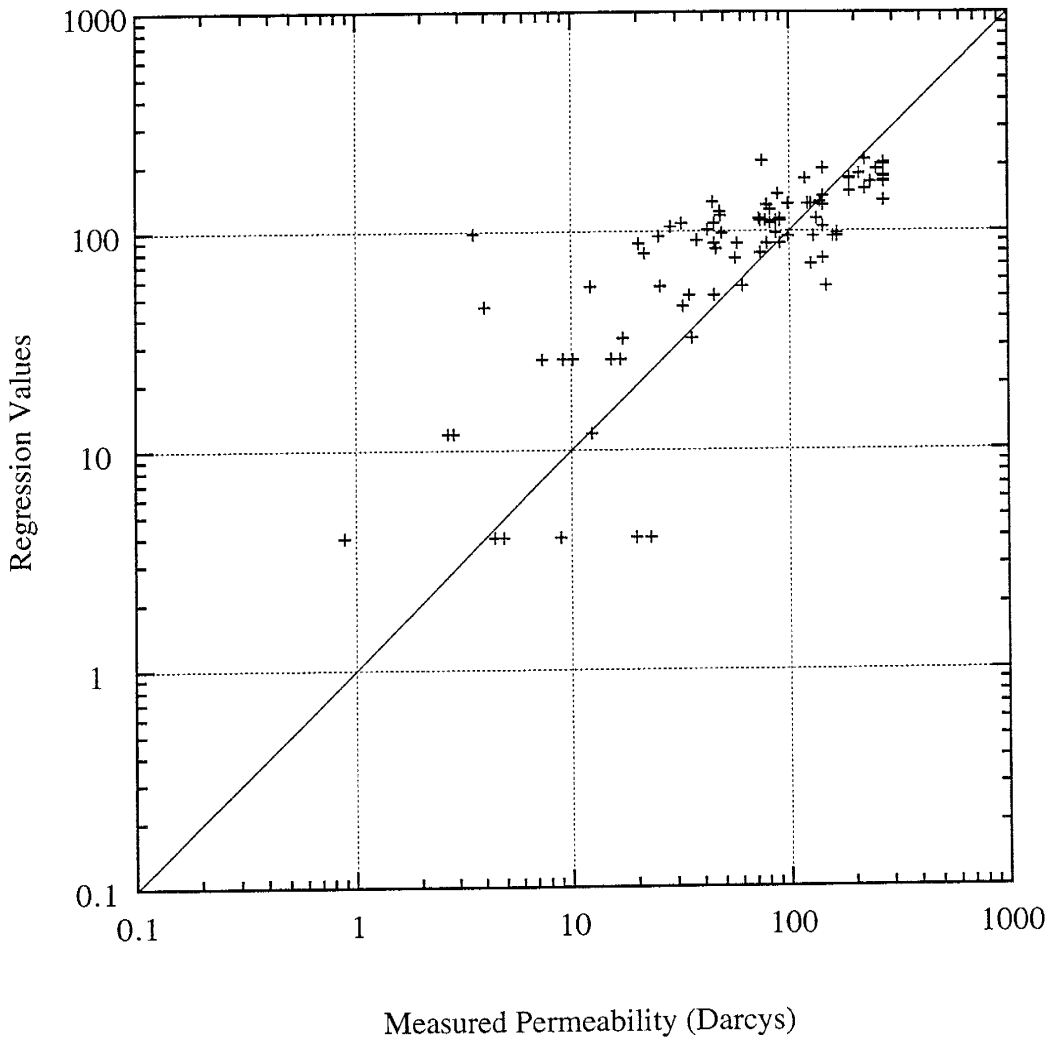

Regression d_{20} phi, complete distribution

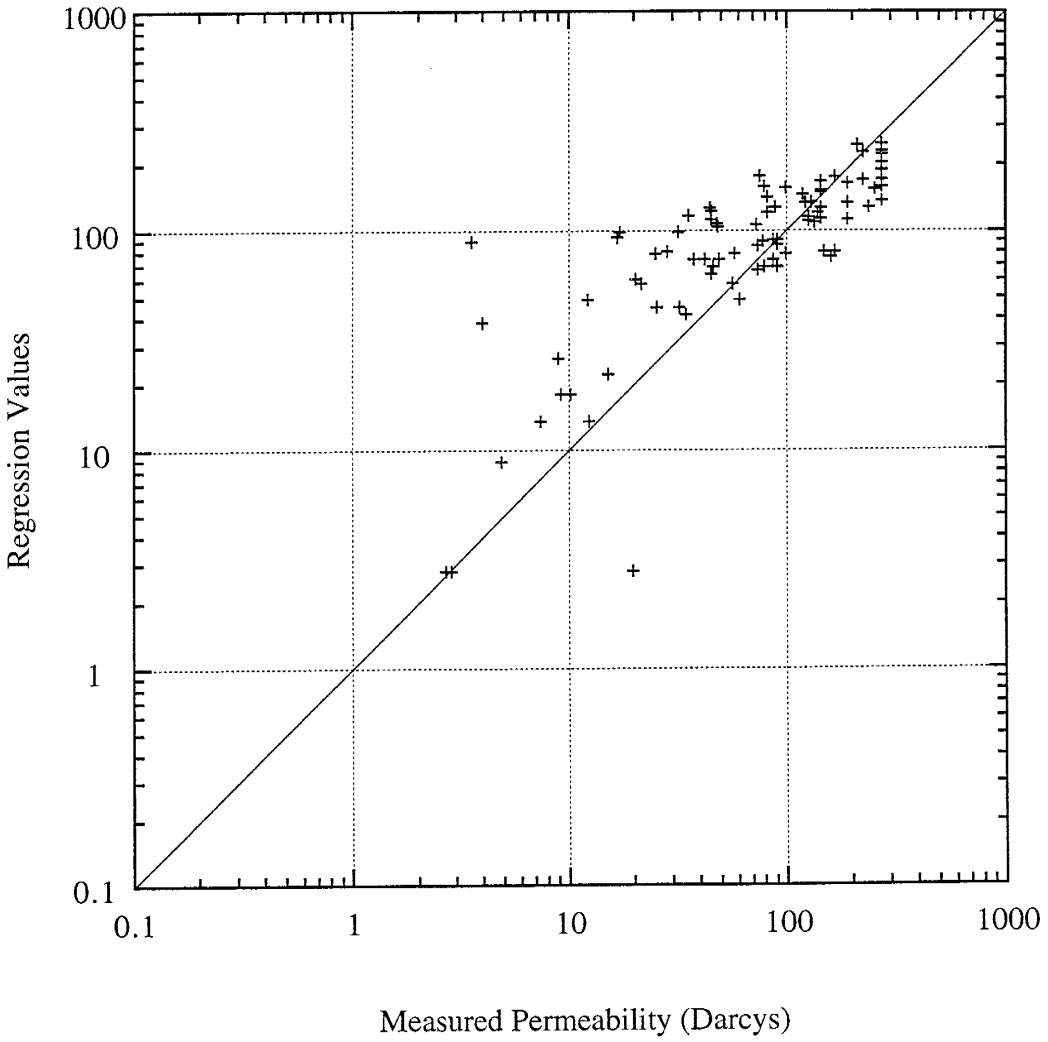

Regression d_{20} phi, cut distribution

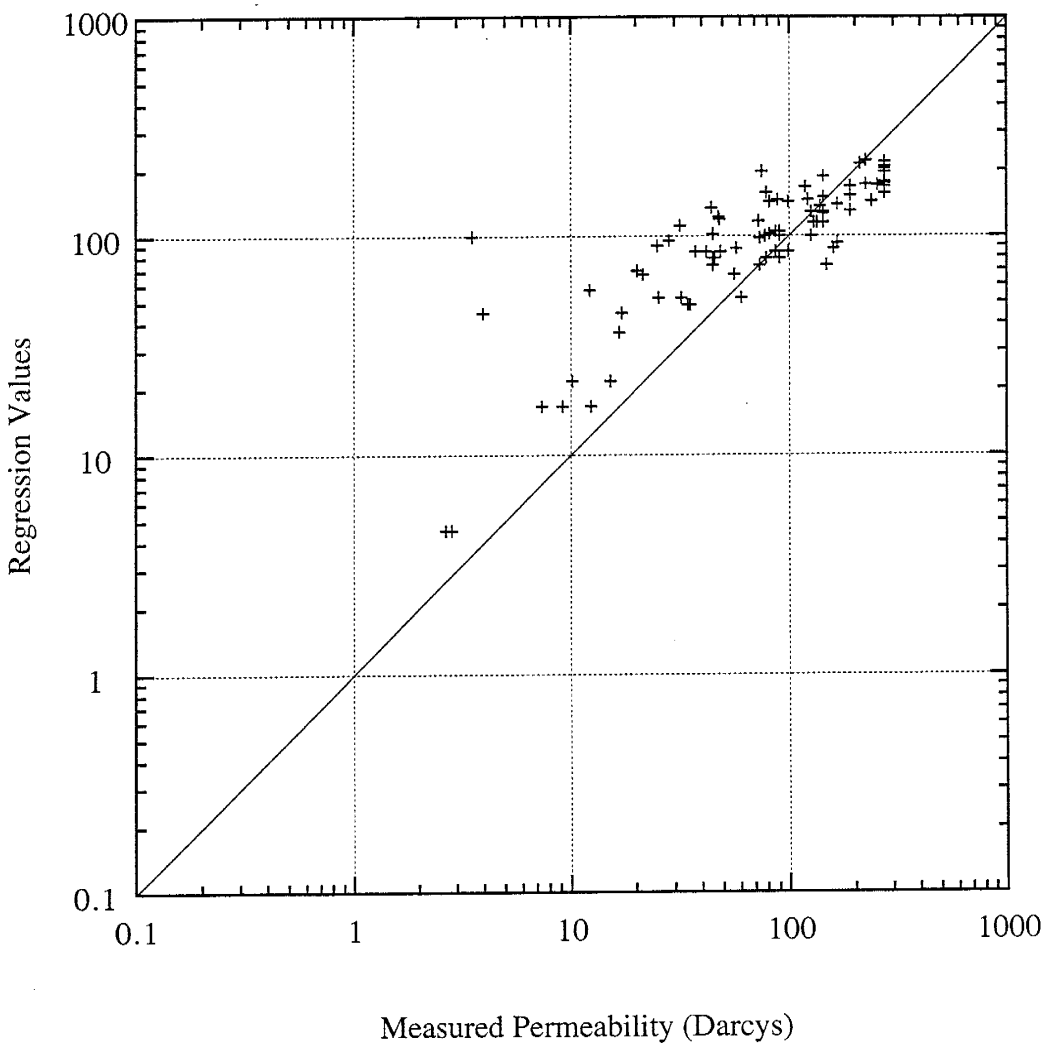

Regression MSP1, complete distribution

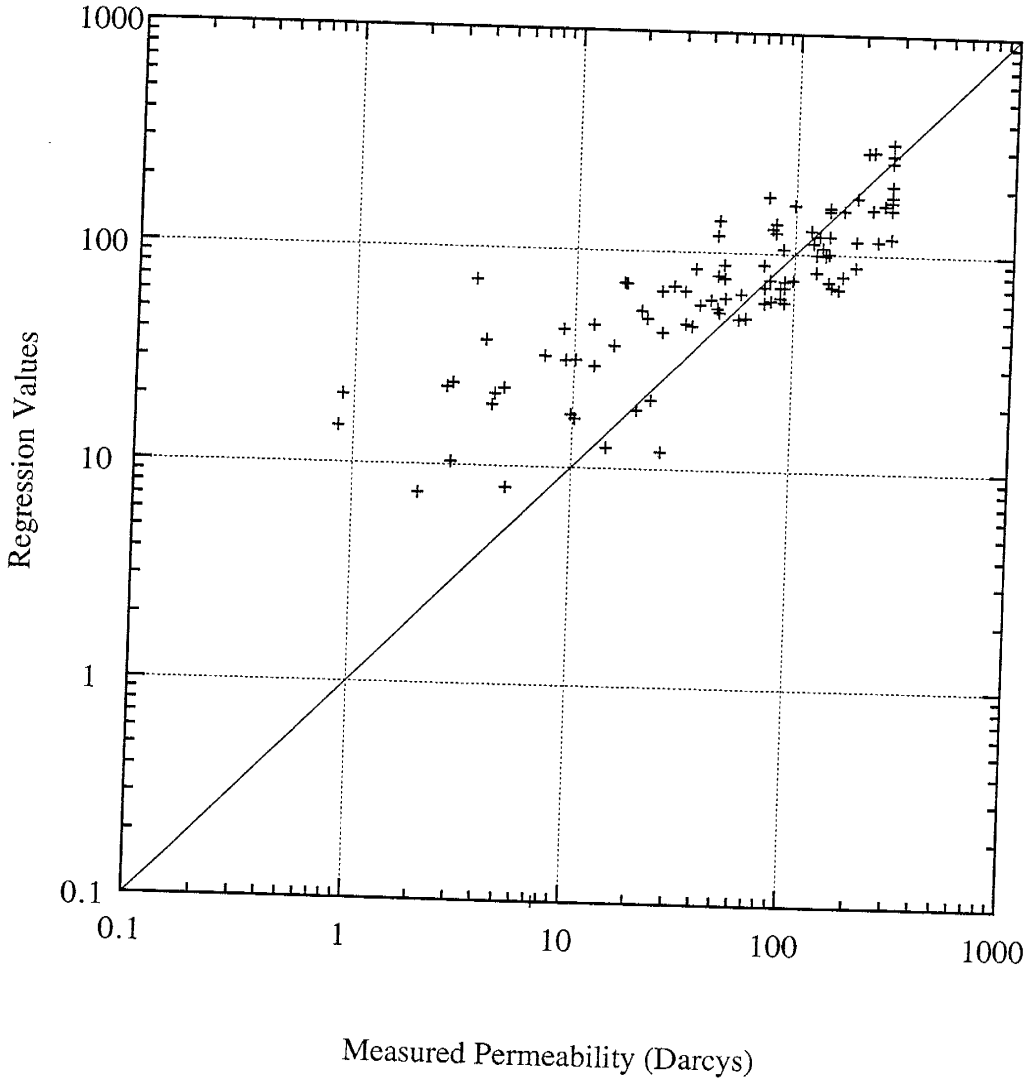

Regression MSP1, cut distribution

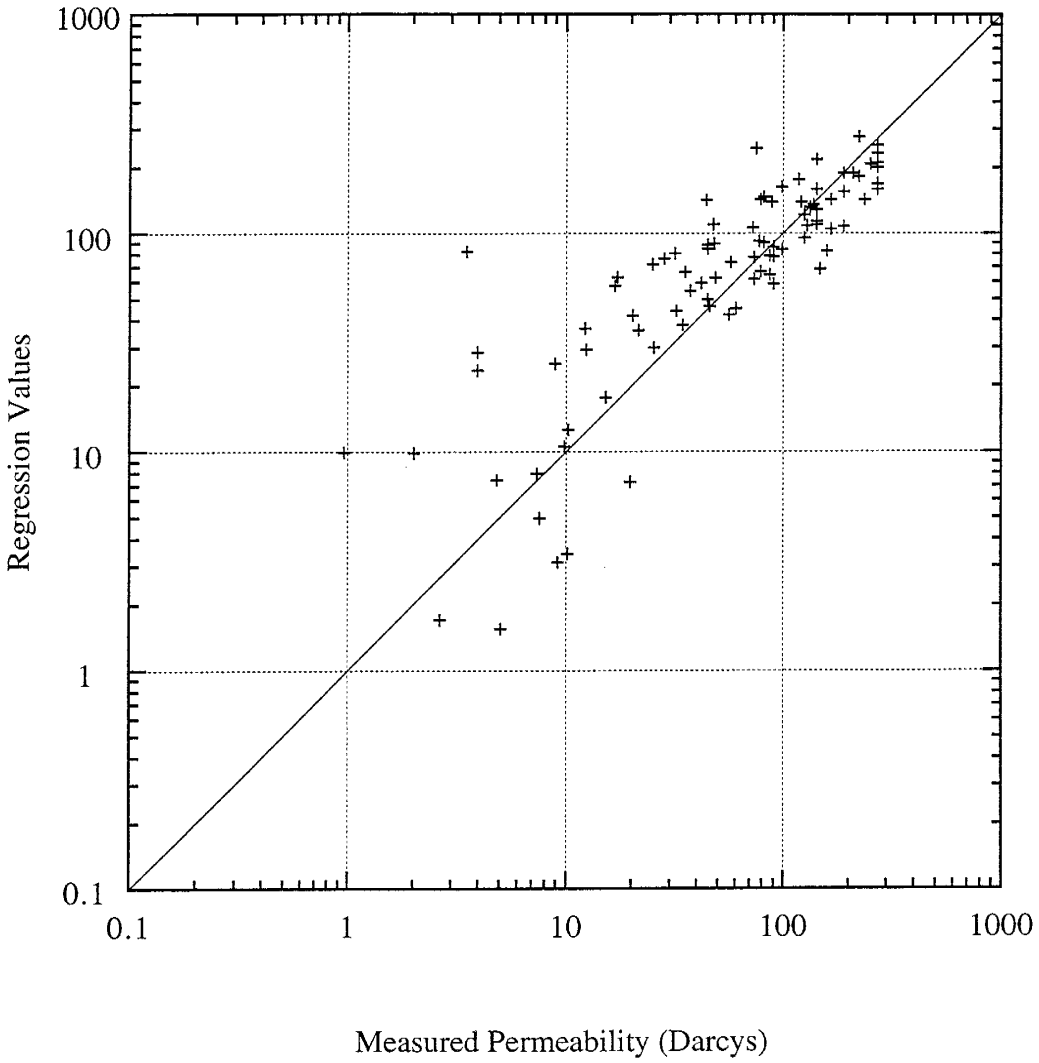

Regression MSP2, complete distribution

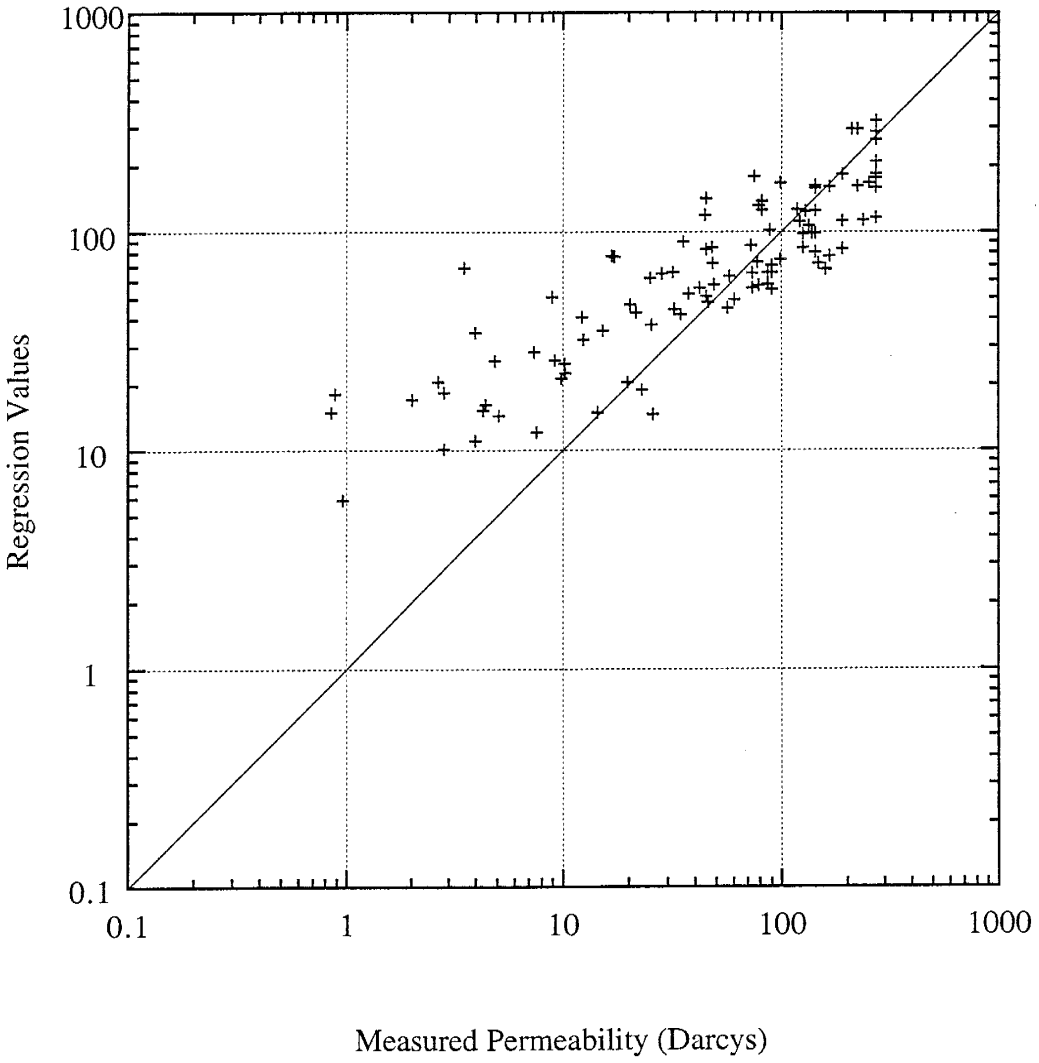

Regression MSP2, cut distribution

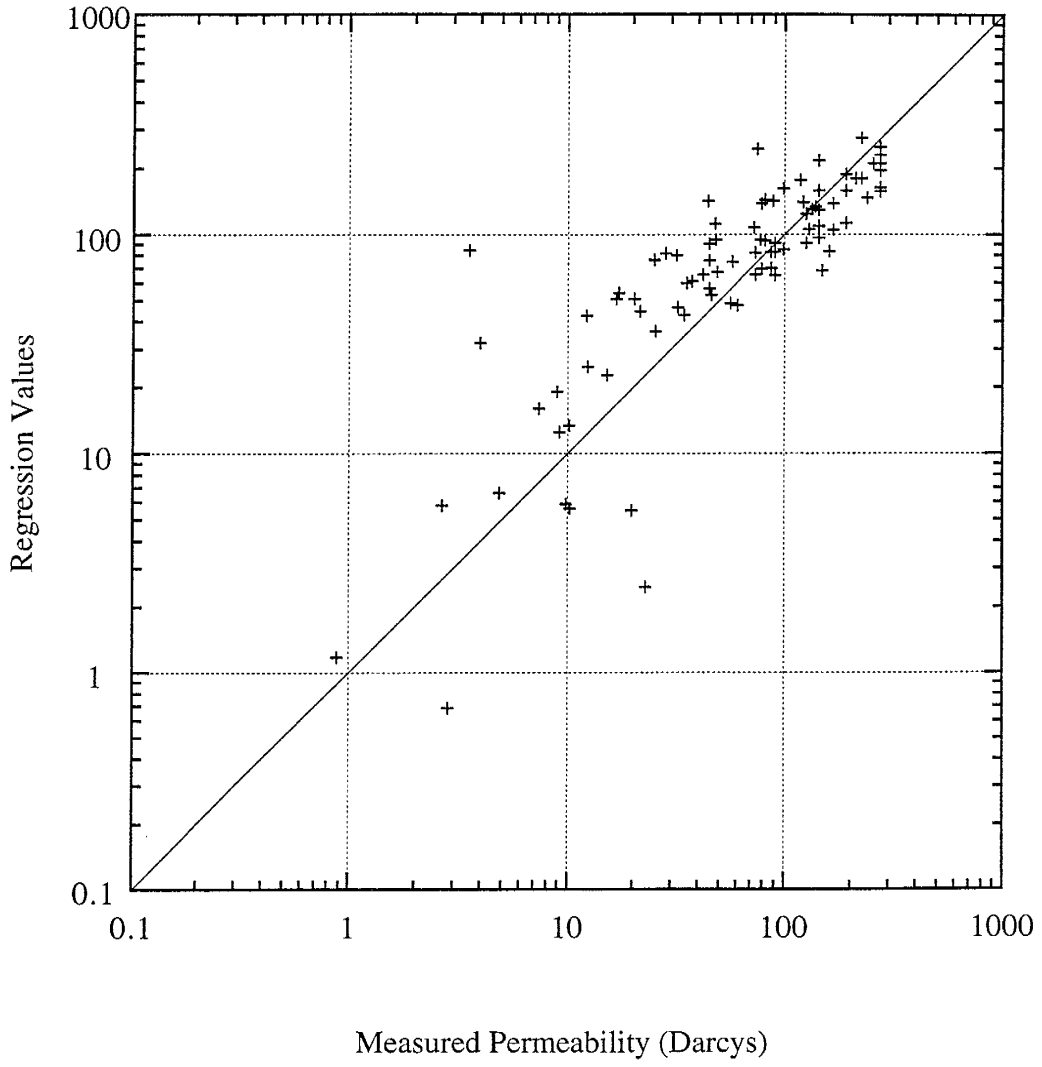

Regression analysis with $\log_{10}$ of measured permeability

	Pearson correlation R	R^2
$\log_{10}$ of measured permeability vs. phi grain size:		
-0.519(d_{10} phi complete) + 3.026	0.851	0.724
-0.462(d_{20} phi complete) + 2.651	0.842	0.709
-0.590(d_{10} phi cut) + 3.298	0.844	0.712
-0.553(d_{20} phi cut) + 2.943	0.854	0.729
$\log_{10}$ of measured permeability vs. entire distribution parameters:		
"LMSP1 COM"		
-0.752(Kruger phi complete) + 0.231(mean complete) - 0.014(% fines complete) + 2.731	0.872	0.760
"LMSP1 CUT"		
-0.456(Kruger phi cut) - 0.145(mean cut) - 0.003(% fines cut) + 2.802	0.887	0.787
"LMSP2 COM"		
-0.799(Kruger phi complete) + 0.249(mean complete) + 2.773	0.871	0.759
"LMSP2 CUT"		
-0.469(Kruger phi cut) - 0.140(mean cut) + 2.815	0.887	0.787
"LMSP3 COM"		
-0.389(d_{10} phi complete) - 0.076(mean complete) - 0.026(% fines complete) + 2.811	0.861	0.741
"LMSP3 CUT"		
-0.202(d_{10} phi cut) - 0.369(mean cut) - 0.010(% fines cut) + 2.820	0.883	0.780
"LMSP4 COM"		
-0.432(d_{10} phi complete) - 0.082(mean complete) + 2.894	0.856	0.733
"LMSP4 CUT"		
-0.221(d_{10} phi cut) - 0.374(mean cut) + 2.865	0.882	0.778

Regression d_{10} phi, complete distribution

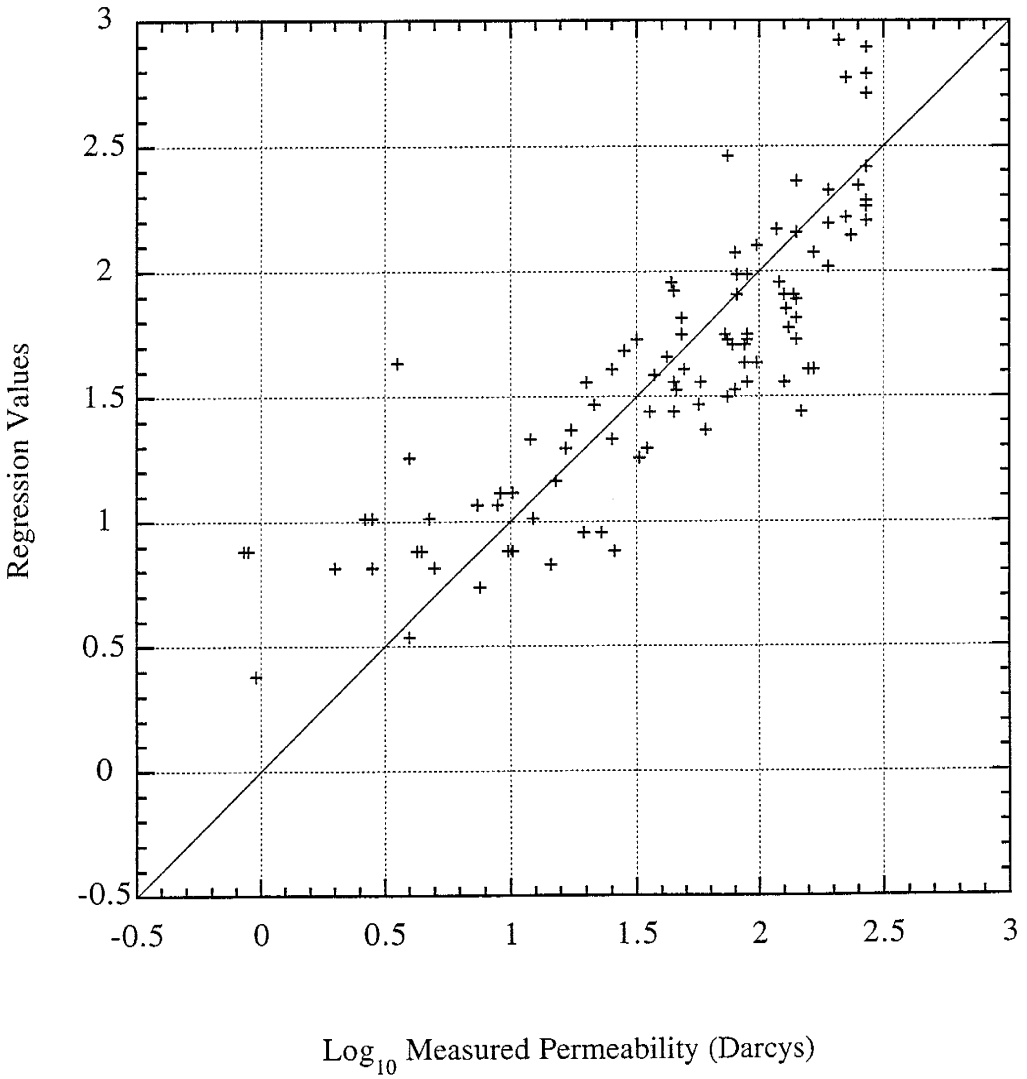

Regression d_{10} phi, cut distribution

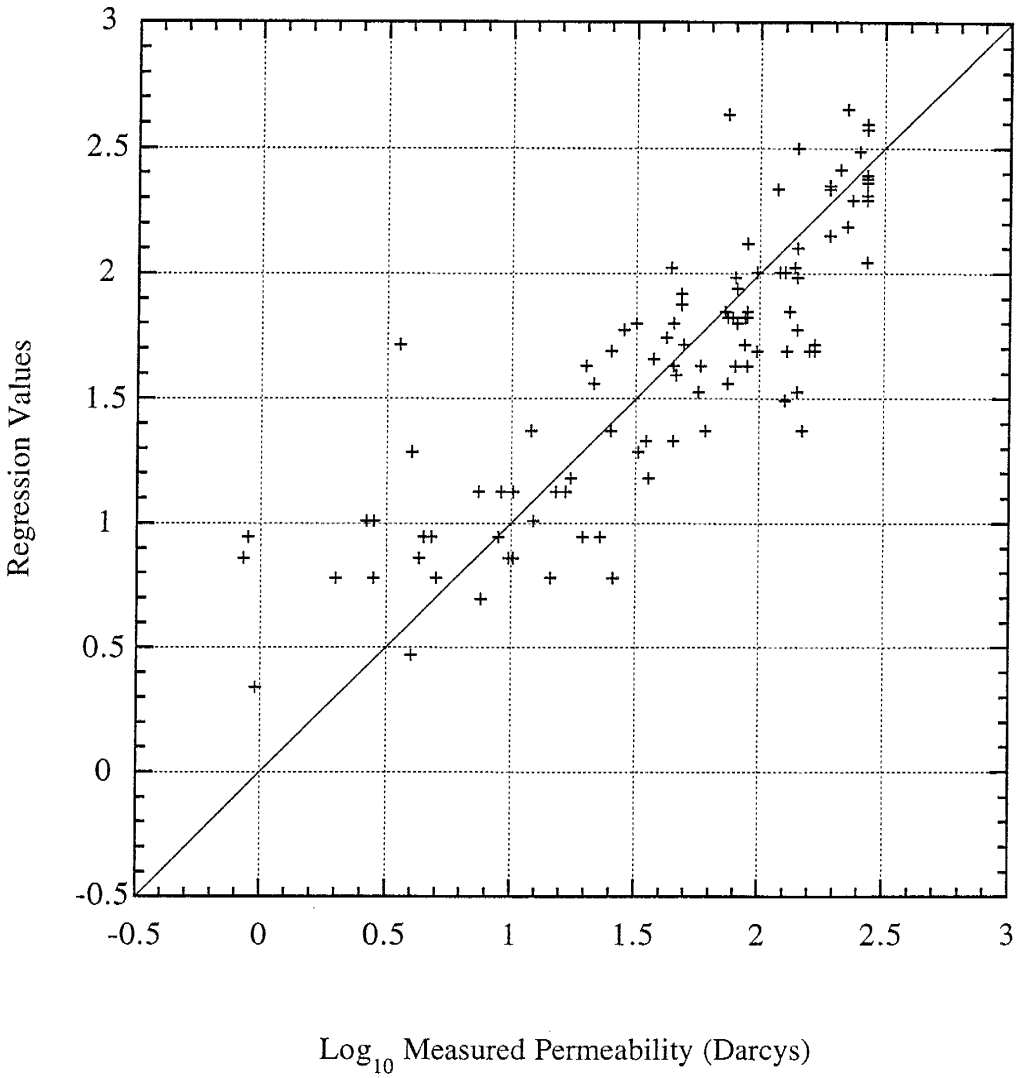

Regression d_{20} phi, complete distribution

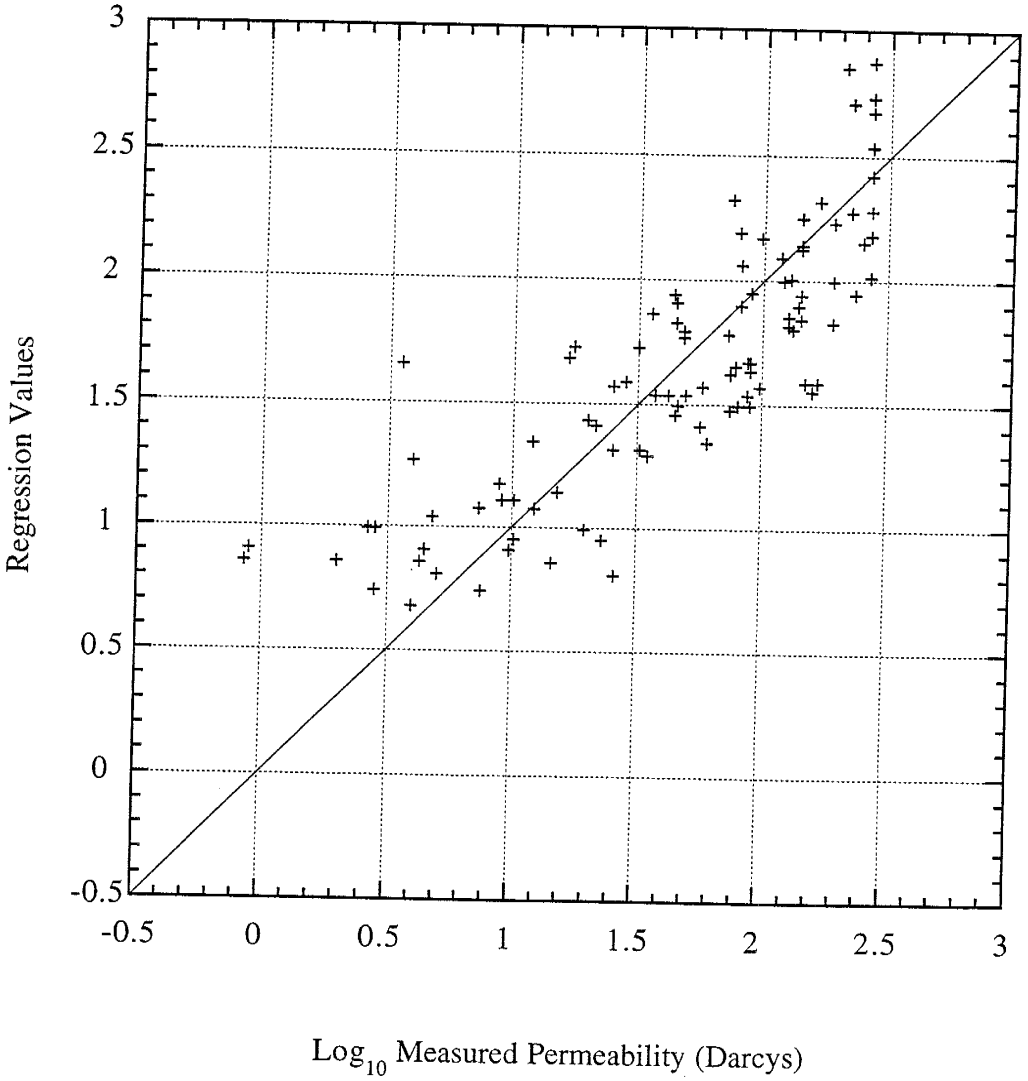

Regression d_{20} phi, cut distribution

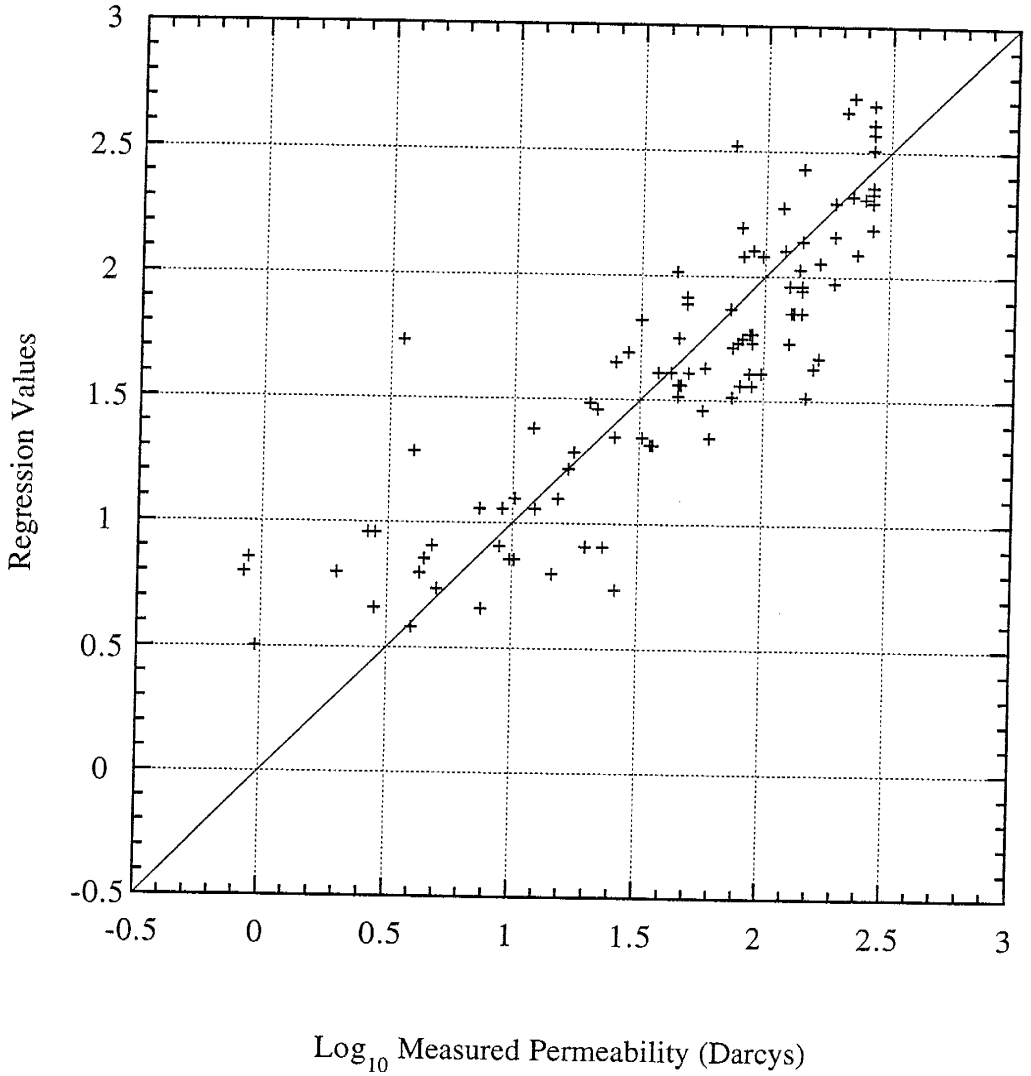

Regression LMSP1, complete distribution

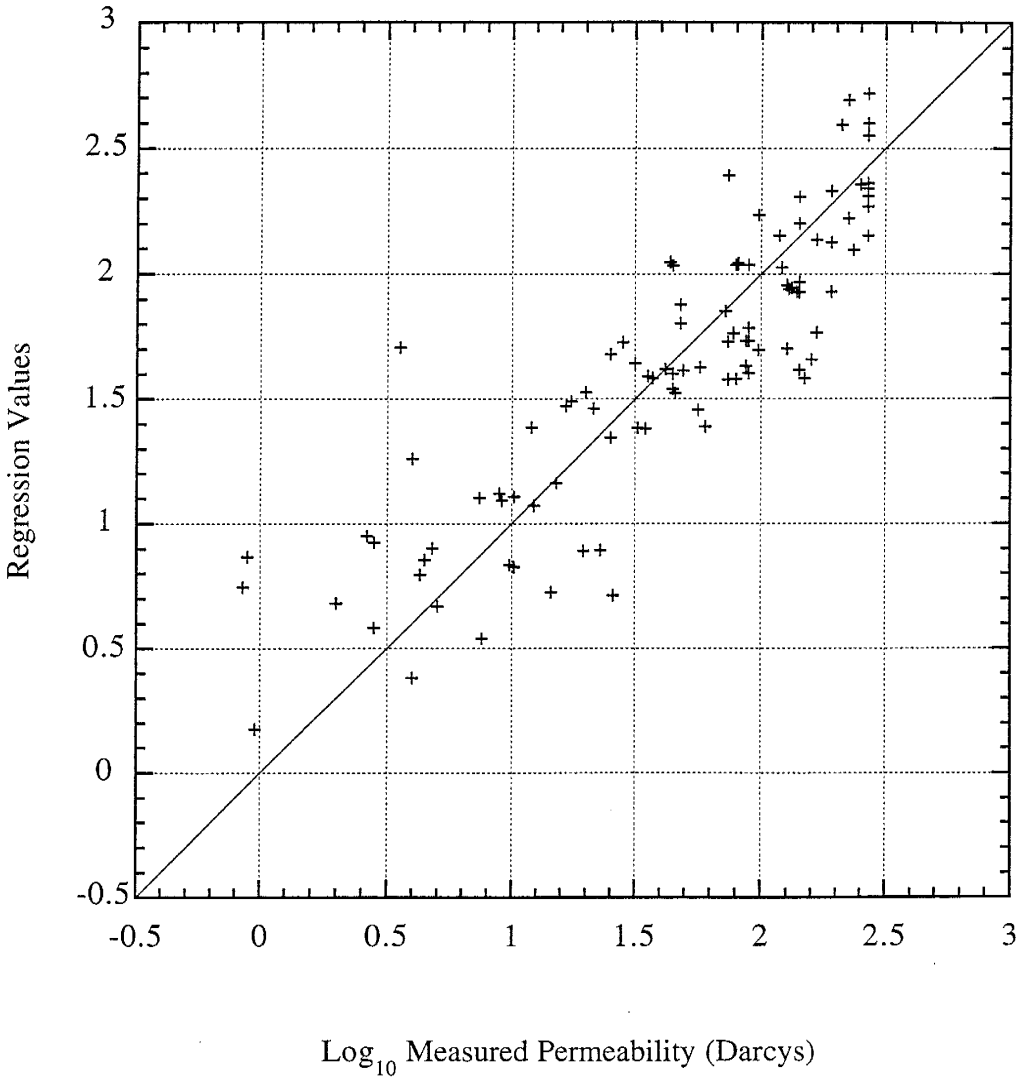

Regression LMSP1, cut distribution

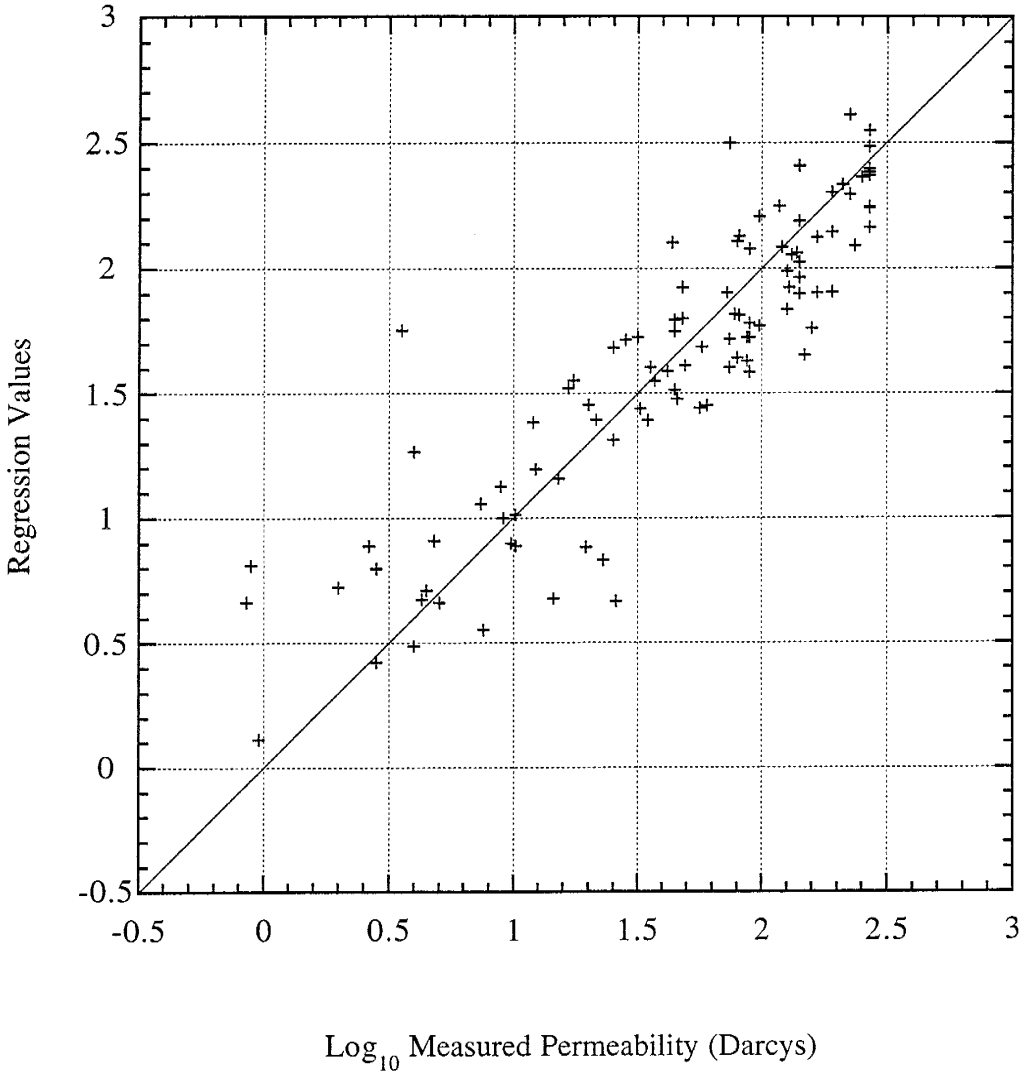

Regression LMSP2, complete distribution

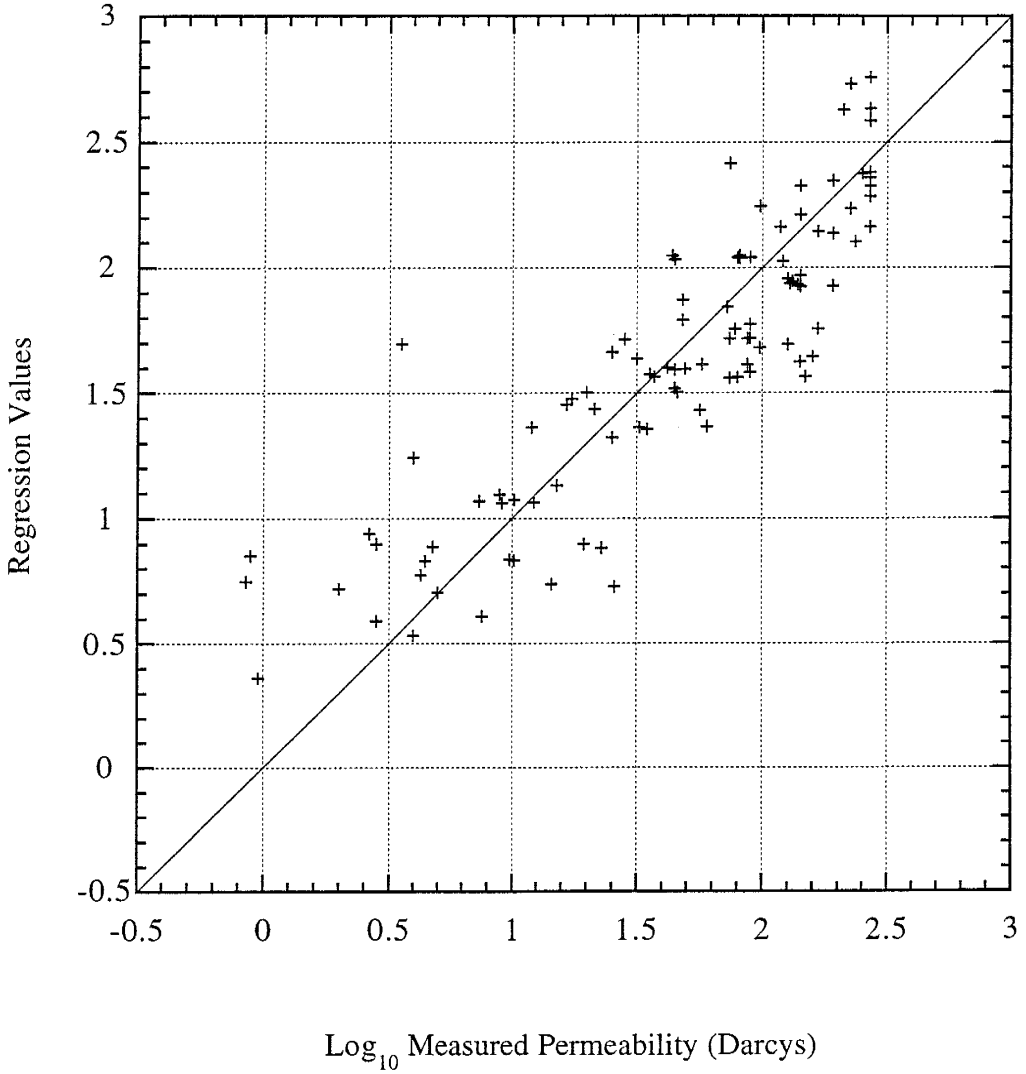

Regression LMSP2, cut distribution

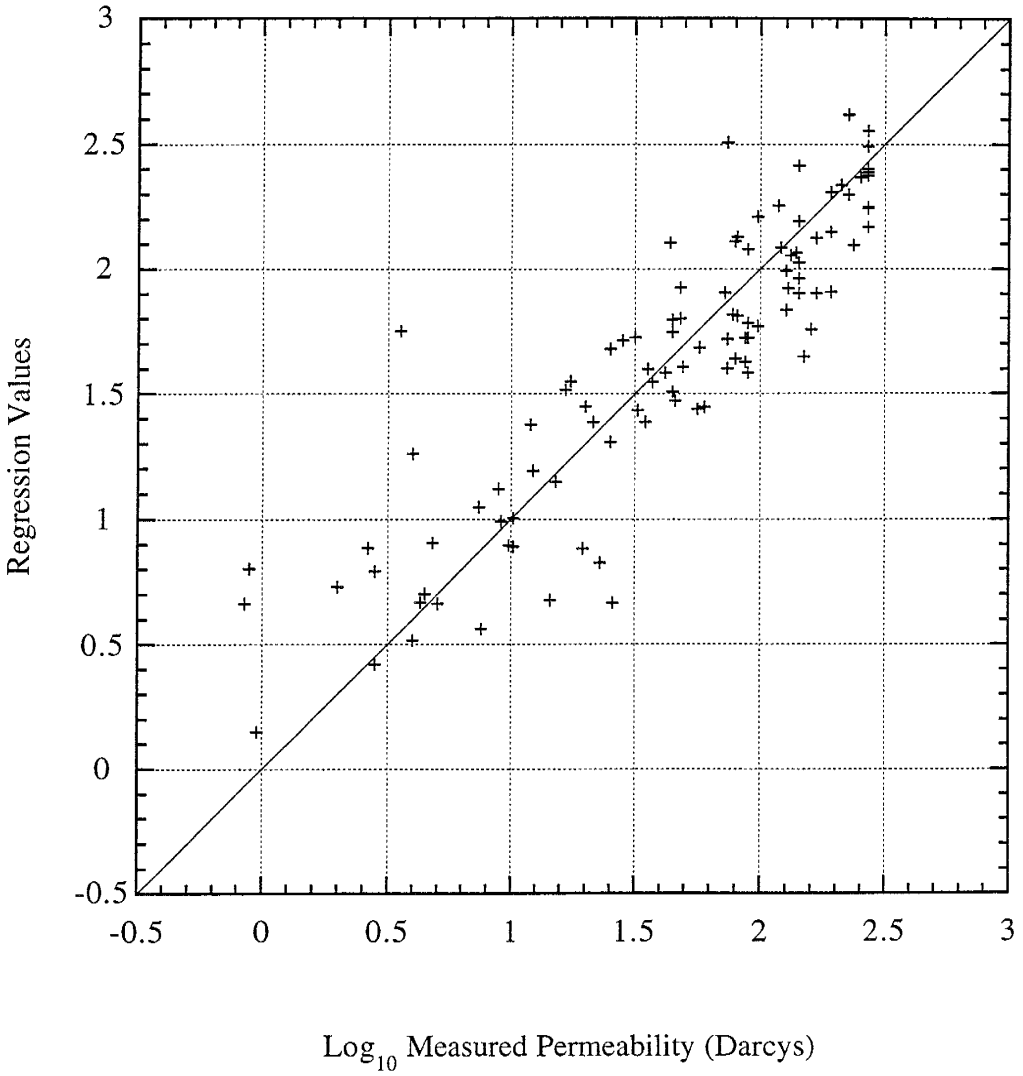

Regression LMSP3, complete distribution

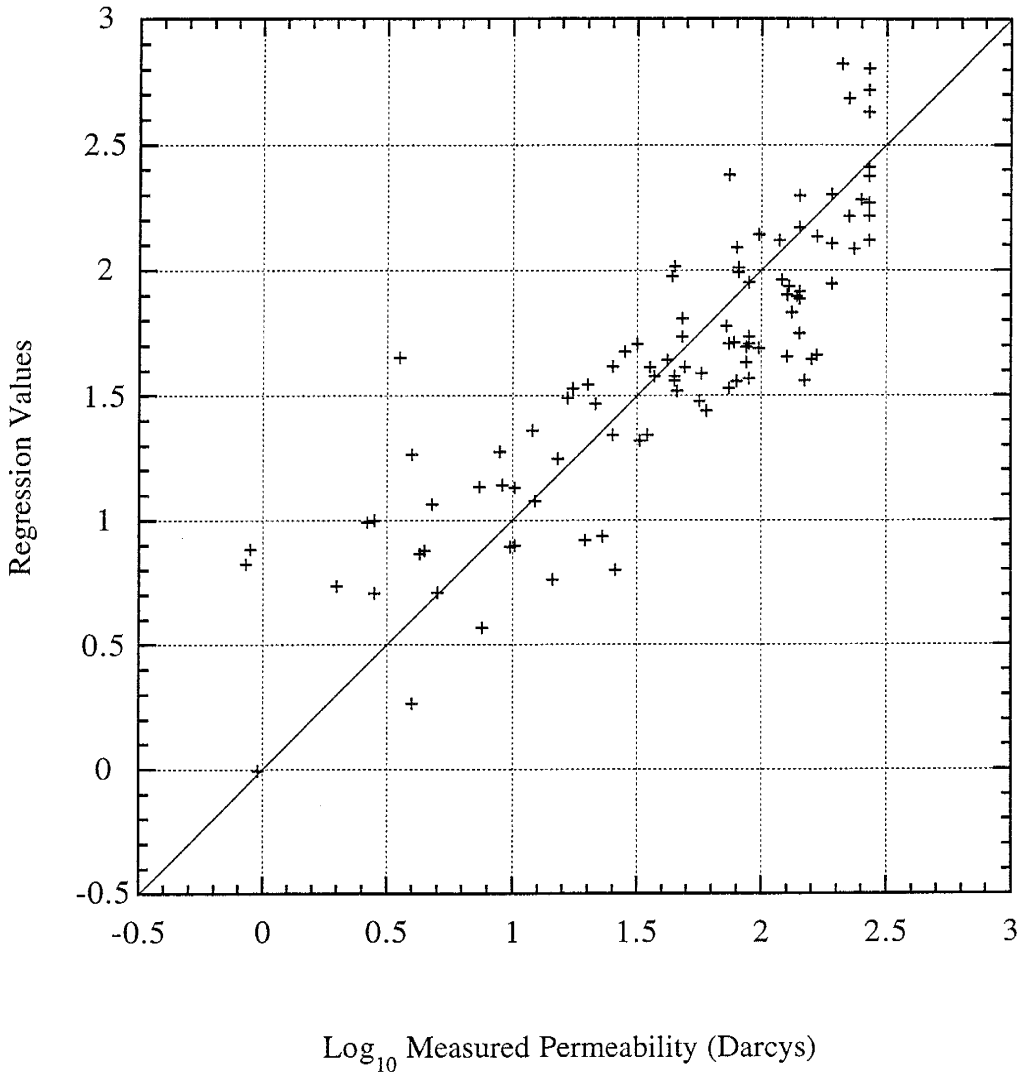

Regression LMSP3, cut distribution

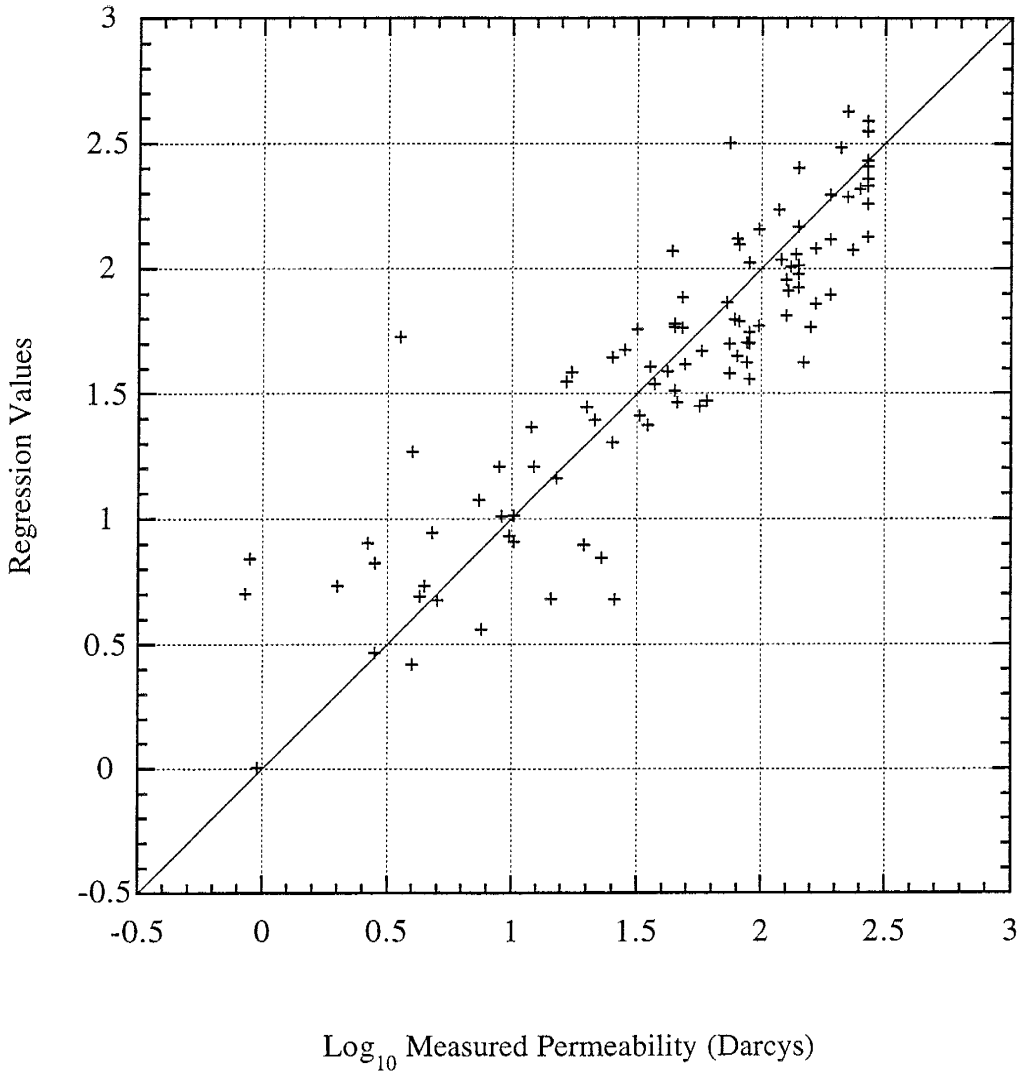

Regression LMSP4, complete distribution

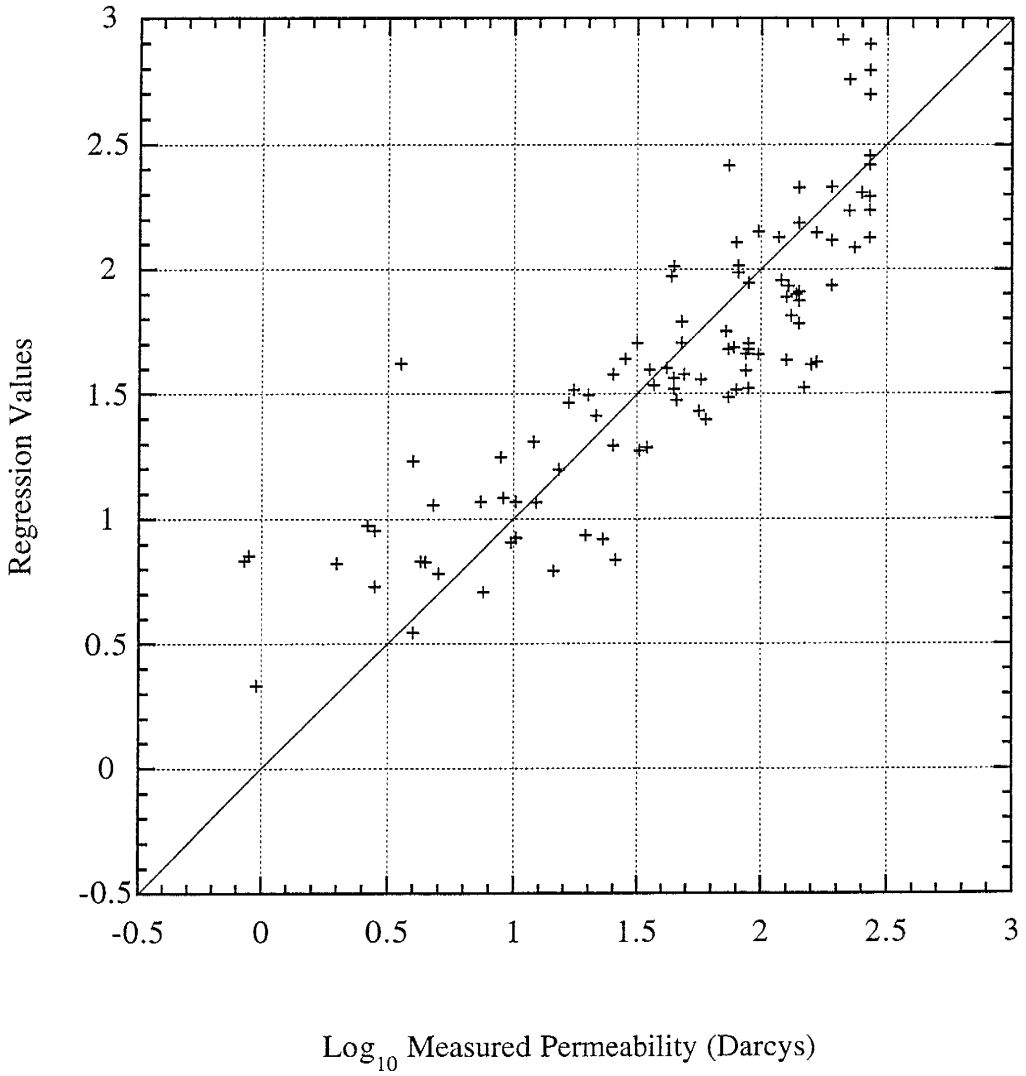

Regression LMSP4, cut distribution

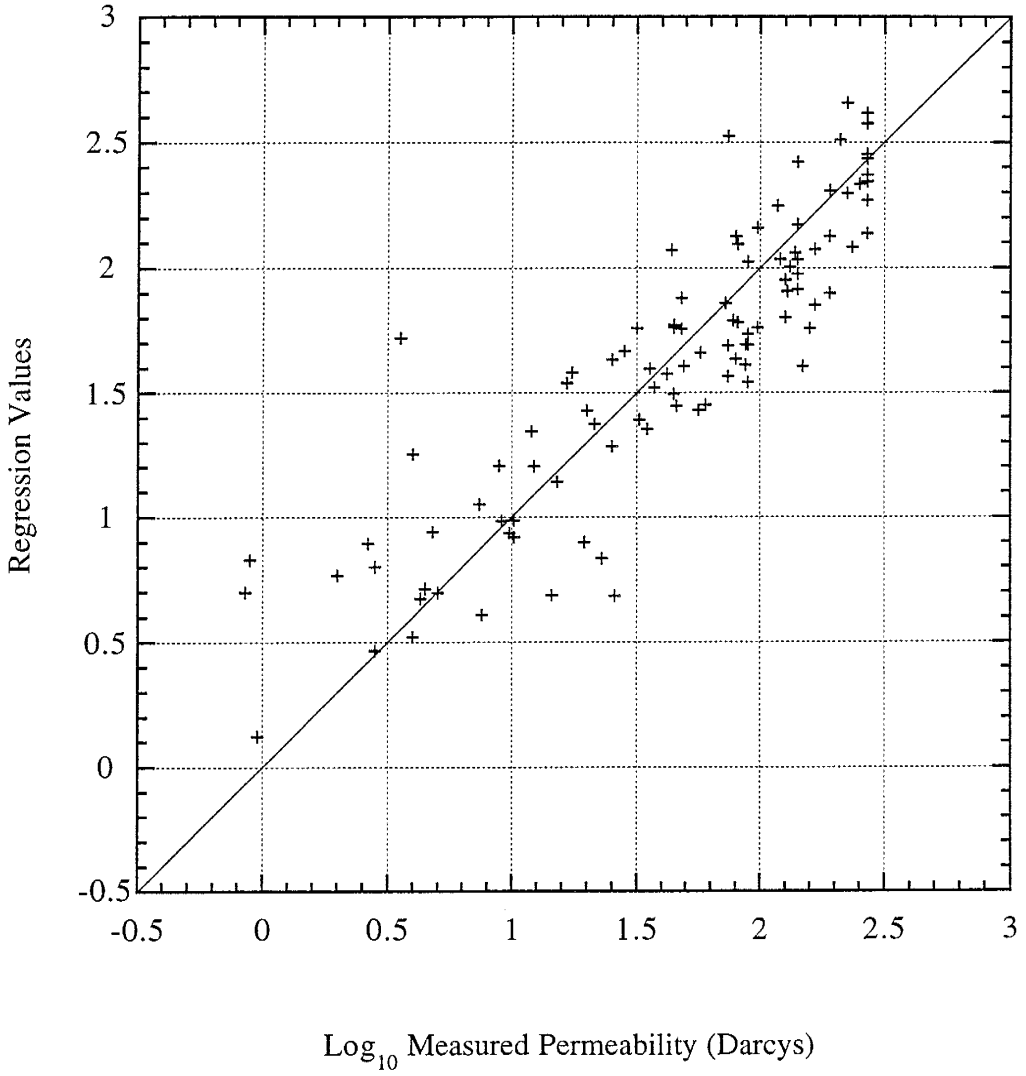

APPENDIX C

Scatter plots of measured permeability and outcrop sample effective diameters and grain size distribution parameters

Pearson correlation coefficients for measured permeability and grain distribution parameters

VARIABLE	COMPLETE SAMPLE	CUT SAMPLE
d_{10}, mm	0.803	0.819
d_{15}, mm	0.794	0.837
d_{17}, mm	0.789	0.839
d_{20}, mm	0.782	0.842
d_{50}, mm	0.571	0.812
Kruger, mm	0.821	0.844
d_{60}/d_{10}, mm	-0.049	0.154
d_{10}^2, mm	0.654	0.754
d_{17}^2, mm	0.636	0.765
d_{20}^2, mm	0.633	0.762
d_{10}, phi	-0.836	-0.796
d_{15}, phi	-0.833	-0.815
d_{17}, phi	-0.827	-0.818
d_{20}, phi	-0.818	-0.823
d_{50}, phi	-0.680	-0.782
Kruger, phi	-0.801	-0.791
d_{60}/d_{10}, phi	-0.509	-0.714
Mean	-0.718	-0.785
Standard Deviation	-0.034	-0.102
Skewness	0.321	0.505
Mean-Cubed Deviation	0.299	0.494
Percent Fines	-0.407	-0.405
Percent Pebbles	0.478	--
Max. Clast Diameter, phi	-0.402	--
Porosity	-0.198	-0.198
Lithification	-0.444	-0.444

Pearson correlation coefficients for $\log_{10}$ of measured permeability and grain distribution parameters

VARIABLE	COMPLETE SAMPLE	CUT SAMPLE
d_{10}, mm	0.669	0.749
d_{15}, mm	0.659	0.747
d_{17}, mm	0.655	0.746
d_{20}, mm	0.649	0.746
d_{50}, mm	0.524	0.734
Kruger, mm	0.723	0.813
d_{60}/d_{10}, mm	0.000	0.218
d_{10}, phi	-0.851	-0.846
d_{15}, phi	-0.842	-0.856
d_{17}, phi	-0.848	-0.861
d_{20}, phi	-0.834	-0.863
d_{50}, phi	-0.741	-0.852
Kruger, phi	-0.858	-0.885
d_{60}/d_{10}, phi	-0.396	-0.668
Mean	-0.776	-0.872
Standard Deviation	-0.018	-0.117
Skewness	0.261	0.439
Mean-Cubed Deviation	0.310	0.458
Percent Fines	-0.634	-0.634
Percent Pebbles	0.397	--
Max. Clast Diameter, phi	-0.430	--
Porosity	-0.161	-0.161
Lithification	-0.611	-0.611

Influence of Porosity on Permeability

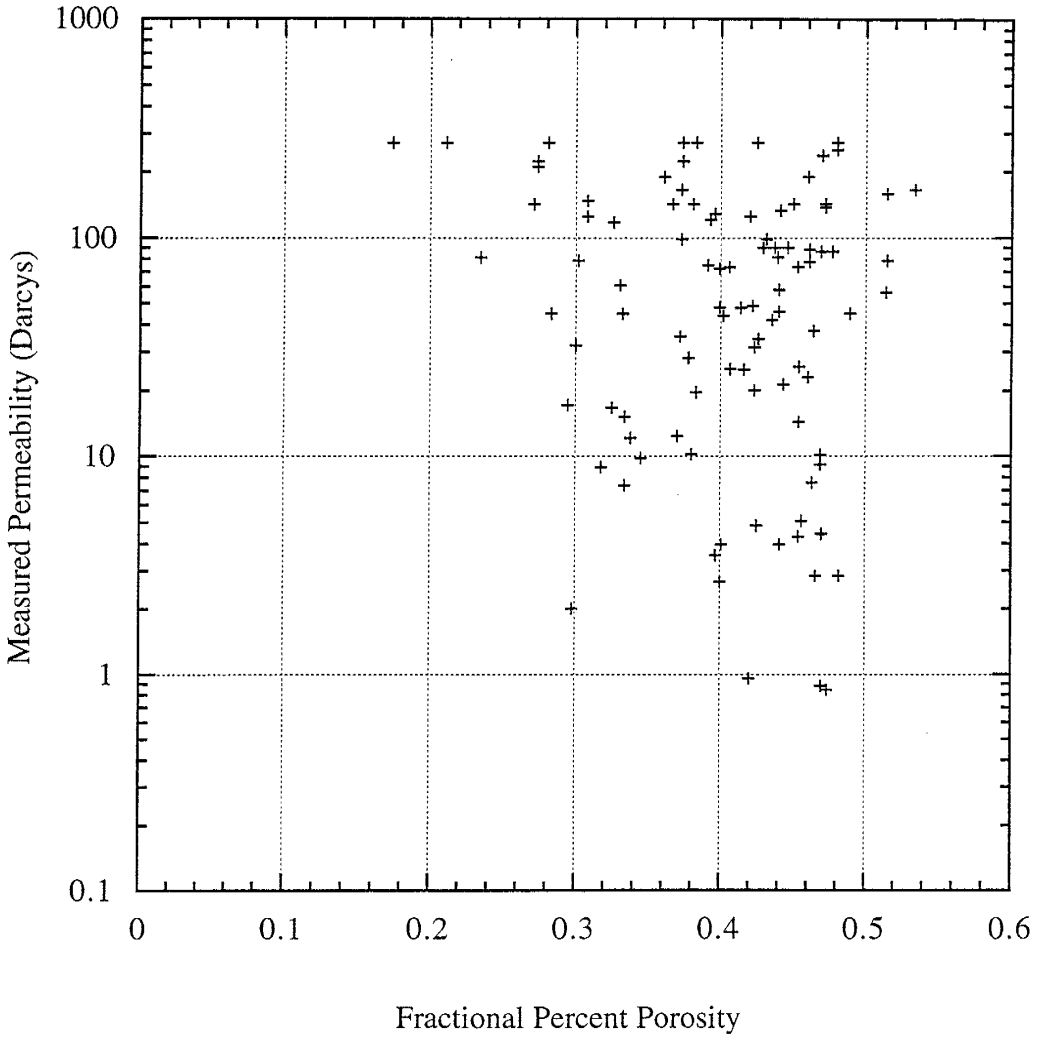

Influence of Cementation on Permeability

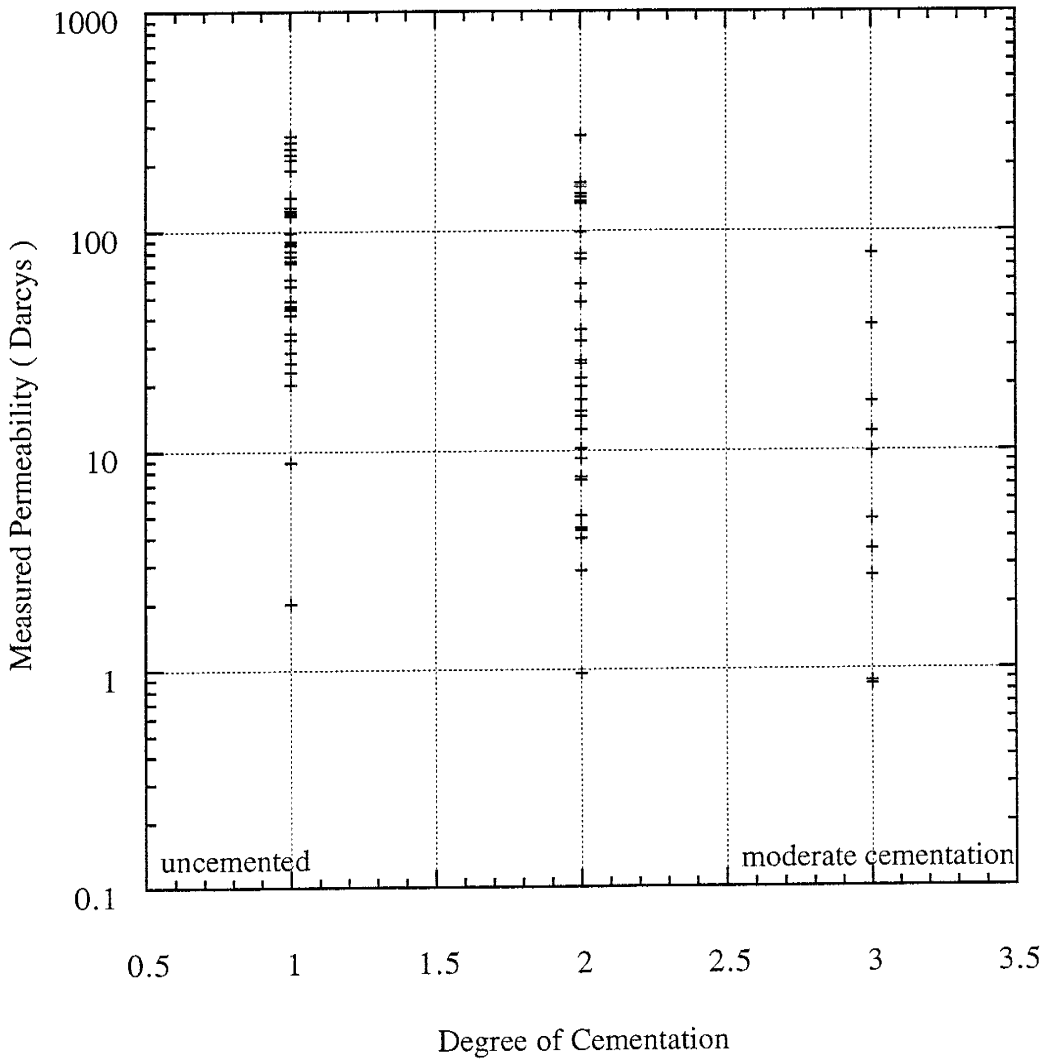

Influence of Mean Grain Size on Permeability

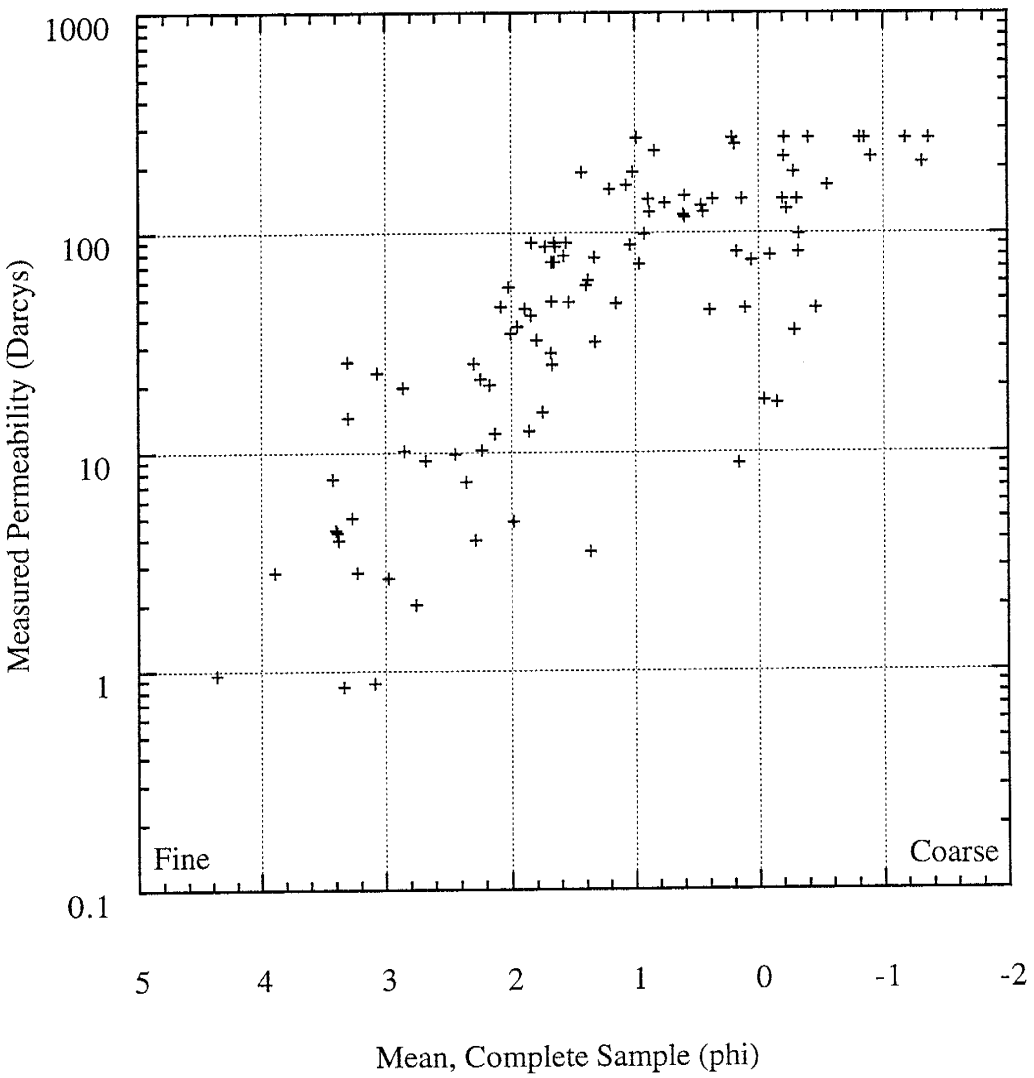

Influence of Mean Grain Size on Permeability

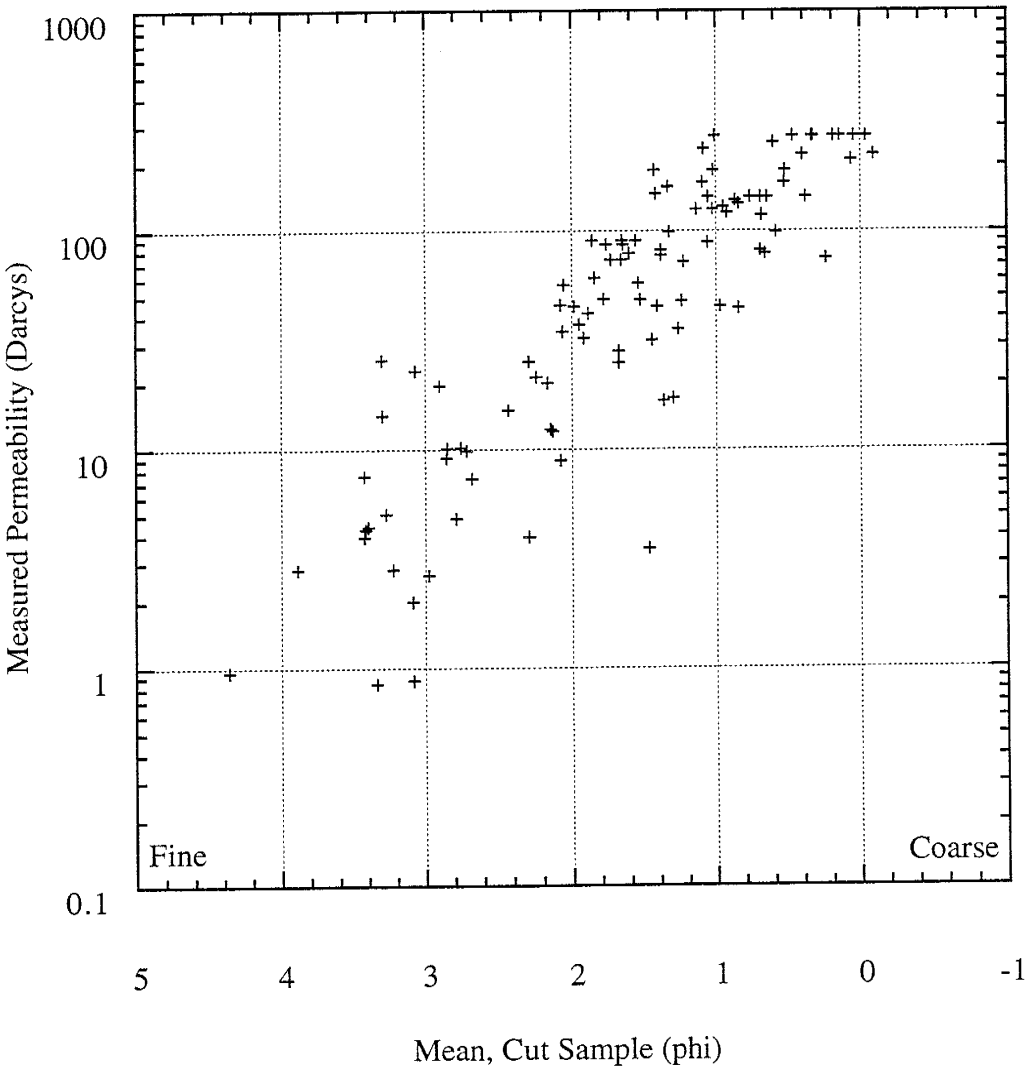

Influence of Standard Deviation on Permeability

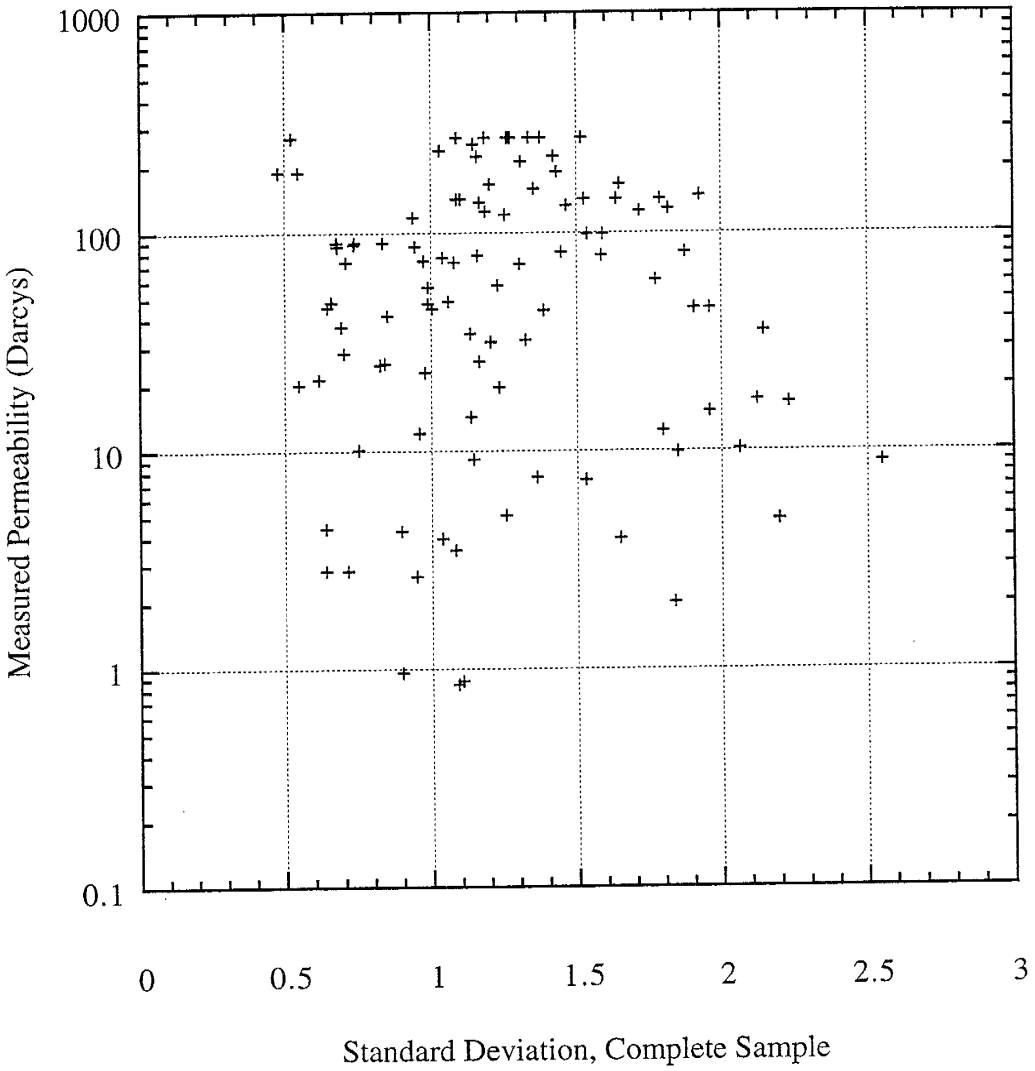

Influence of Standard Deviation on Permeability

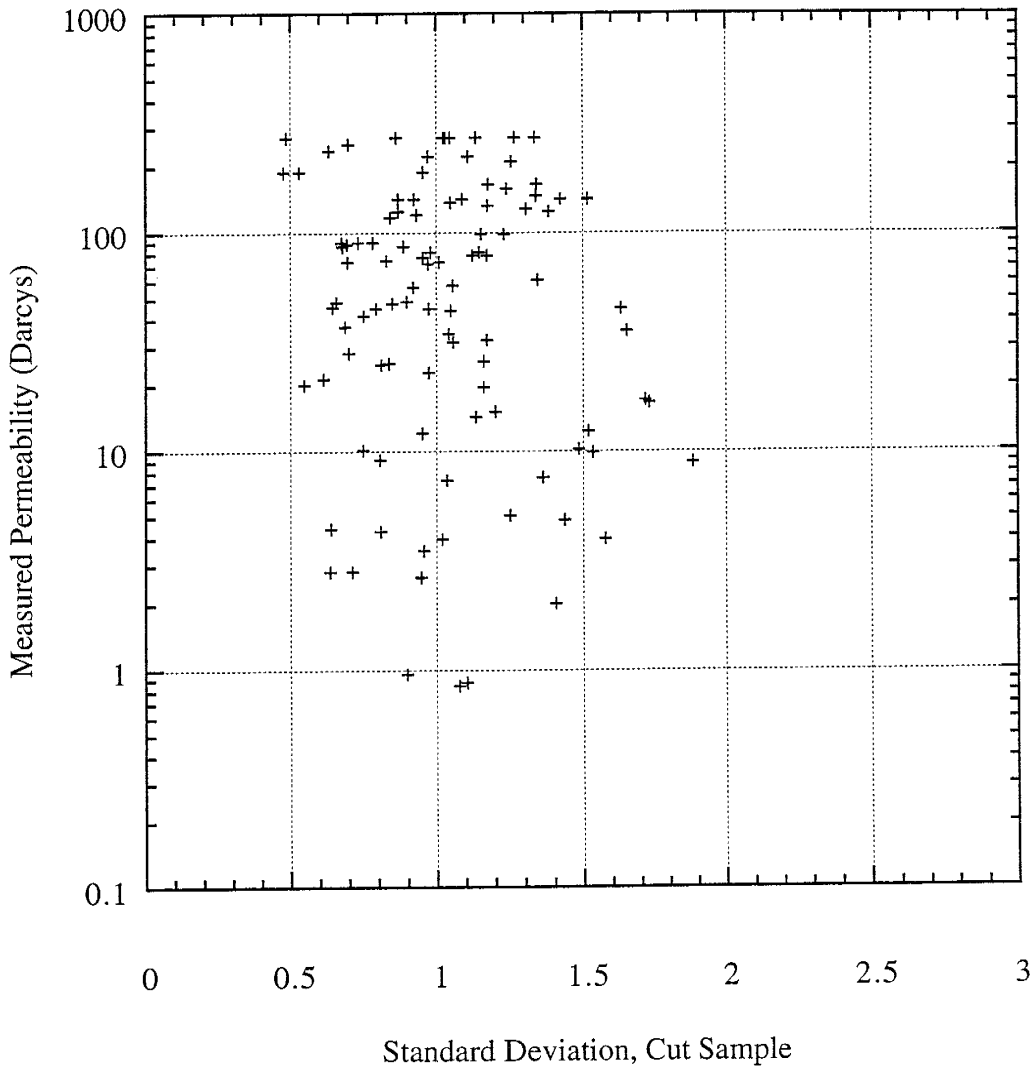

Influence of Skewness on Permeability

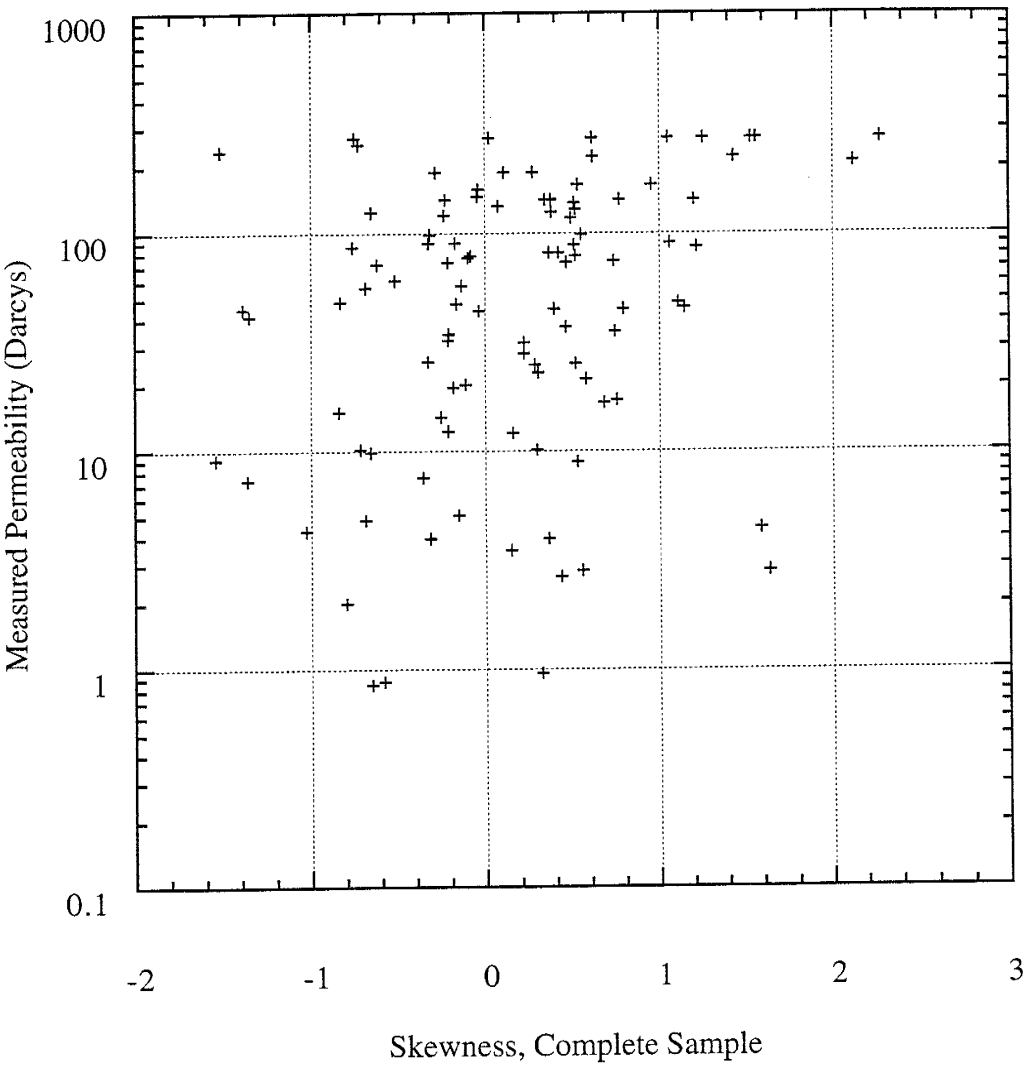

Influence of Skewness on Permeability

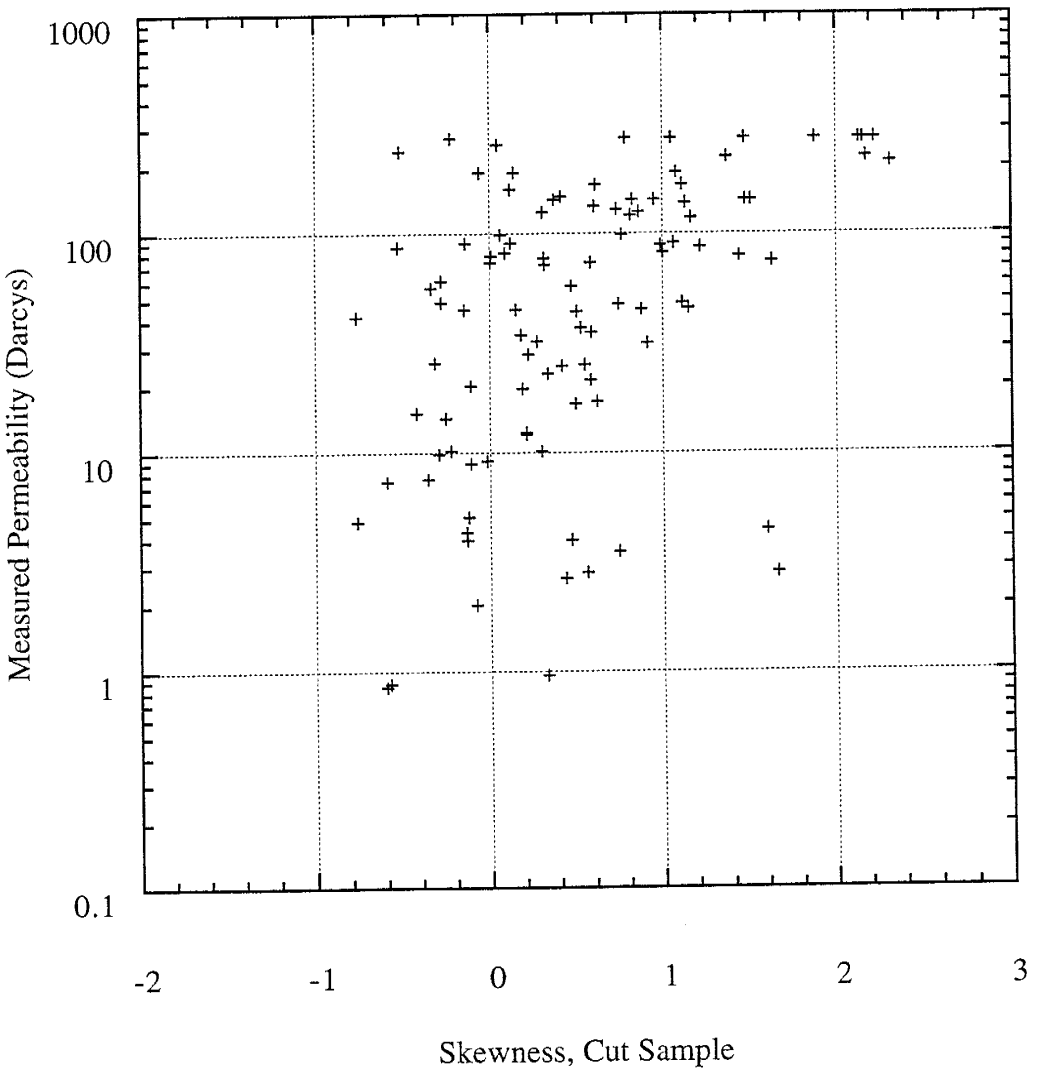

Influence of Percent Fines on Permeability

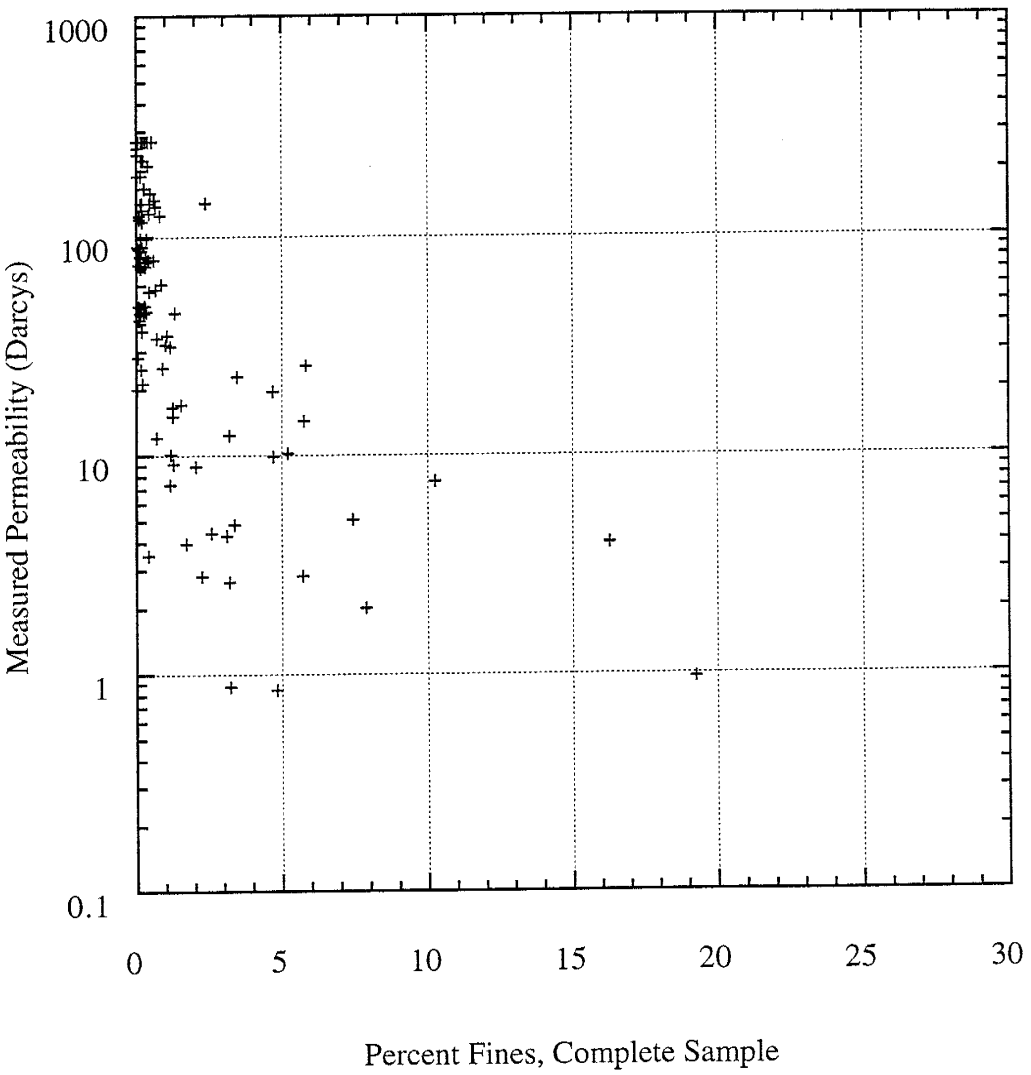

Influence of Percent Fines on Permeability

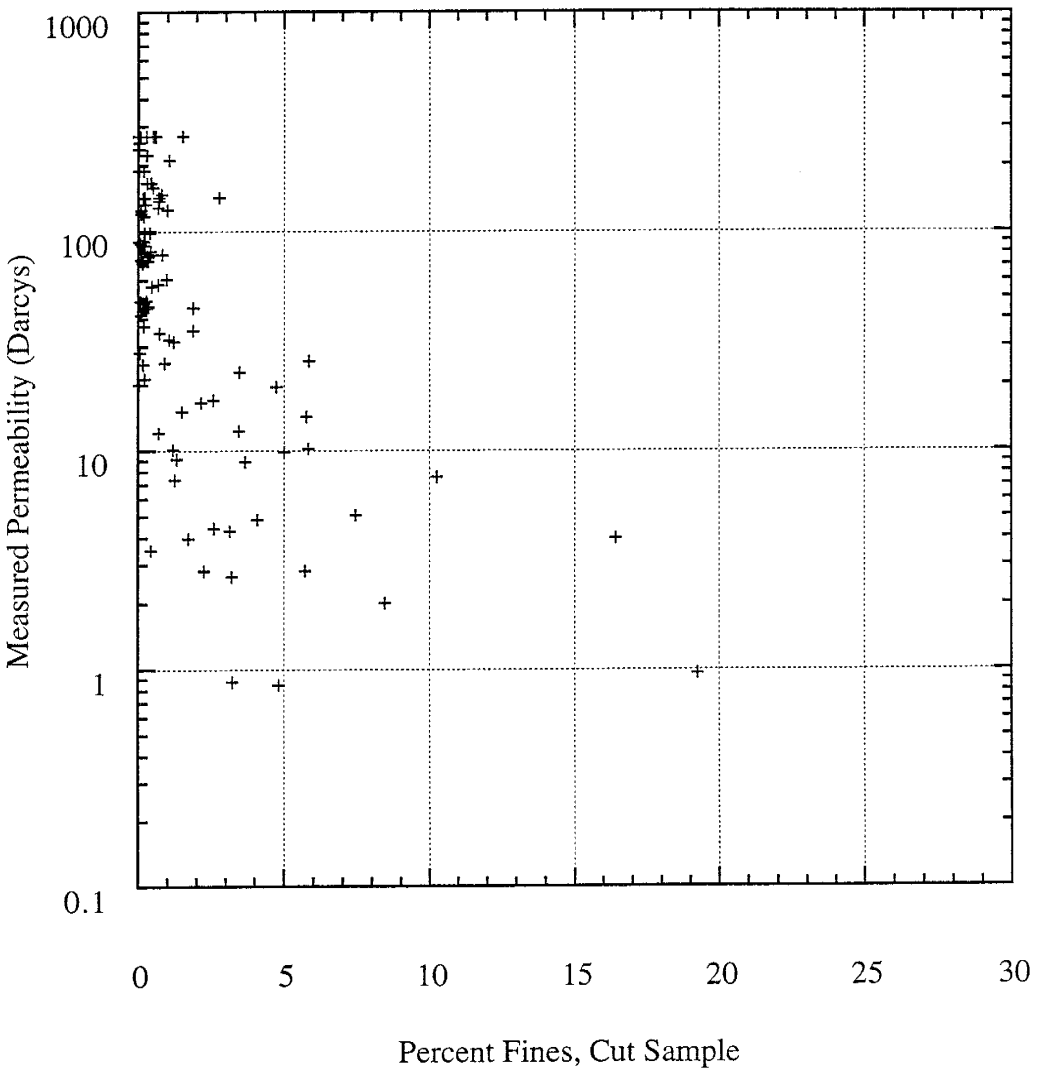

Influence of the Uniformity Coefficient on Permeability

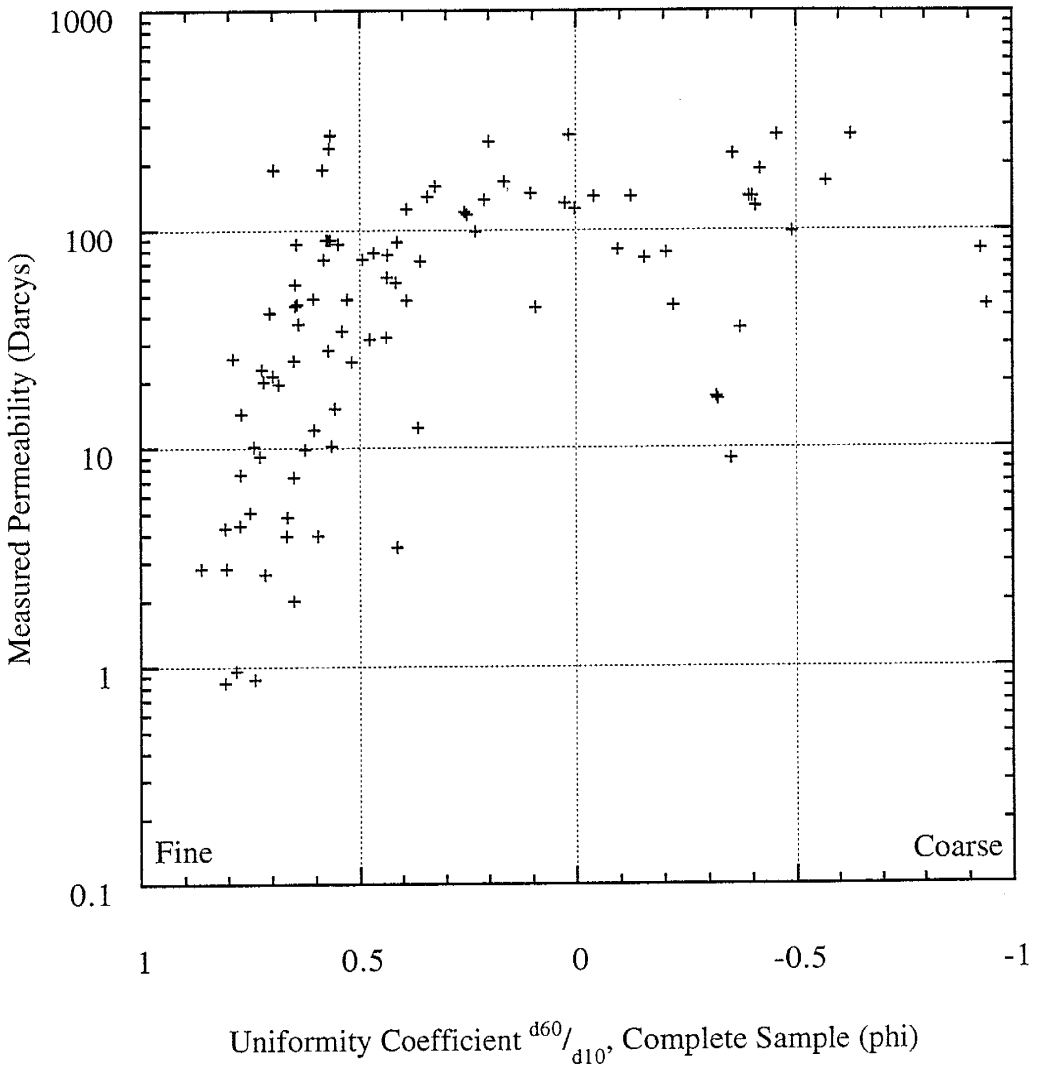

Influence of the Uniformity Coefficient on Permeability

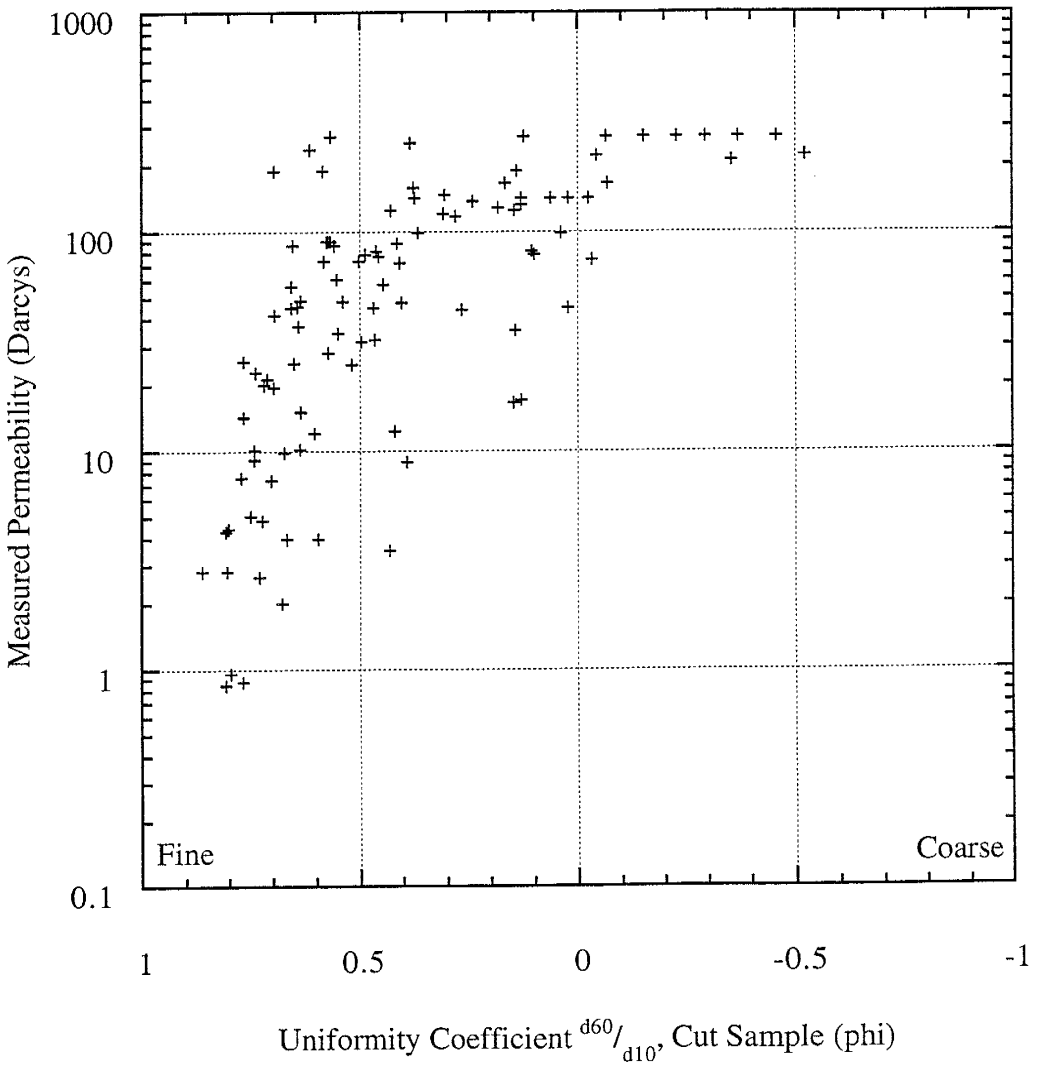

Influence of d_{10} Particle Size on Permeability

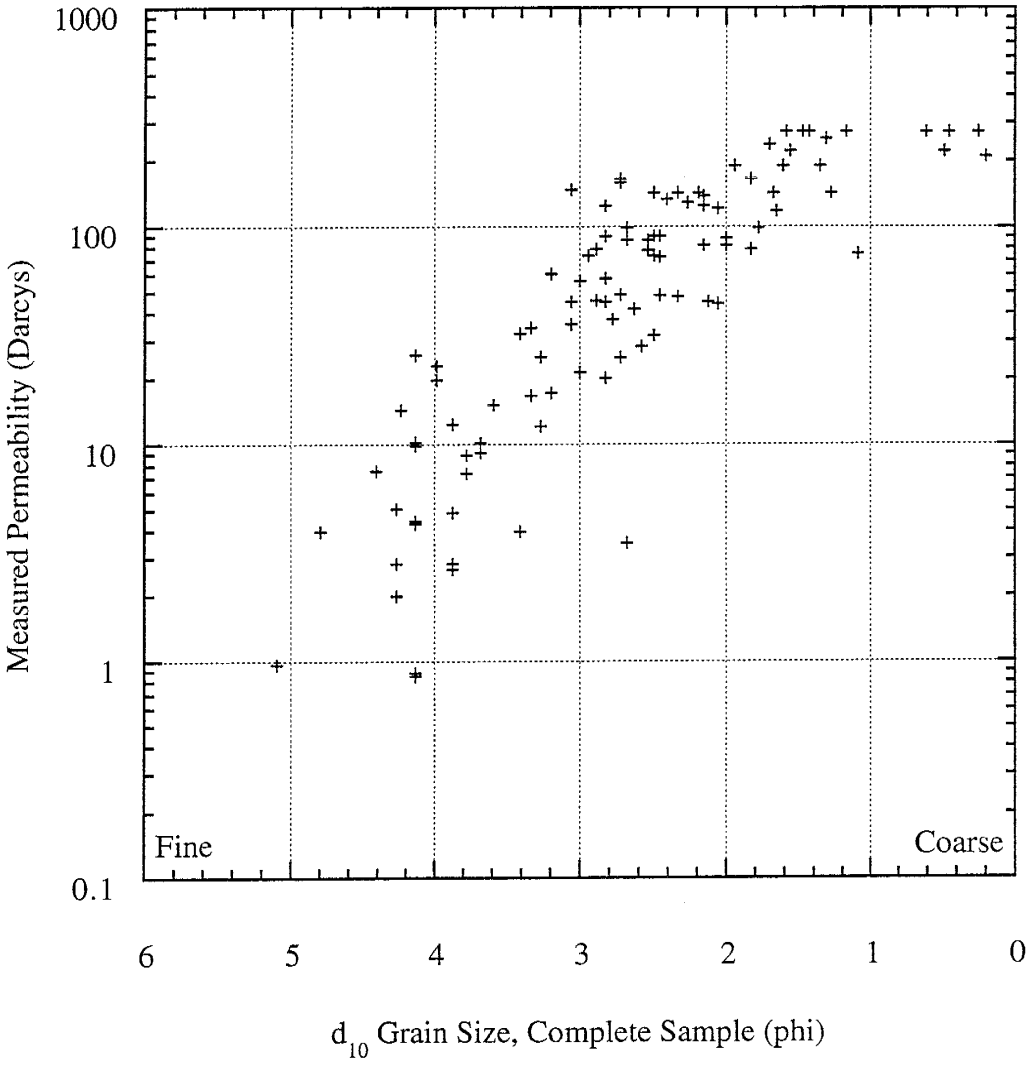

Influence of d_{10} Grain Size on Permeability

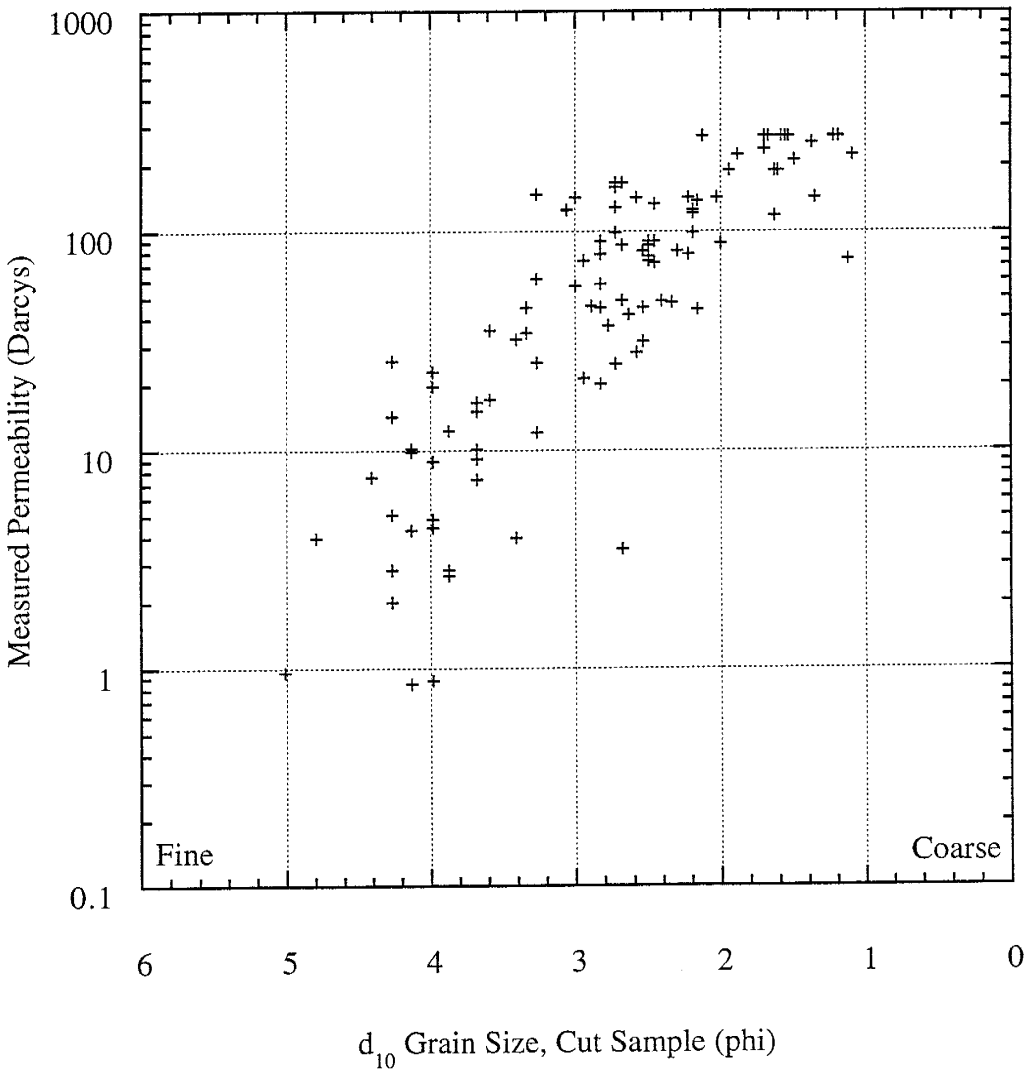

Influence of d_{15} Grain Size on Permeability

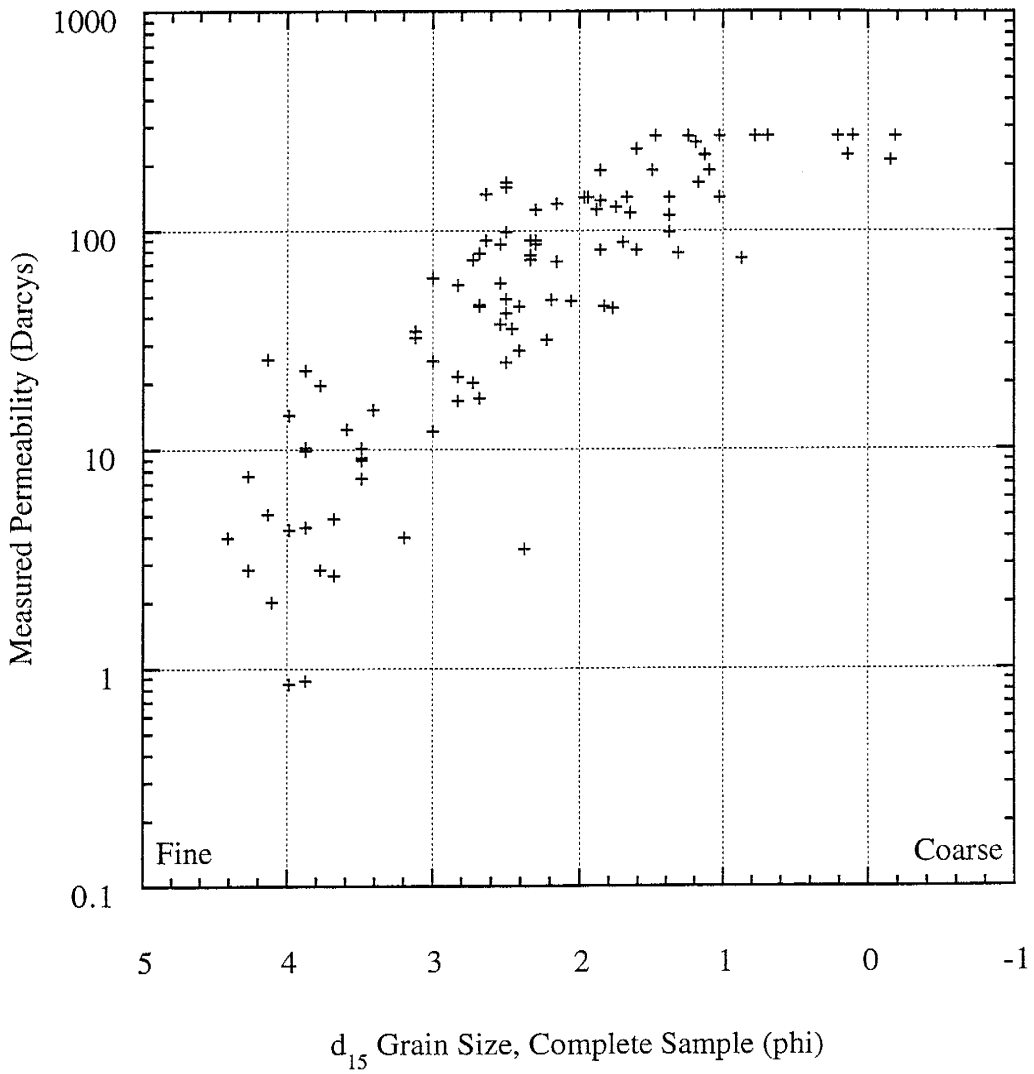

Influence of d_{15} Grain Size on Permeability

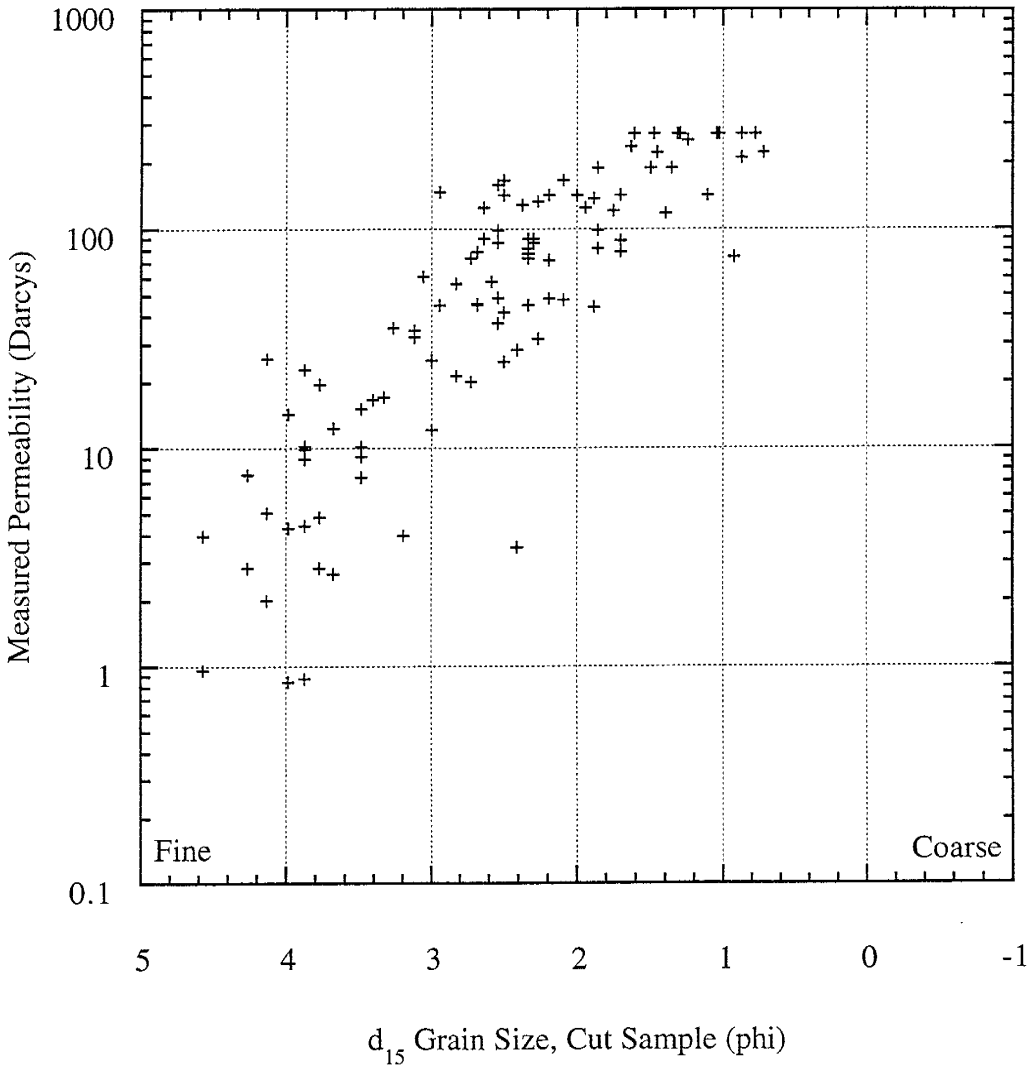

Influence of d_{17} Grain Size on Permeability

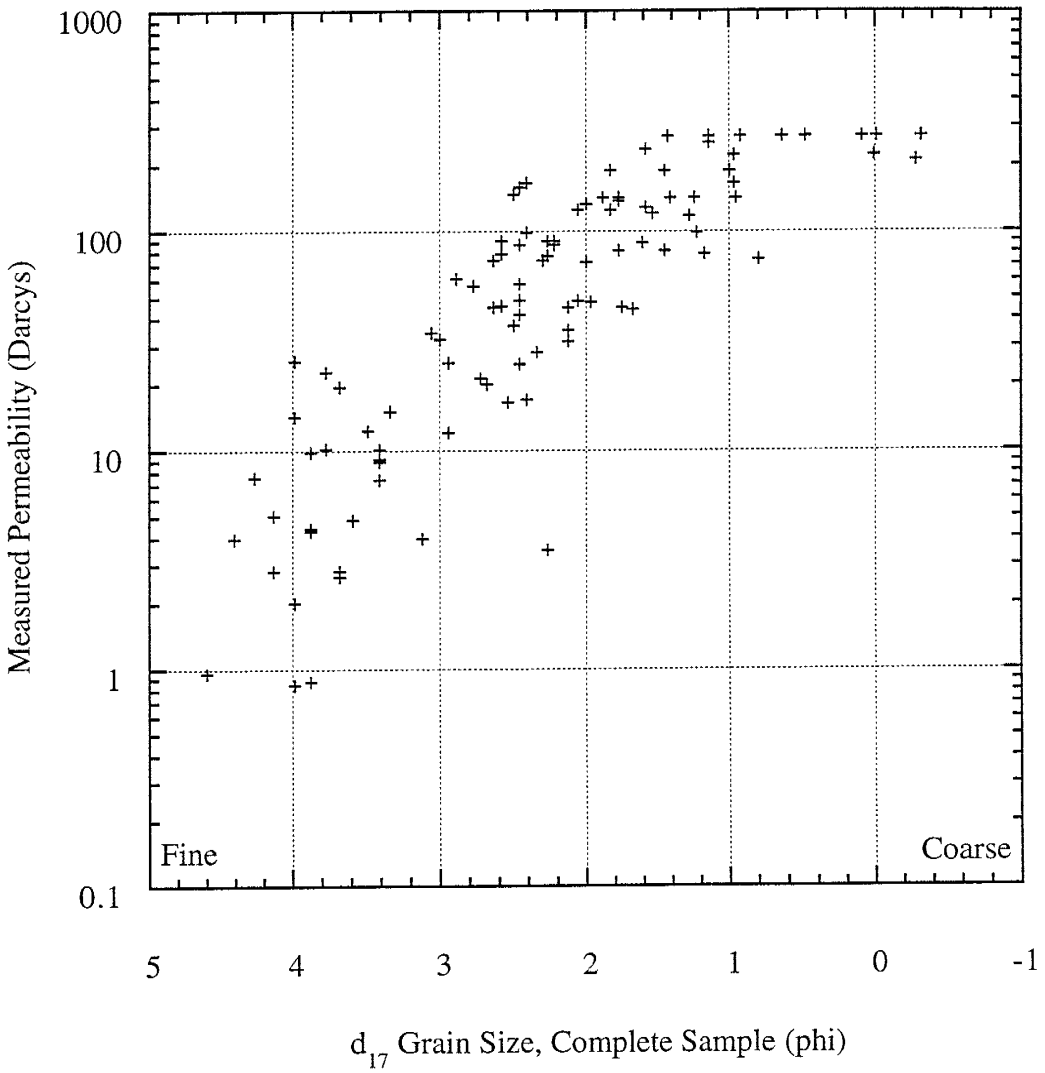

Influence of d_{17} Grain Size on Permeability

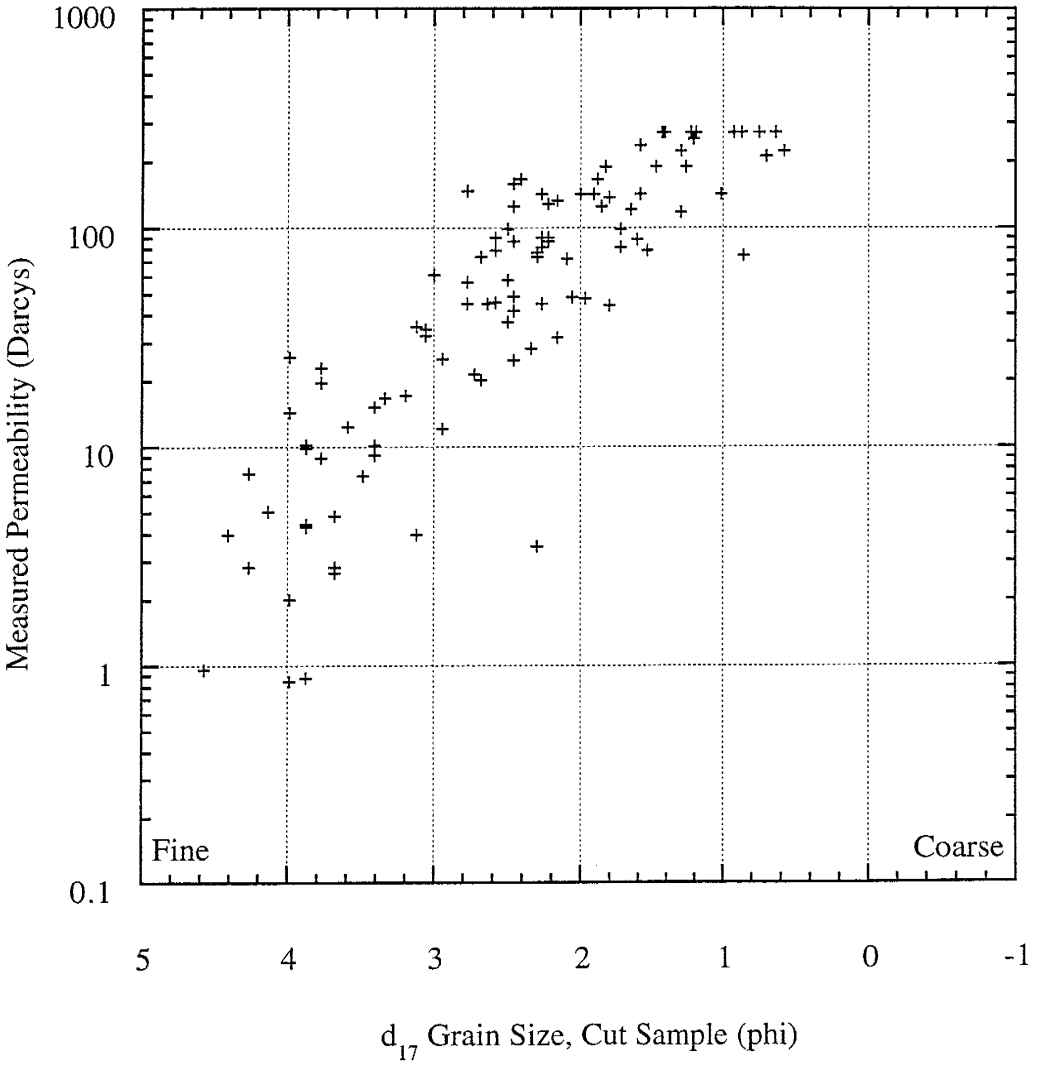

Influence of d_{20} Grain Size on Permeability

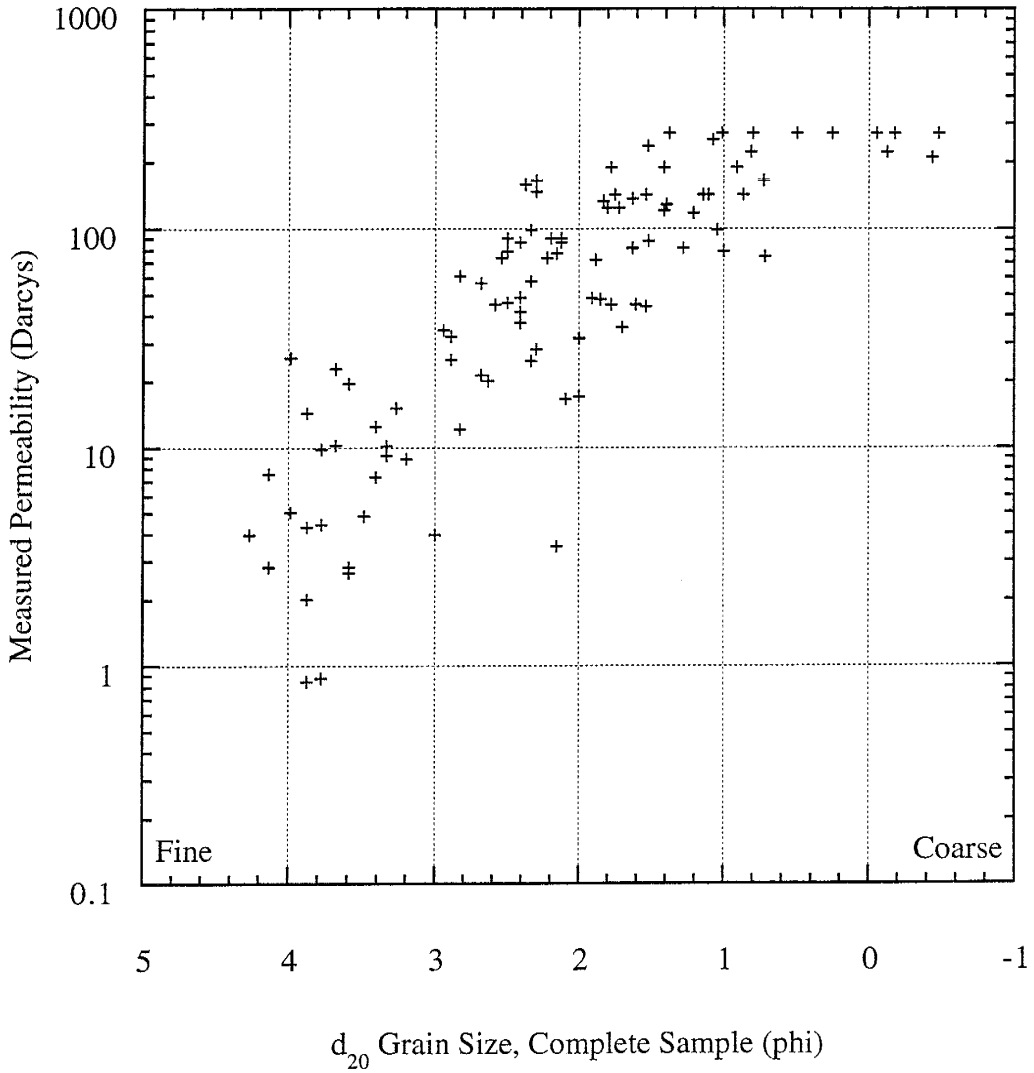

Influence of d_{20} Grain Size on Permeability

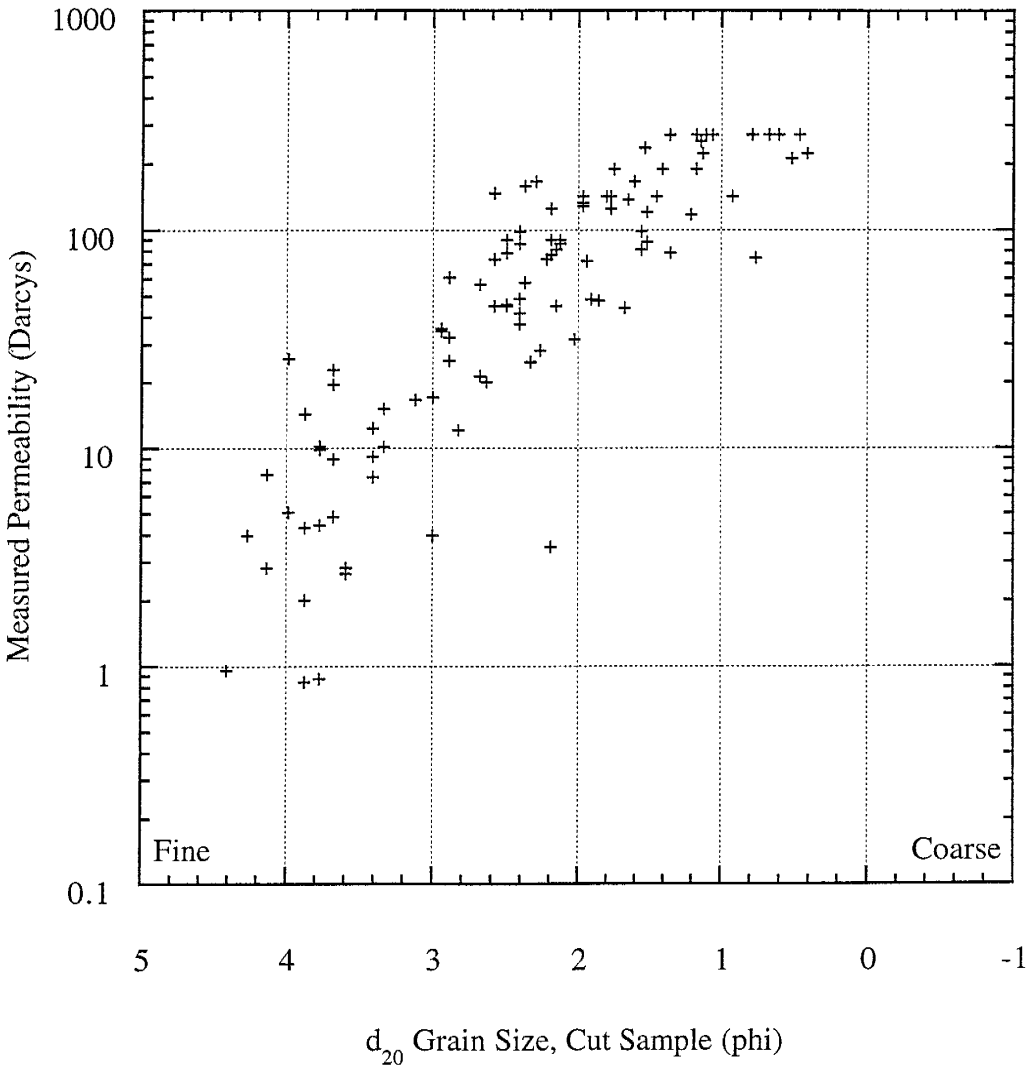

Influence of d_{50} Grain Size on Permeability

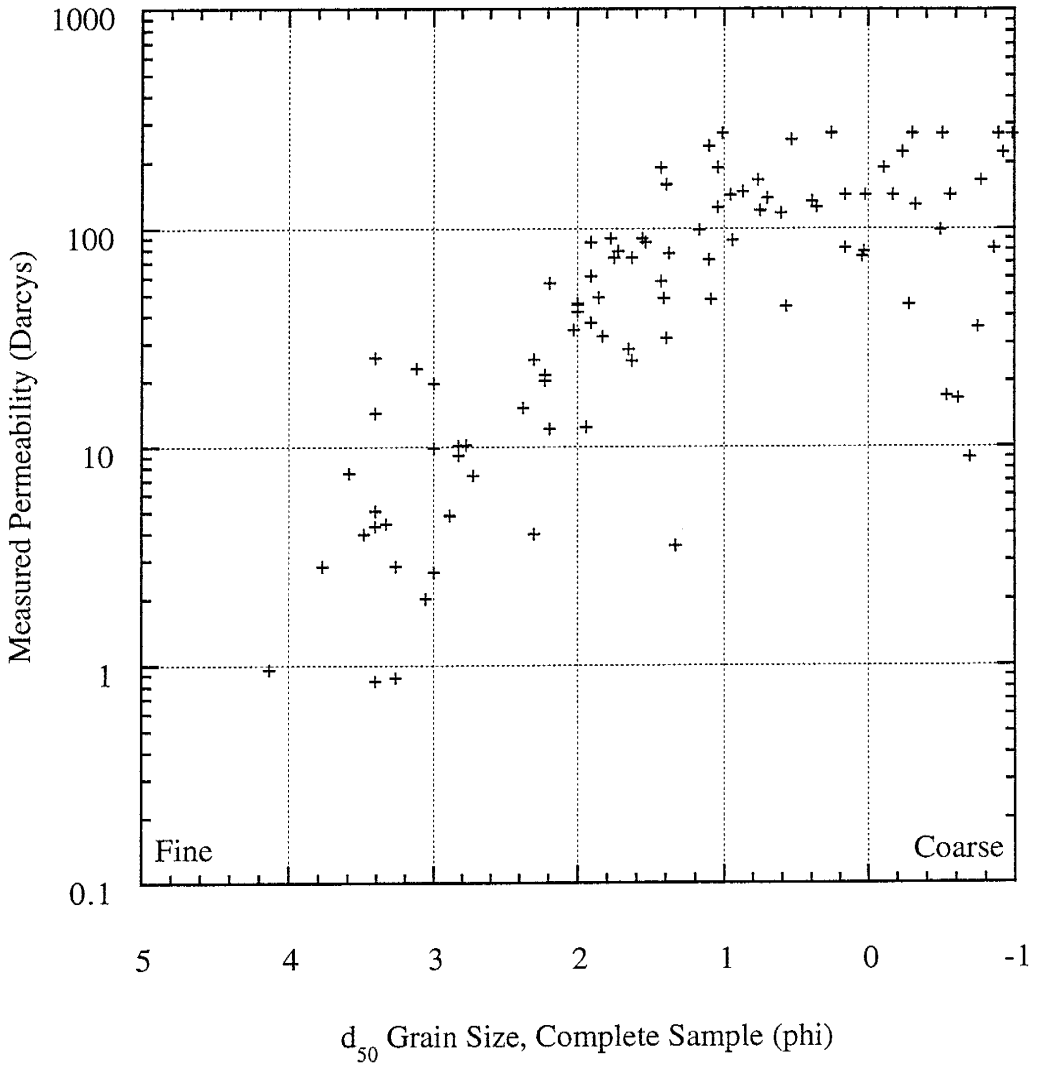

Influence of d_{50} Grain Size on Permeability

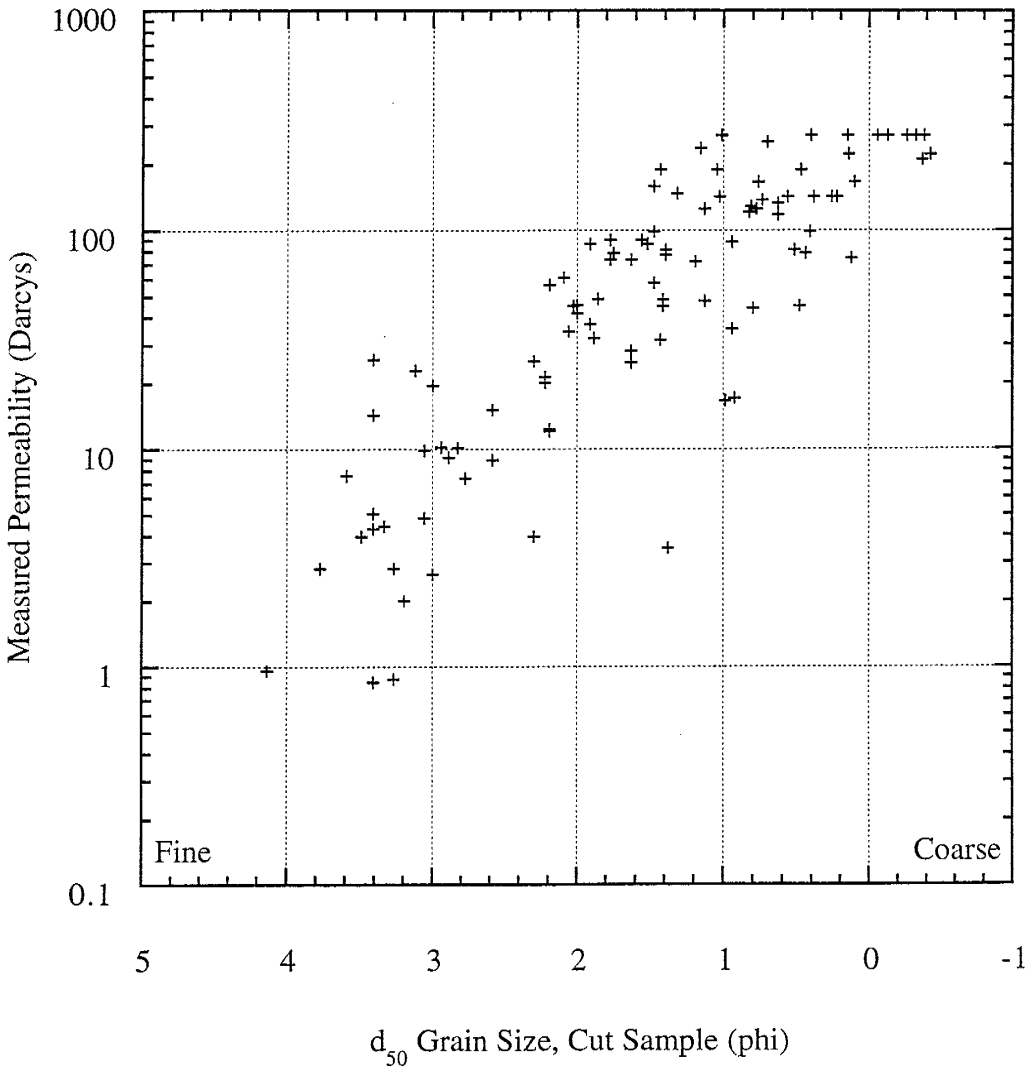

Influence of Kruger Diameter on Permeability

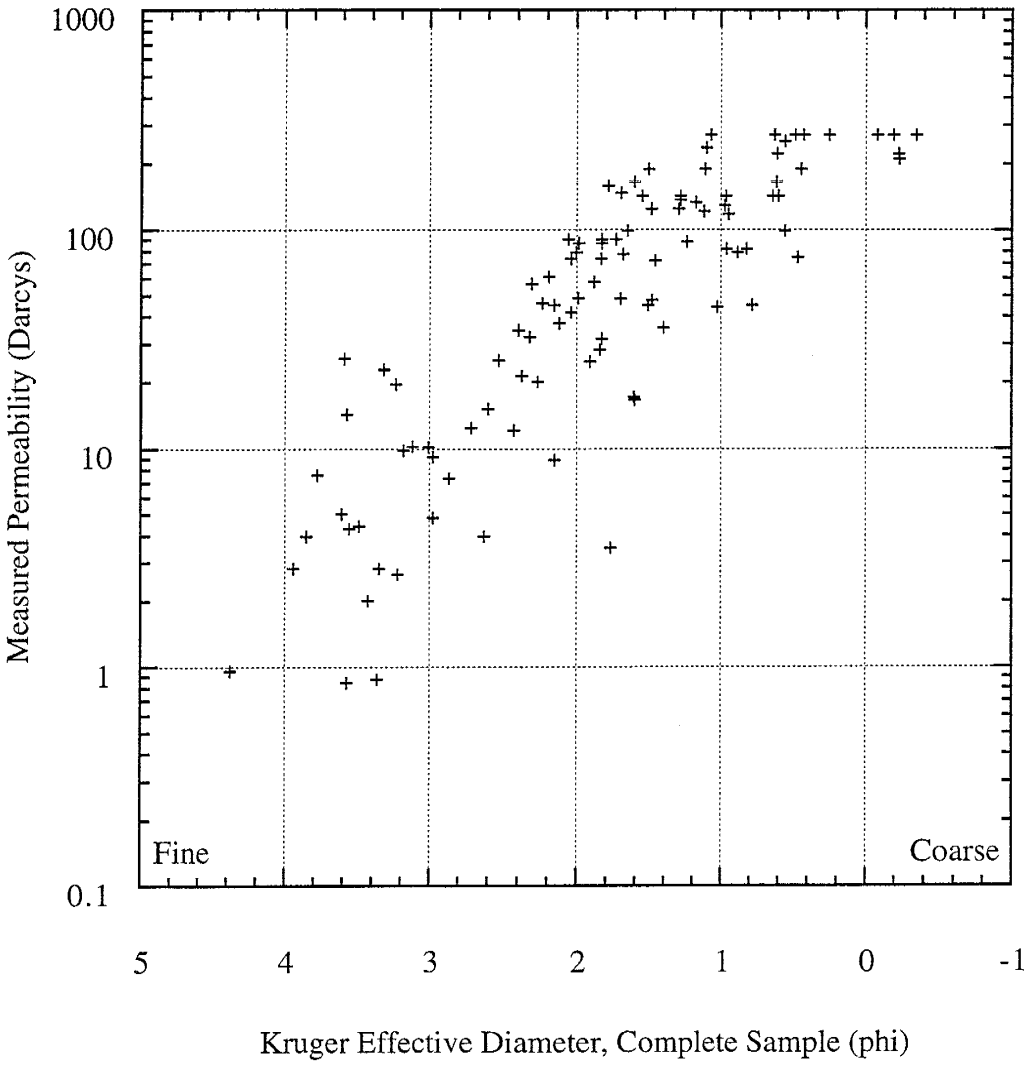

Influence of Kruger Diameter on Permeability

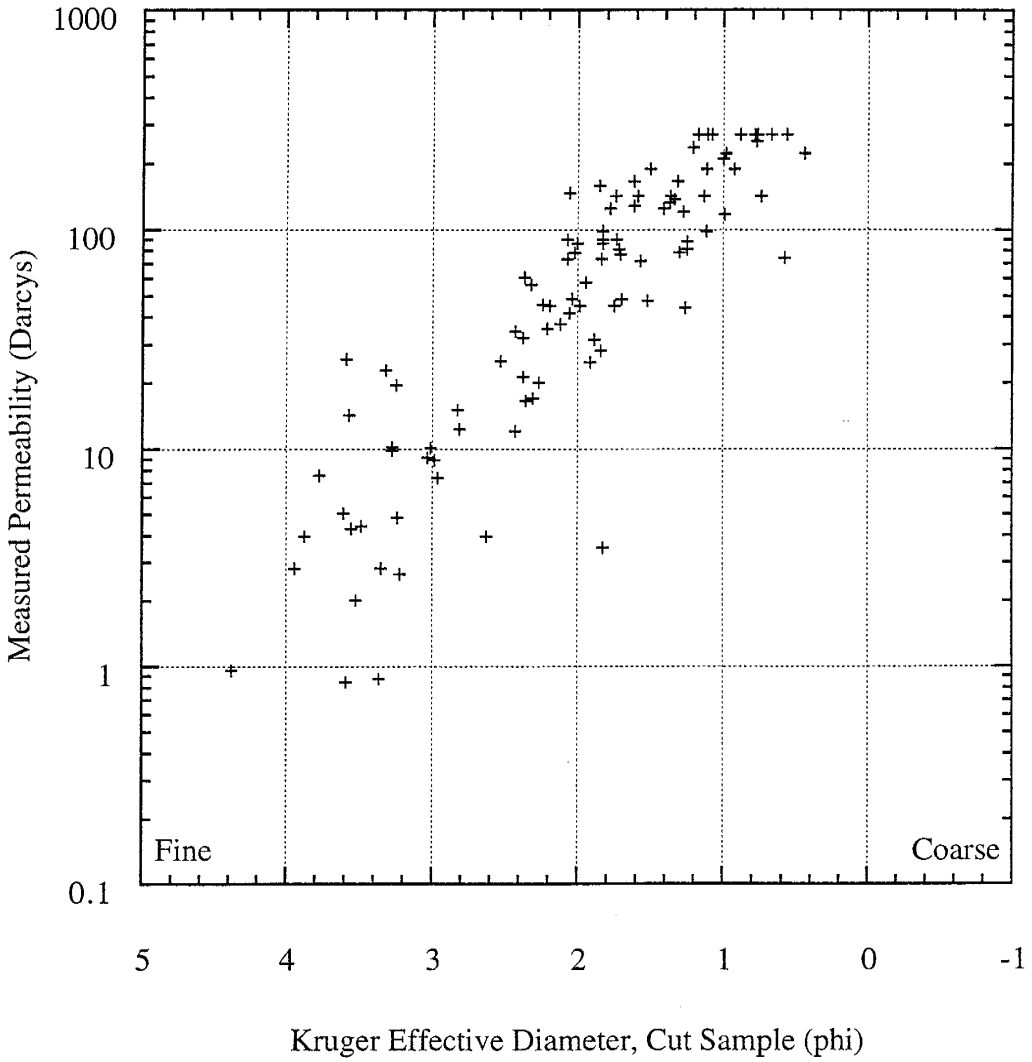

Influence of d_{10} Grain Size Squared on Permeability

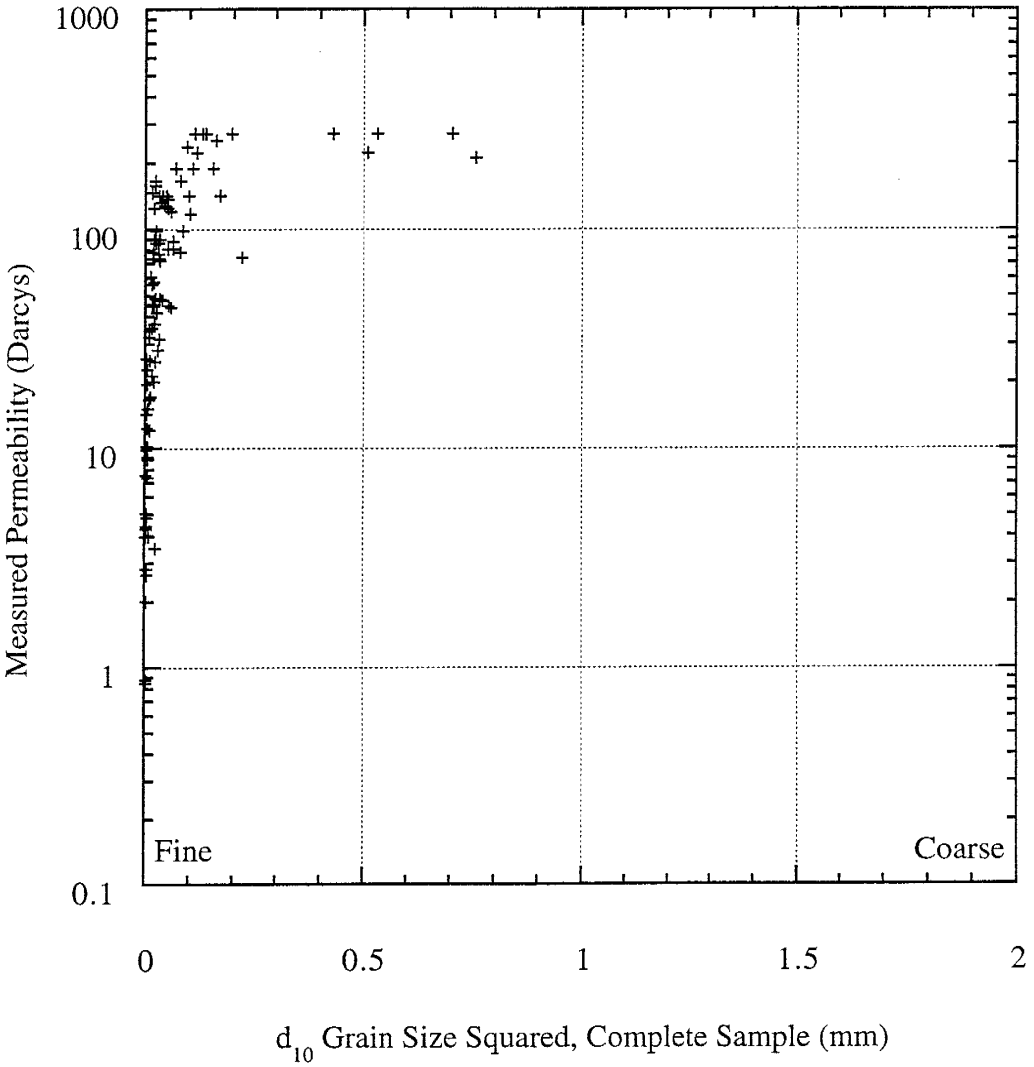

Influence of d_{10} Grain Size Squared on Permeability

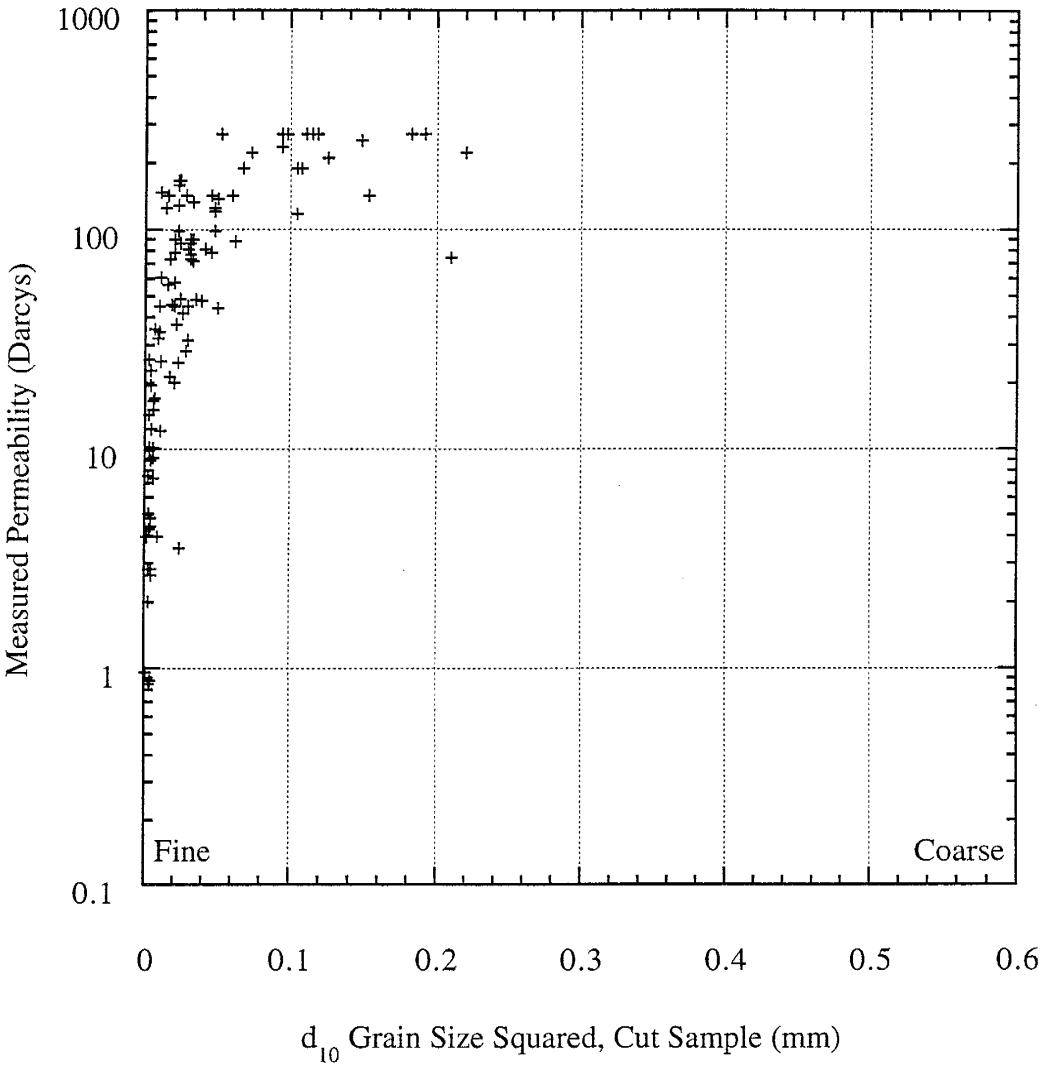

Influence of d_{17} Grain Size Squared on Permeability

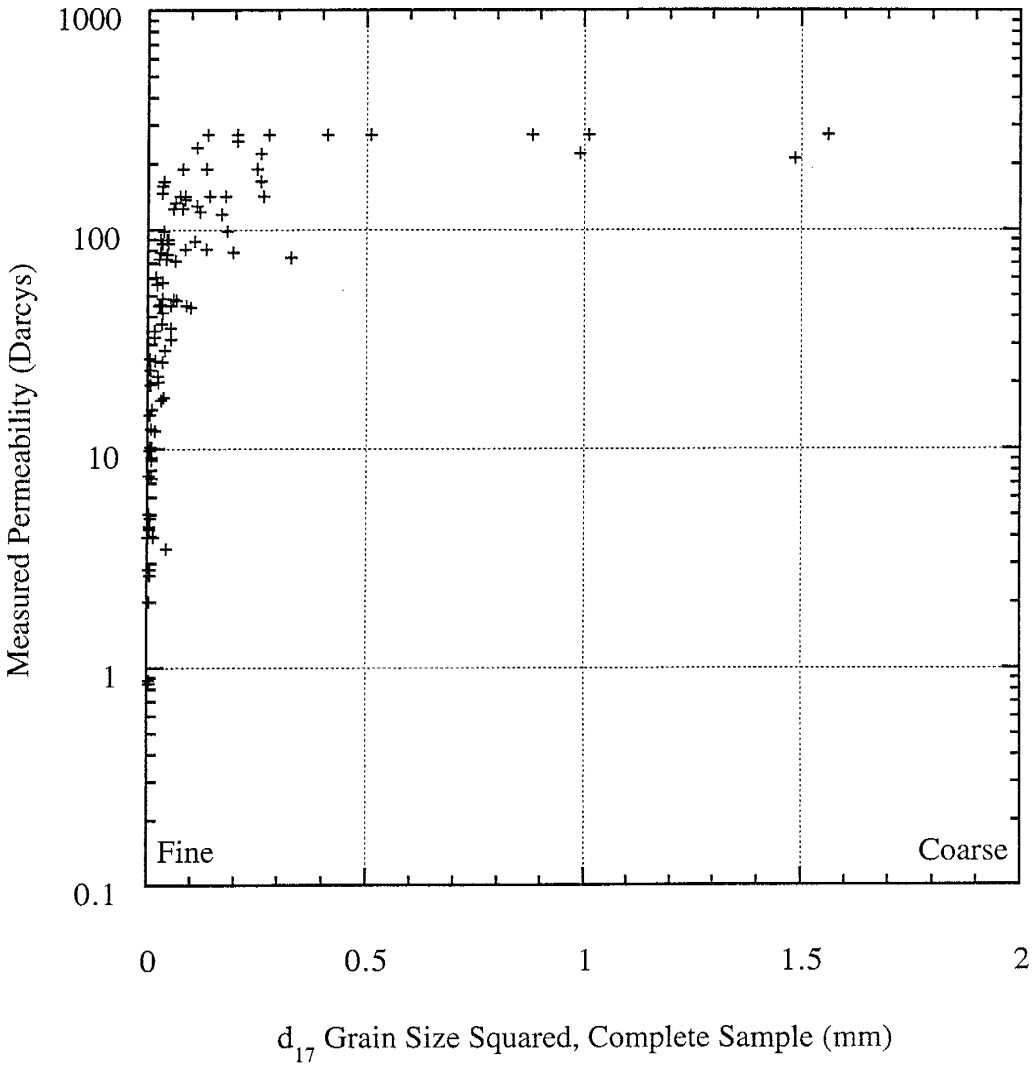

Influence of d_{17} Grain Size Squared on Permeability

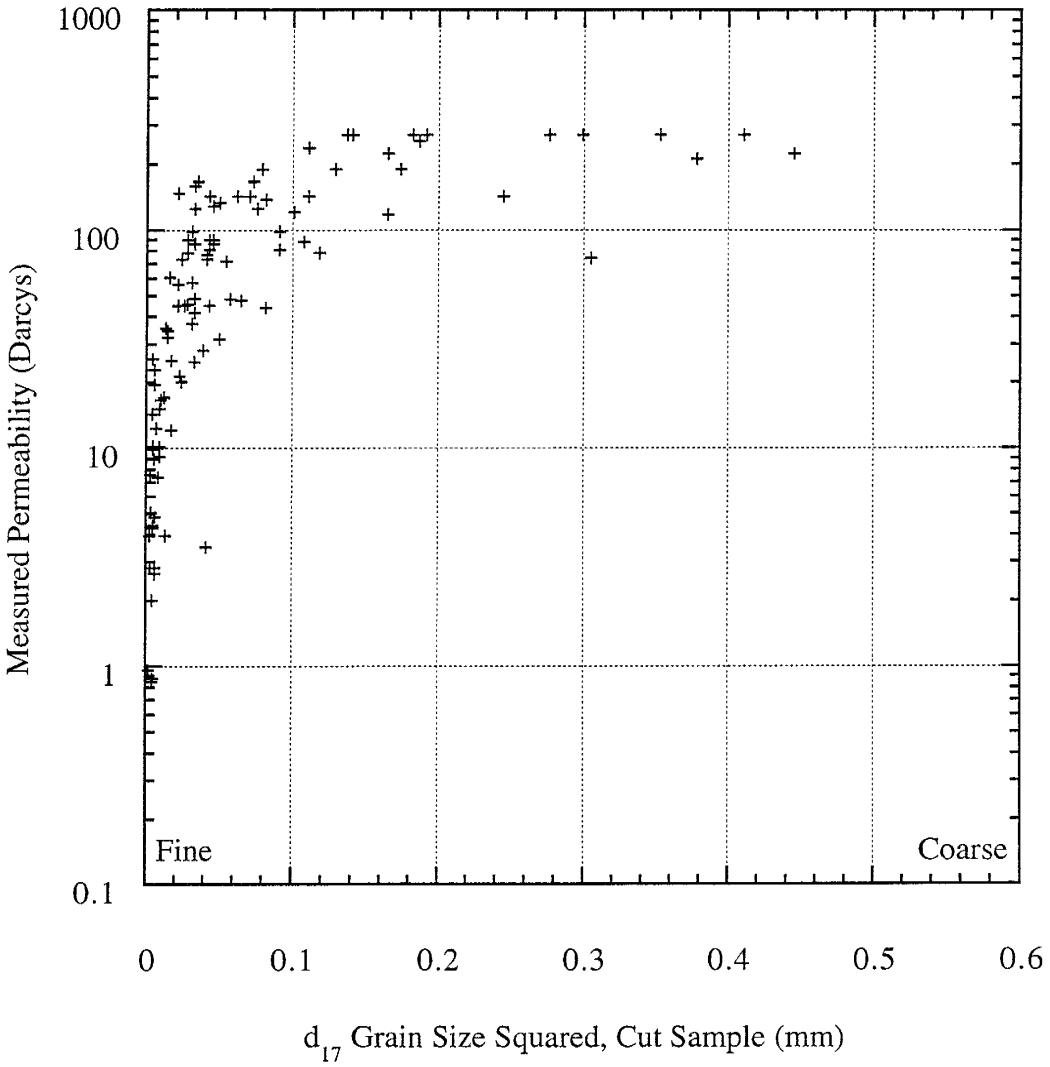

Influence of d_{20} Grain Size Squared on Permeability

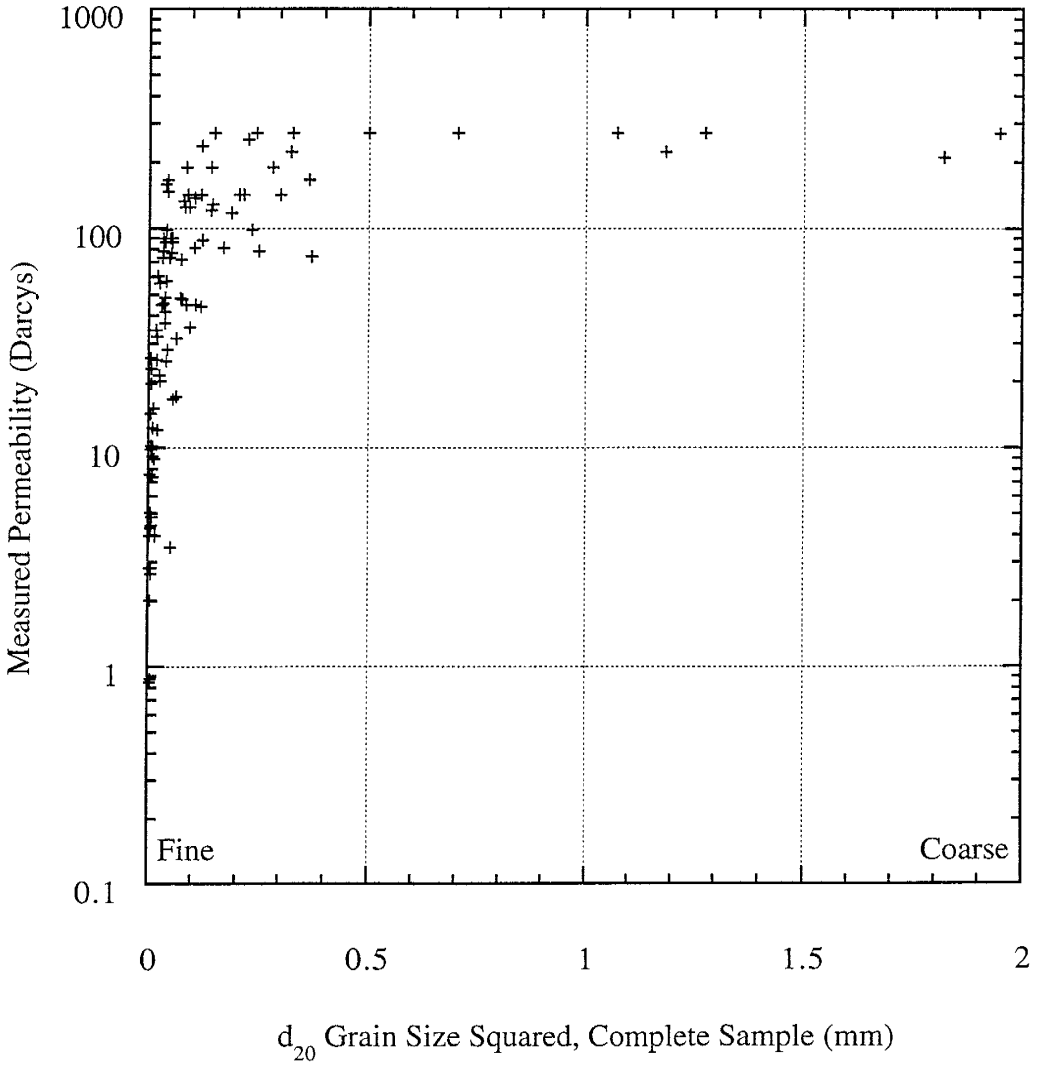

Influence of d_{20} Grain Size Squared on Permeability

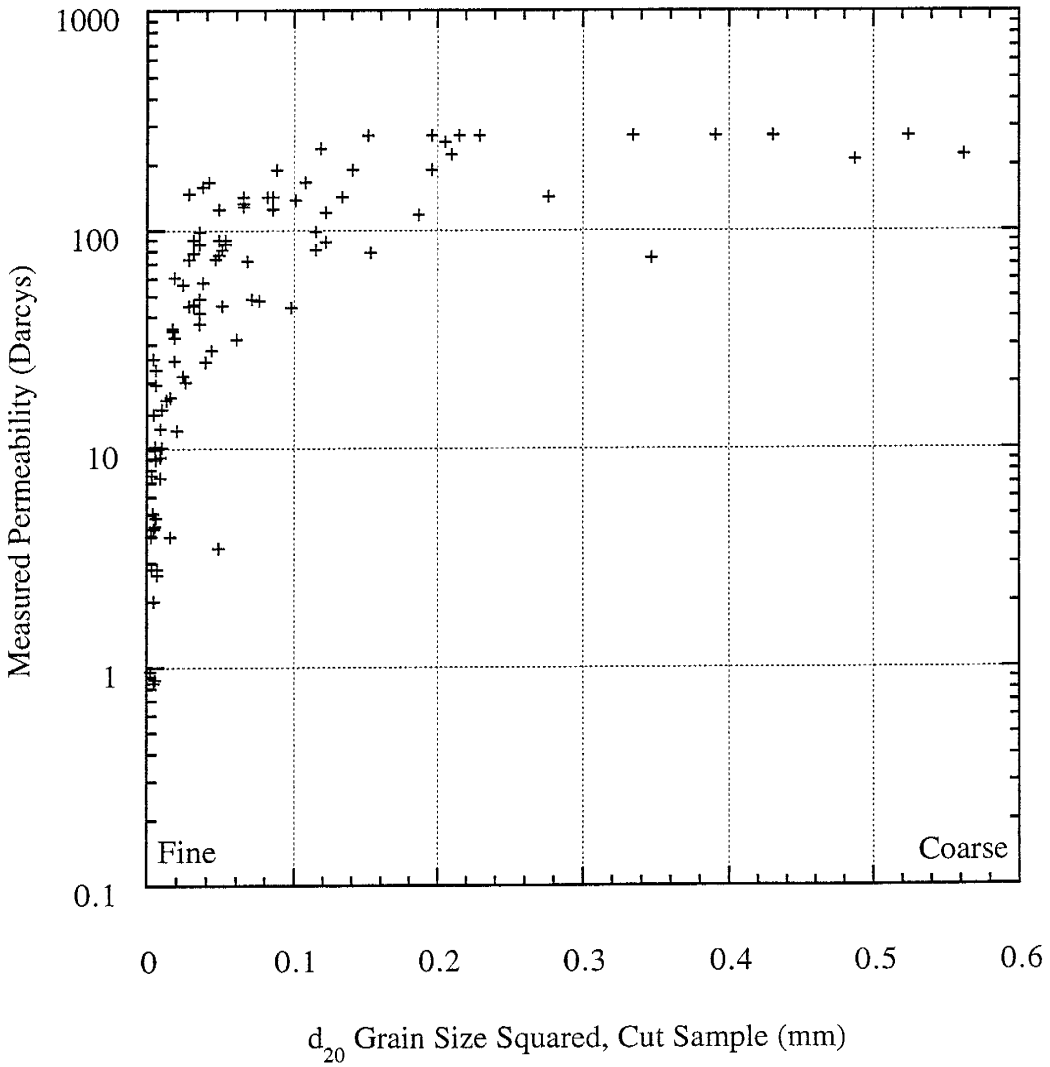

APPENDIX D

Comparison of porosity, permeability and grain size distribution parameters of outcrop sample grouped by bedding type

Permeability by Bedding Type, Sieved Outcrop Samples.

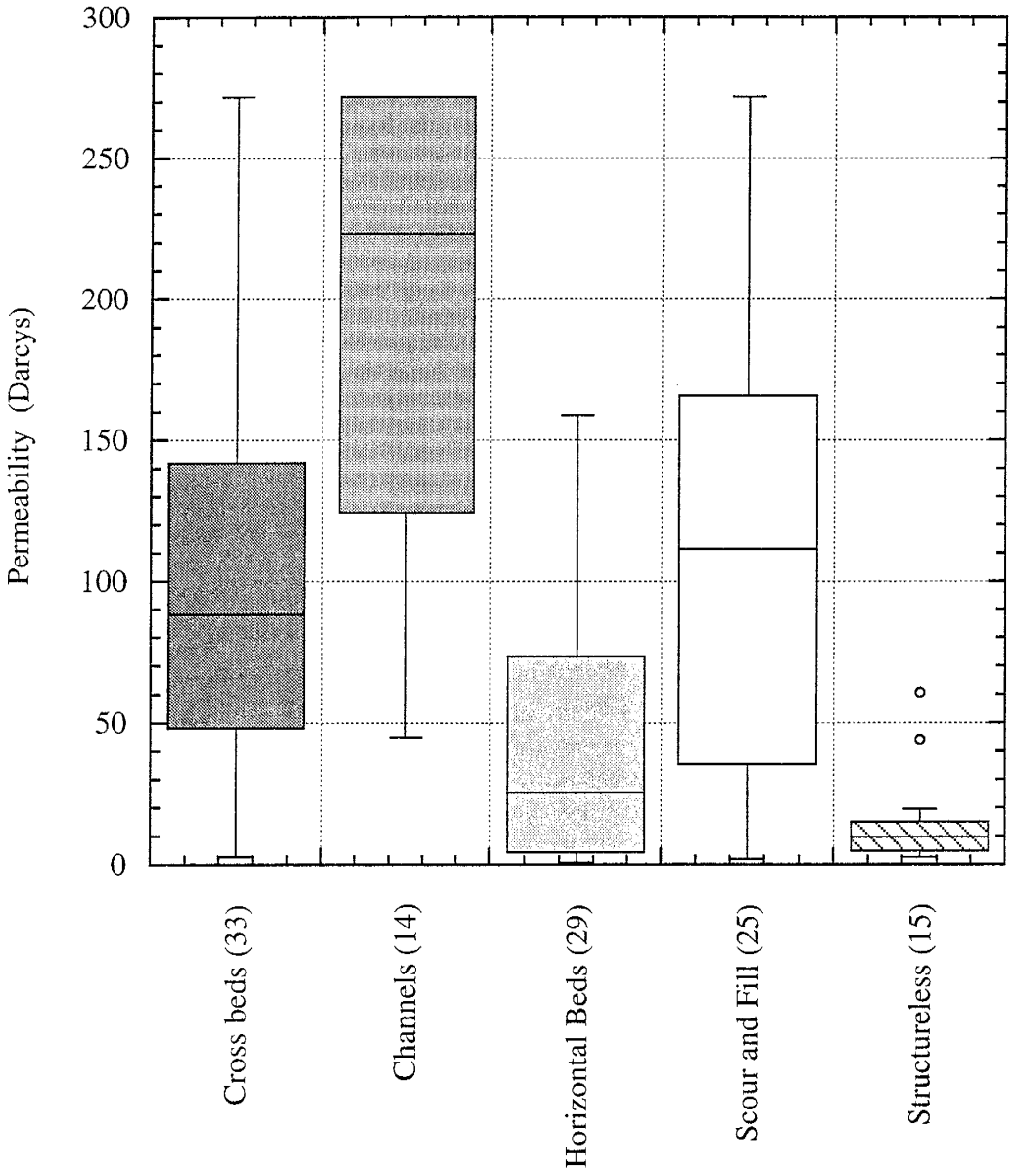

Small circles are data points considered outliers by the graphing program.

Porosity by Bedding Type, Sieved Outcrop Samples

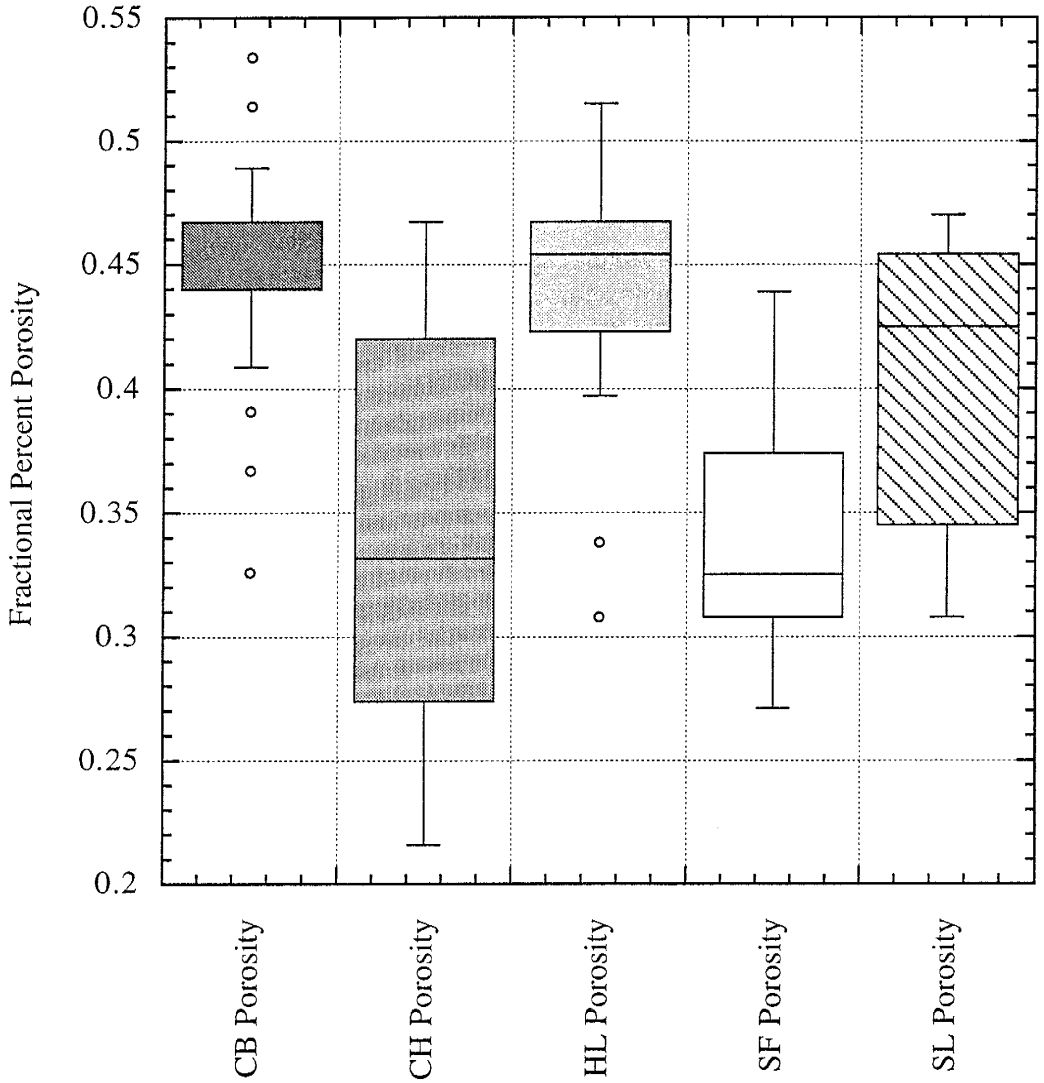

Small circles are data points considered outliers by the graphing program.

Permeability by Bedding Type, Unsieved Permeability Profile Measurements

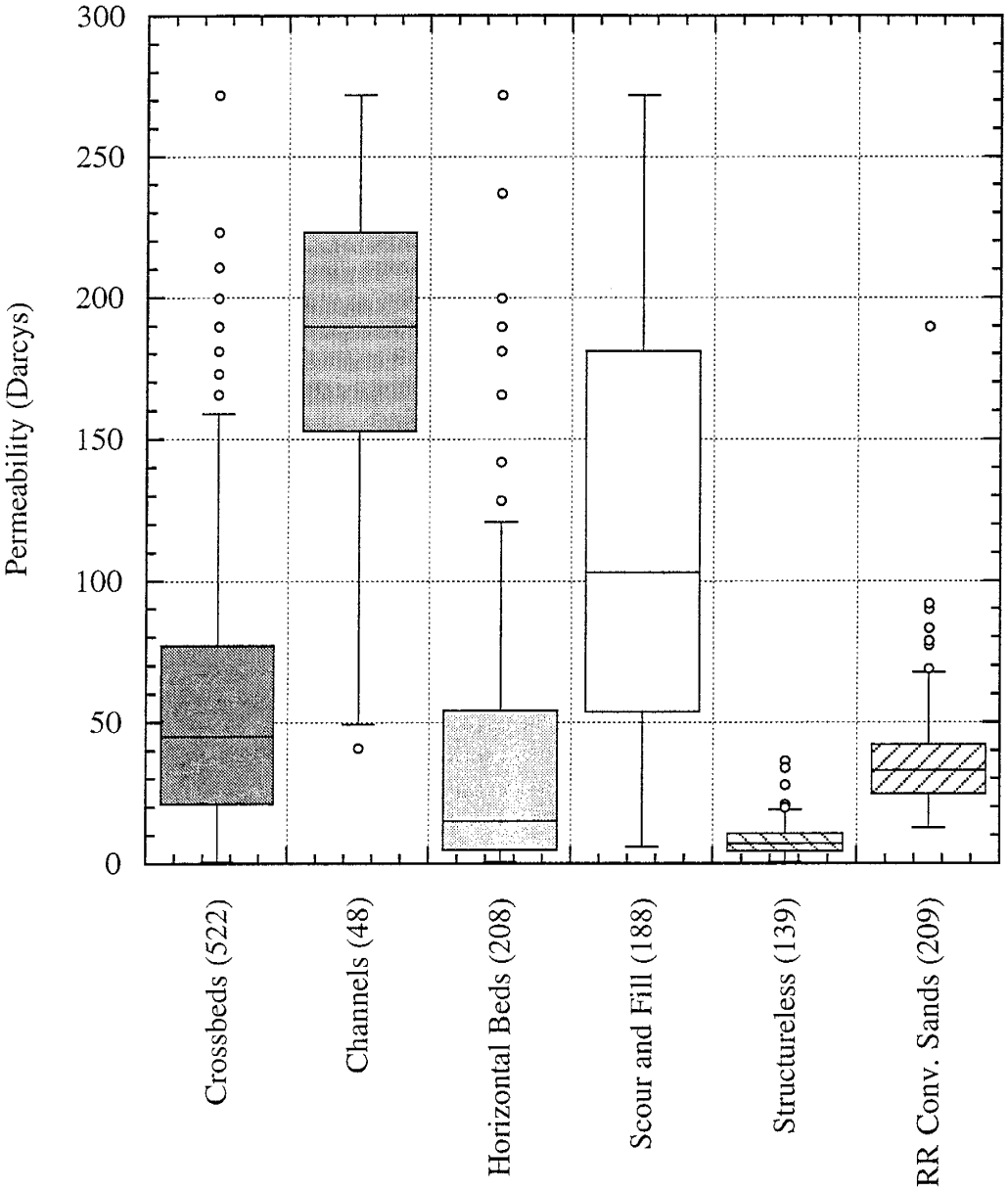

Small circles are data points considered outliers by the graphing program.

Mean, standard deviation and skewness of sieved outcrop samples. Complete samples, grouped by bedding type.

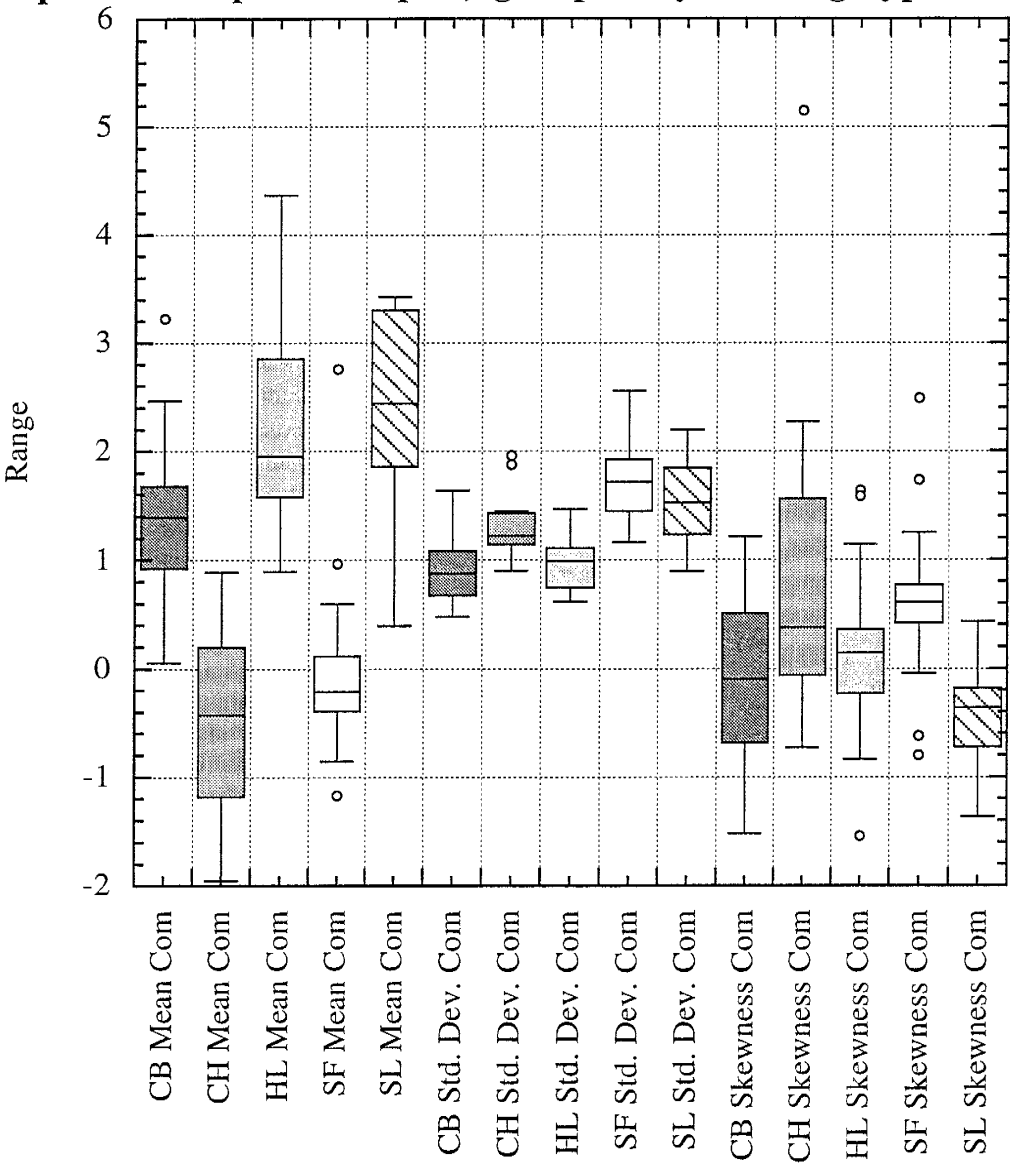

Small circles are data points considered outliers by the graphing program.

Mean, standard deviation and skewness of sieved outcrop samples. Cut samples, grouped by bedding type.

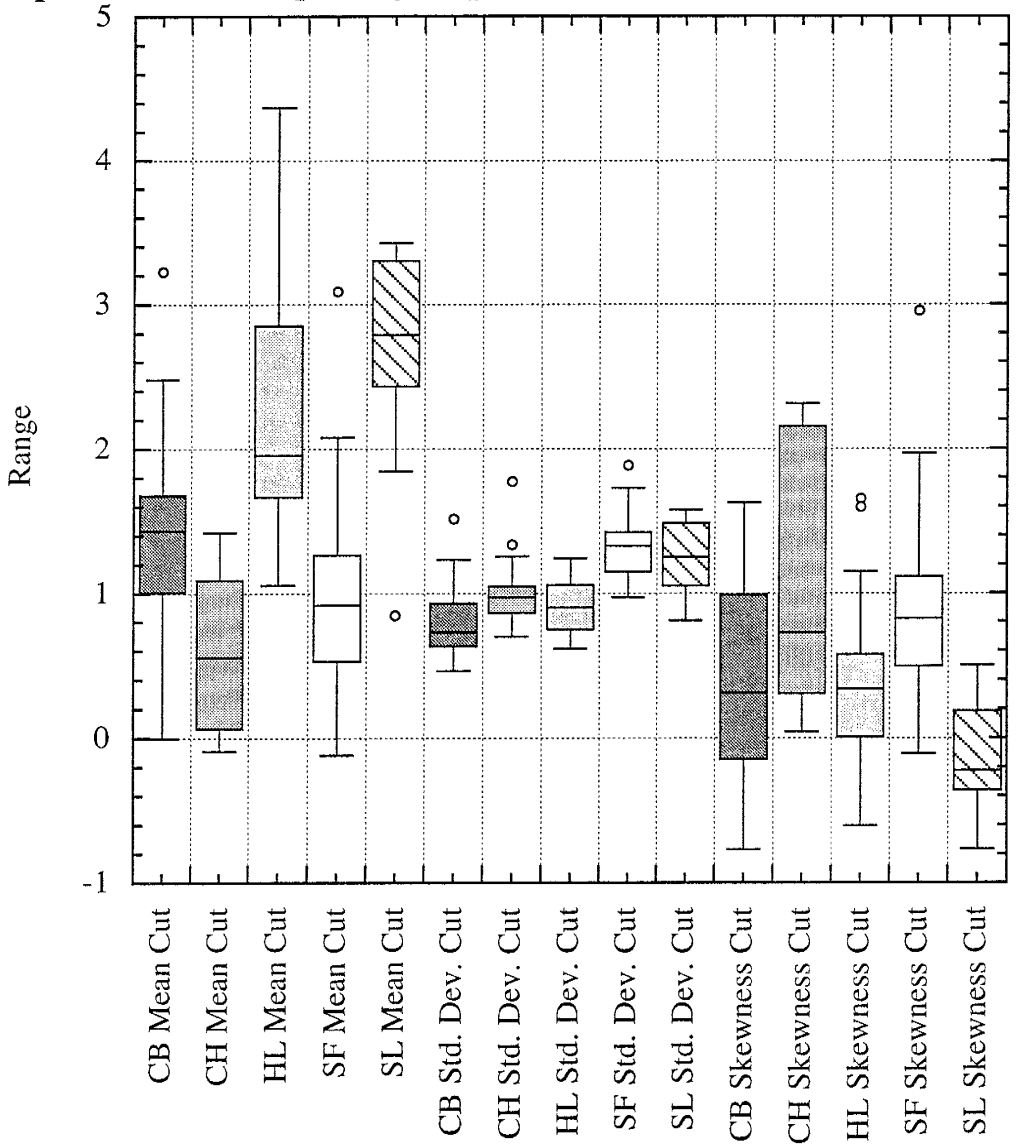

Small circles are data points considered outliers by the graphing program.

Percent Fines by Bedding Type

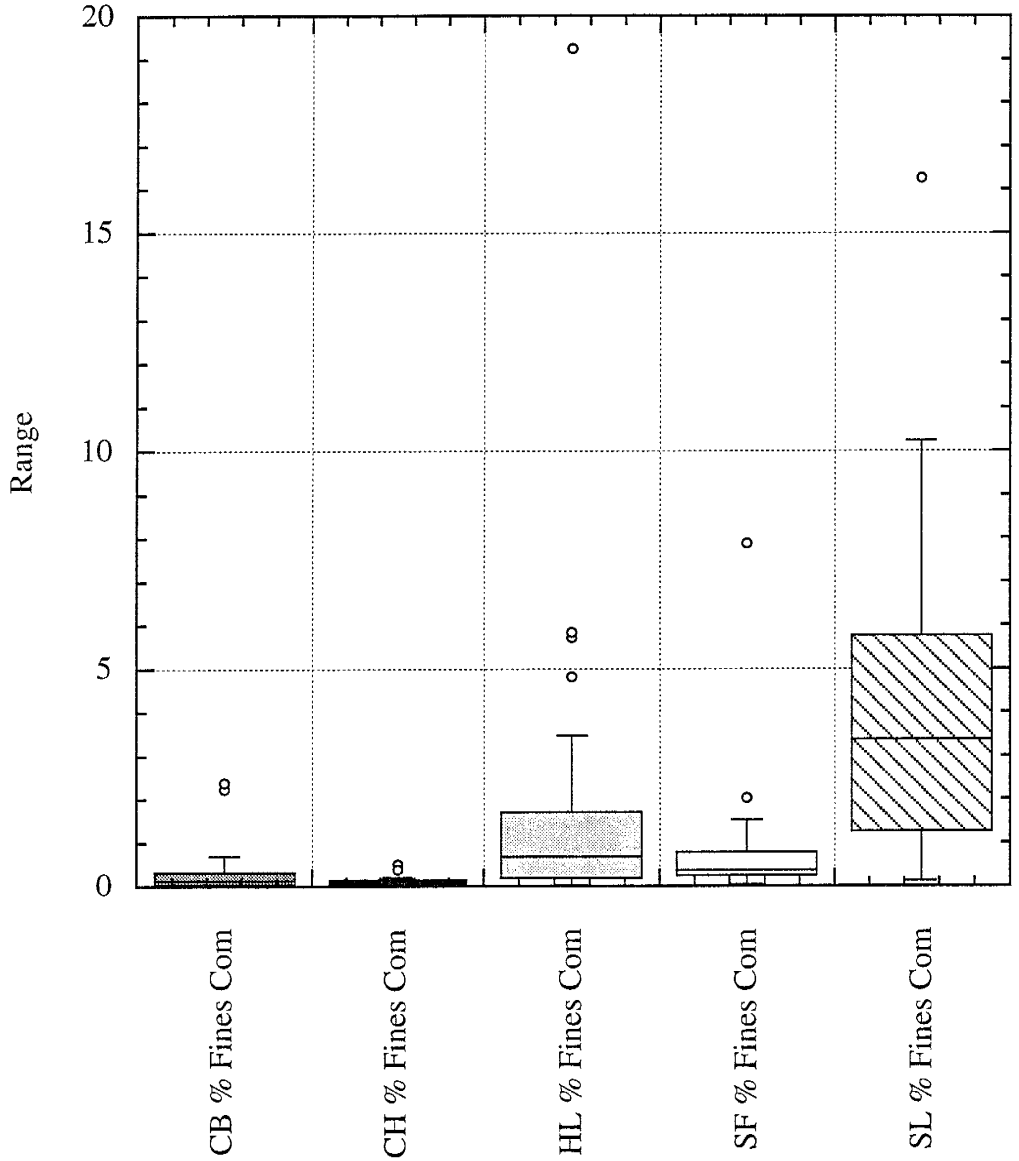

Small circles are data points considered outliers by the graphing program.

Percent Pebbles by Bedding Type

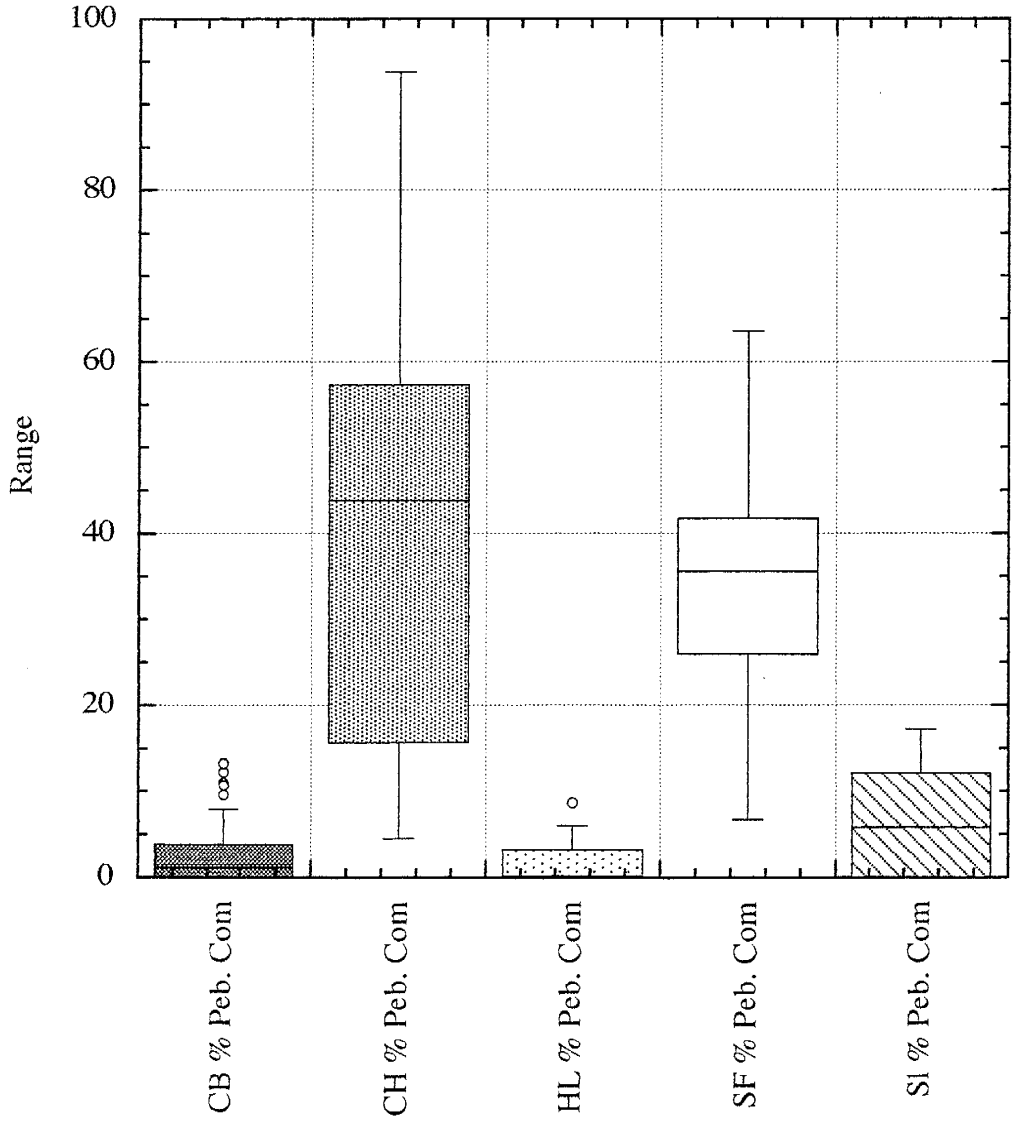

Small circles are data points considered outliers by the graphing program.

Maximum Intermediate Diameter by Bedding Type

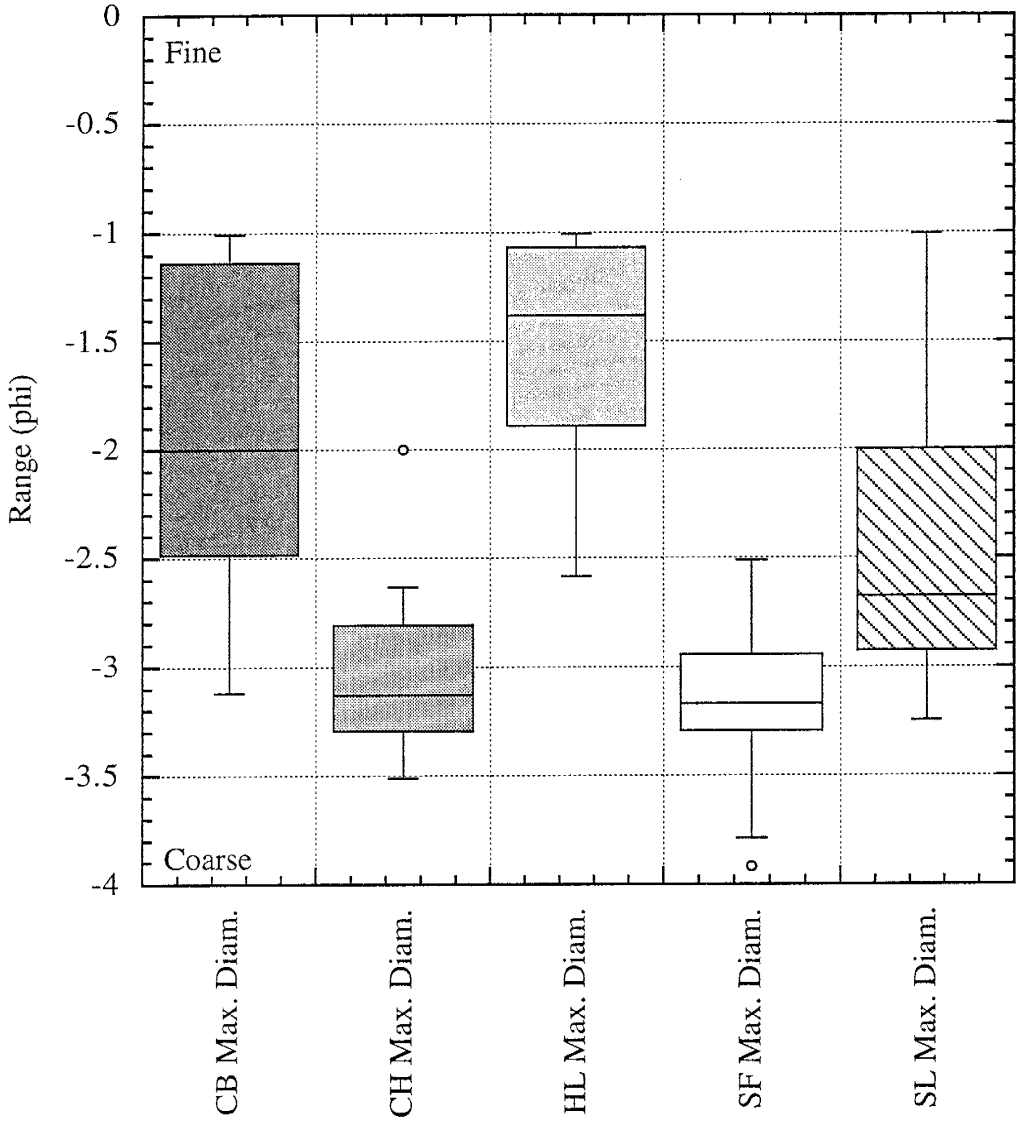

Small circles are data points considered outliers by the graphing program.

Distribution of grain size parameters by grouped bedding type, complete samples

Bedding Type, Parameter	Mean Value	Standard Deviation	Skewness
Crossbeds, mean grain size	1.323	0.677	0.390
Channels, mean grain size	-0.490	0.830	0.096
Horizontal, mean grain size	2.204	0.880	0.743
Scour and fill, mean grain size	-0.072	0.743	2.250
Structureless, mean grain size	2.467	0.886	-0.759
Crossbeds, standard deviations	0.902	0.314	0.629
Channels, standard deviations	1.304	0.303	1.006
Horizontal, standard deviations	0.969	0.233	0.122
Scour and fill, standard deviations	1.722	0.347	0.410
Structureless, standard deviations	1.535	0.402	-0.015
Crossbeds, skewness	-0.051	0.779	-0.236
Channels, skewness	0.968	1.550	1.377
Horizontal, skewness	0.090	0.664	0.281
Scour and fill, skewness	0.638	0.639	0.429
Structureless, skewness	-0.460	0.441	-0.125
Crossbeds, percent fines	0.316	0.552	3.002
Channels, percent fines	0.154	0.138	1.547
Horizontal, percent fines	1.983	3.721	3.668
Scour and fill, percent fines	0.858	1.546	3.968
Structureless, percent fines	4.707	4.159	1.526

Scatter Plot of Mean and Standard Deviation by Bedding Type, Complete Samples

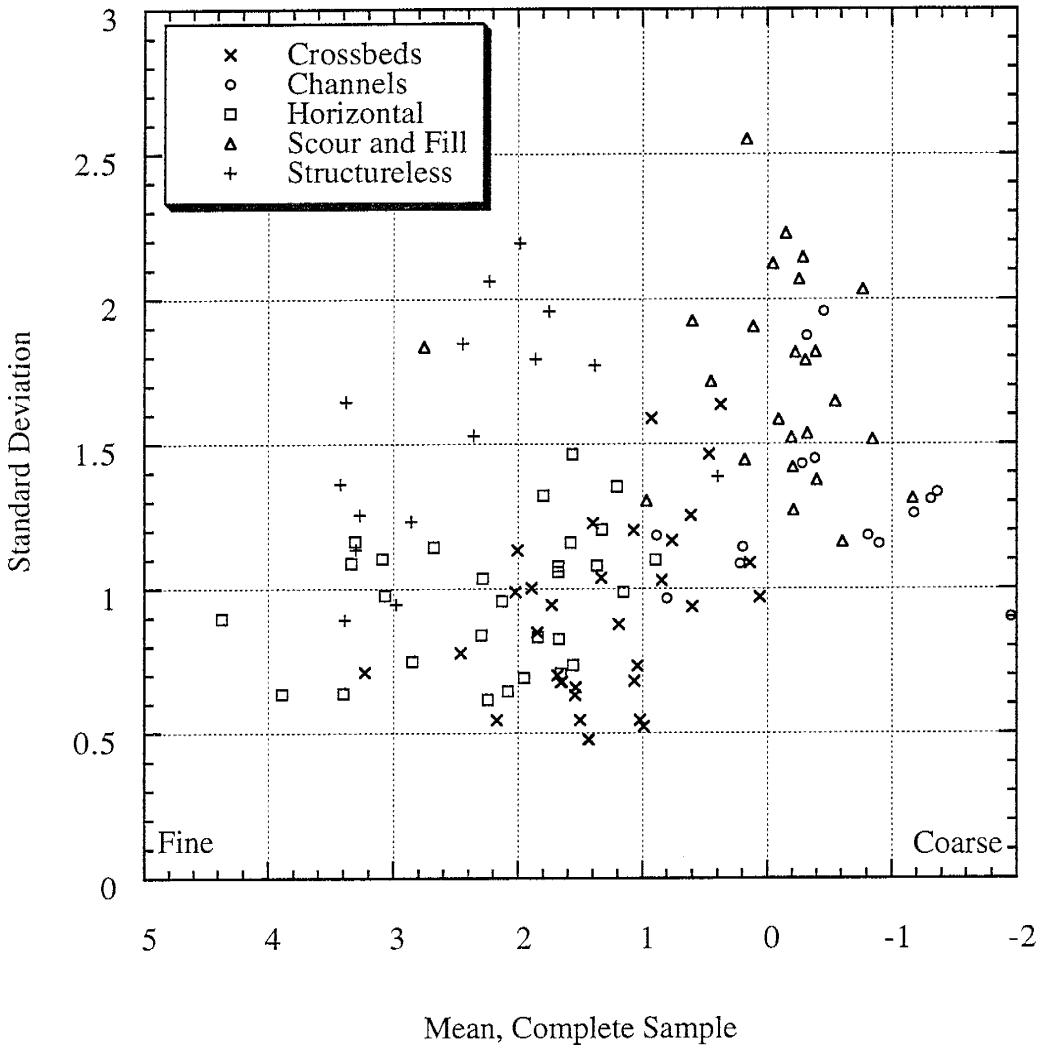

Scatter Plot of Mean and Standard Deviation by Bedding Type, Cut Samples

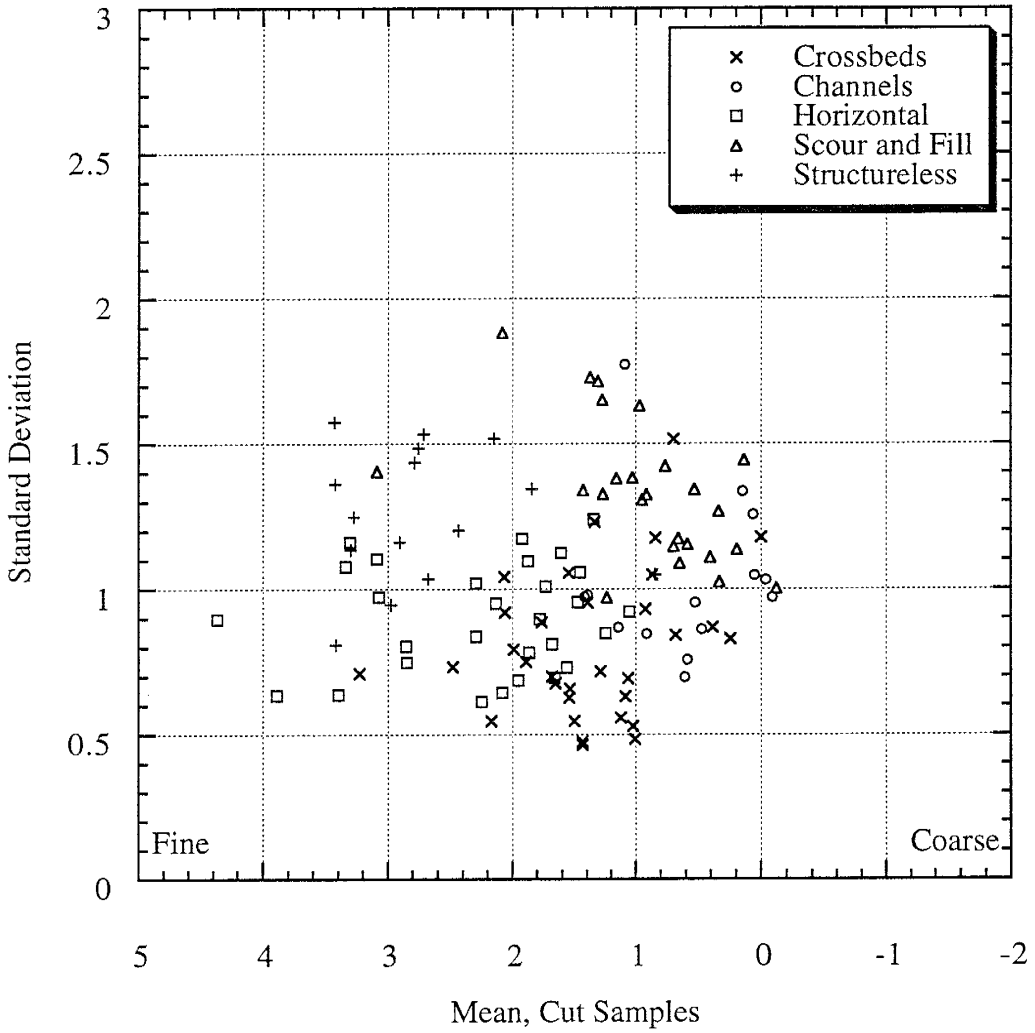

Scatter Plot of Mean and Skewness by Bedding Type, Complete Distribution

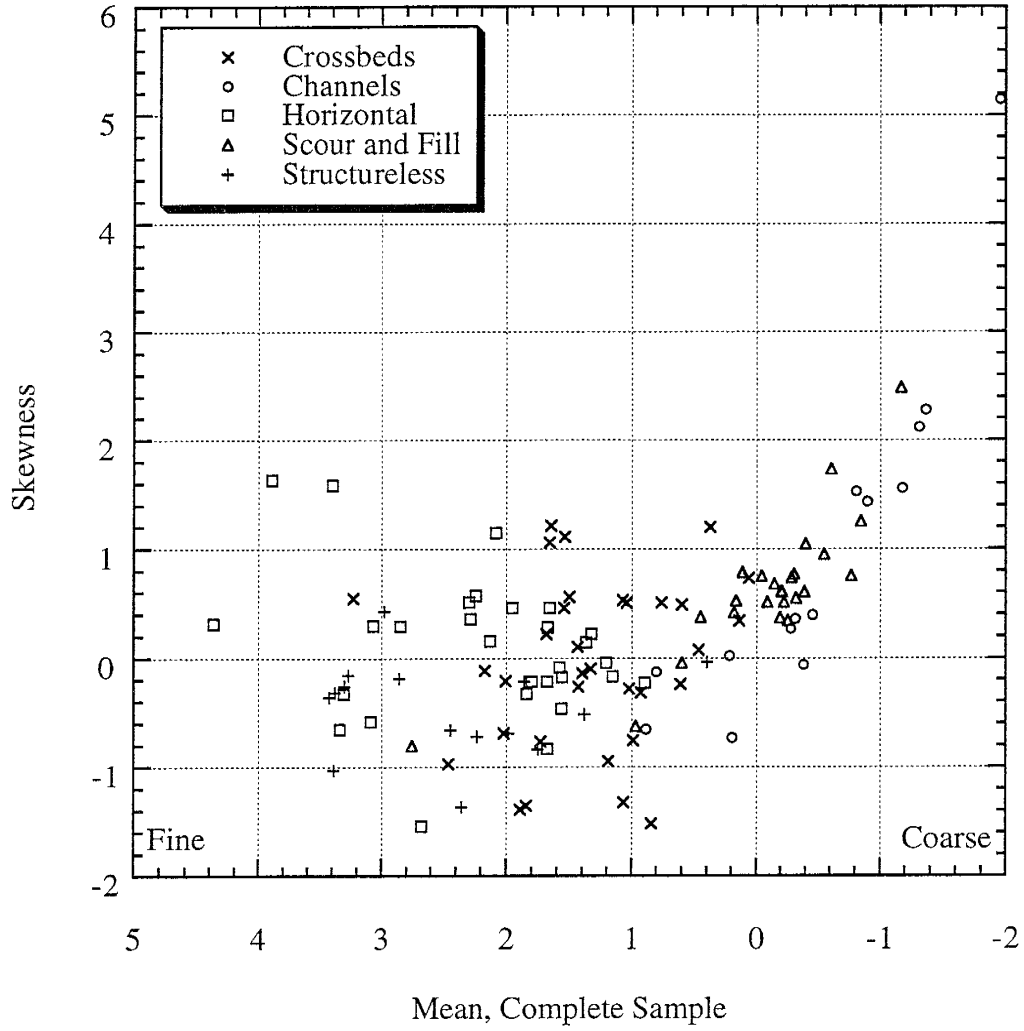

Scatter Plot of Mean and Skewness by Bedding Type, Cut Samples

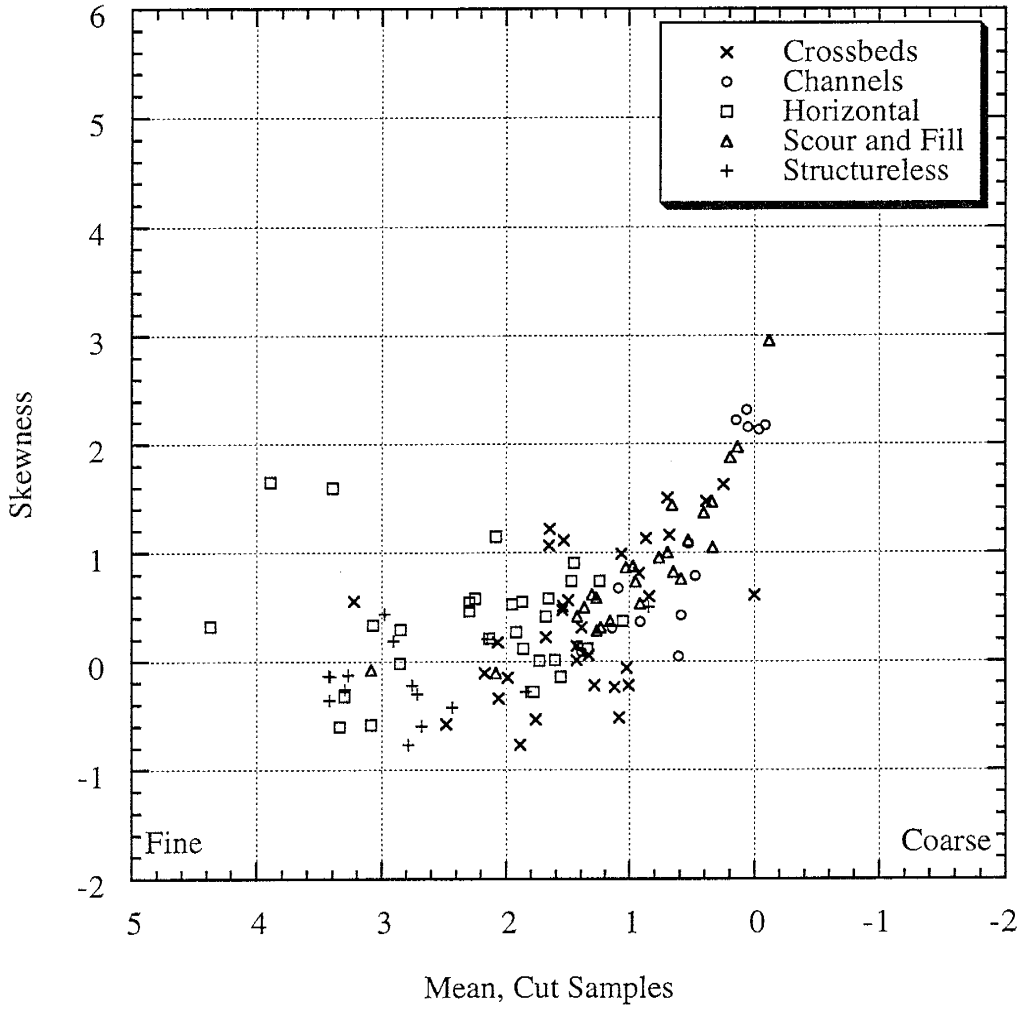

Scatter Plot of Standard Deviation and Skewness by Bedding Type, Complete Samples

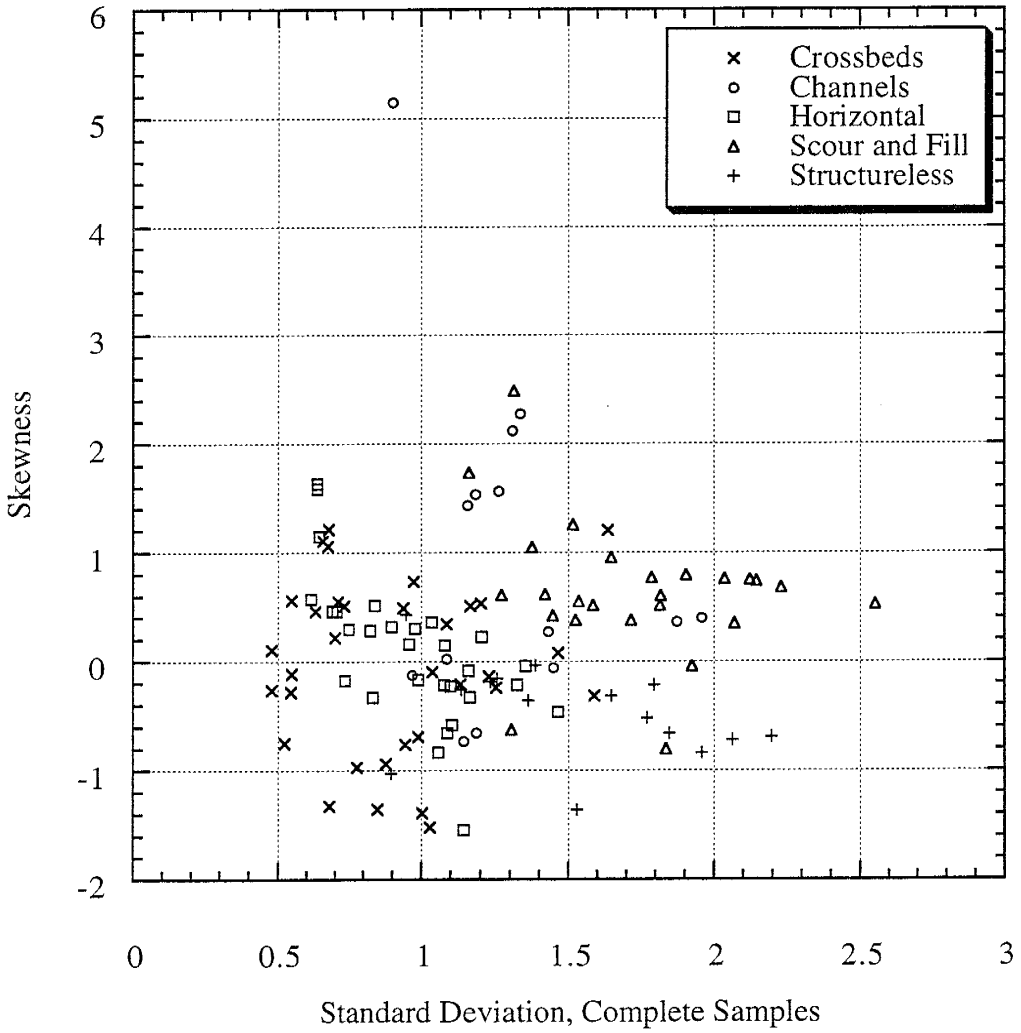

Scatter Plot of Standard Deviation and Skewness by Bedding Type, Cut Samples

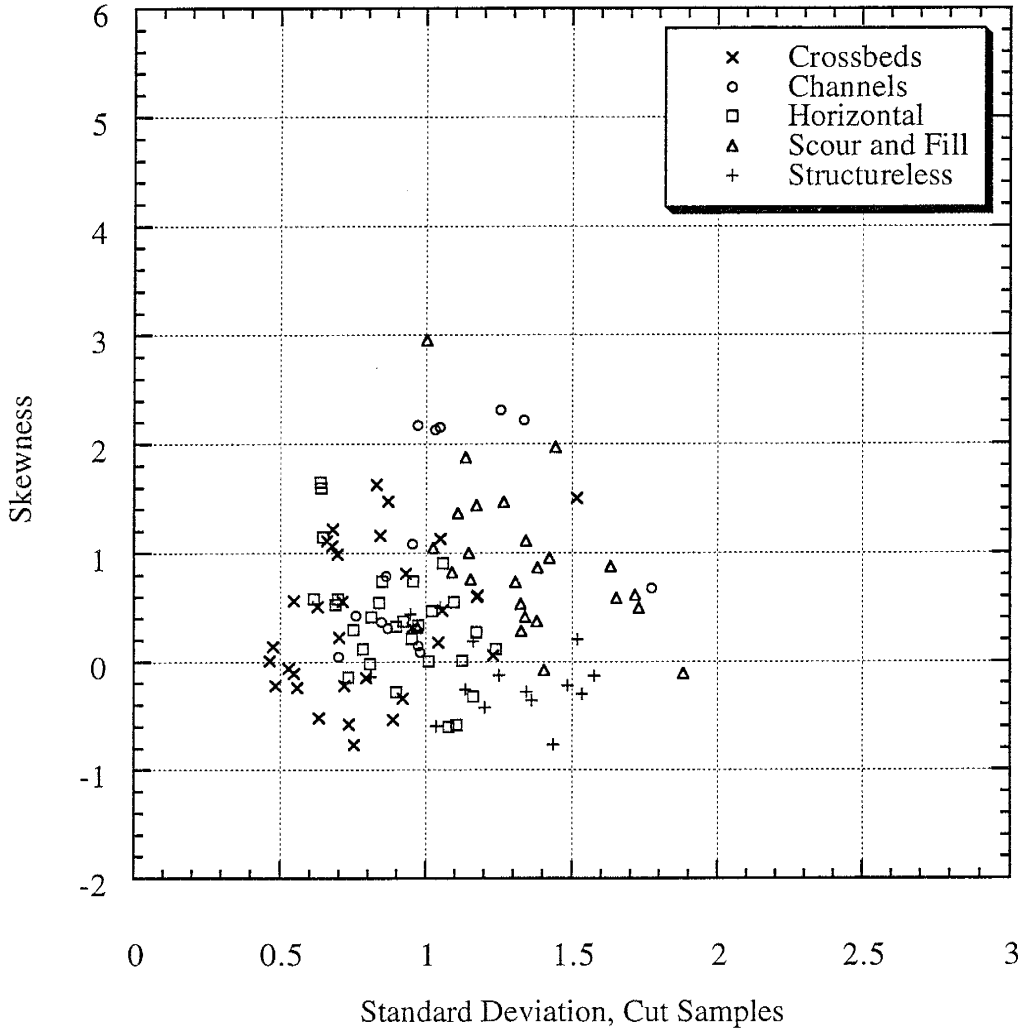

Scatter Plot of Standard Deviation and Mean-Cubed Deviation by Bedding Type, Complete Samples

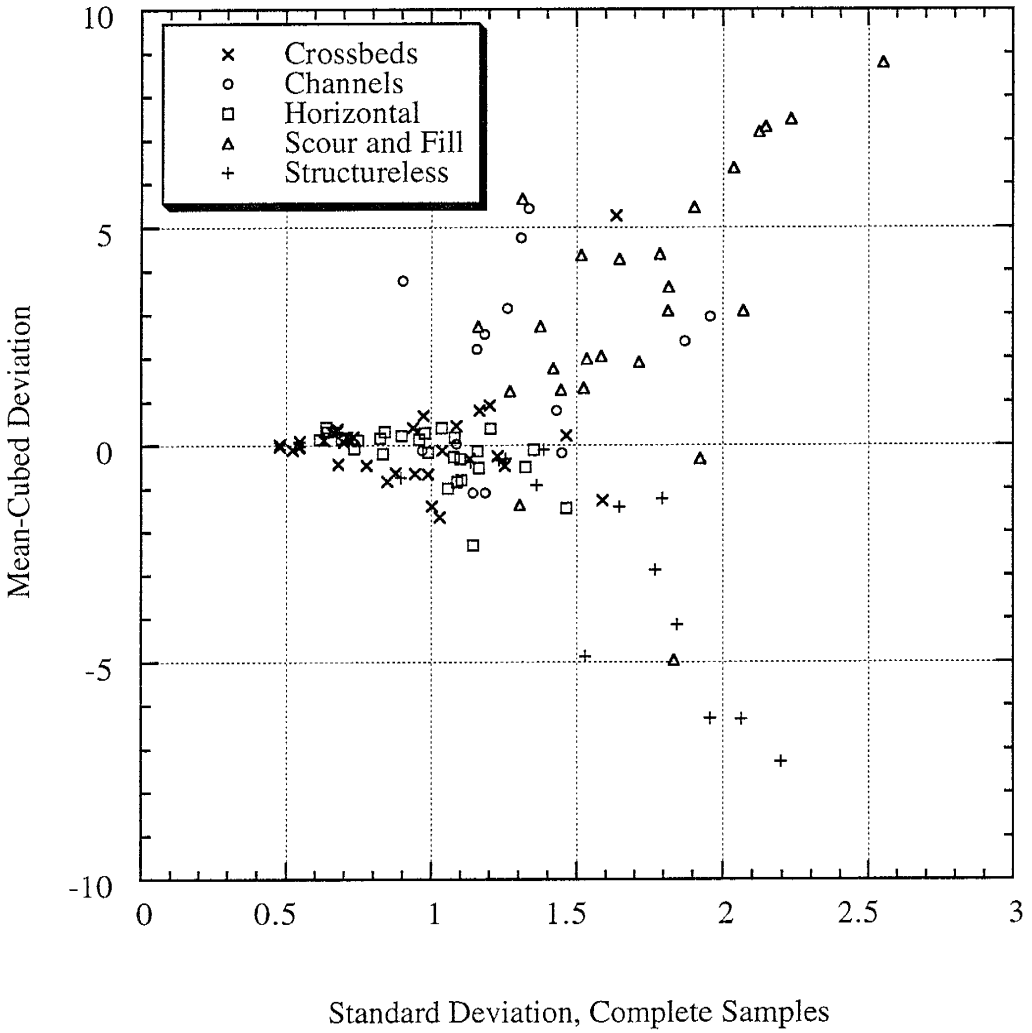

Scatter Plot of Standard Deviation and Mean-Cubed Deviation by Bedding Type, Cut Samples

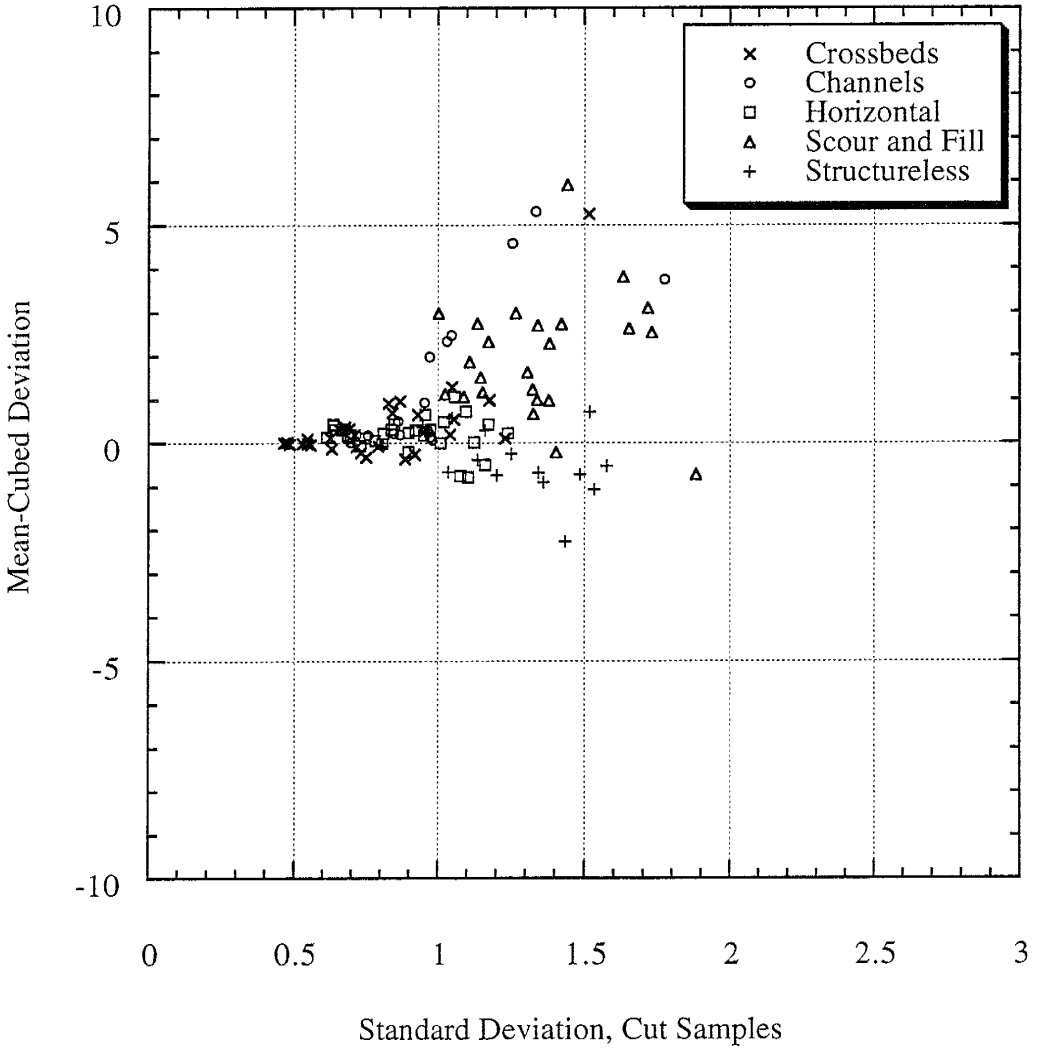

Scatter Plot of Mean Grain Size and Percent Fines by Bedding Type, Complete Samples

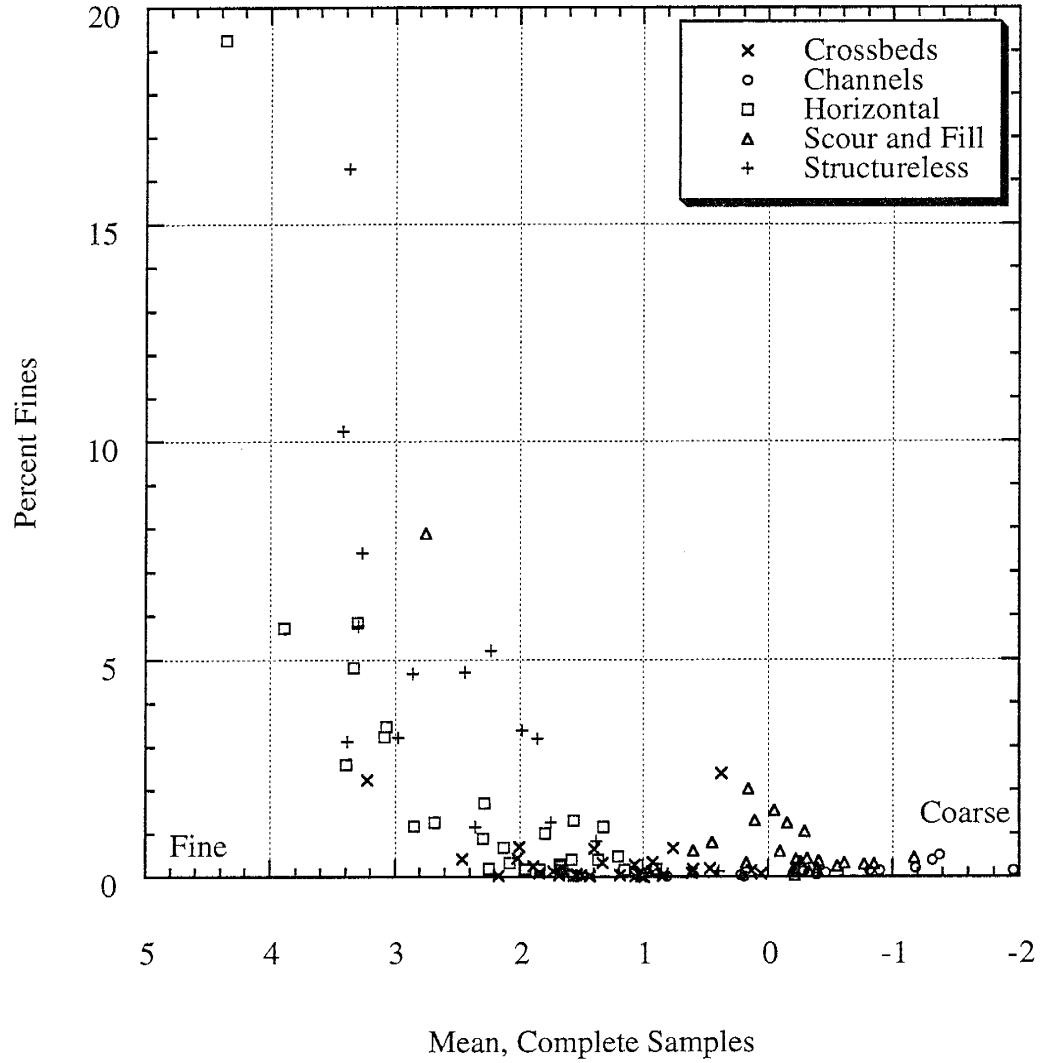

Scatter Plot of Mean Grain Size and Percent Fines by Bedding Type, Cut Samples

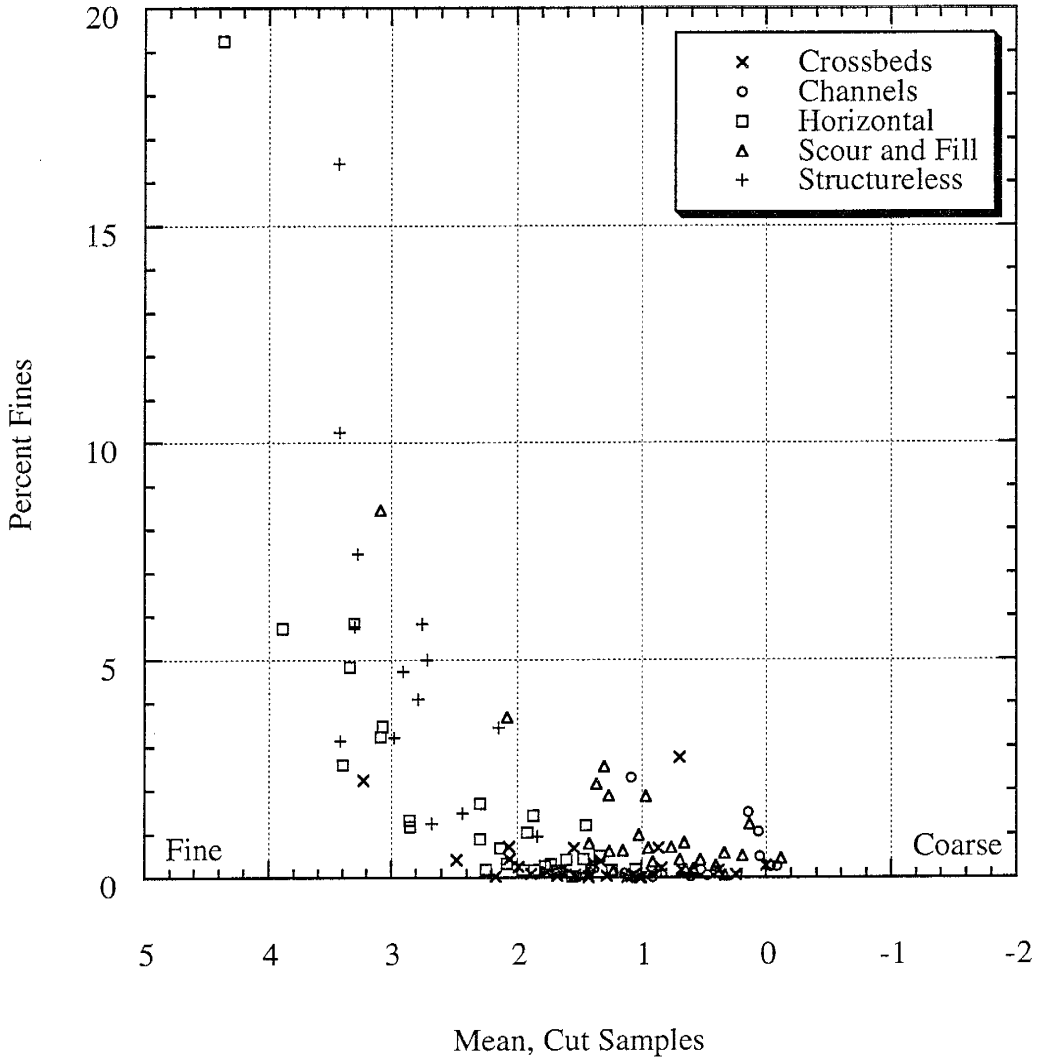

ABBREVIATIONS

CB - CROSSBEDS
CH - CHANNELS
HL - HORIZONTAL LAMINATIONS
SF - SCOUR AND FILL
SL - STRUCTURELESS
C2 - CORONADO 2
M1 - MW1
PS - PSMW-19
-CM - COMPLETE DISTRIBUTION
-CT - CUT DISTRIBUTION
MEAN - MEAN GRAIN SIZE (PHI UNITS)
STDV - STANDARD DEVIATION
SKEW - SKEWNESS
M3DV - MEAN-CUBED DEVIATION
PSLT - PERCENT FINES
PPEB - PERCENT PEBBLES
MAXD - MAXIMUM INTERMEDIATE DIAMETER
POR - PERCENT POROSITY
MSPERM - MEASURED PERMEABILITY
LITH - LITHIFICATION

TOTAL OBSERVATIONS: 33

	CBMEANCM	CBSTDVCM	CBSKEWCM	CBM3DVCM	CBPSLTCM
N OF CASES	33	33	33	33	33
MINIMUM	0.060	0.478	-1.517	-1.656	0.000
MAXIMUM	3.227	1.636	1.214	5.263	2.390
RANGE	3.167	1.158	2.731	6.919	2.390
MEAN	1.323	0.902	-0.051	0.035	0.316
VARIANCE	0.458	0.099	0.607	1.236	0.304
STANDARD DEV	0.677	0.314	0.779	1.112	0.552
STD. ERROR	0.118	0.055	0.136	0.194	0.096
SKEWNESS(G1)	0.390	0.629	-0.236	3.060	3.002
KURTOSIS(G2)	0.482	-0.312	-0.829	13.137	8.298
SUM	43.645	29.772	-1.678	1.147	10.413
C.V.	0.512	0.348	-15.319	31.988	1.748
MEDIAN	1.398	0.878	-0.098	-0.019	0.140

	CBPPEBCM	CBMAXD	CBMEANCT	CBSTDVCT	CBSKEWCT
N OF CASES	33	33	33	33	33
MINIMUM	0.002	-3.121	0.000	0.464	-0.768
MAXIMUM	13.284	-1.007	3.227	1.517	1.626
RANGE	13.282	2.114	3.227	1.053	2.394
MEAN	3.319	-1.968	1.382	0.802	0.381
VARIANCE	19.260	0.548	0.429	0.062	0.444
STANDARD DEV	4.389	0.740	0.655	0.248	0.666
STD. ERROR	0.764	0.129	0.114	0.043	0.116
SKEWNESS(G1)	1.270	0.016	0.328	0.850	0.190
KURTOSIS(G2)	0.101	-1.339	0.704	0.417	-1.024
SUM	109.537	-64.951	45.602	26.465	12.570
C.V.	1.322	-0.376	0.474	0.310	1.749
MEDIAN	1.104	-2.000	1.434	0.733	0.313

	CBM3DVCT	CBPSLTCT	CBPOR	CBMSPERM	CBLITH
N OF CASES	33	33	33	27	27
MINIMUM	-0.373	0.000	0.326	2.830	1.000
MAXIMUM	5.252	2.753	0.534	271.680	2.000
RANGE	5.625	2.753	0.208	268.850	1.000
MEAN	0.400	0.333	0.453	103.023	1.296
VARIANCE	0.938	0.356	0.002	4423.749	0.217
STANDARD DEV	0.969	0.597	0.039	66.511	0.465
STD. ERROR	0.169	0.104	0.007	12.800	0.090
SKEWNESS(G1)	3.962	3.115	-1.197	0.772	0.892
KURTOSIS(G2)	17.386	9.132	2.621	0.090	-1.204
SUM	13.205	11.000	14.941	2781.630	35.000
C.V.	2.420	1.790	0.086	0.646	0.359
MEDIAN	0.126	0.141	0.467	88.150	1.000

TOTAL OBSERVATIONS: 14

	CHMEANCM	CHSTDVCM	CHSKEWCM	CHM3DVCM	CHPSLTCM
N OF CASES	14	14	14	14	14
MINIMUM	-1.951	0.902	-0.729	-1.090	0.021
MAXIMUM	0.886	1.959	5.149	5.420	0.509
RANGE	2.837	1.057	5.878	6.510	0.488
MEAN	-0.490	1.304	0.968	1.825	0.154
VARIANCE	0.688	0.092	2.403	4.494	0.019
STANDARD DEV	0.830	0.303	1.550	2.120	0.138
STD. ERROR	0.222	0.081	0.414	0.567	0.037
SKEWNESS(G1)	0.096	1.006	1.377	0.099	1.547
KURTOSIS(G2)	-0.773	0.294	1.731	-1.165	1.511
SUM	-6.861	18.249	13.545	25.551	2.159
C.V.	-1.693	0.232	1.602	1.162	0.896
MEDIAN	-0.423	1.224	0.378	2.298	0.121

	CHPPEBCM	CHMAXD	CHMEANCT	CHSTDVCT	CHSKEWCT
N OF CASES	14	14	14	14	14
MINIMUM	4.511	-3.511	-0.088	0.698	0.043
MAXIMUM	93.744	-2.000	1.420	1.774	2.314
RANGE	89.233	1.511	1.508	1.076	2.271
MEAN	41.037	-3.005	0.592	1.026	1.065
VARIANCE	644.757	0.154	0.279	0.076	0.848
STANDARD DEV	25.392	0.392	0.528	0.275	0.921
STD. ERROR	6.786	0.105	0.141	0.074	0.246
SKEWNESS(G1)	0.248	1.157	0.244	1.505	0.357
KURTOSIS(G2)	-0.499	1.029	-1.277	1.986	-1.622
SUM	574.522	-42.063	8.292	14.358	14.907
C.V.	0.619	-0.130	0.891	0.268	0.865
MEDIAN	43.811	-3.129	0.557	0.973	0.727

	CHM3DVCT	CHPSLTCT	CHPOR	CHMSPERM	CHLITH
N OF CASES	14	14	14	11	11
MINIMUM	0.015	0.022	0.216	44.981	1.000
MAXIMUM	5.306	2.303	0.467	271.680	2.000
RANGE	5.291	2.281	0.251	226.699	1.000
MEAN	1.623	0.488	0.345	201.321	1.091
VARIANCE	3.316	0.452	0.008	6786.031	0.091
STANDARD DEV	1.821	0.673	0.089	82.377	0.302
STD. ERROR	0.487	0.180	0.024	24.838	0.091
SKEWNESS(G1)	0.858	1.763	0.143	-0.835	2.846
KURTOSIS(G2)	-0.648	1.941	-1.403	-0.747	6.100
SUM	22.715	6.830	4.835	2214.526	12.000
C.V.	1.122	1.379	0.258	0.409	0.276
MEDIAN	0.718	0.221	0.332	223.067	1.000

TOTAL OBSERVATIONS: 29

	HLMEANCM	HLSTDVCM	HLSKEWCM	HLM3DVCM	HLPSLTCM
N OF CASES	29	29	29	29	29
MINIMUM	0.895	0.615	-1.544	-2.311	0.025
MAXIMUM	4.367	1.464	1.636	0.422	19.245
RANGE	3.472	0.849	3.180	2.733	19.220
MEAN	2.204	0.969	0.090	-0.167	1.983
VARIANCE	0.774	0.055	0.441	0.388	13.849
STANDARD DEV	0.880	0.233	0.664	0.623	3.721
STD. ERROR	0.163	0.043	0.123	0.116	0.691
SKEWNESS(G1)	0.743	0.122	0.281	-1.778	3.668
KURTOSIS(G2)	-0.307	-0.839	0.923	3.228	14.247
SUM	63.930	28.110	2.603	-4.830	57.495
C.V.	0.399	0.241	7.401	-3.742	1.877
MEDIAN	1.952	0.989	0.147	0.123	0.686

	HLPPEBCM	HLMAXD	HLMEANCT	HLSTDVCT	HLSKEWCT
N OF CASES	29	29	29	29	29
MINIMUM	0.002	-2.585	1.057	0.614	-0.602
MAXIMUM	8.619	-1.007	4.367	1.241	1.654
RANGE	8.617	1.578	3.310	0.627	2.256
MEAN	1.633	-1.493	2.257	0.902	0.364
VARIANCE	5.311	0.256	0.712	0.034	0.289
STANDARD DEV	2.305	0.506	0.844	0.184	0.538
STD. ERROR	0.428	0.094	0.157	0.034	0.100
SKEWNESS(G1)	1.367	-0.815	0.803	0.046	0.504
KURTOSIS(G2)	1.100	-0.599	-0.241	-1.134	0.436
SUM	47.355	-43.301	65.448	26.153	10.552
C.V.	1.411	-0.339	0.374	0.204	1.478
MEDIAN	0.194	-1.379	1.954	0.898	0.336

	HLM3DVCT	HLPSLTCT	HLPOR	HLMSPERM	HLLITH
N OF CASES	29	29	29	28	27
MINIMUM	-0.788	0.025	0.308	0.850	1.000
MAXIMUM	1.074	19.246	0.515	158.930	4.000
RANGE	1.862	19.221	0.207	158.080	3.000
MEAN	0.177	1.995	0.442	39.962	1.815
VARIANCE	0.155	13.829	0.002	1753.202	0.618
STANDARD DEV	0.394	3.719	0.044	41.871	0.786
STD. ERROR	0.073	0.691	0.008	7.913	0.151
SKEWNESS(G1)	-0.606	3.667	-1.192	1.367	0.814
KURTOSIS(G2)	1.134	14.250	1.962	1.279	0.463
SUM	5.141	57.860	12.832	1118.940	49.000
C.V.	2.221	1.864	0.100	1.048	0.433
MEDIAN	0.221	0.687	0.454	25.495	2.000

TOTAL OBSERVATIONS: 25

	SFMEANCM	SFSTDVCM	SFSKEWCM	SFM3DVCM	SFPSLTCM
N OF CASES	25	25	25	25	25
MINIMUM	-1.169	1.163	-0.801	-4.954	0.046
MAXIMUM	2.756	2.551	2.489	8.773	7.880
RANGE	3.925	1.388	3.290	13.727	7.834
MEAN	-0.072	1.722	0.638	3.256	0.858
VARIANCE	0.552	0.121	0.408	9.380	2.390
STANDARD DEV	0.743	0.347	0.639	3.063	1.546
STD. ERROR	0.149	0.069	0.128	0.613	0.309
SKEWNESS(G1)	2.250	0.410	0.429	-0.447	3.968
KURTOSIS(G2)	6.634	-0.456	2.314	0.519	15.508
SUM	-1.807	43.057	15.948	81.407	21.446
C.V.	-10.280	0.202	1.002	0.941	1.802
MEDIAN	-0.209	1.717	0.611	3.081	0.373

	SFPPEBCM	SFMAXD	SFMEANCT	SFSTDVCT	SFSKEWCT
N OF CASES	25	25	25	25	25
MINIMUM	6.659	-3.916	-0.117	0.971	-0.109
MAXIMUM	63.629	-2.511	3.087	1.883	2.955
RANGE	56.970	1.405	3.204	0.912	3.064
MEAN	33.811	-3.142	0.930	1.334	0.906
VARIANCE	176.502	0.114	0.446	0.059	0.458
STANDARD DEV	13.285	0.338	0.668	0.242	0.677
STD. ERROR	2.657	0.068	0.134	0.048	0.135
SKEWNESS(G1)	-0.068	-0.381	1.307	0.531	1.131
KURTOSIS(G2)	-0.052	-0.136	2.627	-0.428	1.657
SUM	845.270	-78.547	23.246	33.362	22.654
C.V.	0.393	-0.107	0.719	0.181	0.747
MEDIAN	35.570	-3.170	0.917	1.327	0.823

	SFM3DVCT	SFPSLTCT	SFPOR	SFMSPERM	SFLITH
N OF CASES	25	25	25	20	20
MINIMUM	-0.731	0.062	0.271	2.010	1.000
MAXIMUM	5.917	8.442	0.439	271.680	3.000
RANGE	6.648	8.380	0.168	269.670	2.000
MEAN	1.932	1.225	0.345	117.187	1.400
VARIANCE	1.940	3.016	0.002	7872.529	0.463
STANDARD DEV	1.393	1.737	0.048	88.727	0.681
STD. ERROR	0.279	0.347	0.010	19.840	0.152
SKEWNESS(G1)	0.578	3.125	0.353	0.502	1.398
KURTOSIS(G2)	1.098	10.181	-0.987	-0.822	0.612
SUM	48.310	30.631	8.637	2343.749	28.000
C.V.	0.721	1.417	0.139	0.757	0.486
MEDIAN	1.868	0.625	0.325	111.386	1.000

TOTAL OBSERVATIONS: 15

	SLMEANCM	SLSTDVCM	SLSKEWCM	SLM3DVCM	SLPSLTCM
N OF CASES	15	15	15	15	15
MINIMUM	0.398	0.895	-1.361	-7.281	0.141
MAXIMUM	3.426	2.195	0.432	0.368	16.270
RANGE	3.028	1.300	1.793	7.649	16.129
MEAN	2.467	1.535	-0.460	-2.456	4.707
VARIANCE	0.786	0.162	0.194	6.900	17.297
STANDARD DEV	0.886	0.402	0.441	2.627	4.159
STD. ERROR	0.229	0.104	0.114	0.678	1.074
SKEWNESS(G1)	-0.759	-0.015	-0.125	-0.692	1.526
KURTOSIS(G2)	-0.095	-1.109	0.003	-1.080	2.076
SUM	37.012	23.027	-6.897	-36.833	70.610
C.V.	0.359	0.262	-0.958	-1.070	0.884
MEDIAN	2.442	1.529	-0.358	-1.230	3.380

	SLPPEBCM	SLMAXD	SLMEANCT	SLSTDVCT	SLSKEWCT
N OF CASES	15	15	15	15	15
MINIMUM	0.002	-3.248	0.846	0.810	-0.765
MAXIMUM	17.242	-1.007	3.430	1.576	0.501
RANGE	17.240	2.241	2.584	0.766	1.266
MEAN	6.303	-2.309	2.730	1.256	-0.151
VARIANCE	43.314	0.600	0.495	0.055	0.125
STANDARD DEV	6.581	0.775	0.703	0.234	0.354
STD. ERROR	1.699	0.200	0.182	0.060	0.091
SKEWNESS(G1)	0.493	0.714	-1.321	-0.290	0.343
KURTOSIS(G2)	-1.281	-0.802	1.444	-0.986	-0.487
SUM	94.543	-34.635	40.943	18.847	-2.262
C.V.	1.044	-0.335	0.258	0.186	-2.348
MEDIAN	5.829	-2.678	2.788	1.250	-0.223

	SLM3DVCT	SLPSLTCT	SLPOR	SLMSPERM	SLLITH
N OF CASES	15	15	15	15	15
MINIMUM	-2.261	0.169	0.308	2.659	1.000
MAXIMUM	0.721	16.434	0.470	60.662	3.000
RANGE	2.982	16.265	0.162	58.003	2.000
MEAN	-0.419	4.878	0.406	14.819	2.067
VARIANCE	0.568	17.236	0.003	265.527	0.352
STANDARD DEV	0.754	4.152	0.057	16.295	0.594
STD. ERROR	0.195	1.072	0.015	4.207	0.153
SKEWNESS(G1)	-0.578	1.498	-0.423	1.957	0.003
KURTOSIS(G2)	0.579	2.090	-1.370	2.679	-0.001
SUM	-6.289	73.167	6.096	222.285	31.000
C.V.	-1.798	0.851	0.140	1.100	0.287
MEDIAN	-0.523	4.084	0.425	9.836	2.000

TOTAL OBSERVATIONS: 18 Permeability by bedding groups

	CB1	CB2	CB3	CB4	CH1
N OF CASES	5	4	8	8	5
MINIMUM	20.145	88.151	2.828	74.671	210.681
MAXIMUM	189.818	271.680	98.224	165.608	271.680
RANGE	169.673	183.529	95.396	90.937	60.999
MEAN	86.901	196.688	58.176	129.037	249.758
VARIANCE	4139.685	6361.577	896.148	700.906	920.286
STANDARD DEV	64.340	79.759	29.936	26.475	30.336
STD. ERROR	28.774	39.880	10.584	9.360	13.567
SKEWNESS(G1)	0.771	-0.600	-0.470	-0.897	-0.471
KURTOSIS(G2)	-0.551	-1.099	-0.393	0.525	-1.697
SUM	434.506	786.753	465.411	1032.299	1248.788
C.V.	0.740	0.406	0.515	0.205	0.121
MEDIAN	86.397	213.461	56.932	134.886	271.680

	CH2	HL1	HL2	SF1	SF2
N OF CASES	6	17	8	13	6
MINIMUM	44.981	3.525	0.848	35.455	8.899
MAXIMUM	271.680	158.933	45.843	271.680	147.170
RANGE	226.699	155.408	44.995	236.225	138.271
MEAN	160.956	57.279	17.125	156.502	51.203
VARIANCE	8534.561	2019.518	227.497	6355.770	2765.330
STANDARD DEV	92.383	44.939	15.083	79.723	52.586
STD. ERROR	37.715	10.899	5.333	22.111	21.468
SKEWNESS(G1)	0.016	0.879	0.675	0.335	1.110
KURTOSIS(G2)	-1.532	0.005	-0.371	-1.114	-0.145
SUM	965.738	973.746	136.996	2034.520	307.219
C.V.	0.574	0.785	0.881	0.509	1.027
MEDIAN	157.183	47.679	15.776	141.959	31.081

	SL1
N OF CASES	14
MINIMUM	2.010
MAXIMUM	19.681
RANGE	17.671
MEAN	8.534
VARIANCE	28.192
STANDARD DEV	5.310
STD. ERROR	1.419
SKEWNESS(G1)	0.639
KURTOSIS(G2)	-0.611
SUM	119.481
C.V.	0.622
MEDIAN	7.462

TOTAL OBSERVATIONS: 18 Permeability by bedding groups

	CB1	CB2	CB3	CB4	CH1
N OF CASES	5	4	8	8	5
MINIMUM	20.145	88.151	2.828	74.671	210.681
MAXIMUM	189.818	271.680	98.224	165.608	271.680
RANGE	169.673	183.529	95.396	90.937	60.999
MEAN	86.901	196.688	58.176	129.037	249.758
VARIANCE	4139.685	6361.577	896.148	700.906	920.286
STANDARD DEV	64.340	79.759	29.936	26.475	30.336
STD. ERROR	28.774	39.880	10.584	9.360	13.567
SKEWNESS(G1)	0.771	-0.600	-0.470	-0.897	-0.471
KURTOSIS(G2)	-0.551	-1.099	-0.393	0.525	-1.697
SUM	434.506	786.753	465.411	1032.299	1248.788
C.V.	0.740	0.406	0.515	0.205	0.121
MEDIAN	86.397	213.461	56.932	134.886	271.680

	CH2	HL1	HL2	SF1	SF2
N OF CASES	6	17	8	13	6
MINIMUM	44.981	3.525	0.848	35.455	8.899
MAXIMUM	271.680	158.933	45.843	271.680	147.170
RANGE	226.699	155.408	44.995	236.225	138.271
MEAN	160.956	57.279	17.125	156.502	51.203
VARIANCE	8534.561	2019.518	227.497	6355.770	2765.330
STANDARD DEV	92.383	44.939	15.083	79.723	52.586
STD. ERROR	37.715	10.899	5.333	22.111	21.468
SKEWNESS(G1)	0.016	0.879	0.675	0.335	1.110
KURTOSIS(G2)	-1.532	0.005	-0.371	-1.114	-0.145
SUM	965.738	973.746	136.996	2034.520	307.219
C.V.	0.574	0.785	0.881	0.509	1.027
MEDIAN	157.183	47.679	15.776	141.959	31.081

	SL1
N OF CASES	14
MINIMUM	2.010
MAXIMUM	19.681
RANGE	17.671
MEAN	8.534
VARIANCE	28.192
STANDARD DEV	5.310
STD. ERROR	1.419
SKEWNESS(G1)	0.639
KURTOSIS(G2)	-0.611
SUM	119.481
C.V.	0.622
MEDIAN	7.462

Mean grain size, complete sample

Kolmogorov-Smirnov two sample test results

Maximum differences for pairs of variables

	Crossbeds	Channels	Horizontal	Scour and Fill	Structureless
Crossbeds	0.000				
Channels	0.786	0.000			
Horizontal	0.483	1.000	0.000		
Scour and Fill	0.760	0.357	0.920	0.000	
Structureless	0.600	0.929	0.333	0.933	0.000

Two-sided probabilities

	Crossbeds	Channels	Horizontal	Scour and Fill	Structureless
Crossbeds	1.00				
Channels	0.00	1.00			
Horizontal	0.002	0.000	1.000		
Scour and Fill	0.000	0.264	0.000	1.000	
Structureless	0.006	0.000	0.341	0.000	1.000

Measured Permeability, permeability profile measurements

Kolmogorov-Smirnov two sample test results

Maximum differences for pairs of variables

	Crossbeds	Channels	Horizontal	Scour and Fill	Structureless
Crossbeds	0.000				
Channels	0.708	0.000			
Horizontal	0.226	0.792	0.000		
Scour and Fill	0.500	0.438	0.537	0.000	
Structureless	0.676	1.000	0.439	0.942	0.000

Two-sided probabilities

	Crossbeds	Channels	Horizontal	Scour and Fill	Structureless
Crossbeds	1.000				
Channels	0.000	1.000			
Horizontal	0.000	0.000	1.000		
Scour and Fill	0.000	0.000	0.000	1.000	
Structureless	0.000	0.000	0.000	0.000	1.000

Measured Permeability, sieved outcrop samples

Kolmogorov-Smirnov two sample test results

Maximum differences for pairs of variables

	Crossbeds	Channels	Horizontal	Scour and Fill	Structureless
Crossbeds	0.000				
Channels	0.727	0.000			
Horizontal	0.500	0.727	0.000		
Scour and Fill	0.111	0.500	0.421	0.000	
Structureless	0.800	0.909	0.467	0.900	0.000

Two-sided probabilities

	Crossbeds	Channels	Horizontal	Scour and Fill	Structureless
Crossbeds	1.000				
Channels	0.003	1.000			
Horizontal	0.002	0.003	1.000		
Scour and Fill	0.999	0.188	0.058	1.000	
Structureless	0.000	0.000	0.065	0.000	1.000

APPENDIX E

Comparison of grain size distribution statistics of well cuttings

Scatter Plot of Mean and Standard Deviation of Well Cuttings and Outcrop Samples.

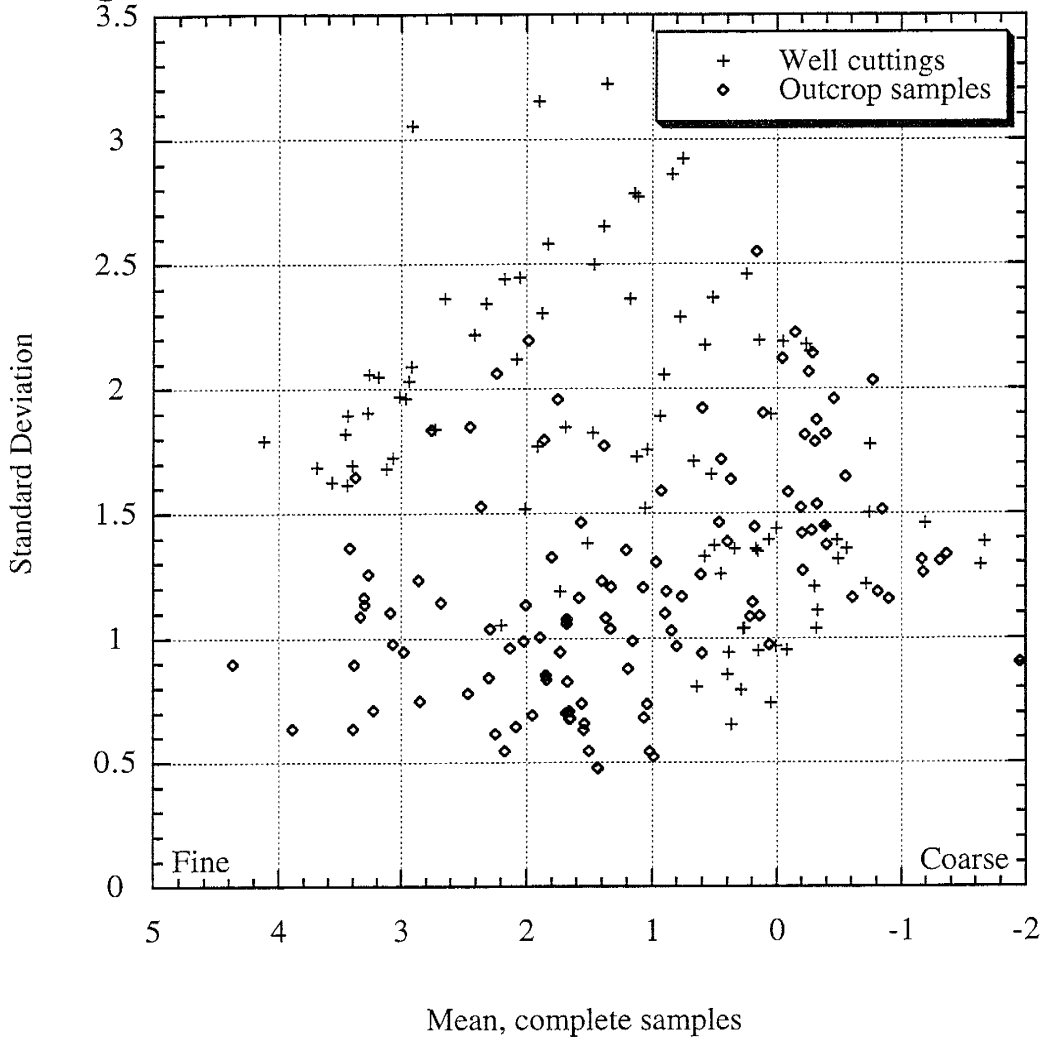

Scatter Plot of Mean and Skewness of Well Cuttings and Outcrop Samples

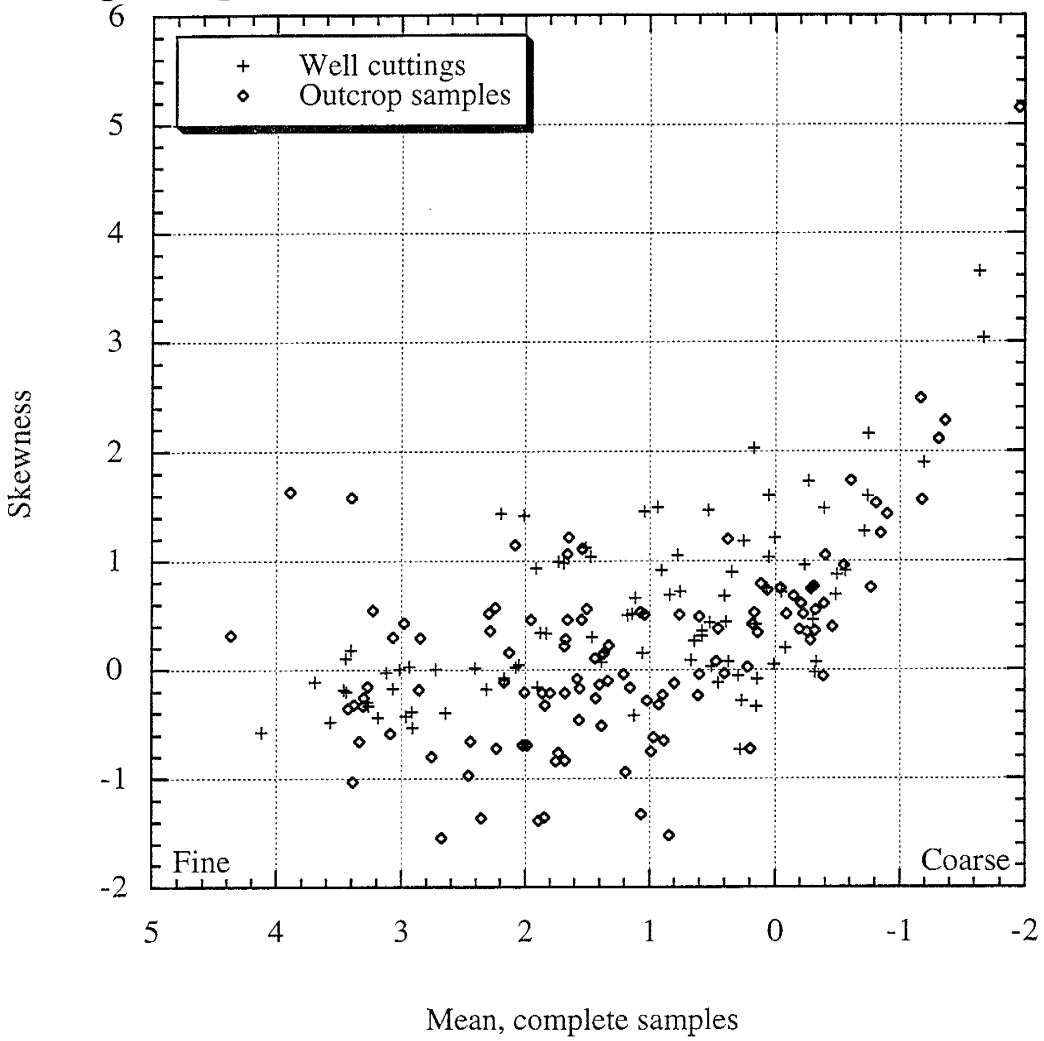

Scatter Plot of Mean and Standard Deviation of Well Cuttings, Complete Samples

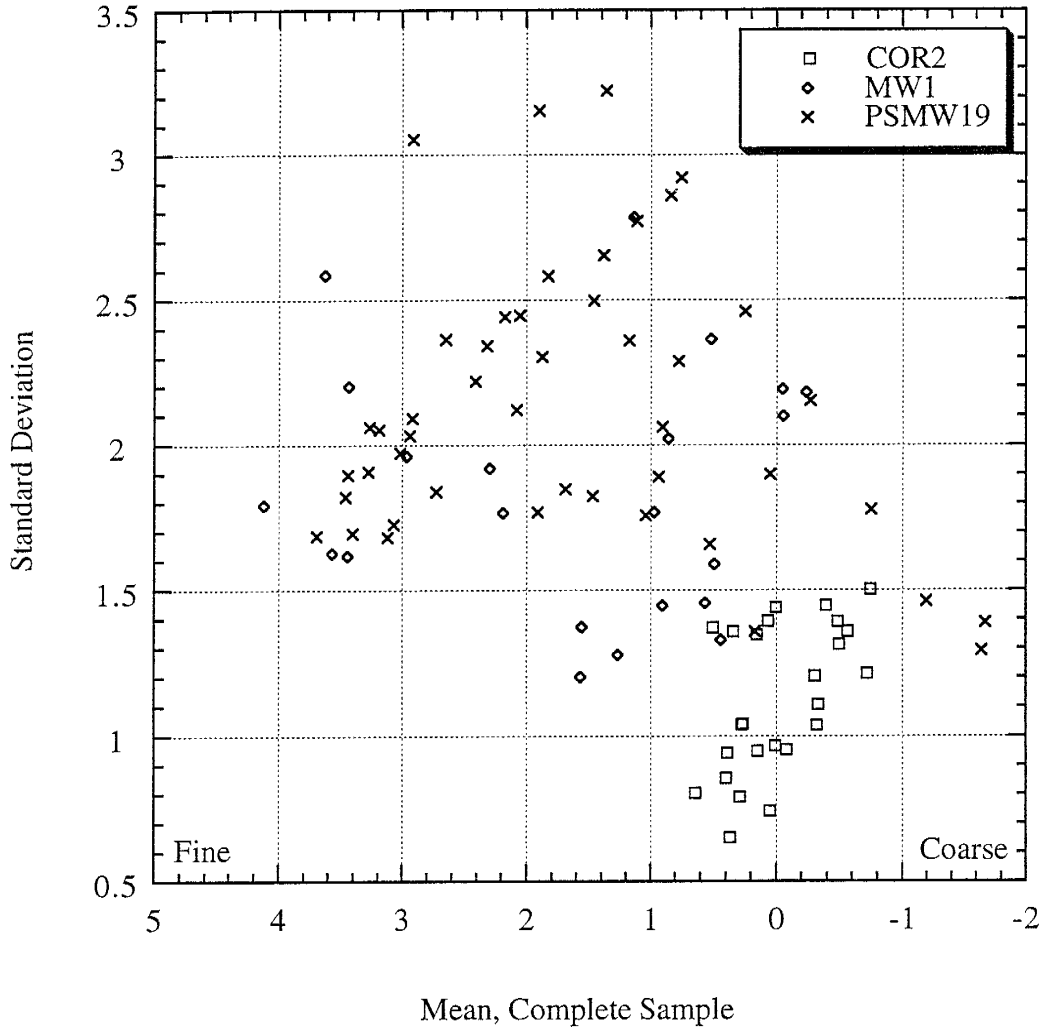

Scatter Plot of Mean and Standard Deviation of Well Cuttings, Cut Samples

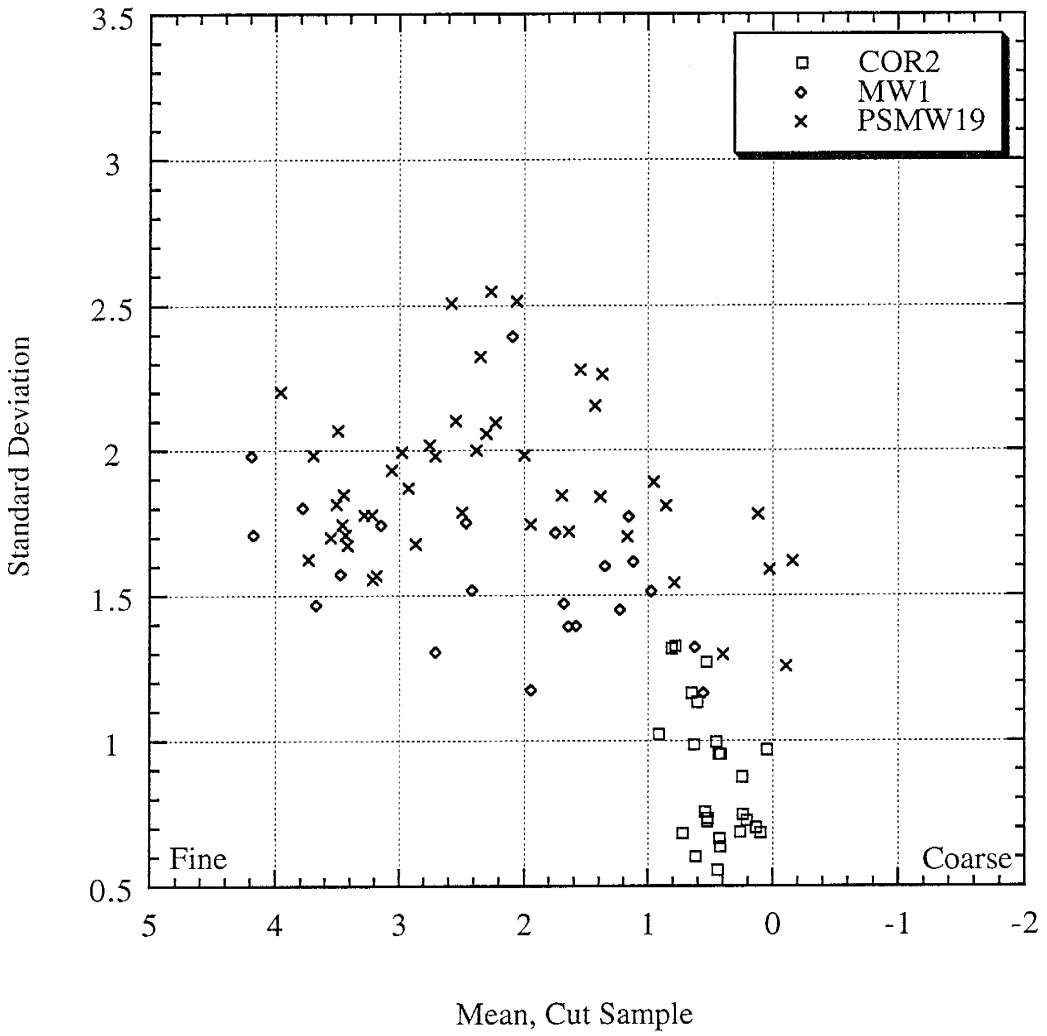

Scatter Plot of Mean and Skewness of Well Cuttings, Complete Samples

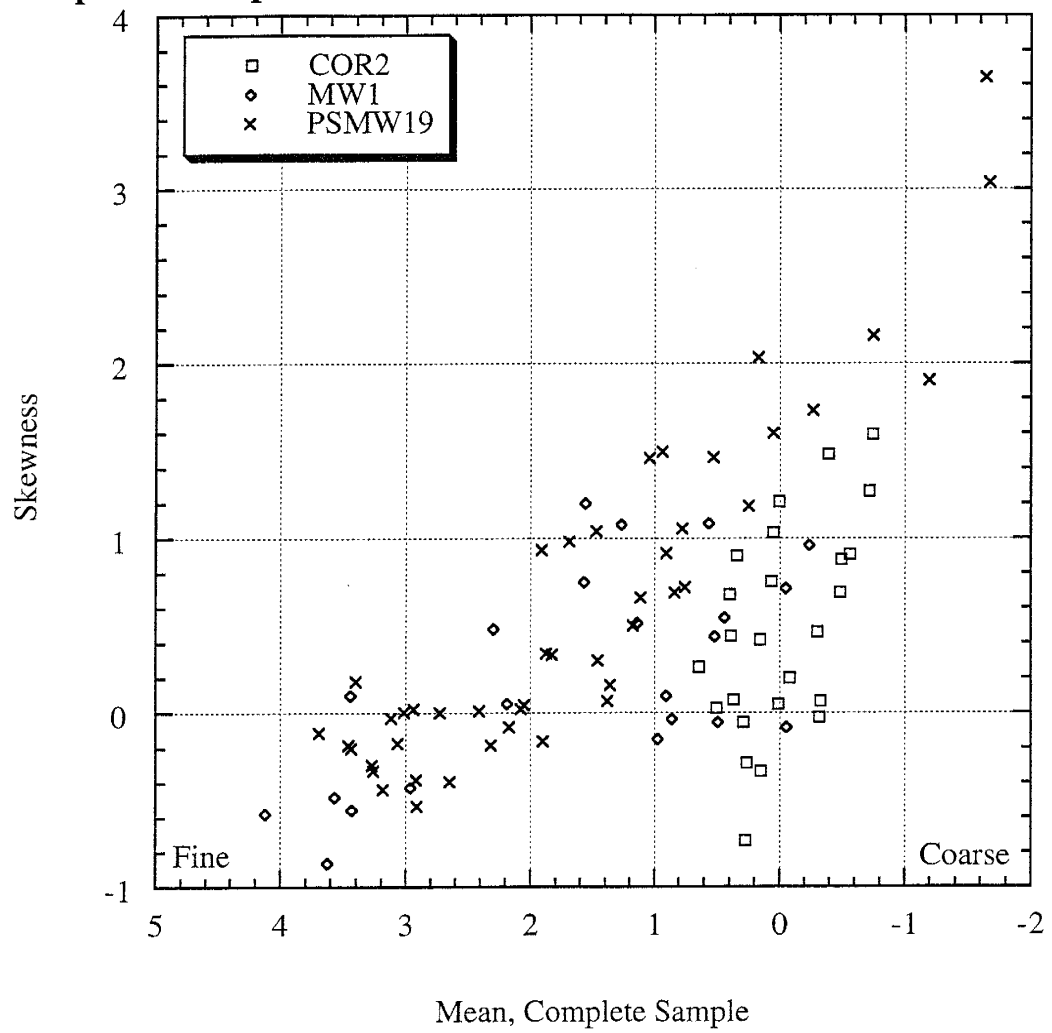

Scatter Plot of Mean and Skewness of Well Cuttings, Cut Samples

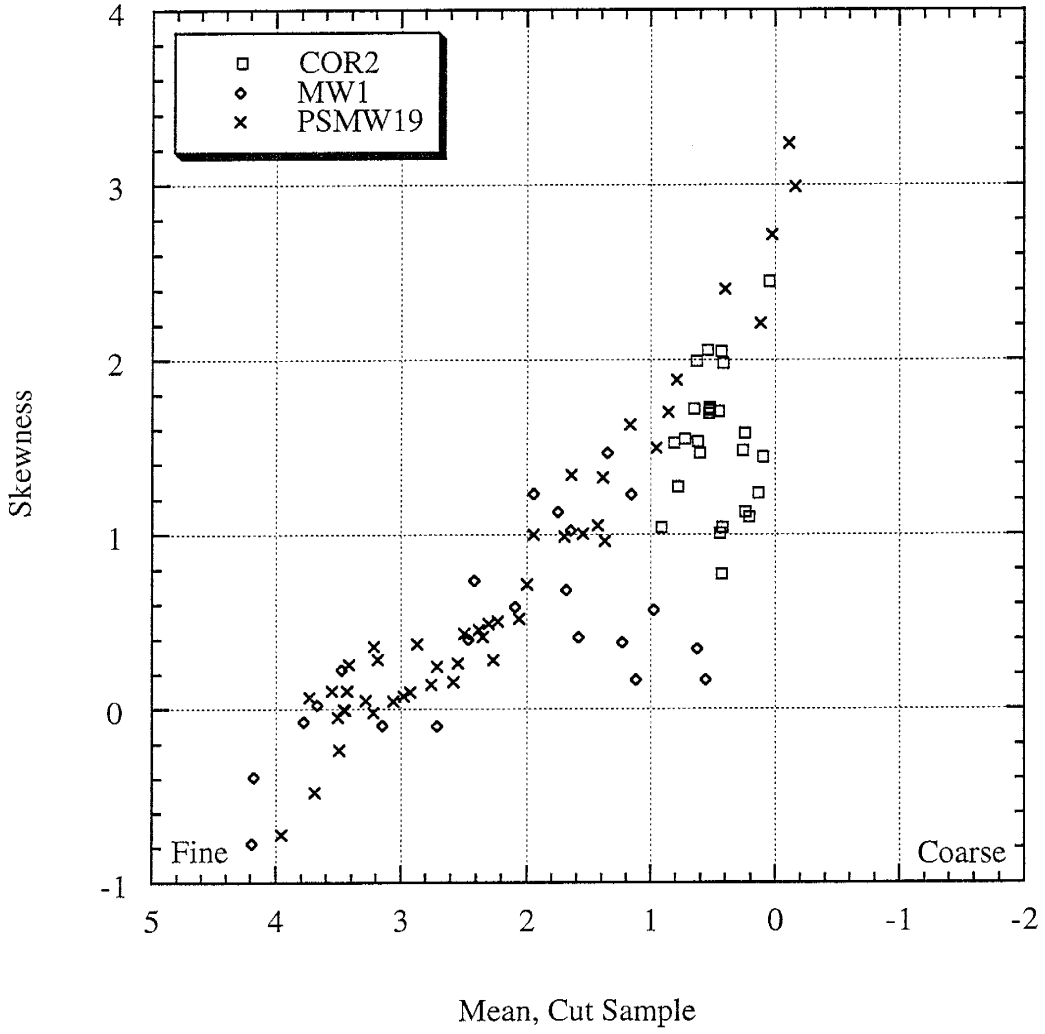

Scatter Plot of Standard Deviation and Skewness of Well Cuttings, Complete Samples

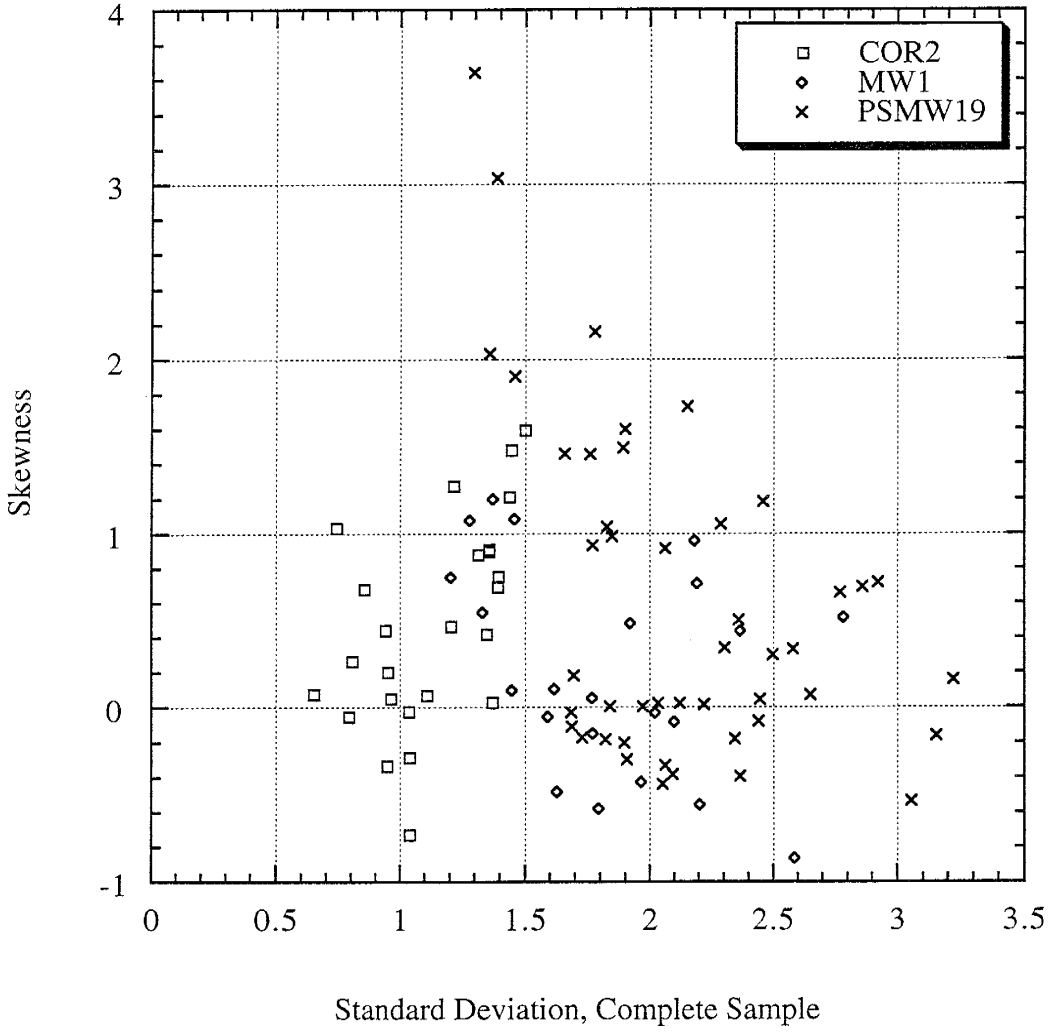

Scatter Plot of Standard Deviation and Skewness of Well Cuttings, Cut Samples

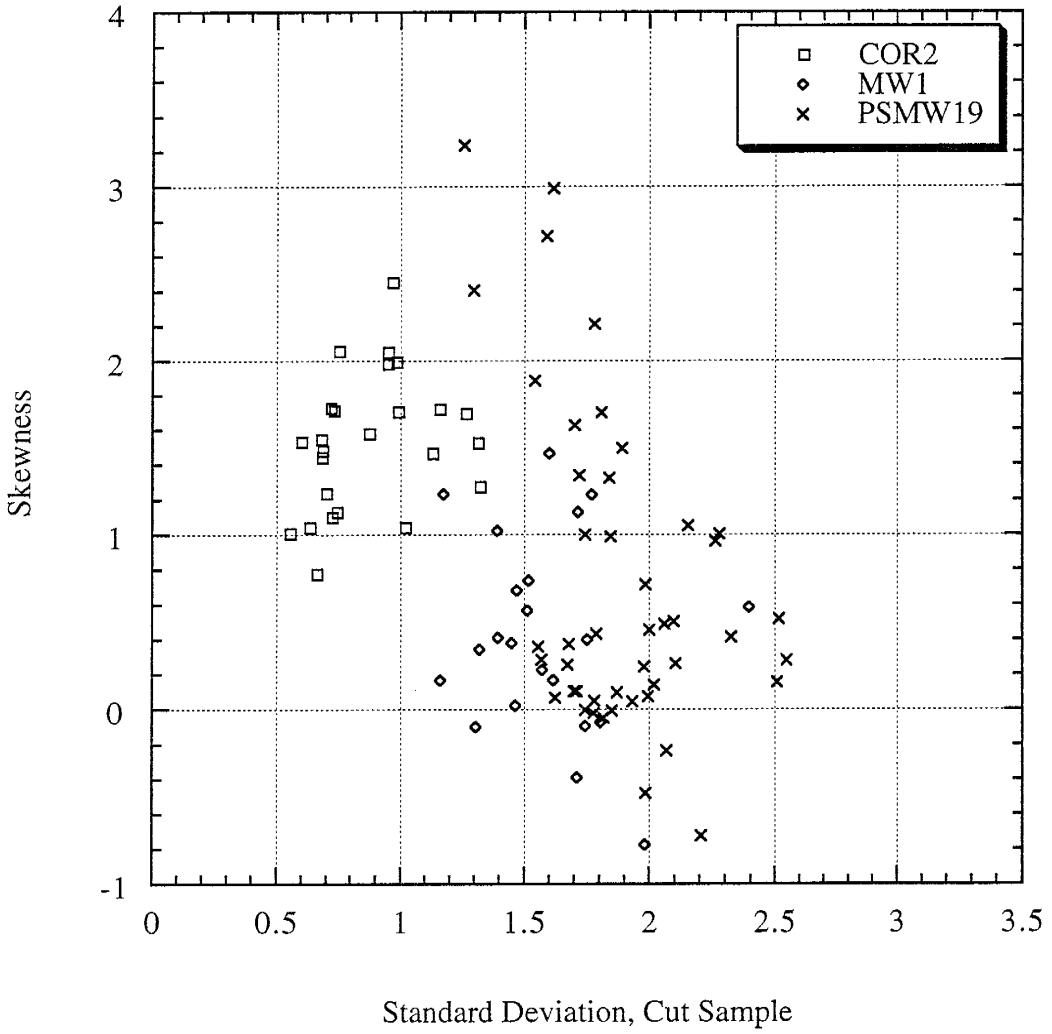

Scatter Plot of Mean and Percent Fines of Well Cuttings, Complete Samples

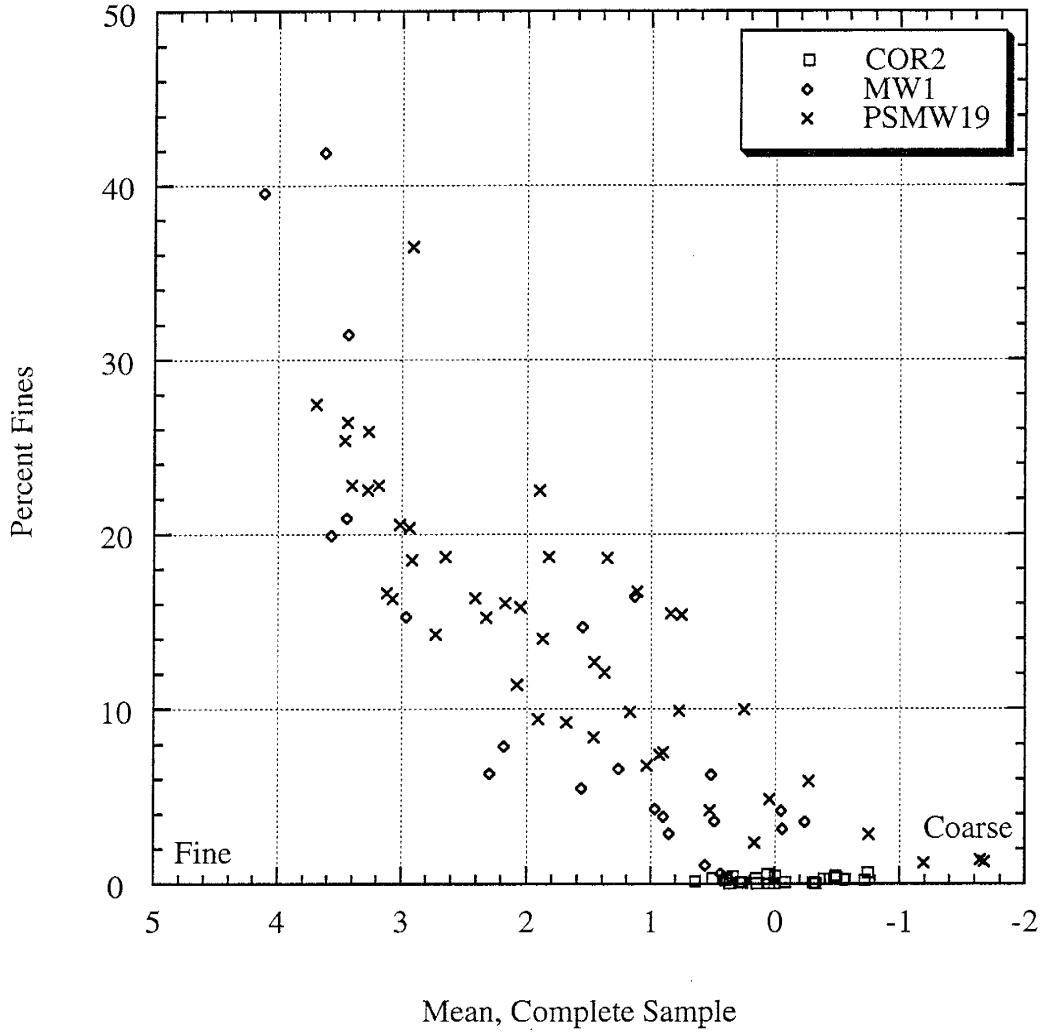

Scatter Plot of Mean and Percent Fines of Well Cuttings, Cut Samples

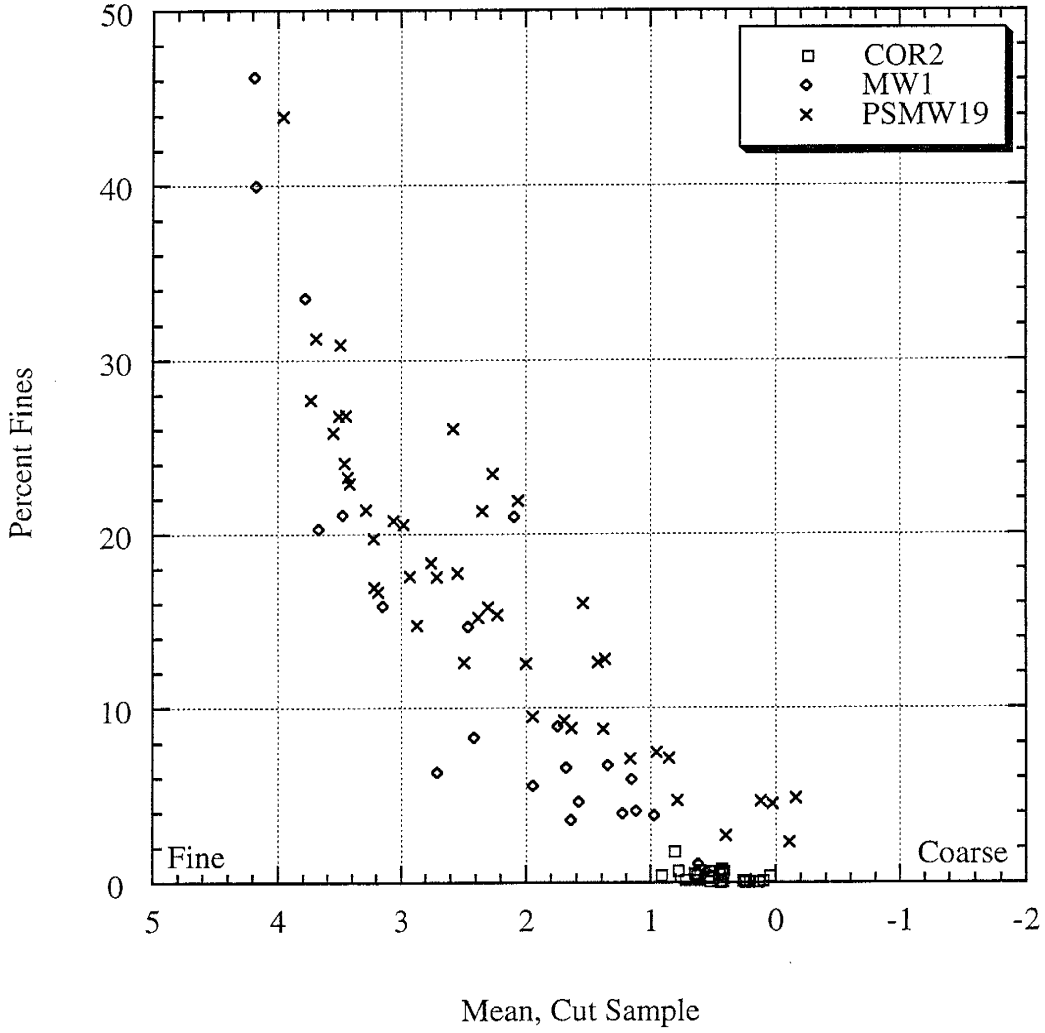

Mean, Standard Deviation and Skewness of Well Cuttings, Complete Samples

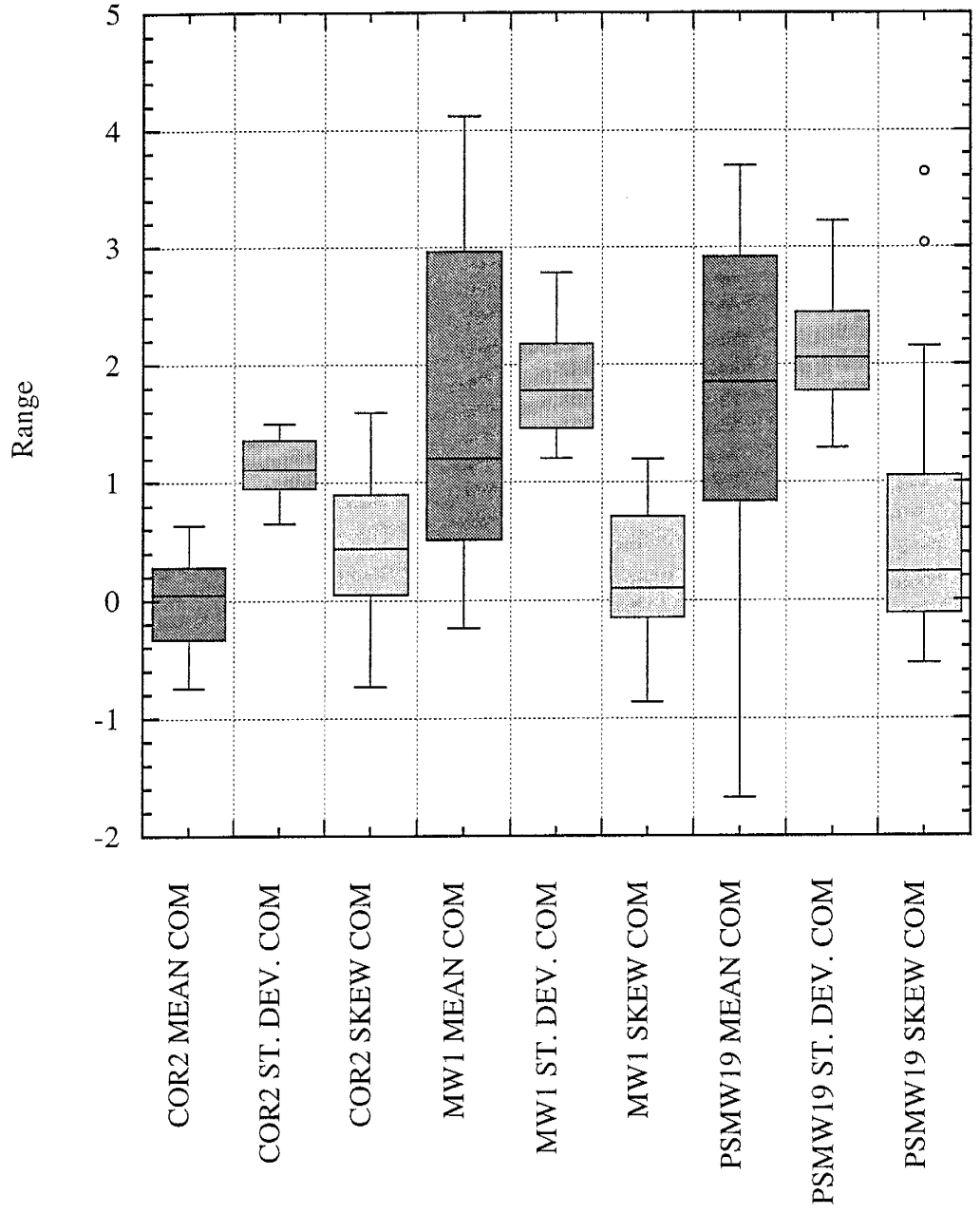

Small circles are data points considered outliers by the graphing program.

Mean, Standard Deviation and Skewness of Well Cuttings, Cut Samples

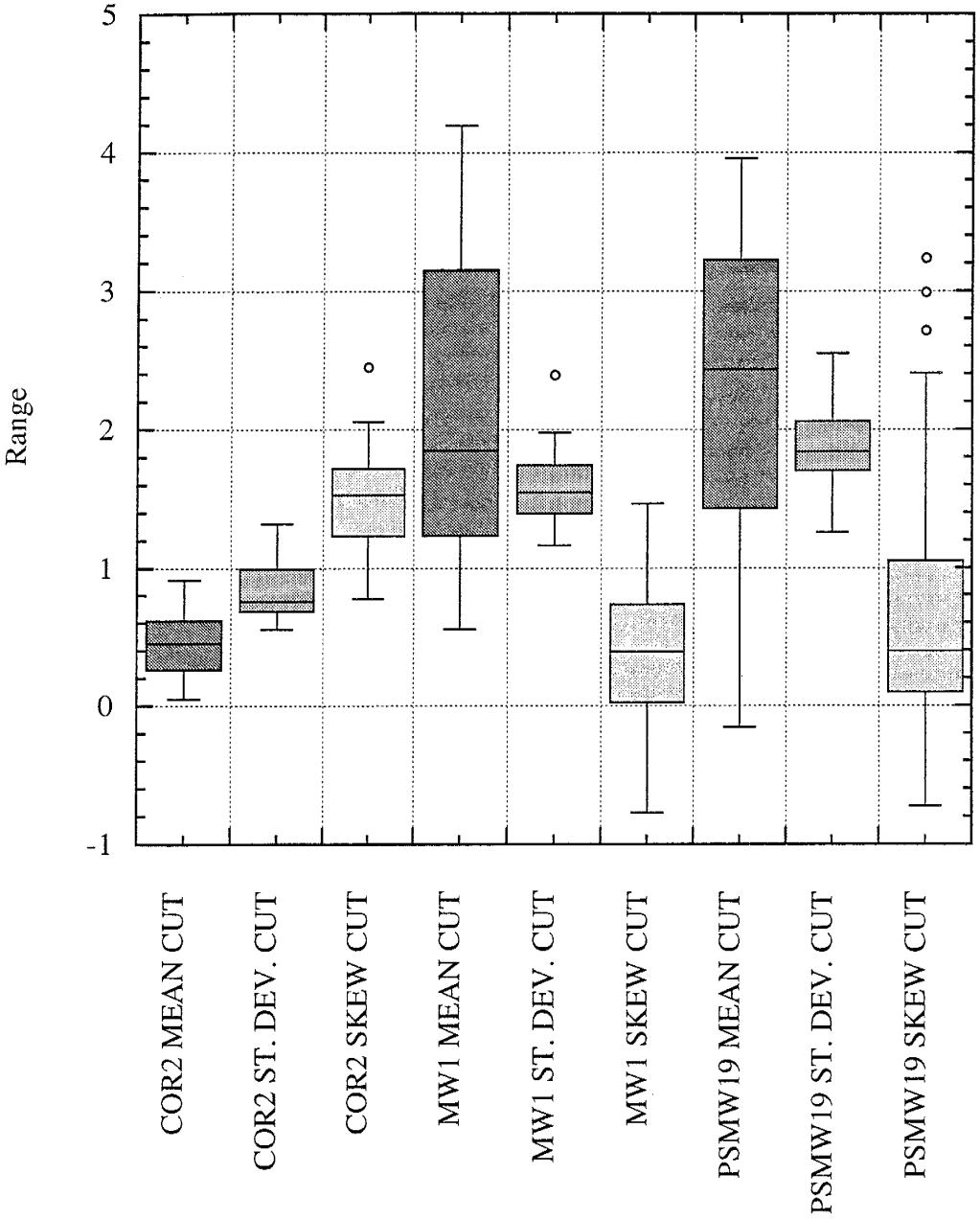

Small circles are data points considered outliers by the graphing program.

Percent Fines of Well Cuttings

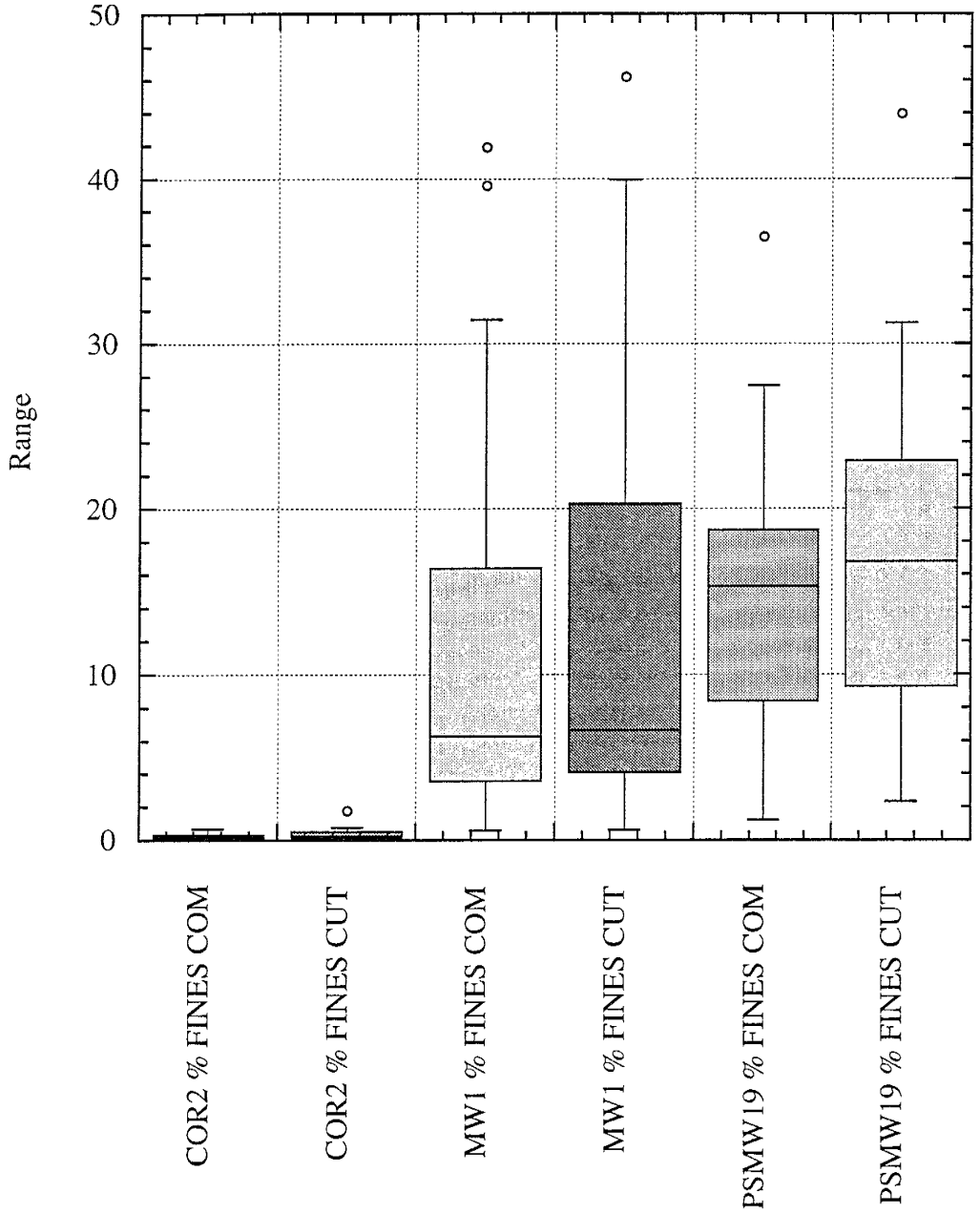

Small circles are data points considered outliers by the graphing program.

ABBREVIATIONS

CB - CROSSBEDS
CH - CHANNELS
HL - HORIZONTAL LAMINATIONS
SF - SCOUR AND FILL
SL - STRUCTURELESS
C2 - CORONADO 2
M1 - MW1
PS - PSMW-19
-CM - COMPLETE DISTRIBUTION
-CT - CUT DISTRIBUTION
MEAN - MEAN GRAIN SIZE (PHI UNITS)
STDV - STANDARD DEVIATION
SKEW - SKEWNESS
M3DV - MEAN-CUBED DEVIATION
PSLT - PERCENT FINES
PPEB - PERCENT PEBBLES
MAXD - MAXIMUM INTERMEDIATE DIAMETER
POR - PERCENT POROSITY
MSPERM - MEASURED PERMEABILITY
LITH - LITHIFICATION

Well Colorado 7

TOTAL OBSERVATIONS: 25

	C2MEANCM	C2STDVCM	C2SKEWCM	C2M3DVCM	C2PFINCM
N OF CASES	25	25	25	25	25
MINIMUM	-0.742	0.652	-0.731	-0.820	0.048
MAXIMUM	0.639	1.503	1.594	5.413	0.698
RANGE	1.381	0.851	2.325	6.233	0.650
MEAN	-0.022	1.129	0.479	1.132	0.249
VARIANCE	0.158	0.065	0.353	2.520	0.035
STANDARD DEV	0.398	0.255	0.594	1.587	0.188
STD. ERROR	0.080	0.051	0.119	0.317	0.038
SKEWNESS(G1)	-0.291	-0.198	0.067	1.201	0.677
KURTOSIS(G2)	-1.073	-1.255	-0.695	0.696	-0.555
SUM	-0.551	28.223	11.971	28.294	6.223
C.V.	-18.060	0.226	1.241	1.403	0.754
MEDIAN	0.050	1.109	0.441	0.420	0.238

	C2PPEB	CRMAXDIA	C2MEANCT	C2STDVCT	C2SKEWCT
N OF CASES	25	25	25	25	25
MINIMUM	3.383	-3.138	0.047	0.555	0.773
MAXIMUM	60.493	-1.070	0.913	1.325	2.451
RANGE	57.110	2.068	0.866	0.770	1.678
MEAN	21.664	-2.491	0.468	0.874	1.529
VARIANCE	250.085	0.222	0.051	0.054	0.159
STANDARD DEV	15.814	0.471	0.226	0.231	0.399
STD. ERROR	3.163	0.094	0.045	0.046	0.080
SKEWNESS(G1)	0.926	1.241	-0.054	0.601	0.194
KURTOSIS(G2)	-0.114	1.495	-0.660	-0.818	-0.342
SUM	541.590	-62.268	11.693	21.855	38.235
C.V.	0.730	-0.189	0.484	0.265	0.261
MEDIAN	18.347	-2.609	0.452	0.756	1.530

	C2M3DVCT	C2PFINCT
N OF CASES	25	25
MINIMUM	0.172	0.051
MAXIMUM	3.478	1.767
RANGE	3.306	1.716
MEAN	1.286	0.373
VARIANCE	1.098	0.145
STANDARD DEV	1.048	0.380
STD. ERROR	0.210	0.076
SKEWNESS(G1)	0.806	2.046
KURTOSIS(G2)	-0.594	5.141
SUM	32.159	9.330
C.V.	0.815	1.019
MEDIAN	0.889	0.254

Well MW 1

TOTAL OBSERVATIONS: 22

	M1MEANCM	M1STDVCM	M1SKEWCM	M1M3DVCM	M1PFINCM
N OF CASES	22	22	22	21	22
MINIMUM	-0.236	1.204	-0.862	-5.933	0.609
MAXIMUM	4.121	2.782	1.198	11.063	41.902
RANGE	4.357	1.578	2.060	16.996	41.293
MEAN	1.617	1.843	0.218	1.590	11.809
VARIANCE	1.866	0.185	0.360	18.073	147.767
STANDARD DEV	1.366	0.430	0.600	4.251	12.156
STD. ERROR	0.291	0.092	0.128	0.928	2.592
SKEWNESS(G1)	0.456	0.422	0.009	0.651	1.367
KURTOSIS(G2)	-1.135	-0.593	-1.049	0.063	0.745
SUM	35.573	40.556	4.788	33.385	259.789
C.V.	0.845	0.233	2.756	2.674	1.029
MEDIAN	1.203	1.781	0.100	0.436	6.298

	M1PPEBCM	M1MAXDIA	M1MEANCT	M1STDVCT	M1SKEWCT
N OF CASES	22	22	22	22	22
MINIMUM	0.002	-3.797	0.557	1.163	-0.774
MAXIMUM	40.278	-1.070	4.193	2.393	1.464
RANGE	40.276	2.727	3.636	1.230	2.238
MEAN	10.117	-2.912	2.171	1.582	0.424
VARIANCE	161.174	0.651	1.298	0.076	0.317
STANDARD DEV	12.695	0.807	1.139	0.276	0.563
STD. ERROR	2.707	0.172	0.243	0.059	0.120
SKEWNESS(G1)	1.265	0.836	0.446	0.986	0.002
KURTOSIS(G2)	0.267	-0.037	-1.017	1.600	-0.451
SUM	222.576	-64.067	47.763	34.810	9.336
C.V.	1.255	-0.277	0.525	0.174	1.327
MEDIAN	4.505	-2.897	1.848	1.545	0.391

	M1M3DVCT	M1PFINCT
N OF CASES	22	22
MINIMUM	-6.011	0.628
MAXIMUM	8.031	46.199
RANGE	14.042	45.571
MEAN	1.636	12.854
VARIANCE	9.336	162.381
STANDARD DEV	3.056	12.743
STD. ERROR	0.651	2.717
SKEWNESS(G1)	0.040	1.385
KURTOSIS(G2)	0.807	0.884
SUM	35.990	282.792
C.V.	1.868	0.991
MEDIAN	1.138	6.655

Well PSMW-19

TOTAL OBSERVATIONS: 46

	PSMEANCM	PSSTDVCM	PSSKEWCM	PSM3DVCM	PSPFINCM
N OF CASES	46	46	46	45	46
MINIMUM	-1.672	1.293	-0.532	-5.210	1.226
MAXIMUM	3.695	3.221	3.643	17.905	36.460
RANGE	5.367	1.928	4.175	23.115	35.234
MEAN	1.652	2.123	0.592	4.356	14.318
VARIANCE	1.955	0.224	0.896	40.239	63.875
STANDARD DEV	1.398	0.473	0.947	6.343	7.992
STD. ERROR	0.206	0.070	0.140	0.946	1.178
SKEWNESS(G1)	-0.621	0.522	1.237	0.557	0.302
KURTOSIS(G2)	-0.258	-0.296	1.233	-0.575	-0.182
SUM	75.990	97.638	27.211	196.006	658.623
C.V.	0.846	0.223	1.600	1.456	0.558
MEDIAN	1.852	2.056	0.243	4.697	15.316

	PSPPEBCM	PSMAXDIA	PSMEANCT	PSSTDVCT	PSSKEWCT
N OF CASES	46	46	46	46	46
MINIMUM	0.321	-3.982	-0.157	1.257	-0.723
MAXIMUM	70.814	-1.202	3.958	2.547	3.237
RANGE	70.493	2.780	4.115	1.290	3.960
MEAN	17.061	-2.614	2.265	1.886	0.714
VARIANCE	335.968	0.375	1.312	0.083	0.827
STANDARD DEV	18.329	0.613	1.145	0.288	0.910
STD. ERROR	2.703	0.090	0.169	0.042	0.134
SKEWNESS(G1)	1.394	0.047	-0.580	0.365	1.150
KURTOSIS(G2)	1.328	0.558	-0.672	0.119	0.671
SUM	784.783	-120.249	104.182	86.748	32.852
C.V.	1.074	-0.234	0.506	0.152	1.274
MEDIAN	11.488	-2.585	2.434	1.841	0.394

	PSM3DVCT	PSPFINCT
N OF CASES	46	46
MINIMUM	-7.736	2.334
MAXIMUM	12.635	43.960
RANGE	20.371	41.626
MEAN	3.998	16.799
VARIANCE	21.013	77.834
STANDARD DEV	4.584	8.822
STD. ERROR	0.676	1.301
SKEWNESS(G1)	0.097	0.478
KURTOSIS(G2)	-0.363	0.356
SUM	183.899	772.767
C.V.	1.147	0.525
MEDIAN	3.069	16.798

APPENDIX F

Outcrop sketches and range of permeability measurements by outcrop

Strike of outcrop photos. Measured from base of sampling profile to left, looking right. Base of profiles are marked on outcrop mosaics.

Clarke Carr
1-2 140 degrees
2-3 180
3-4 180
4-5 225
5-6 230
6-7 235
7-8 205

Rio Bravo lower (west)
1-2 165 degrees
2-3 163
3-4 158
4-5 090

Rio Bravo upper (east)
1-2 180 degrees
2-3 170
3-4 175
4-5 100

Railroad lower (south)
1-2 210 degrees
2-3 230
3-4 240
4-5 275
5-6 275

Railroad upper (north)
1-2 310 degrees
2-3 310
3-4 290

Bear Canyon
1-2 270 degrees
2-3 270
3-4 285
4-5 285

Four Hills
1-2 045 degrees
2-3 020
3-4 005
4-5 005
5-6 360
6-7 360
7- 345

Tijeras Arroyo
1-2 275 degrees
2-3 275
3-4 270

Edith Gravels
1-2 180 degrees
2-3 200
(30m gap)
4-5 170

Clarke Carr

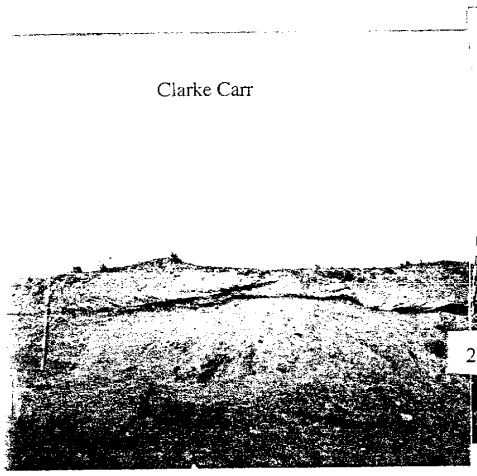

2

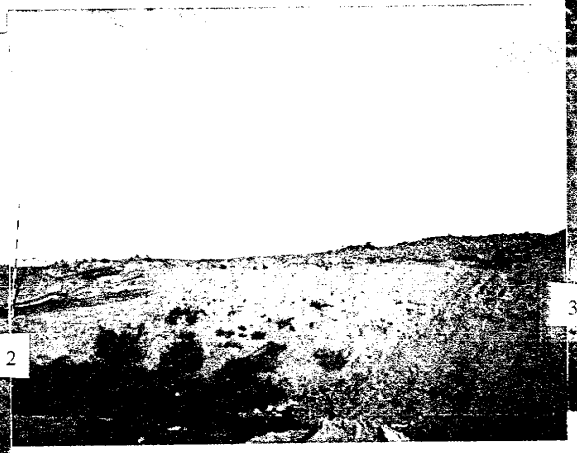

3

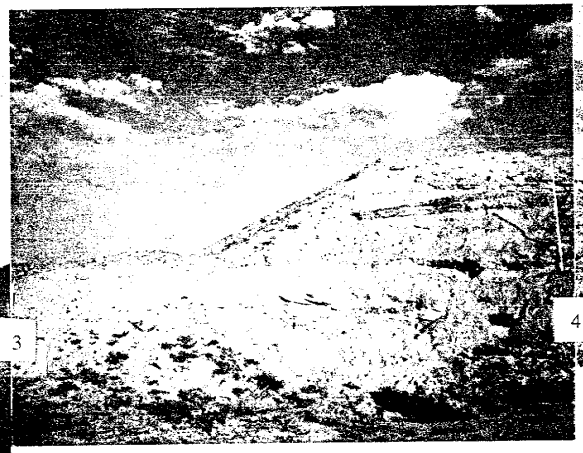

4

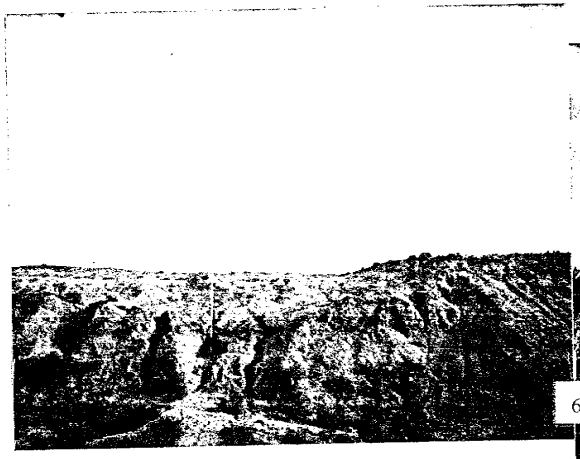

6

7

8

Clarke Carr

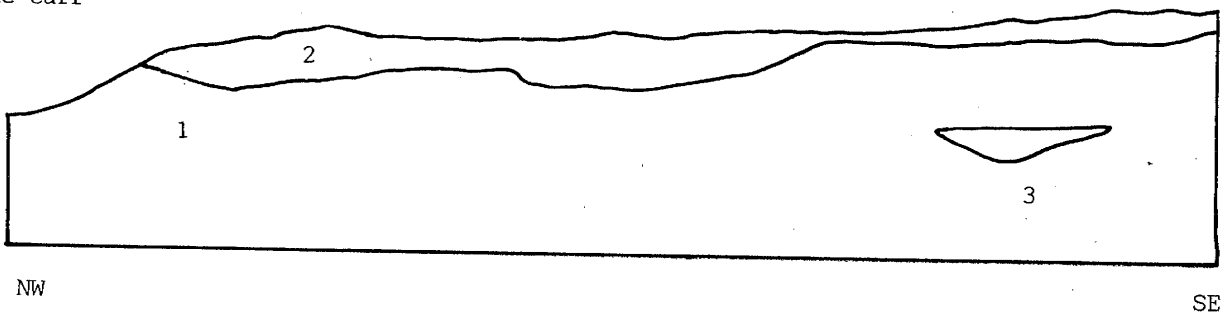

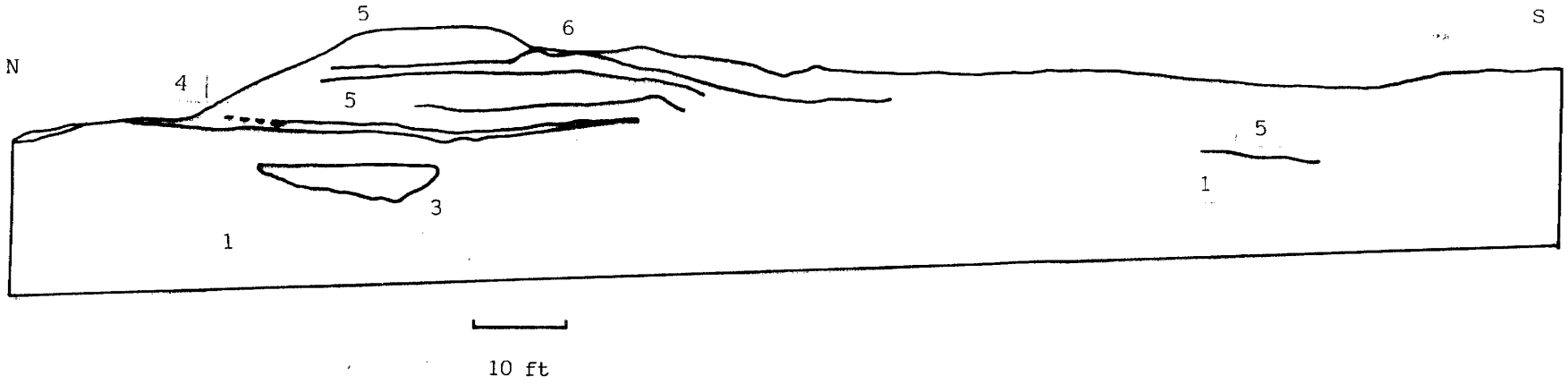

1. Horizontal laminations, low angle crossbeds and foresets. Fine to medium sand. Pumice-rich laminations along silica sands.

2. Large foresets or lateral accretion deposits. Beds may be entirely of pumice.

3. Coarse channels. Mafic gravels and large pumice clasts, very coarse sand matrix.

4. Thin bed of silts and clasts of reworked fine overbank deposits.

5. Interbedded coarse sand beds and gravels with coarse sand matrix.

6. Well sorted fine to medium sand. Horizontal laminations and local climbing ripples.

Clarke Carr

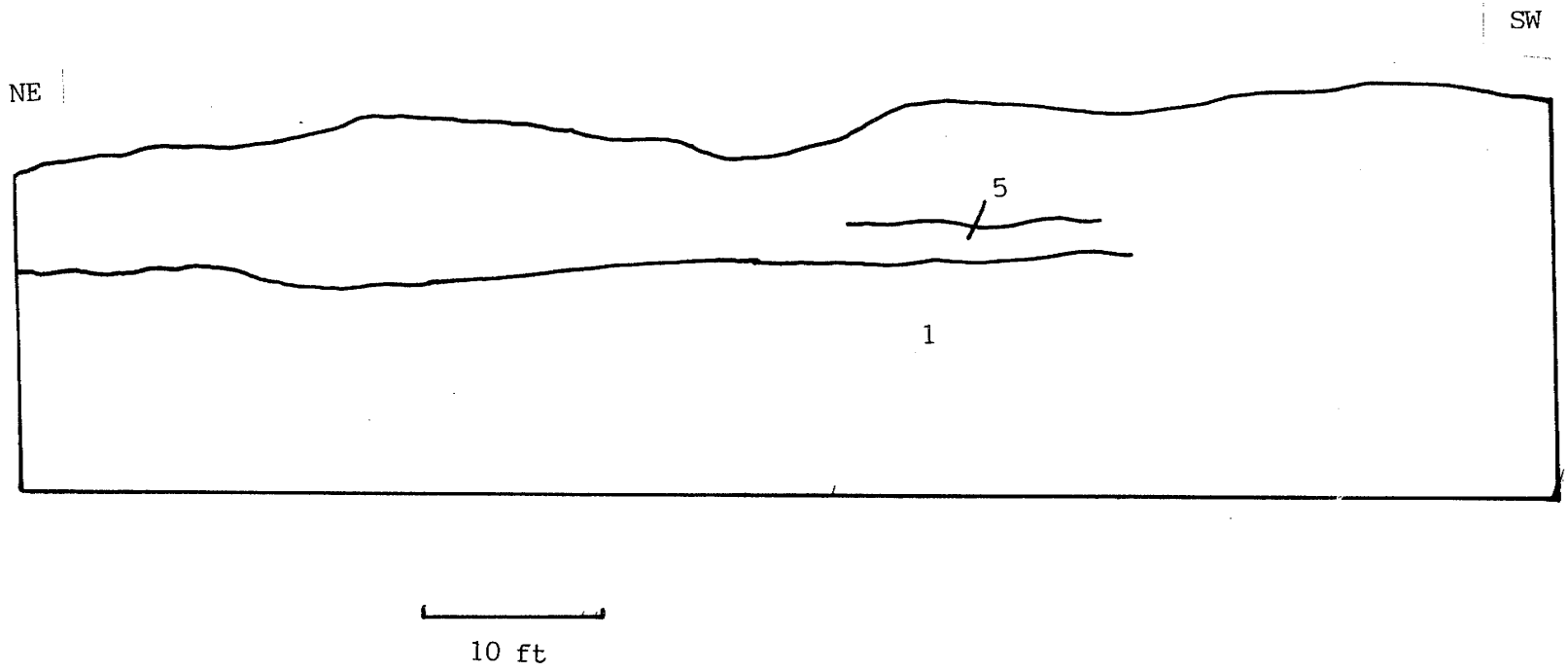

Rio Bravo upper (east)
1
2
3
4
5

Rio Bravo Upper

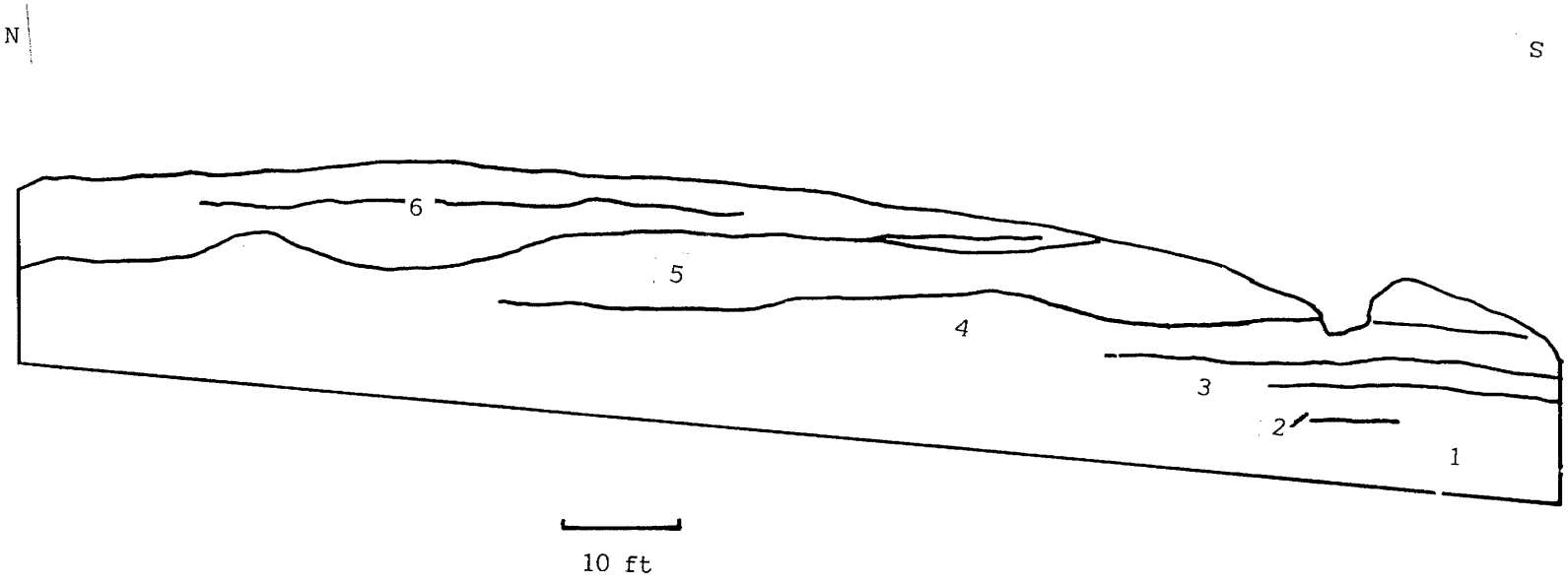

1. Same as lower Rio Bravo.

2. Same as lower Rio Bravo.

3. Same as lower Rio Bravo.

4. Same as lower Rio Bravo.

5. Fine sand, horizontal laminations to structureless. Cements are weak to moderate, locally well-developed concretions along bedding planes.

6. Horizontal beds and laminations, low angle crossbeds and foresets. Medium to coarse sands, local pebble and small gravel scours. Locally moderately to highly cemented.

Rio Bravo lower (west)

Rio Bravo Lower

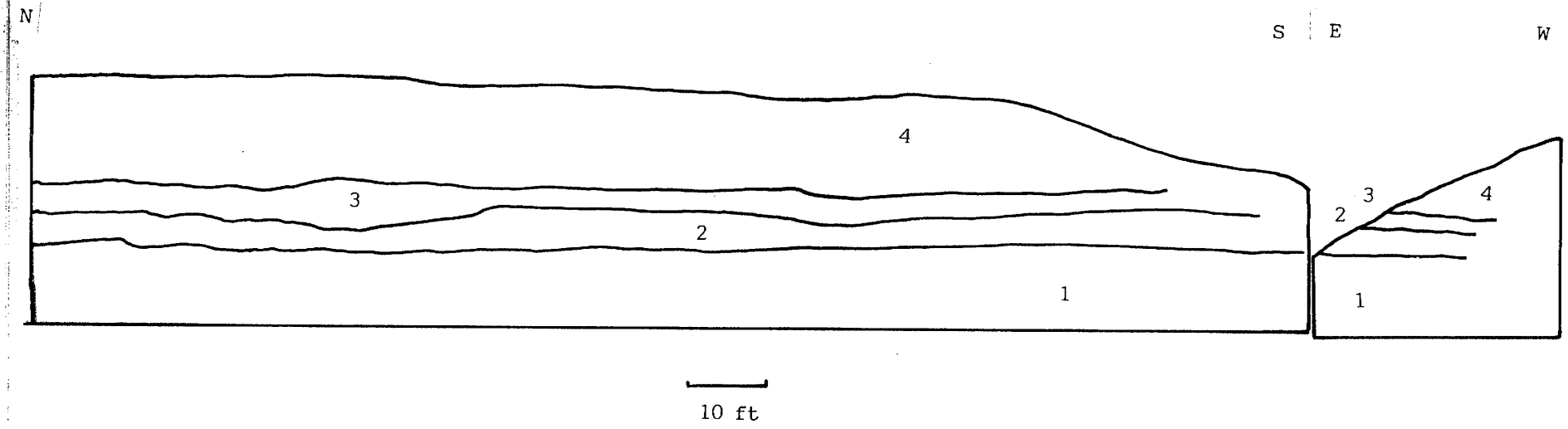

1. Crossbeds, horizontal beds, and low angle foresets. Fine to medium sand, moderate to poor sorting.

2. Horizontal beds and laminations. Medium to coarse sand, moderate sorting. Local thin gravel scours into bed 1.

3. Gravels with a coarse sand matrix. Large-scale foresets and horizontal bedding.

4. Horizontal laminations, low angle crossbeds and foresets. Medium to coarse sand with pebbles.

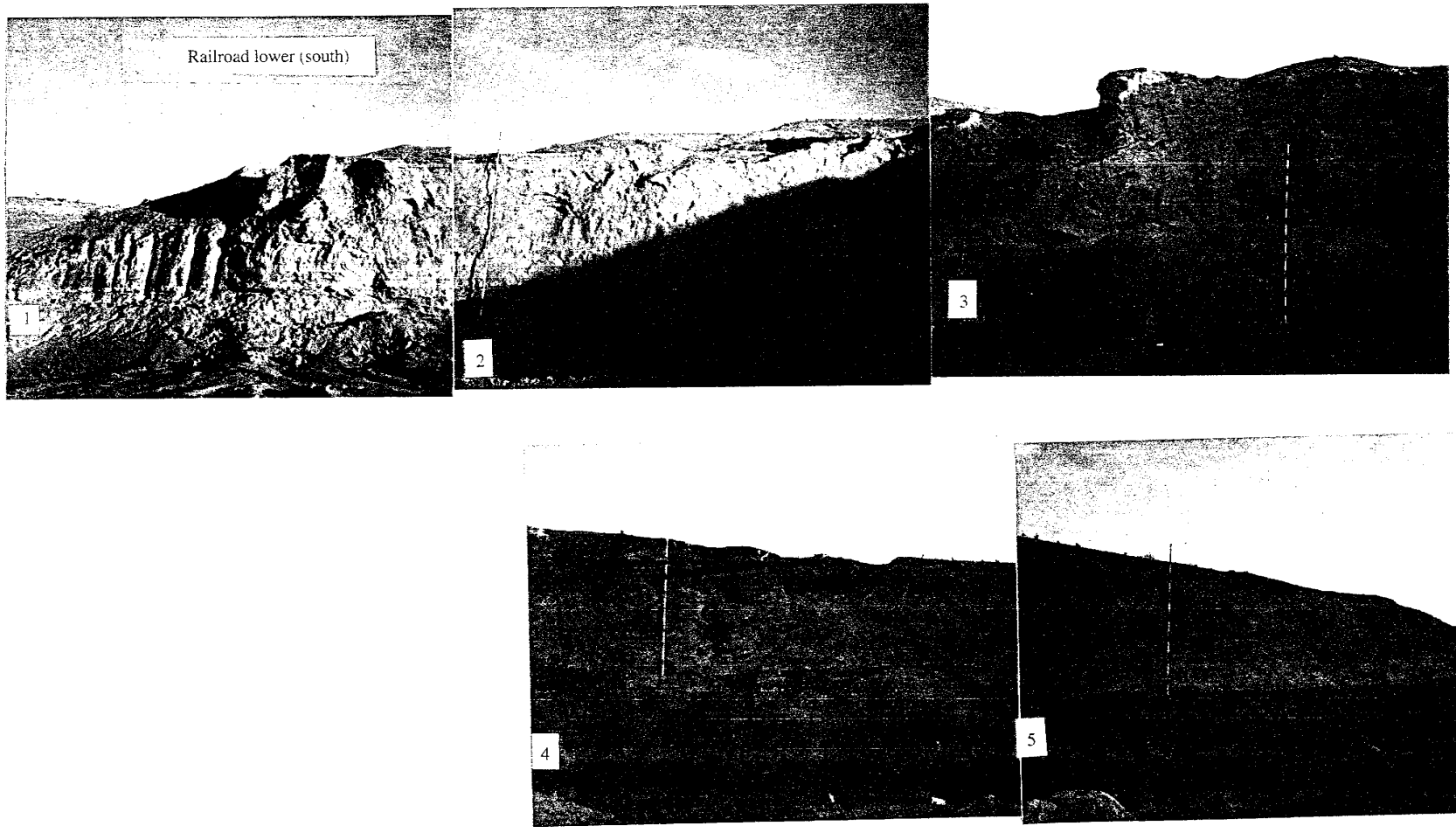
Railroad lower (south)
1
2
3
4
5
6

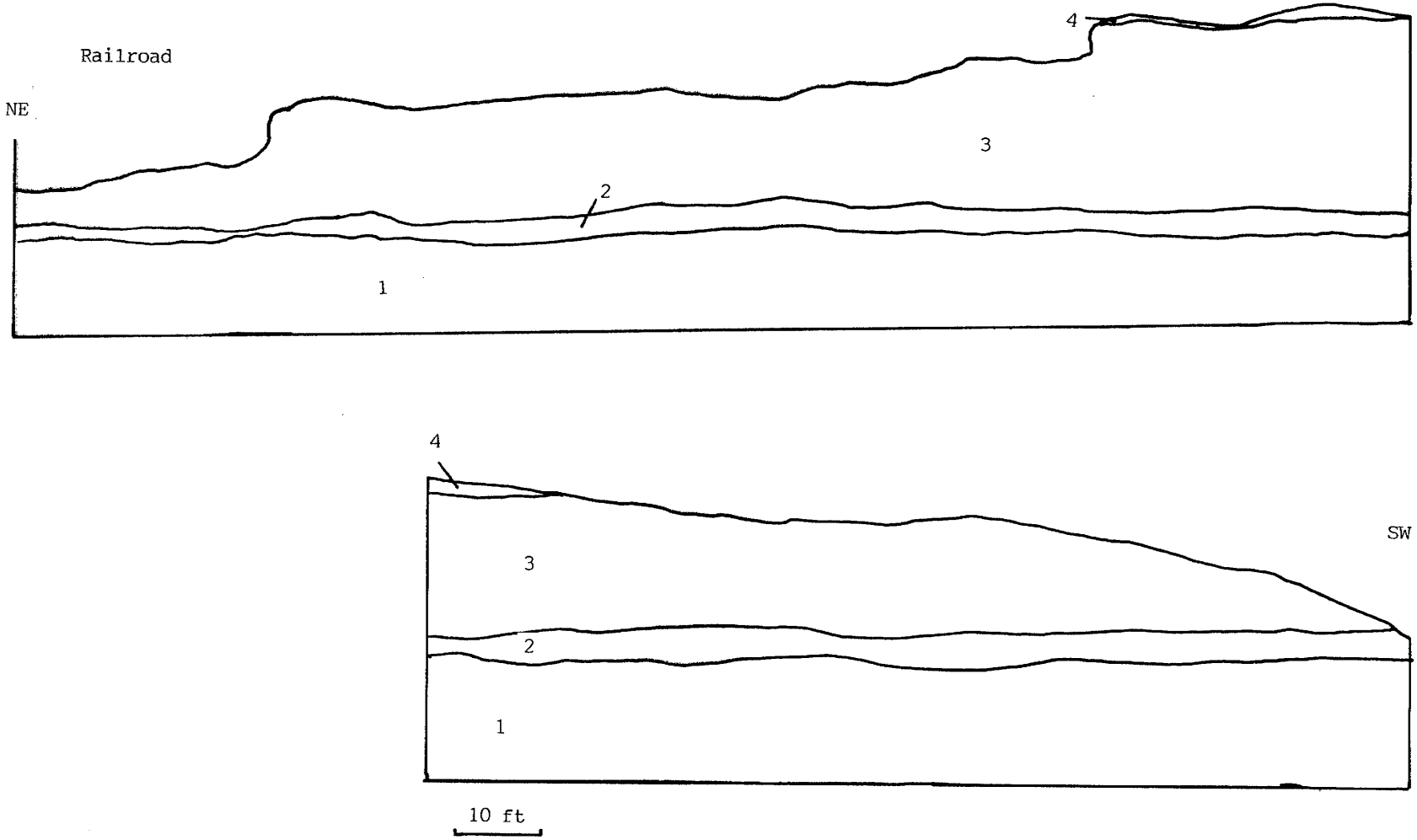

1. Clean river sands with gravel channels. Trough crossbeds and minor channels Medium to coarse sand, no fines.

2. Structureless and horizontally laminated fine to very fine sands. Bed is moderately cemented with well-developed laminar cements near the top. Laminar cements extend into overlying bed.

3. Well-sorted medium sand. Large-scale convoluted bedding. Possibly eolian in origin. Local dendritic cementation near top of beds.

4. Gravel beds/channels with coarse sand matrix. Exposure is limited, continuity undetermined.

Railroad upper (north)

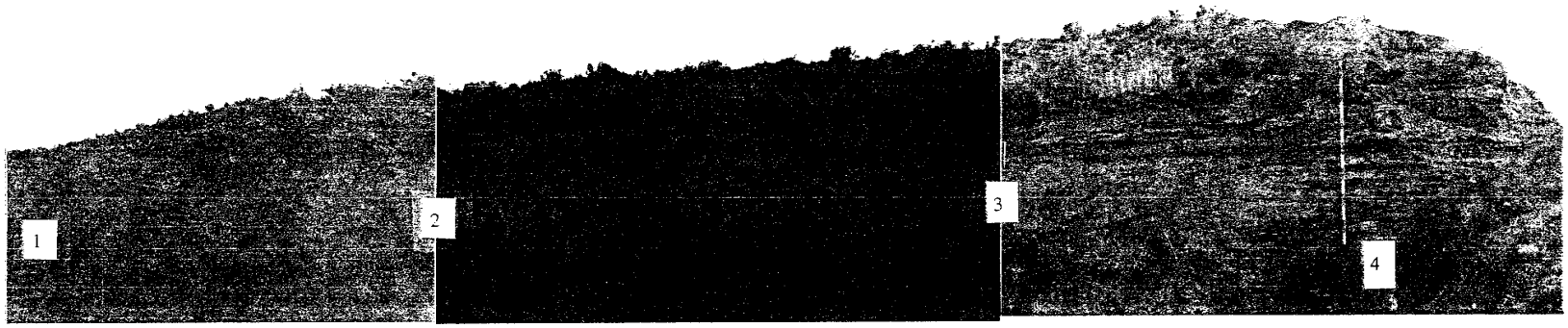

Bear Canyon

Bear Canyon

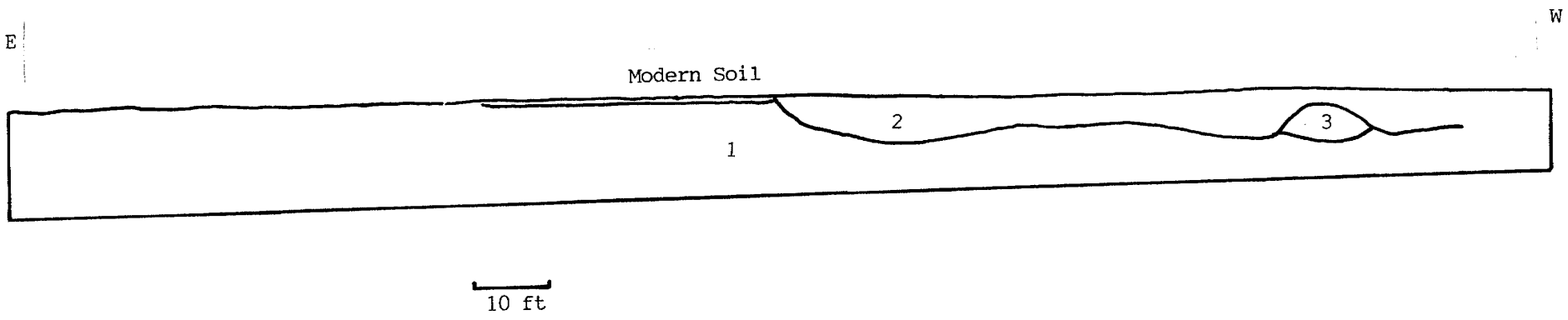

1. Horizontal beds, crude to well-defined, scour and fill structures common. Poorly sorted gravels and pebbles to very fine sand.

2. Channels. Well to poorly sorted granules and pebbles. Locally well sorted with open matrix. Scouring into lower beds.

3. Structureless paleosol. Medium sand to silt with 10 percent granules. Moderate cementation.

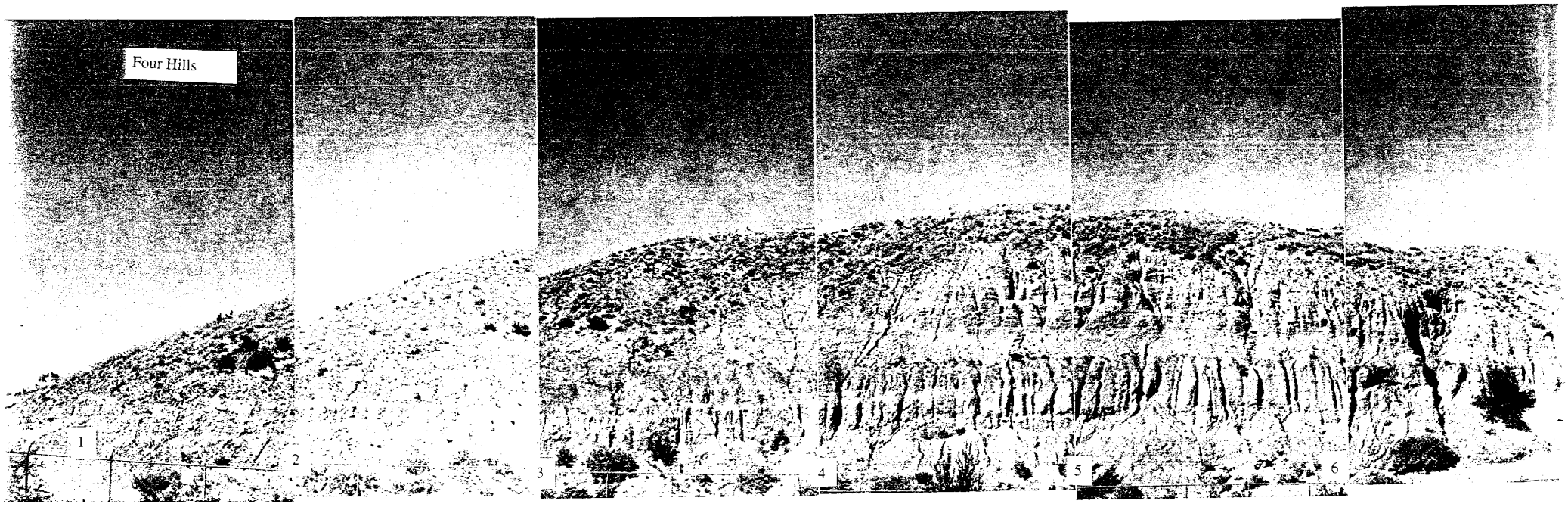
Four Hills
1
2
3
4
5
6

Four Hills

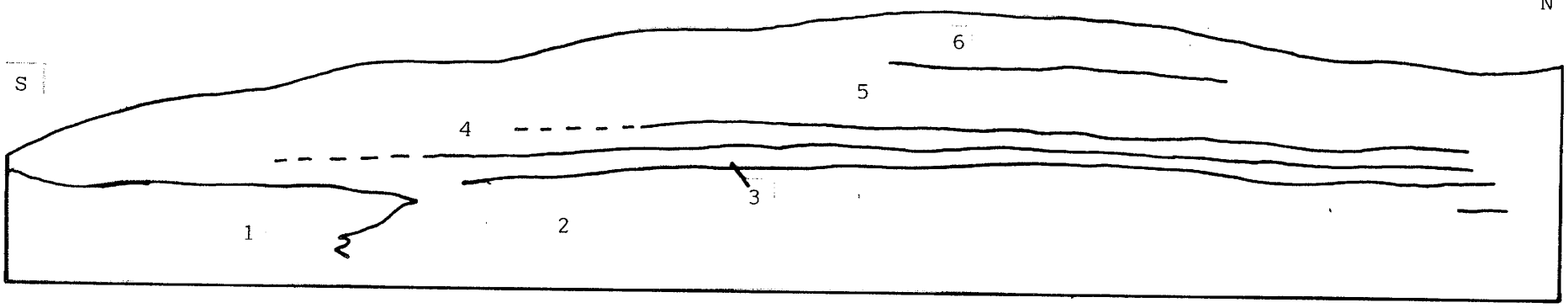

10 ft

1. Coarse channel deposits. Crude horizontal bedding within channel deposits. Poorly sorted with few fines, very coarse sand and gravel matrix.

2. Very fine sand and silt. Up to 10 percent very coarse sand and gravels in matrix. Structureless with few horizontal laminations.

3. Horizontal bedding to shallow scour and fill. Fine sand with granules and pebbles.

4. Coarse channels. Poorly sorted with medium sand matrix. Locally open matrix without fines.

5. Horizontal beds and shallow scour and fill structures. Fine to medium sand with granules, poorly sorted.

6. Coarse float. Interpreted as channel deposits.

Tijeras Arroyo

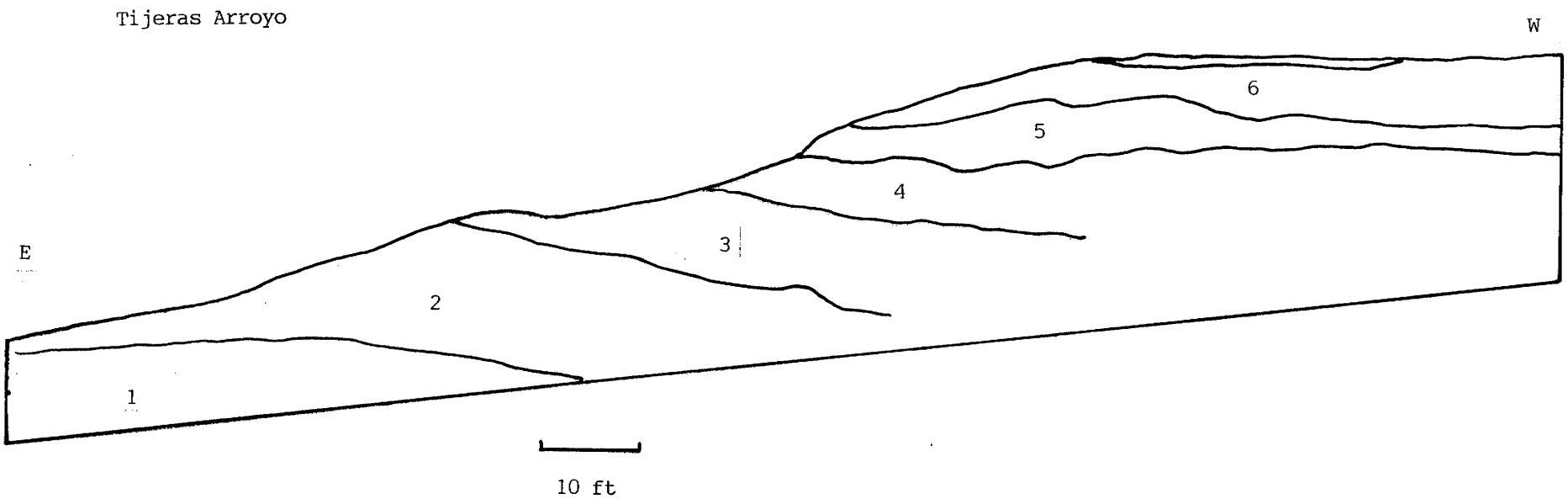

1. Interbedded silts and very fine sands. Structureless to weak local horizontal laminations.

2. Coarse channel sequence. Top and bottom of bed are coarse clasts up to 30 cm in diameter, open matrix. Poorly sorted fine sand to granules, forming crude horizontal beds located between larger channels.

3. Very fine sand and silt. Structureless with local horizontal laminations.

4. Coarse horizontal beds and scours. Local open matrix, but generally fine sand.

5. Very fine sand and silt. Structureless with local horizontal laminations.

6. Coarse channel poorly sorted. Very coarse sand matrix.

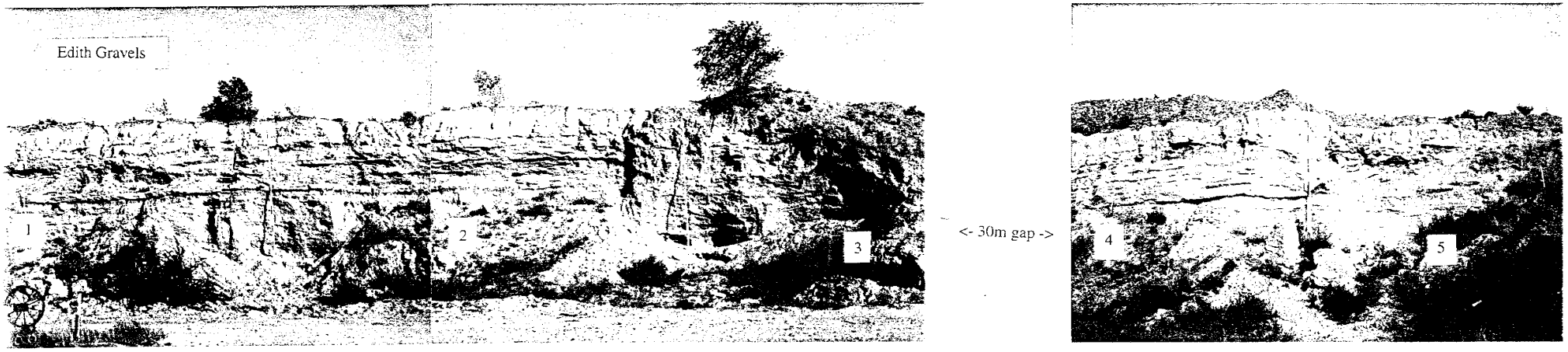
Edith Gravels
1
2
3
<- 30m gap ->
4
5

Edith Gravels

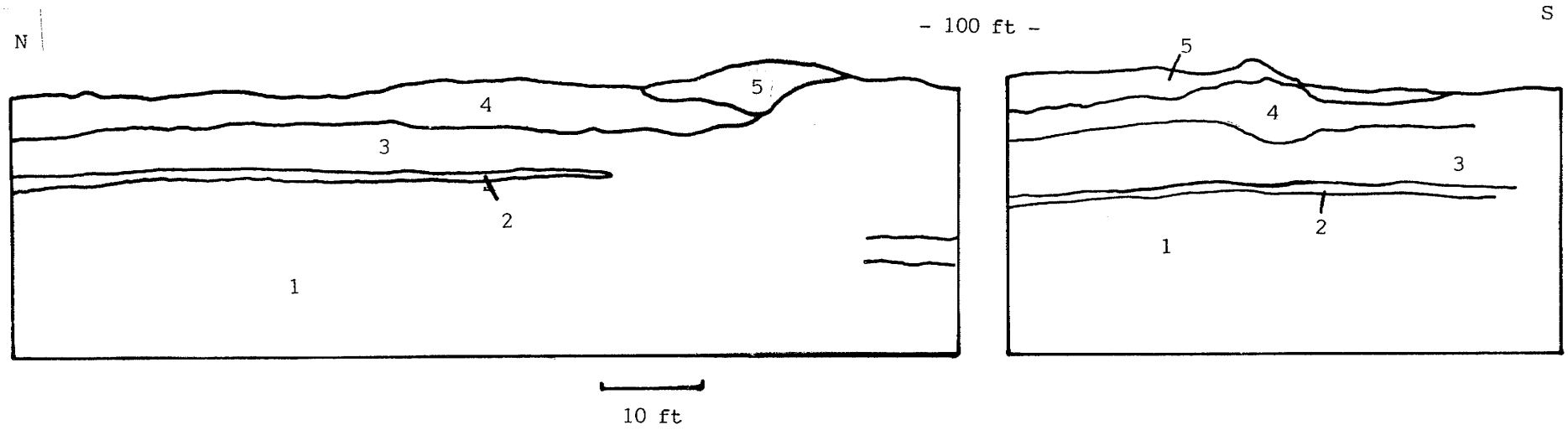

1. Trough crossbeds and small channels. Course to very coarse sand with a high percentage of pumice clasts.

2. Discontinuous bed of silts up to 1 foot thick.

3. Trough crossbeds, channels and foresets. Large-scale convoluted bedding Course sands with abundant pumice.

4. Structureless silts and very fine sand.

5. Gravels with a coarse sand matrix. Scours into underlying silts.

Outcrop permeability profile data

	CC	RB	RR	LD (sands)	EG	BC	FH	TA
Number of cases	74	116	496	20	134	68	211	91
Minimum	6.17	3.55	0.52	25.24	0.67	3.69	1.49	5.17
Maximum	223.07	271.68	223.07	137.13	223.07	223.07	271.68	271.68
Range	216.9	268.13	222.55	111.89	222.4	219.38	270.19	266.51
Mean	88.886	50.201	42.126	71.25	55.755	90.996	83.369	98.102
Variance	3198.071	1861.085	1640.732	885.427	2760.119	3996.929	8013.277	8100.613
Standard Deviation	56.551	43.14	40.506	29.756	52.537	63.221	89.517	90.003
Standard Error	6.574	4.005	1.819	6.654	4.538	7.667	6.163	9.435
Skewness	0.664	1.977	1.636	0.497	1.029	0.386	0.915	0.407
Kurtosis	-0.397	5.919	3.044	-0.348	0.776	-1.052	-0.5	-1.444
Sum	6577.54	5823.37	20894.54	1424.99	7471.23	6187.75	17590.9	8927.29
Coefficient of Varience	0.636	0.859	0.962	0.418	0.942	0.695	1.074	0.917
Median	74.67	42.59	32.86	66.9	49.42	90.94	37.63	67.89

Bear Canyon Permeability Profile Measurements

Location	Height (cm)	Time (sec.)	Darcys	Structure
BC1 left side, at plastic	0	0.84	189.82	SF
BC1	15	0.85	180.95	SF
BC1	30	2.47	24.99	SF
BC1	45	2.75	21.96	SF
BC1	60	0.99	111.17	SF
BC1	75	1.04	98.22	SF
BC1	90	1.31	61.47	SF
BC1	105	1.26	65.91	SF
BC1	120	1.13	81.56	SF
BC1	135	1.42	53.64	SF
BC1	150	1.03	100.55	SF
BC1	165	0.97	117.45	SF
BC1	180	1.04	98.22	SF
BC1	195	1.02	102.99	SF
BC1	210	1.45	51.86	SF
BC1	225	1.56	46.29	SF
BC2	0	0.83	199.67	SF
BC2	15	1.02	102.99	SF
BC2	30	1.08	89.98	SF
BC2	45	0.92	137.13	SF
BC2	60	0.85	180.95	SF
BC2	75	3	19.83	SF
BC2	90	0.99	111.17	SF
BC2	105	14.56	3.69	SL
BC2	120	1.94	33.99	SF
BC2	135	3.56	16.31	SF
BC2	150	3.74	15.44	SF
BC2	165	3.24	18.15	SF
BC2	180	5.89	9.43	SF
BC3	0	1.54	47.21	SF
BC3	15	1.16	77.27	SF
BC3	30	1.49	49.68	SF
BC3	45	1.31	61.47	SF
BC3	60	0.99	111.17	SF
BC3	75	0.83	199.67	SF
BC3	90	0.88	158.93	SF
BC3	105	1.03	100.55	SF
BC3	120	0.85	180.95	SF
BC3	135	0.96	120.88	SF
BC3	150	0.88	158.93	SF
BC3	165	0.88	158.93	CH
BC3	180	0.86	172.91	CH
BC3	195	1.12	83.11	SF
BC3	210	0.83	199.67	SF
BC3	225	1.07	91.90	SF
BC3	240	0.84	189.82	SF
BC3	255	1.07	91.90	SF
BC3	270	8.9	6.12	SF
BC3	285	2.1	30.63	SF
BC3	300	3.73	15.48	SF
BC4	0	1.06	93.91	SF
BC4	15	1.7	40.79	SF
BC4	30	0.91	141.96	SF
BC4	45	0.86	172.91	SF
BC4	60	1.59	44.98	SF

BC4	75	3.05	19.46	SF
BC4	90	2.85	21.06	SL
BC4	105	2.99	19.91	SL
BC4	120	2.26	27.90	SL
BC4	135	6.2	8.93	SL
BC4	150	6.41	8.62	SL
BC4	165	0.84	189.82	CH
BC4	180	0.81	223.07	CH
BC4	195	0.84	189.82	SF
BC4	210	1.67	41.85	SF
BC4	225	1.11	84.72	SF
BC4	240	0.99	111.17	SF
BC4	255	1.06	93.91	SF

Clarke Carr Permeability Profile Measurements

Location	Height (cm)	Time (sec.)	Darcys	Structure
CC1,180 cm rt. of stake 1	0	1.31	61.47	CB
CC1	15	1.27	64.97	CB
CC1	30	1.2	72.25	CB
CC1	45	1.74	39.46	CB
CC1	60	1.24	67.89	CB
CC1	75	0.88	158.93	CH
CC1	90	0.94	128.46	CH
CC1	105	1.18	74.67	CH
CC1	120	0.85	180.95	CH
CC1	135	0.88	158.93	CH
CC2	0	0.84	189.82	CB
CC2	15	8.82	6.17	SL
CC3	0	1.05	96.01	CB
CC3	15	1.33	59.87	CB
CC3	30	1.16	77.27	CB
CC3	45	1.34	59.10	CB
CC3	60	0.81	223.07	CH
CC3	75	0.81	223.07	CH
CC3	90	0.86	172.91	CH
CC3	105	0.89	152.81	CH
CC3	120	1.18	74.67	CB
CC3	135	0.91	141.96	CB
CC3	150	0.91	141.96	CB
CC3	165	unconsolidated.		CB
CC3	180	1.31	61.47	CB
CC3, 5 cm below sp. 21	195	1.11	84.72	CB
CC3	210-325	float, m-c sand.		CB
CC3	325	0.92	137.13	CB
CC3	340	0.89	152.81	CB
CC3	340-415	float, m-c sand.		CB
CC3, 5 cm below sp. 27	415	0.92	137.13	CB
CC3	430	0.81	223.07	CB
CC3	430-490	float, gravel .		CH
CC3	490-575	float, c-vc sanc.		CB
CC3	575-695	float, f. sand .		HL
CC4	0	0.9	147.17	CB
CC4	15	0.86	172.91	CB
CC4	30	1.78	38.22	CB
CC4	45	0.99	111.17	CB
CC4, 90 cm rt. of sp. 35	60	6.43	8.59	HL
CC4	75	1.74	39.46	HL
CC4	90	6.74	8.18	HL
CC5	0	1.2	72.25	CB
CC5	15	1.14	80.07	CB
CC5	30	0.84	189.82	CH
CC5	45	1.2	72.25	CB
CC5	60	1.13	81.56	CB
CC5	75	1.35	58.36	CB
CC5	80-165	too coarse .		CH
CC6	0	2.59	23.59	HL
CC6	15	1.75	39.14	HL
CC6	30	1.64	42.97	HL
CC6, at sp. 40	45	2.75	21.96	HL
CC6	60	1.07	91.90	HL
CC6	75	1.15	78.64	HL

CC6		90	0.85	180.95	HL
CC6		105	1.11	84.72	HL
CC6		120	0.99	111.17	HL
CC6		135	1.14	80.07	HL
CC6		150	1.05	96.01	HL
CC6		165	1	108.29	HL
CC6		180	0.94	128.46	HL
CC6		195	0.94	128.46	HL
CC6		210	1.27	64.97	HL
CC6		225	1.14	80.07	HL
CC6, 30 cm rt. of sp. 45		240	1.27	64.97	HL
CC6	245-320	too coarse	.		CH
CC6		320	1.2	72.25	CB
CC6		335	0.99	111.17	CB
CC6		350	1.21	71.11	CB
CC6	360-480	float	.		CH
CC7		0	1.59	44.98	CB
CC7		15	1.52	48.16	CB
CC7		30	1.77	38.53	CB
CC7		45	2.45	25.24	CB
CC7		60	2.68	22.65	CB
CC7		75	2.5	24.63	CB
CC7		90	1.25	66.89	CB
CC7		105	2.6	23.48	HL
CC7		120	1.63	43.35	HL
CC7	130-165	float	.		
CC7		165	2.99	19.91	CB
CC7		180	3.04	19.53	CB
CC7		195	3.56	16.31	CB
CC7	200-425	float	.		CH

Edith Gravels Permeability Profile Measurements

Location	Height (cm)	Time (sec.)	Darcys	Structure
EG1 left, between stakes	0	1.06	93.91	CB
EG1	15	0.94	128.46	CB
EG1	30	1	108.29	CB
EG1	45	0.87	165.61	CB
EG1	60	1.55	46.74	CB
EG1	75	1.34	59.10	CB
EG1	90	1.07	91.90	CB
EG1	105	1.02	102.99	CB
EG1	120	1.17	75.95	CB
EG1	135	1.02	102.99	CB
EG1	150	1.41	54.27	CB
EG1	165	1.17	75.95	CB
EG1	180	1.35	58.36	CB
EG1	195	1.87	35.71	CB
EG1	210	1.12	83.11	CB
EG1	225	1.14	80.07	CB
EG1	240	0.9	147.17	CB
EG1	255	1.78	38.22	CB
EG1	270	1.06	93.91	CB
EG1	285	42.84	1.24	SL
EG1	300	78.54	0.67	SL
EG1	315	1.83	36.78	CB
EG1	330	1.44	52.44	CB
EG1	345	0.99	111.17	CB
EG1	360	1.06	93.91	CB
EG1	375	0.89	152.81	CB
EG1	390	1.16	77.27	CB
EG1	405	1.59	44.98	CB
EG1	420	1.95	33.75	CB
EG1	435	1.09	88.15	CB
EG1	450	2.32	27.00	CB
EG1	465	1.34	59.10	CB
EG1	480	1.49	49.68	CB
EG1	495	2.2	28.86	CB
EG1	510	1.3	62.31	CB
EG1	525	7.62	7.19	SL
EG1	540	18.32	2.92	SL
EG1	555	14.87	3.61	SL
EG1	570	11.93	4.52	SL
EG1	585	29.5	1.80	SL
EG1	600	16.29	3.29	SL
EG1	615	32.93	1.61	SL
EG2	0	1.06	93.91	CB
EG2	15	1.01	105.57	CB
EG2	30	1.18	74.67	CB
EG2	45	1.09	88.15	CB
EG2	60	1.74	39.46	CB
EG2	75	1.86	35.97	CB
EG2	90	0.89	152.81	CH
EG2	105	0.83	199.67	CB
EG2	120	1.27	64.97	CB
EG2	135	0.89	152.81	CB
EG2	150	0.9	147.17	CB
EG2	165	1.09	88.15	CB
EG2	180	0.98	114.21	CB

EG2	195	1.09	88.15	CB
EG2	210	1.29	63.17	CB
EG2	225	1.5	49.16	CB
EG2	240	1.91	34.71	CB
EG2	255	1.21	71.11	CB
EG2	270	1.44	52.44	CB
EG2	285	1.85	36.24	CB
EG2	300	3.56	16.31	CB
EG2	315	63.94	0.83	SL
EG2	330	72.79	0.73	SL
EG2	345	1.27	64.97	CB
EG2	360	1.29	63.17	CB
EG2	375	1.24	67.89	CB
EG2	390	1.08	89.98	CB
EG2	405	2.59	23.59	CB
EG2	420	1.04	98.22	CB
EG2	435	1.49	49.68	CB
EG2	450	1.01	105.57	CB
EG2	465	1.09	88.15	CB
EG2	480	1.41	54.27	CB
EG2	495	2.69	22.55	CB
EG2	510	1.21	71.11	CB
EG2	525	57.4	0.92	SL
EG2	540	11.97	4.51	SL
EG2	555	10.46	5.18	SL
EG2	570	20.09	2.66	SL
EG2	585	10.73	5.04	SL
EG2	600	51.66	1.02	SL
EG2	615	27.32	1.95	SL
EG2	630	18.61	2.87	SL
EG3	0	1.28	64.06	CB
EG3	15	3.81	15.12	CB
EG3	30	too tight		HL
EG3	45	12.54	4.30	HL
EG3	60	24.69	2.16	HL
EG3	75	22.91	2.33	HL
EG3	90	28.46	1.87	HL
EG3	105	58.53	0.90	HL
EG3	120	1.35	58.36	CB
EG3	135	27.41	1.94	HL
EG3	150	1.21	71.11	CB
EG3	165	71.65	0.74	HL
EG3	180	22.84	2.33	HL
EG3	195	1.53	47.68	CB
EG3	210	1.57	45.84	CB
EG3	225	2.69	22.55	CB
EG3	240	3.49	16.68	CB
EG3	255	13.56	3.97	SL
EG3	270	16.05	3.34	SL
EG3	285	13.12	4.10	SL
EG3	300	29.19	1.82	SL
EG3	315	54.2	0.98	SL
EG4, 3m left of stake	0	1.3	62.31	CB
EG4	15	0.81	223.07	CB
EG4	30	1.03	100.55	CB
EG4	45	0.97	117.45	CB
EG4	60	1.46	51.30	CB
EG4	75	3.63	15.96	CB

EG4	90	6.05	9.16	CB
EG4	105	33.09	1.60	SL
EG4	120	1.1	86.40	CB
EG4	135	0.82	210.68	CB
EG4	150	0.88	158.93	CB
EG4	165	0.91	141.96	CB
EG4	180	0.81	223.07	CB
EG4	195	0.99	111.17	CB
EG4	210	8.89	6.12	CB
EG4	225	0.93	132.64	CB
EG4	240	1.28	64.06	CB
EG4	255	1.81	37.35	CB
EG4	270	1.46	51.30	CB
EG4	285	2.24	28.21	CB
EG4	300	1.53	47.68	CB
EG4	315	4.22	13.51	CB
EG4	330	20.85	2.56	SL
EG4	345	24.29	2.19	SL
EG4	360	25.59	2.08	SL
EG4	375	12.27	4.39	SL
EG4	390	11.22	4.82	SL
EG4	405	7.72	7.09	SL

Four Hills Permeability Profile Measurements

Location	Height (cm)	Time (sec.)	Darcys	Structure
FH1, 15 m from south side	0	0.78	271.68	CH
FH1	15	0.81	223.07	CH
FH1	30	0.85	180.95	CH
FH1	45	0.84	189.82	CH
FH1	60	too coarse	.	CH
FH1	75	0.82	210.68	CH
FH1	90	too coarse	.	CH
FH2	0	1	108.29	SF
FH2	15	0.79	253.15	SF
FH2	30	1.05	96.01	SF
FH2	45	0.77	293.32	SF
FH2	60	1.34	59.10	SF
FH2	75	too coarse	.	SF
FH2	90	0.78	271.68	SF
FH2	105	0.8	237.10	SF
FH2	120	0.85	180.95	SF
FH2	135	float	.	SF
FH2	150	float	.	SF
FH2	165	0.81	223.07	CH
FH2	180	0.81	223.07	CH
FH3	0	15.35	3.49	SL
FH3	15	22.39	2.38	SL
FH3	30	35.59	1.49	SL
FH3	45	22.08	2.42	SL
FH3	60	3.26	18.02	SL
FH3	75	6.91	7.96	SL
FH3	90	10.69	5.06	SL
FH3	105	13.74	3.91	SL
FH3	120	18.6	2.87	SL
FH3	135	8.76	6.22	SL
FH3	150	3.87	14.86	SL
FH3	165	12.12	4.45	SL
FH3	180	8.79	6.20	SL
FH3	195	11.47	4.71	SL
FH3	210	8.18	6.68	SL
FH3	225	9.68	5.61	SL
FH3	240	14.97	3.58	SL
FH3	255	10.37	5.22	SL
FH3	270	2.1	30.63	SF
FH3	285	5.33	10.49	SL
FH3	300	6.22	8.90	SL
FH3	315	3.66	15.81	SL
FH3	330	5.04	11.14	SL
FH3	345	8.69	6.27	SL
FH3	360	7.15	7.68	SL
FH3	375	2.61	23.38	HL
FH3	390	4.56	12.41	HL
FH3	405	2.05	31.60	HL
FH3	420	0.87	165.61	SF
FH3	240 cm	float	.	SF
FH3	660	0.89	152.81	SF
FH3	675	0.81	223.07	SF
FH3	690	0.81	223.07	SF
FH3	705	1.02	102.99	SF
FH3	720	1.65	42.59	SF

FH3	735	1.31	61.47	SF
FH3	750	29.99	1.77	SL
FH3	765	2.95	20.22	SL
FH3	780	0.78	271.68	SF
FH3	795	4.77	11.82	SL
FH3	810	1.03	100.55	SF
FH3	825	1.02	102.99	SF
FH3	840	1.24	67.89	SF
FH3	855	1.29	63.17	SF
FH3	870	1.91	34.71	SF
FH3	105 cm float			SF
FH3	975	0.94	128.46	SF
FH3	990	1.06	93.91	SF
FH3	1005	0.87	165.61	SF
FH3	1020	1.06	93.91	SF
FH3	1035	1.1	86.40	SF
FH3	1050	2.03	32.01	SF
FH3 1.5m rt., .6m below sp	1065	2.34	26.71	SF
FH4	0	5.04	11.14	SL
FH4	15	4.7	12.01	SL
FH4	30	7.88	6.94	SL
FH4	45	10.02	5.41	SL
FH4	60	7.37	7.44	SL
FH4	75	9.95	5.45	SL
FH4	90	8.63	6.32	SL
FH4	105	10.87	4.98	SL
FH4	120	8.2	6.66	SL
FH4	135	5.38	10.38	SL
FH4	150	7.69	7.12	SL
FH4	165	5.81	9.57	SL
FH4	180	5.91	9.39	SL
FH4	195	7.31	7.51	SL
FH4	210	6.4	8.63	SL
FH4	225	5.28	10.59	SL
FH4	240	5	11.23	SL
FH4	255	7.31	7.51	SL
FH4	270	7.52	7.29	SL
FH4	285	6.31	8.76	SL
FH4	300	5.15	10.88	SL
FH4	315	5.66	9.84	SL
2.1m left, 45cm below sp.20	330	5.25	10.66	SL
FH4	120 cm float			SF
FH4	450	0.78	271.68	SF
FH4	465	0.81	223.07	SF
FH4	480	0.77	293.32	SF
FH4	495	0.77	293.32	SF
FH4	510	1.25	66.89	SF
FH4	525	0.85	180.95	SF
FH4	540	0.84	189.82	SF
FH4	555	0.88	158.93	SF
FH4	570	1.09	88.15	SF
FH4	585	0.86	172.91	SF
FH4	600	0.86	172.91	SF
FH4	615	0.98	114.21	SF
FH4	630	0.92	137.13	SF
FH4	645	0.78	271.68	SF
FH4	660	0.77	293.32	SF
FH4 sp. 23	675	0.81	223.07	SF

FH4	690	0.81	223.07	SF
FH4	705	0.84	189.82	SF
FH4	720	2.65	22.95	SF
FH4	735	3.63	15.96	SF
FH4	750	1.49	49.68	SF
FH4	765	0.99	111.17	SF
FH4	780	1.59	44.98	SF
FH4	795	1.14	80.07	SF
FH4	810	1.03	100.55	SF
FH4	825	1.31	61.47	SF
FH4	840	0.96	120.88	SF
FH4	855	1.45	51.86	SF
FH4	870	0.98	114.21	SF
FH4	885	1.06	93.91	SF
FH4	900	1.11	84.72	SF
FH4	915	1.1	86.40	SF
FH4	930	0.77	293.32	SF
FH4	945	0.79	253.15	SF
FH4	960	0.84	189.82	SF
FH4	975	0.99	111.17	SF
FH4	990	0.85	180.95	SF
FH4	1005	1.09	88.15	SF
FH5	0	4.31	13.20	SL
FH5	15	10.51	5.15	SL
FH5	30	10.15	5.34	SL
FH5	45	10.32	5.25	SL
FH5	60	8.12	6.73	SL
FH5	75	10.16	5.33	SL
FH5	90	4.39	12.93	SL
FH5	105	9.88	5.49	SL
FH5	120	8.58	6.35	SL
FH5	135	2.04	31.80	SF
FH5	150	5.09	11.02	SF
FH5	165	7.08	7.76	SL
FH5	180	5.59	9.97	SL
FH5	195	4.75	11.87	SL
FH5	210	4.08	14.02	SL
FH5	225	1.85	36.24	SL
FH5	240	5.16	10.86	SL
FH5	255	1.88	35.46	SF
FH5	270	1.59	44.98	SF
FH5	285	4.78	11.79	SL
FH5	300	6.45	8.56	SL
FH5	315	1.94	33.99	SL
FH5	330	7.38	7.43	SL
FH5	345	4.83	11.66	SL
FH5	360	7.26	7.56	SL
FH5	375	3.86	14.90	SL
FH5	390	4.92	11.43	SL
FH5	405	7.8	7.02	SL
FH5	420	2.26	27.90	SL
FH5	435	3.1	19.09	SL
FH5	450	1.52	48.16	SF
FH5	465	0.91	141.96	SF
FH5	480	0.91	141.96	SF
FH5	495	0.84	189.82	SF
FH5	510	0.9	147.17	SF
FH5	525	1.04	98.22	SF

FH5	540	0.81	223.07	SF
FH5	555	0.9	147.17	SF
FH5 2.4m rt. of sp. ___	570	0.78	271.68	SF
FH5	585	too coarse	.	CH
FH5	600	too coarse	.	CH
FH5	615	too coarse	.	CH
FH5	630	1.2	72.25	SF
FH5	645	0.84	189.82	SF
FH5	660	0.95	124.55	SF
FH5	675	0.81	223.07	SF
FH5	690	1.13	81.56	SF
FH5	705	1.2	72.25	SF
FH5	720	1.12	83.11	SF
FH5	735	0.78	271.68	SF
FH5	750	0.93	132.64	SF
FH5	765	0.79	253.15	SF
FH5	780	0.86	172.91	SF
FH5	795	1.02	102.99	SF
FH5	810	0.93	132.64	SF
FH5	825	0.79	253.15	SF
FH5	840	1.2	72.25	SF
FH5	855	1.8	37.63	SF
FH5	870	1.65	42.59	SF
FH5	885	0.81	223.07	SF
FH5	900	1.06	93.91	SF
FH5	915	1.18	74.67	SF
FH5	930	2.29	27.44	SF
FH5	945	2.07	31.20	SF
FH5	960	0.97	117.45	SF
FH6	0	3.85	14.95	SL
FH6	15	6.33	8.74	SL
FH6	30	9.57	5.67	SL
FH6	45	7.33	7.49	SL
FH6	60	7.77	7.04	SL
FH6	75	6.6	8.36	SL
FH6	90	9.16	5.94	SL
FH6	105	9.85	5.51	SL
FH6	120	1.44	52.44	SF
FH6	135	10.38	5.22	SL
FH6	150	7.45	7.36	SL
FH6	165	4.23	13.47	SL
FH6	180	7.09	7.75	SL
FH6	195	4.92	11.43	SL
FH6	210	6.31	8.76	SL
FH6	225	2.58	23.70	HL
FH6	240	0.84	189.82	SF
FH6	255	float	.	SF
FH6	270	float	.	SF
FH6	285	0.84	189.82	SF
FH6	300	0.8	237.10	SF
FH6	315	0.78	271.68	SF
FH6	330	too coarse	.	CH
FH6	345	too coarse	.	CH
FH6	360	0.87	165.61	SF
FH6	375	0.93	132.64	SF

Los Duranes Permeability Profile Measurements

	Time	Darcys
sands	1.57	45.84
	1.51	48.66
	1.08	89.98
	2.45	25.24
	1.19	73.44
	1.08	89.98
	1.18	74.67
	1.27	64.97
	1.44	52.44
	1.02	102.99
	0.92	137.13
	2.34	26.71
	1.57	45.84
	1.01	105.57
	1.53	47.68
	1.34	59.10
	1.26	65.91
	0.96	120.88
	1.24	67.89
	1.14	80.07
silts	18.86	2.83
	12.17	4.43
	30.18	1.76
	23.6	2.26
	52.35	1.01
	67.52	0.78
	59.65	0.89
	10.87	4.98
	15.77	3.40

Rio Bravo Permeability Profile Measurements

Location	Height (cm)	Time (sec.)	Darcys	Structure
RB1	0	0.87	165.608492	HL
RB1	15	1.51	48.6563462	HL
RB1	30	1.78	38.2229912	HL
RB1	45	1.39	55.56121	HL
RB1	60	1.47	50.7460481	HL
RB1	75	0.96	120.884461	HL
RB1	90	1.15	78.6446521	HL
RB1	105	2.28	27.5884587	CB
RB1	120	1.1	86.396668	CB
RB2	0	1.66	42.2145617	HB
RB2	15	2.72	22.2514525	HB
RB2	30	1.81	37.3460005	HB
RB2	45	1.53	47.678635	HB
RB2	60	1.22	69.9984575	HB
RB2	75	0.98	114.213647	HB
RB2	90	1.43	53.0370843	HB
RB2	105	1.78	38.2229912	HB
RB2	120	1.8	37.6335884	CB
RB2	135	0.91	141.959431	CB
RB2	150	too coarse	.	CB
RB2	165	1.64	42.9674784	CB
RB3	0	1.31	61.4738203	HL
RB3	15	1.38	56.2330386	CH
RB3	30	1.49	49.6777812	HL
RB3	45	1.58	45.4076369	HL
RB3 1.2m rt. of sp3	60	3.62	16.0088892	HL
RB3	75	1.37	56.9225138	HL
RB3	90	1.23	68.9268511	HL
RB3	105	1.26	65.9137192	CB
RB3	120	1.05	96.0140172	CB
RB3	135	1.15	78.6446521	CB
RB3	150	0.92	137.130067	CB
RB3	165	1.32	60.6616058	CB
RB3	180	1.43	53.0370843	CB
RB3	195	too coarse	.	CB
RB3	210	0.78	271.680365	CB
RB4 corner of lower outcrop	0	1.49	49.6777812	HL
RB4	15	1.55	46.7418126	HL
RB4	30	2.88	20.8002227	HL
RB4	45	1.84	36.5103091	HL
RB4	60	1.77	38.5250505	HL
RB4	75	1.75	39.1445287	HL
RB4	90	3.69	15.6692344	HL
RB4	105	1.41	54.2677678	HL
RB4	120	1.89	35.2014229	HL
RB4	135	1.5	49.1614107	CH
RB4	150	1.05	96.0140172	HL
RB4	165	1.07	91.900949	HL
RB4	180	1.33	59.8720938	HL
RB4	195	1	108.289727	HL
RB4 sp. 9	210	0.87	165.608492	HL
RB4	225	1.41	54.2677678	HL
RB4	240	1.16	77.2702017	HL
RB4	255	1.59	44.9806861	HL
RB4	270	0.91	141.959431	HL

RB4 5cm up, 50cm rt.of sp8	285	too coarse	.	CH
RB5 north end,upper outcrop	0	8.38	6.51112626	CB
RB5	15	14.74	3.64203333	CB
RB5	30	10.25	5.28572869	CB
RB5	45	15.1	3.5534821	CB
RB5	60	9.52	5.7046985	CB
RB5	75	8.88	6.13091766	CB
RB5	90	5.16	10.8581836	HL
RB5	105	1.05	96.0140172	HL
RB5	120	1.85	36.2404075	HL
RB5	135	1.99	32.8576641	HL
RB5	150	4.34	13.0969351	HL
RB5	165	2.06	31.4017798	HL
RB5	180	1.91	34.7050016	HL
RB5	195	3.34	17.5319802	HL
RB5	210	3.06	19.3830035	HL
RB5 25 cm rt. of sp.37	225	0.84	189.817552	CH
RB5	240	1.88	35.4552662	CB
RB5	255	1.11	84.7163436	CB
RB5	270	1.16	77.2702017	CB
RB5	285	1.09	88.1507282	CB
RB5	300	1.75	39.1445287	CB
RB5	315	2.69	22.5470629	CB
RB5	330	2.38	26.1547227	CB
RB5	345	1.34	59.1043163	CB
RB6	0	1.52	48.1622083	HL
RB6	15	2.37	26.2911223	HL
RB6	30	2.23	28.3683377	HL
RB6	45	1.34	59.1043163	HL
RB6	60	5.34	10.4662796	HL
RB6	75	8.51	6.40779256	HL
RB6	90	7.62	7.18917584	HL
RB6	105	8.85	6.15246971	HL
RB6	120	10.81	5.00389682	HL
RB6	135	10.86	4.98019084	HL
RB6	150	11.59	4.65805128	HL
RB6	165	8.57	6.36120189	HL
RB6	180	6.97	7.8926946	HL
RB6	195	12.37	4.35699285	HL
RB6	210	9.34	5.81844643	HL
RB6	225	10.69	5.06172459	HL
RB6	240	2.89	20.7159356	CB
RB6	255	4.14	13.7924355	CB
RB6	270	4.01	14.2861214	CB
RB6	285	7.47	7.34011212	CB
RB6	300	5.58	9.98604012	CB
RB7	0	1.33	59.8720938	CB
RB7	15	2.23	28.3683377	CB
RB7	30	2.45	25.2394091	CB
RB7	45	1.34	59.1043163	CB
RB7	60	1.35	58.3573605	CB
RB7 sp. 20	75	1.47	50.7460481	CB
RB7	90	1.49	49.6777812	HL
RB7	105	1.52	48.1622083	HL
RB7	120	1.48	50.2058548	HL
RB7	135	1.38	56.2330386	HL
RB7	150	1.04	98.2239489	HL
RB7 sp. 24	165	3.13	18.8837593	HL

RB7	180	1.92	34.4622532	OB
RB7	195	2.12	30.2567757	OB
RB7 30 cm above sp. 23	210	1.85	36.2404075	OB
RB7	225	1.69	41.1360684	HL
RB7	240	1.21	71.1066327	HL
RB7	255	1.05	96.0140172	HL

Railroad Permeability Profile Measurements

Location	Height (cm)	Time (sec.)	Darcys	Structure
RR1	0	1.85	36.24	CB
RR1	15	1.06	93.91	CB
RR1	30	1.53	47.68	CB
RR1	45	3.26	18.02	CB
RR1	60	5.24	10.68	CB
RR1	75	8.18	6.68	CB
RR1	90	1.56	46.29	CB
RR1	105	1.15	78.64	CB
RR1	120	1.27	64.97	CB
RR1	135	4.25	13.40	CB
RR1	150	14.31	3.75	CB
RR1	165	14.77	3.63	CB
RR1	180	1.29	63.17	CB
RR1	195	1.34	59.10	CB
RR1	210	2.84	21.14	CB
RR1	225	4.55	12.44	CB
RR1	240	23.12	2.31	CB
RR1	255	1.36	57.63	CB
RR1	270	1.28	64.06	CB
RR1	285	3.24	18.15	CB
RR1	300	6.13	9.04	CB
RR1	315	21.46	2.49	CB
RR1	330	1.04	98.22	CB
RR1	345	1.45	51.86	CB
RR1	360	1.87	35.71	CB
RR1	375	6.97	7.89	CB
RR1	390	3.74	15.44	CB
RR1	405	1.81	37.35	CB
RR1	420	1.51	48.66	CB
RR1	435	2.52	24.39	CB
RR1	450	4.67	12.09	CB
RR1	465	14.94	3.59	CB
RR1	480	1.13	81.56	CB
RR1	495	1.34	59.10	CB
RR1	510	4.1	13.94	CB
RR1	525	3.1	19.09	CB
RR1	540	13.7	3.92	CB
RR1	555	1.36	57.63	CB
RR1	570	1.65	42.59	CB
RR1	585	2.51	24.51	CB
RR1	600	3.09	19.17	CB
RR1	615	9.56	5.68	CB
RR1	630	37.81	1.40	HL
RR1	645	73.02	0.72	HL
RR1	660	102.49	0.52	HL
RR1	675	33.2	1.60	HL
RR1	690	39.95	1.33	HL
RR1	705	30.9	1.72	HL
RR1	720	24.08	2.21	HL
RR1	735	16.52	3.24	HL
RR1	750	2.07	31.20	Con sand
RR1	765	1.99	32.86	Con sand
RR1	780	2.59	23.59	Con sand
RR1	795	1.59	44.98	Con sand
RR1	810	2.65	22.95	Con sand

RR1	825	2.74	22.06	Con sand
RR1	840	2.38	26.15	Con sand
RR1	855	2.94	20.30	Con sand
RR1	870	3.54	16.42	Con sand
RR1	885	2.28	27.59	Con sand
RR1	900	2.39	26.02	Con sand
RR2	0	1.52	48.16	CB
RR2	15	2	32.64	CB
RR2	30	55.13	0.96	CB
RR2	45	33.36	1.59	CB
RR2	60	1.84	36.51	CB
RR2	75	2.3	27.29	CB
RR2	90	4.71	11.98	CB
RR2	105	31.91	1.66	CB
RR2	120	53.61	0.99	CB
RR2	135	3.7	15.62	CB
RR2	150	1.78	38.22	CB
RR2	165	2.85	21.06	CB
RR2	180	3.06	19.38	CB
RR2	195	35.96	1.48	CB
RR2	210	24.07	2.21	CB
RR2	225	4.88	11.53	CB
RR2	240	1.2	72.25	CB
RR2	255	1.9	34.95	CB
RR2	270	3.57	16.26	CB
RR2	285	64.27	0.82	CB
RR2	300	52.93	1.00	CB
RR2	315	3.2	18.41	CB
RR2	330	2.2	28.86	CB
RR2	345	1.38	56.23	CB
RR2	360	2.84	21.14	CB
RR2	375	17.49	3.06	CB
RR2	390	37.05	1.43	CB
RR2	405	3.17	18.61	CB
RR2	420	2.3	27.29	CB
RR2	435	2.55	24.04	CB
RR2	450	3.57	16.26	CB
RR2	465	14.91	3.60	CB
RR2	480	24.65	2.16	CB
RR2	495	3.08	19.24	CB
RR2	510	1.37	56.92	CB
RR2	525	2.44	25.37	CB
RR2	540	4.12	13.87	CB
RR2	555	43.21	1.23	CB
RR2	570	17.64	3.03	CB
RR2	585	0.9	147.17	CB
RR2	600	2.81	21.41	CB
RR2	615	2.74	22.06	CB
RR2	630	2.02	32.22	CB
RR2	645	29.31	1.81	CB
RR2	660	24.05	2.22	CB
RR2	675	10.99	4.92	HL
RR2	690	18.24	2.93	HL
RR2	705	23.46	2.27	HL
RR2	720	17.65	3.03	HL
RR2	735	19.39	2.76	HL
RR2	750	15.58	3.44	HL
RR2	765	46.03	1.15	HL

RR2	780	32.2	1.65	HL
RR2	795	14.63	3.67	HL
RR2	810	24.7	2.16	HL
RR2	825	5.65	9.85	HL
RR2	840	4.25	13.40	HL
RR2	855	4.2	13.58	HL
RR2	870	1.77	38.53	Con Sand
RR2	885	1.56	46.29	Con Sand
RR2	900	1.96	33.53	Con Sand
RR2	915	1.38	56.23	Con Sand
RR2	930	1.97	33.30	Con Sand
RR2	945	1.73	39.79	Con Sand
RR2	960	1.91	34.71	Con Sand
RR2	975	2.53	24.27	Con Sand
RR2	990	1.07	91.90	Con Sand
RR2	1005	1.65	42.59	Con Sand
RR2	1020	1.99	32.86	Con Sand
RR2	1035	1.9	34.95	Con Sand
RR2	1050	1.4	54.91	Con Sand
RR2	1065	1.43	53.04	Con Sand
RR2	1080	1.37	56.92	Con Sand
RR2	1095	2.36	26.43	Con Sand
RR2	1110	1.84	36.51	Con Sand
RR2	1125	1.84	36.51	Con Sand
RR2	1140	2.79	21.59	Con Sand
RR2	1155	1.24	67.89	Con Sand
RR3	0	1.03	100.55	CB
RR3	15	1.28	64.06	CB
RR3	30	2.04	31.80	CB
RR3	45	1.21	71.11	CB
RR3	60	44.77	1.18	CB
RR3	75	12.52	4.30	CB
RR3	90	1.08	89.98	CB
RR3	105	1.5	49.16	CB
RR3	120	3.06	19.38	CB
RR3	135	1.71	40.45	CB
RR3	150	17.45	3.07	CB
RR3	165	44.71	1.19	CB
RR3	180	1.05	96.01	CB
RR3	195	1.06	93.91	CB
RR3	210	1.62	43.75	CB
RR3	225	1.59	44.98	CB
RR3	240	32.32	1.64	CB
RR3	255	45.88	1.15	CB
RR3	270	1.18	74.67	CB
RR3	285	4.26	13.37	CB
RR3	300	1.96	33.53	CB
RR3	315	1.66	42.21	CB
RR3	330	25.77	2.07	CB
RR3	345	44.89	1.18	CB
RR3	360	2.23	28.37	CB
RR3	375	1.58	45.41	CB
RR3	390	1.63	43.35	CB
RR3	405	1.8	37.63	CB
RR3	420	5.07	11.07	CB
RR3	435	70.91	0.75	CB
RR3	450	1.16	77.27	CB
RR3	465	1.02	102.99	CB

RR3	480	2.52	24.39	CB
RR3	495	2.4	25.89	CB
RR3	510	3.25	18.09	CB
RR3	525	46.17	1.15	CB
RR3	540	1.19	73.44	CB
RR3	555	1.66	42.21	CB
RR3	570	1.78	38.22	CB
RR3	585	9.61	5.65	CB
RR3	600	50	1.06	CB
RR3	615	1.31	61.47	CB
RR3	630	1.32	60.66	CB
RR3	645	1.88	35.46	CB
RR3	660	2.41	25.75	CB
RR3	675	49	1.08	CB
RR3	690	65.75	0.80	HL
RR3	705	40.01	1.33	HL
RR3	720	23.48	2.27	HL
RR3	735	26.2	2.03	HL
RR3	750	28.63	1.86	HL
RR3	765	29.23	1.82	HL
RR3	780	17.71	3.02	HL
RR3	795	22.8	2.34	HL
RR3	810	20.37	2.62	HL
RR3	825	4.14	13.79	HL
RR3	840	6.81	8.09	HL
RR3	855	13.38	4.02	HL
RR3	870	5.81	9.57	HL
RR3	885	10.4	5.21	HL
RR3	900	12.88	4.18	HL
RR3	915	4.6	12.29	HL
RR3	930	3.94	14.57	HL
RR3	945	1.55	46.74	Con sand
RR3	960	1.12	83.11	Con sand
RR3	975	1.81	37.35	Con sand
RR3	990	1.51	48.66	Con sand
RR3	1005	1.7	40.79	Con sand
RR3	1020	1.45	51.86	Con sand
RR3	1035	1.9	34.95	Con sand
RR3	1050	1.8	37.63	Con sand
RR3	1065	3.65	15.86	Con sand
RR3	1080	4.45	12.74	Con sand
RR3	1095	2.05	31.60	Con sand
RR3	1110	1.3	62.31	Con sand
RR3	1125	1.08	89.98	Con sand
RR3	1140	2.06	31.40	Con sand
RR3	1155	2.15	29.72	Con sand
RR4	0	1.59	44.98	CB
RR4	15	3.59	16.16	CB
RR4	30	1.76	38.83	CB
RR4	45	1.15	78.64	CB
RR4	60	1.81	37.35	CB
RR4	75	1.66	42.21	CB
RR4	90	53.15	1.00	CB
RR4	105	1.2	72.25	CB
RR4	120	1.96	33.53	CB
RR4	135	1.2	72.25	CB
RR4	150	1.16	77.27	CB
RR4	165	1.25	66.89	CB

RR4	180	33.89	1.57	CB
RR4	195	1.22	70.00	CB
RR4	210	1.68	41.49	CB
RR4	225	1.22	70.00	CB
RR4	240	1.27	64.97	CB
RR4	255	1.47	50.75	CB
RR4	270	2.28	27.59	CB
RR4	285	1.3	62.31	CB
RR4	300	1.79	37.93	CB
RR4	315	1.27	64.97	CB
RR4	330	1.08	89.98	CB
RR4	345	1.56	46.29	CB
RR4	360	7.6	7.21	CB
RR4	375	10	5.42	CB
RR4	390	0.85	180.95	CB
RR4	405	2.02	32.22	CB
RR4	420	1.16	77.27	CB
RR4	435	1.02	102.99	CB
RR4	450	1.29	63.17	CB
RR4	465	2.66	22.85	CB
RR4	480	6.44	8.58	CB
RR4	495	0.91	141.96	CB
RR4	510	1.65	42.59	CB
RR4	525	1.56	46.29	CB
RR4	540	1.07	91.90	CB
RR4	555	1.2	72.25	CB
RR4	570	3.13	18.88	CB
RR4	585	24.33	2.19	CB
RR4	600	0.92	137.13	CB
RR4	615	1.76	38.83	CB
RR4	630	1.49	49.68	CB
RR4	645	1.13	81.56	CB
RR4	660	1.96	33.53	CB
RR4	675	7.45	7.36	CB
RR4	690	6.31	8.76	CB
RR4	705	1.08	89.98	CB
RR4	720	1.57	45.84	CB
RR4	735	1.61	44.15	CB
RR4	750	1.13	81.56	CB
RR4	765	1.65	42.59	CB
RR4	780	2.02	32.22	CB
RR4	795	56.45	0.94	CB
RR4	810	82.06	0.64	HL
RR4	825	52.34	1.01	HL
RR4	840	45.74	1.16	HL
RR4	855	16.45	3.26	HL
RR4	870	14.14	3.80	HL
RR4	885	4.48	12.65	HL
RR4	900	4.2	13.58	HL
RR4	915	2.76	21.87	HL
RR4	930	16.34	3.28	HL
RR4	945	4.24	13.44	HL
RR4	960	1.24	67.89	con sand
RR4	975	1.23	68.93	con sand
RR4	990	2.61	23.38	con sand
RR4	1005	1.99	32.86	con sand
RR4	1020	2.37	26.29	con sand
RR4	1035	2.25	28.05	con sand

RR4	1050	2.87	20.89	con sand
RR4	1065	2.77	21.78	con sand
RR4	1080	1.85	36.24	con sand
RR4	1095	2.62	23.27	con sand
RR4	1110	2.7	22.45	con sand
RR4	1125	1.88	35.46	con sand
RR4	1140	2.02	32.22	con sand
RR4	1155	1.74	39.46	con sand
RR4	1170	1.71	40.45	con sand
RR4	1185	1.07	91.90	con sand
RR4	1200	1.89	35.20	con sand
RR4	1215	1.73	39.79	con sand
RR4	1230	3.06	19.38	con sand
RR4	1245	2.2	28.86	con sand
RR4	1260	1.6	44.56	con sand
RR4	1275	1.59	44.98	con sand
RR4	1290	1.88	35.46	con sand
RR4	1305	2.52	24.39	con sand
RR4	1320	2.16	29.54	con sand
RR4	1335	2.29	27.44	con sand
RR4	1350	2.78	21.68	con sand
RR4	1365	1.83	36.78	con sand
RR4	1380	1.4	54.91	con sand
RR4	1395	1.66	42.21	con sand
RR4	1410	1.38	56.23	con sand
RR4	1425	1.85	36.24	con sand
RR4	1440	1.98	33.08	con sand
RR5	0	0.99	111.17	CB
RR5	15	1.13	81.56	CB
RR5	30	0.96	120.88	CB
RR5	45	1.22	70.00	CB
RR5	60	2.84	21.14	CB
RR5	75	5.16	10.86	CB
RR5	90	37.85	1.40	CB
RR5	105	0.99	111.17	CB
RR5	120	1.07	91.90	CB
RR5	135	1.89	35.20	CB
RR5	150	1.78	38.22	CB
RR5	165	1.13	81.56	CB
RR5	180	3.88	14.82	CB
RR5	195	70.91	0.75	CB
RR5	210	0.91	141.96	CB
RR5	225	2.02	32.22	CB
RR5	240	1	108.29	CB
RR5	255	1.6	44.56	CB
RR5	270	1.28	64.06	CB
RR5	285	1.44	52.44	CB
RR5	300	12.34	4.37	CB
RR5	315	64.85	0.82	CB
RR5	330	1.16	77.27	CB
RR5	345	1.85	36.24	CB
RR5	360	0.95	124.55	CB
RR5	375	1.33	59.87	CB
RR5	390	2.2	28.86	CB
RR5	405	1.57	45.84	CB
RR5	420	24.96	2.13	CB
RR5	435	24.27	2.19	CB
RR5	450	1.13	81.56	CB

RR5	465	1.7	40.79	CB
RR5	480	1	108.29	CB
RR5	495	1.1	86.40	CB
RR5	510	2.07	31.20	CB
RR5	525	2.35	26.57	CB
RR5	540	9.17	5.93	CB
RR5	555	20.7	2.58	CB
RR5	570	1.2	72.25	CB
RR5	585	1.83	36.78	CB
RR5	600	1.45	51.86	CB
RR5	615	1.2	72.25	CB
RR5	630	2.39	26.02	CB
RR5	645	1.75	39.14	CB
RR5	660	5.33	10.49	CB
RR5	675	71.56	0.74	CB
RR5	690	1.58	45.41	CB
RR5	705	1.05	96.01	CB
RR5	720	1.38	56.23	CB
RR5	735	2.58	23.70	CB
RR5	750	2.41	25.75	CB
RR5	765	5.12	10.95	CB
RR5	780	14.09	3.81	CB
RR5	795	1.1	86.40	CB
RR5	810	1.33	59.87	CB
RR5	825	1.05	96.01	CB
RR5	840	3.91	14.69	CB
RR5	855	1.71	40.45	CB
RR5	870	3.85	14.95	CB
RR5	885	9.81	5.53	CB
RR5	900	57.06	0.93	HL
RR5	915	51.31	1.03	HL
RR5	930	72.08	0.73	HL
RR5	945	78.95	0.67	HL
RR5	960	15.46	3.47	HL
RR5	975	25.86	2.06	HL
RR5	990	6.41	8.62	HL
RR5	1005	10.47	5.17	HL
RR5	1020	6.16	8.99	HL
RR5	1035	1.16	77.27	con sand
RR5	1050	1.63	43.35	con sand
RR5	1065	2.41	25.75	con sand
RR5	1080	1.51	48.66	con sand
RR5	1095	2.06	31.40	con sand
RR5	1110	2.28	27.59	con sand
RR5	1125	1.75	39.14	con sand
RR5	1140	2.11	30.44	con sand
RR5	1155	3.24	18.15	con sand
RR5	1170	1.46	51.30	con sand
RR5	1185	1.4	54.91	con sand
RR5	1200	2.91	20.55	con sand
RR5	1215	2.92	20.47	con sand
RR5	1230	2.81	21.41	con sand
RR5	1245	2.77	21.78	con sand
RR5	1260	2.04	31.80	con sand
RR5	1275	1.96	33.53	con sand
RR5	1290	2.8	21.50	con sand
RR5	1305	2.89	20.72	con sand
RR5	1320	2.81	21.41	con sand

RR5	1335	1.63	43.35	con sand
RR5	1350	1.78	38.22	con sand
RR5	1365	2.11	30.44	con sand
RRU2	0	1.05	96.01	CB
RRU2	15	3.38	17.30	CB
RRU2	30	4.59	12.32	CB
RRU2	45	1.5	49.16	CB
RRU2	60	1.41	54.27	CB
RRU2	75	1.54	47.21	CB
RRU2	90	1.74	39.46	CB
RRU2	105	0.92	137.13	CB
RRU2	120	1.27	64.97	CB
RRU2	135	1.41	54.27	CB
RRU2	150	3.62	16.01	CB
RRU2	165	0.89	152.81	CB
RRU2	180	1.52	48.16	CB
RRU2	195	2.44	25.37	CB
RRU2	210	1.19	73.44	CB
RRU2	225	0.87	165.61	CB
RRU2	240	1.94	33.99	CB
RRU3	0	2	32.64	CB
RRU3	15	2.79	21.59	CB
RRU3	30	0.85	180.95	CB
RRU3	45	0.86	172.91	CB
RRU3	60	0.81	223.07	CB
RRU3	75	1.91	34.71	CB
RRU3	90	0.83	199.67	CB
RRU3	105	0.91	141.96	CB
RRU3	120	1.09	88.15	CB
RRU3	135	1.64	42.97	CB
RRU3	150	0.89	152.81	CB
RRU3	165	0.84	189.82	CB
RRU3	180	0.85	180.95	CB
RRU4	0	2.06	31.40	CB
RRU4	15	3.56	16.31	CB
RRU4	30	0.84	189.82	CB
RRU4	45	0.93	132.64	CB
RRU4	60	1.32	60.66	CB
RRU4	75	1.63	43.35	CB
RRU4	90	2.26	27.90	CB
RRU4	105	1.44	52.44	CB
RRU4	120	1.51	48.66	HL
RRU4	135	2.16	29.54	HL
RRU4	150	1.26	65.91	HL
RRU4	165	1.33	59.87	HL
RRU4	180	2.38	26.15	CB
RRU4	195	0.95	124.55	CB
RRU4	210	1.38	56.23	CB
RRU4	225	18.49	2.89	CB
RRU4	240	9.62	5.64	CB
RRU4	255	3.59	16.16	CB
RRU4	270	1.53	47.68	CB
RRU4	285	0.83	199.67	CB
RRU4	300	0.84	189.82	CB
RRU4	315	0.91	141.96	CB
RRU4	330	1.23	68.93	CB
RRU4	345	2.43	25.49	CB

RRU4	360	0.85	180.95	CB
RRU4	375	0.88	158.93	CB
RRU4	390	0.95	124.55	CB
RRU4	405	1.43	53.04	CB
RRU4	420	3.67	15.76	CB
RRU4	435	2.13	30.07	HL
RRU4	450	1.94	33.99	HL
RRU4	465	1.13	81.56	HL
RRU5	0	0.99	111.17	CB
RRU5	15	2.02	32.22	CB
RRU5	30	0.93	132.64	CB
RRU5	45	1.51	48.66	CB
RRU5	60	1.38	56.23	CB
RRU5	75	1.02	102.99	CB
RRU5	90	1.04	98.22	CB
RRU5	105	1.15	78.64	HL
RRU5	120	1.14	80.07	HL
RRU5	135	1.91	34.71	HL
RRU5	150	1.59	44.98	HL
RRU5	165	1.01	105.57	HL
RRU5	180	0.94	128.46	HL
RRU5	195	2.35	26.57	HL
RRU5	210	2.14	29.89	HL
RRU5	225	3.06	19.38	HL
RRU5	240	12.08	4.46	HL
RRU5	255	12.85	4.19	HL
RRU5	270	0.95	124.55	CB
RRU5	285	1.33	59.87	CB
RRU5	300	1.13	81.56	CB
RRU5	315	1.34	59.10	CB
RRU5	330	1.42	53.64	CB
RRU5	345	1.23	68.93	Con. sand
RRU5	360	1.09	88.15	Con. sand
RRU5	375	1.02	102.99	Con. sand
RRU5	390	0.96	120.88	Con. sand
RRU5	405	1.24	67.89	Con. sand

Tijeras Arroyo Permeability Profile Measurements

Location	Height (cm)	Time (sec.)	Darcys	Structure
TA1 2.4 m rt. of left edge	0	7.38	7.43	SL
TA1	15	8.23	6.63	SL
TA1	30	7.17	7.66	SL
TA1	45	6.6	8.36	HL
TA1	60	0.85	180.95	SF
TA1	75	0.84	189.82	SF
TA1	90	1.08	89.98	SF
TA1	105	10.48	5.17	HL
TA1	120	6.43	8.59	HL
TA1	135	9.71	5.59	HL
TA1	150	4.92	11.43	HL
TA2 sp. 3	0	1.24	67.89	SF
TA2	15	too coarse	.	CH
TA2	30	1.7	40.79	CH
TA2	45	0.82	210.68	CH
TA2	60	2.12	30.26	HL
TA2	75	0.85	180.95	CH
TA2	90	0.84	189.82	CH
TA2	105	1.3	62.31	CH
TA2	120	3.61	16.06	SL
TA2	135	5.24	10.68	SL
TA2	150	7.08	7.76	SL
TA3 sp. 6	0	9.58	5.67	HL
TA3	15	too coarse	.	CH
TA3	30	0.88	158.93	CH
TA3	45	0.79	253.15	CH
TA3	60	too coarse	.	CH
TA3	75	0.81	223.07	CH
TA3	90	0.84	189.82	HL
TA3	105	0.91	141.96	HL
TA3	120	0.79	253.15	CH
TA3	135	0.88	158.93	CH
TA3	150	6.5	8.49	HL
TA4	0	0.78	271.68	HL
TA4	15	too coarse	.	HL
TA4	30	0.85	180.95	HL
TA4	45	0.83	199.67	HL
TA4	60	1.31	61.47	SF
TA4	75	2.21	28.69	SF
TA4	90	1.76	38.83	SF
TA4	105	0.82	210.68	HB
TA4	120	0.86	172.91	HB
TA4	135	0.79	253.15	CH
TA4 50 cm right of sp.9	150	0.82	210.68	CH
TA5 90 cm left of sp.11	0	0.87	165.61	SF
TA5	15	0.85	180.95	SF
TA5	30	1.54	47.21	SF
TA5	45	1.2	72.25	SF
TA5	60	4.97	11.31	HL
TA5	75	2.45	25.24	SF
TA5	90	4.36	13.03	HL
TA5	105	6.04	9.18	HL
TA5	120	5.65	9.85	HL
TA5	135	3.92	14.65	HL
TA5	150	6.19	8.94	HL

TA6 25 cm rt. of sp.11	0	7.56	7.25	HL
TA6 sp.14.	15	6.56	8.41	HL
TA6	30	6.01	9.23	HL
TA6	45	4.29	13.26	HL
TA6	60	5.63	9.89	HL
TA6	75	7.74	7.07	HL
TA6	90	5.69	9.78	HL
TA6	105	6.34	8.72	HL
TA6	120	1.79	37.93	HB
TA6	135	0.8	237.10	HB
TA6	150	0.8	237.10	HB
TA7 sp.14	0	too coarse .		CH
TA7	15	too coarse .		CH
TA7	30	0.86	172.91	CH
TA7	45	0.81	223.07	CH
TA7	60	0.79	253.15	CH
TA7	75	too coarse .		CH
TA7	90	0.81	223.07	CH
TA7	105	0.83	199.67	CH
TA7	120	0.81	223.07	CH
TA7	135	1.09	88.15	HB
TA7	150	0.99	111.17	HB
TA8	0	0.82	210.68	CH
TA8	15	0.91	141.96	CH
TA8	30	1.06	93.91	CH
TA8	45	1.09	88.15	CH
TA8	60	too coarse .		CH
TA8	75	0.9	147.17	CH
TA8	90	2.96	20.14	SF
TA8	105	2.81	21.41	SF
TA8	120	1.14	80.07	HB
TA8	135	1.08	89.98	HB
TA8 45 cm left of sp 17	150	2.14	29.89	SF
TA9	0	0.88	158.93	SF
TA9 sp.18	15	0.93	132.64	SF
TA9	30	3.89	14.77	HL
TA9	45	0.81	223.07	SF
TA9	60	0.85	180.95	SF
TA9	75	1.94	33.99	SL
TA9	90	7.2	7.63	SL
TA9	105	4.4	12.90	SL
TA9	120	4.88	11.53	SL
TA9	135	9.8	5.54	SL
TA9	150	0.81	223.07	SF

Dan Four Hills

MAGNETIC DECLINATION	
Degrees	12
Minutes	30
Declination	EAST
Radians	0.2182

REFERENCE AZIM	
Inverse?	0
Degrees	12.5
Radians	0.2182

INSTRUMENT POSITION	
North	0.00
East	0.00
Elevation	5970.00
Instrument Height	4.76

BACKSIGHT	
North	0.00
East	0.00

	ANGLE RT			ZENITH								
SHO	D	M	S	D	M	S	STADIA	ROD	DESCRIPTION	N COOD	E COOD	ELV
1	243	33	2	95	1	40	245.55	5	top of concrete diversion	-58.74	-236.48	5948.32
2	256	16	50	93	10	42	220.73	5	top of red sand\base gvl sand	-4.68	-220.00	5957.54
3	278	29	0	94	38	5	173.23	5		61.63	-160.69	5955.81
4	288	59	57	93	48	54	185.6	5		96.54	-157.55	5957.44
5	304	5	55	92	6	5	212.86	5		154.45	-146.06	5961.96
6	310	18	20	92	2	8	234.02	5	porosity 1	186.18	-141.29	5961.45
7	319	34	39	93	30	28	233.61	5	fence corner	205.64	-108.98	5955.49
8	314	47	30	90	2	45	269	5		226.35	-145.36	5969.54
9	313	9	15	87	47	18	275.29	5		226.95	-155.08	5980.38
10	311	39	0	86	57	33	289.36	5	out of sight ?in gully?	233.88	-168.99	5985.09
11	321	40	32	89	42	52	327.93	5		295.17	-142.85	5971.39
12	316	24	23	85	17	40	370.48	5		315.12	-190.04	6000.05
13	310	44	19	82	26	17	395.34	5		311.24	-232.51	6021.33
14	304	23	31	81	34	29	360.15	5		257.29	-240.83	6021.96
15	290	30	20	79	55	56	312.96	5		165.27	-254.43	6023.63
16	280	10	5	81	42	30	263.46	5		99.42	-238.05	6007.36
17	290	12	12	83	38	30	236.03	5		125.96	-196.18	5995.74
18	282	59	2	88	36	44	199.28	5		85.69	-179.79	5974.58
19	293	25	55	89	11	8	203.42	5		119.35	-164.68	5972.65
20	306	23	41	88	41	16	236.57	5		178.16	-155.45	5975.18
21	313	52	27	88	46	35	270.63	5		225.24	-149.80	5975.54
22	307	21	42	86	23	18	253.8	5		193.26	-162.96	5985.72
23	302	37	24	86	16	30	237.67	5		167.71	-166.99	5985.17
24	294	53	11	85	59	40	220.3	5		133.11	-174.19	5985.11
25	276	50	55	88	9	44	199.32	5		65.97	-187.87	5976.15
26	244	20	35	104	34	22	135.54	5	base of trib channel (modern)	-28.90	-123.63	5936.75

Oct 6, 1994

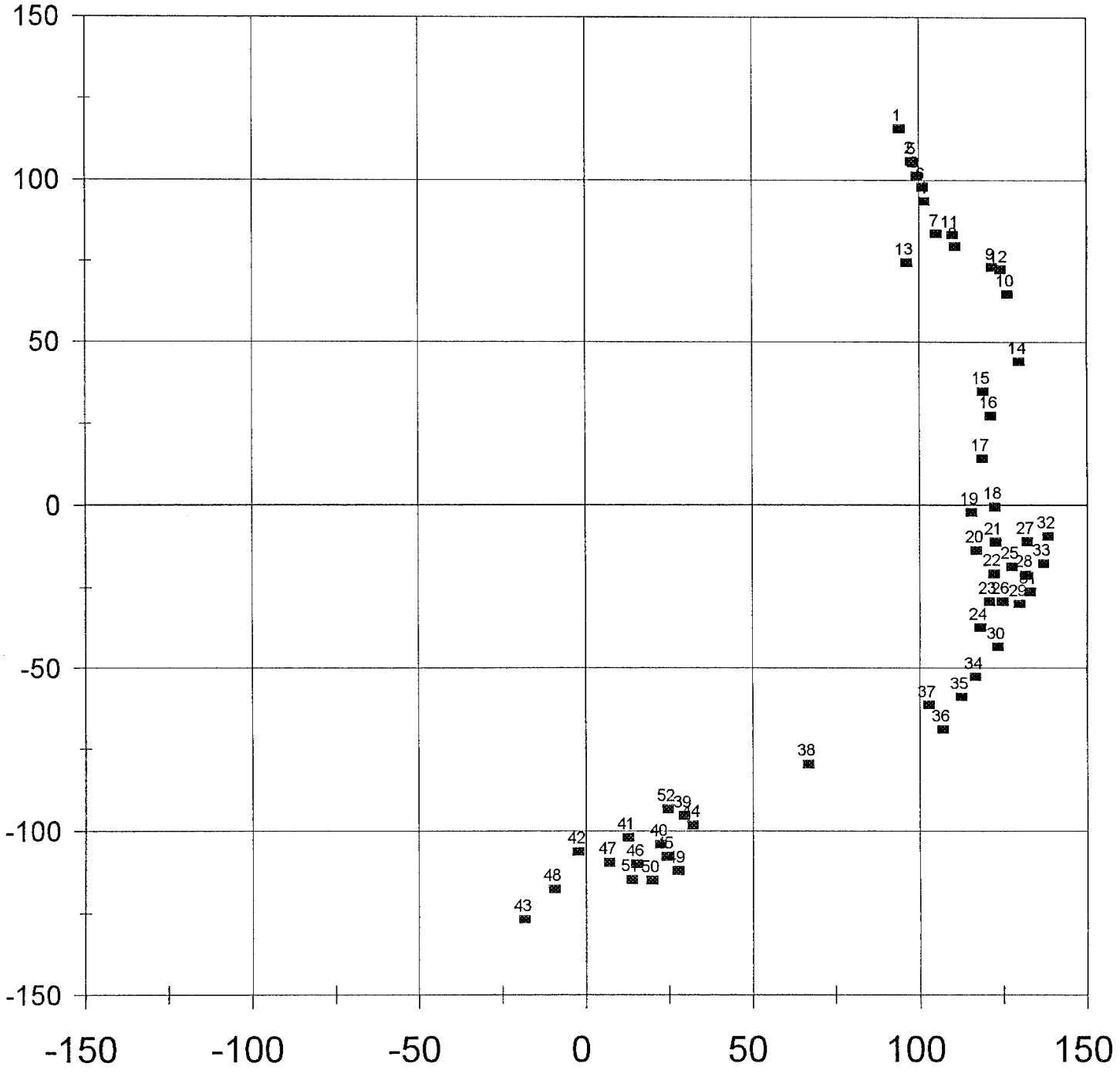
150
100
50
0
-50
-100
-150
-150
-100
-50
0
50
100
150
1
2
3
4
5
6
7
8
9
10
11
12
13
14
15
16
17
18
19
20
21
22
23
24
25
26
27
28
29
30
31
32
33
34
35
36
37
38
39
40
41
42
43
44
45
46
47
48
49
50
51
52

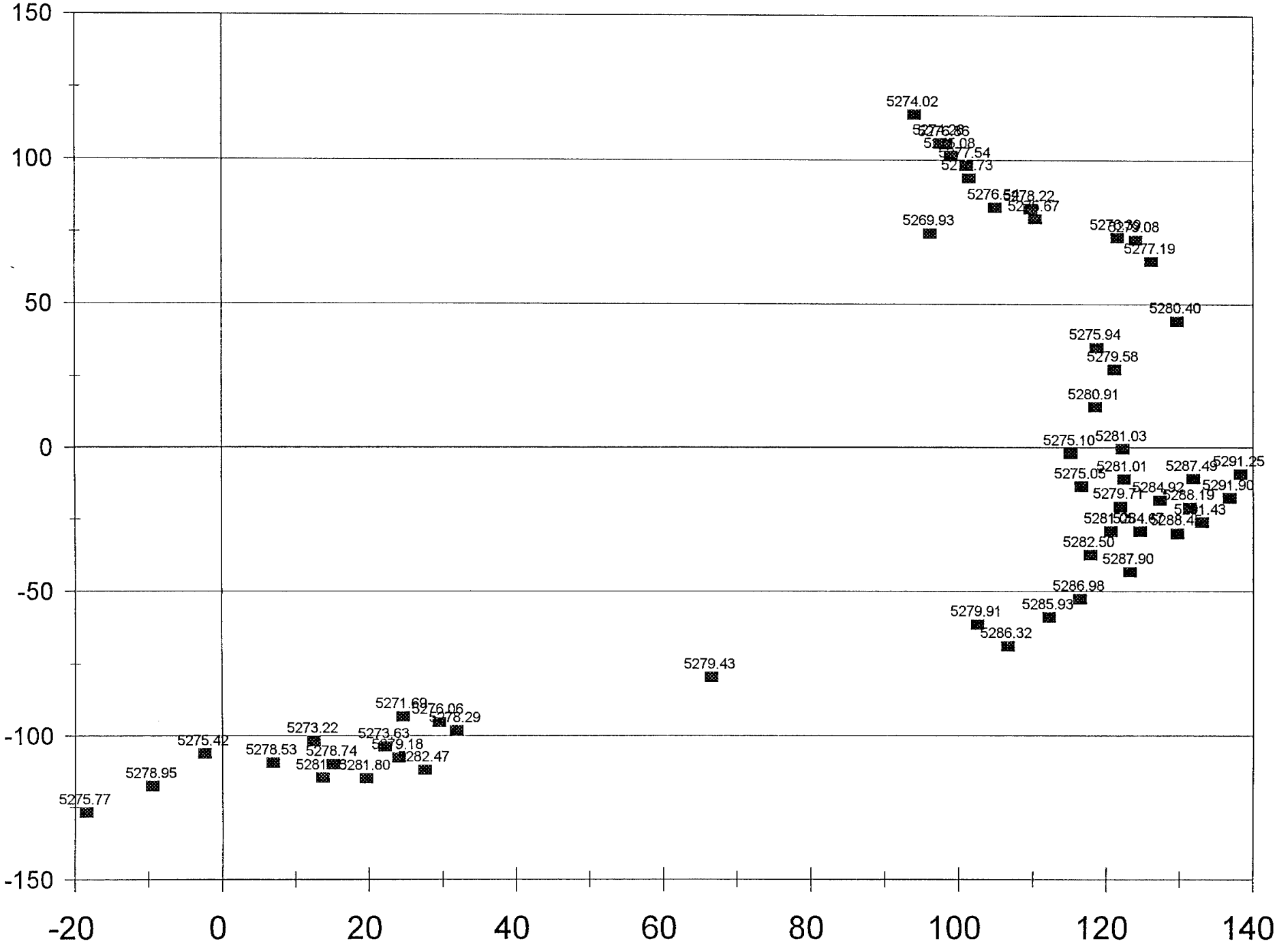
150
100
50
0
-50
-100
-150
-20
0
20
40
60
80
100
120
140
5274.02
5269.93
5277.19
5280.40
5275.94
5279.58
5280.91
5275.10
5281.03
5281.01
5287.49
5291.25
5275.05
5284.92
5279.71
5288.19
5282.50
5287.90
5286.98
5285.93
5279.91
5286.32
5279.43
5271.69
5276.06
5278.29
5273.22
5273.63
5275.42
5278.53
5278.74
5282.47
5281.80
5278.95
5275.77

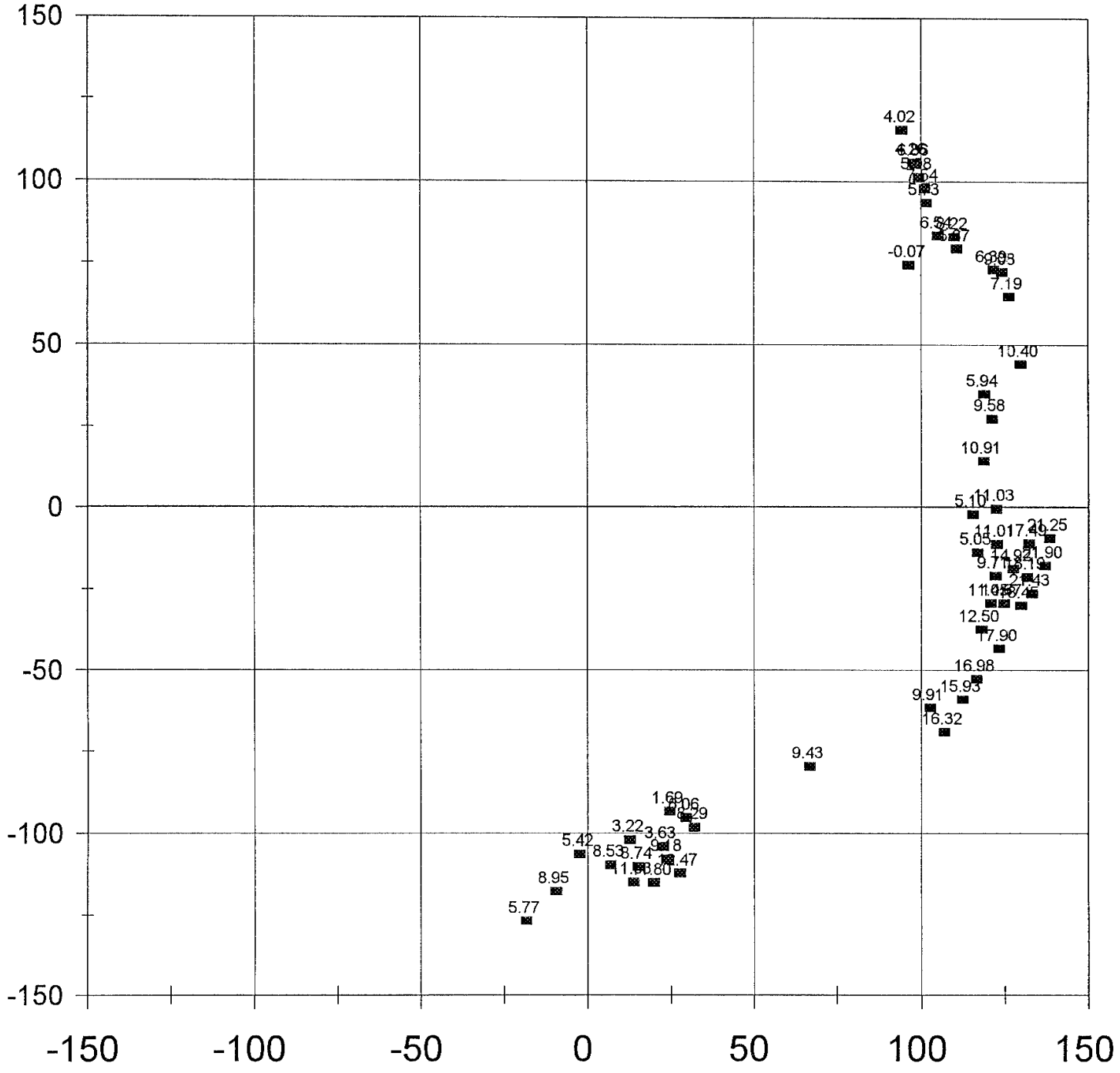
150
100
50
0
-50
-100
-150
-150
-100
-50
0
50
100
150
4.02
-0.07
7.19
10.40
5.94
9.58
10.91
11.03
5.10
21.25
21.90
12.50
7.90
16.98
15.93
9.91
16.32
9.43
1.69
3.22
3.63
5.42
8.53
8.74
8.95
5.77

MAGNETIC DECLINATION		REFERENCE AZIM	
Degrees	12	Inverse?	0
Minutes	30	Degrees	12.5
Declination	EAST	Radians	0.2182
Radians	0.2182		

INSTRUMENT POSITION		BACKSIGHT	
North	0.00	North	0.00
East	0.00	East	0.00
Elevation	5490.00		
Instrument Height	4.94		

Tijeras Arroyo

DESCRIPTION	N COOD	E COOD	ELV
coarse/fine 2' above channel	-95.81	-21.24	5449.52
top of fine	-81.15	-26.24	5453.53
	-74.42	-24.71	5452.57
	-69.37	-26.14	5456.06
	-64.09	-27.13	5456.72
	-57.13	-28.51	5457.43
	-44.32	-33.94	5458.90
	-51.00	-34.02	5465.57
	-36.52	-34.92	5466.61
	-29.09	-36.58	5463.57
boulder bed	-18.40	-38.37	5466.35
contact	-26.63	-40.14	5472.59
same contact	-16.93	-43.58	5474.02
same contact	-6.17	-45.67	5473.42
bottom of red sd soil	-15.86	-47.37	5480.31
top of gvl 0?	-8.28	-50.61	5479.97
	10.24	-56.68	5474.82
	36.28	-66.61	5481.09
surface of ground above gully	29.70	-68.23	5490.68
	19.31	-62.80	5489.41
	8.20	-56.67	5488.91
	-12.83	-52.12	5487.18
	33.39	-68.84	5489.38
bottom of contact	-42.35	-38.63	5472.22
surface 5?	-98.42	-22.98	5453.47

Eubank Dump Survey
(Tijeras Arroyo)

MAGNETIC DECLINATION		REFERENCE AZIM	
Degrees	12	Inverse?	0
Minutes	30	Degrees	12.5
Declination	EAST	Radians	0.2182
Radians	0.2182		

INSTRUMENT POSITION		BACKSIGHT	
North	0.00	North	0.00
East	0.00	East	0.00
Elevation	5490.00		
Instrument Height	4.94		

	ANGLE RT			ZENITH								
SHO	D	M	S	D	M	S	STADIA	ROD	DESCRIPTION	N COOD	E COOD	ELV
1	180	0	0	112	23	3	114.78	5	coarse/fine 2' above channel	-95.81	-21.24	5449.52
2	185	25	16	113	6	58	100.83	5	top of fine	-81.15	-26.24	5453.53
3	185	52	5	115	28	46	96.22	5		-74.42	-24.71	5452.57
4	188	8	53	114	33	35	89.61	5		-69.37	-26.14	5456.06
5	190	26	43	115	30	52	85.45	5		-64.09	-27.13	5456.72
6	194	0	55	116	58	53	80.4	5		-57.13	-28.51	5457.43
7	204	56	44	119	4	16	73.08	5		-44.32	-33.94	5458.90
8	201	12	20	115	35	55	75.38	0		-51.00	-34.02	5465.57
9	211	13	0	119	16	51	66.42	0		-36.52	-34.92	5466.61
10	219	0	9	119	25	52	61.61	5		-29.09	-36.58	5463.57
11	231	52	37	118	59	50	55.63	5	boulder bed	-18.40	-38.37	5466.35
12	223	56	30	114	53	9	58.54	0	target at contact 0	-26.63	-40.14	5472.59
13	236	16	18	114	6	30	56.12	0	same	-16.93	-43.58	5474.02
14	249	48	15	115	2	0	56.14	0	same	-6.17	-45.67	5473.42
15	238	59	0	106	19	28	54.24	0	red s soil/gravel top	-15.86	-47.37	5480.31
16	248	12	45	106	16	40	55.65	0	top of gravel	-8.28	-50.61	5479.97
17	267	44	28	104	42	30	61.57	0	check this	10.24	-56.68	5479.82
18	286	4	20	96	39	22	76.88	0	check this	36.28	-66.61	5486.09
19	281	1	36	89	25	40	74.42	0	check, surface	29.70	-68.23	5495.68
20	274	35	43	94	48	42	66.17	0	target @ 0	19.31	-62.80	5489.41
21	265	43	46	96	0	41	57.89	0	ditto	8.20	-56.67	5488.91
22	243	40	33	98	13	30	54.8	0	ditto	-12.83	-52.12	5487.18
23	283	22	21	94	9	16	76.91	0	ditto	33.39	-68.84	5489.38
24	209	52	35	111	37	31	66.33	0	contact	-42.35	-38.63	5472.22
25	180	38	35	109	50	30	114.23	0	check, surface	-98.42	-22.98	5458.47

Eubank S Dump

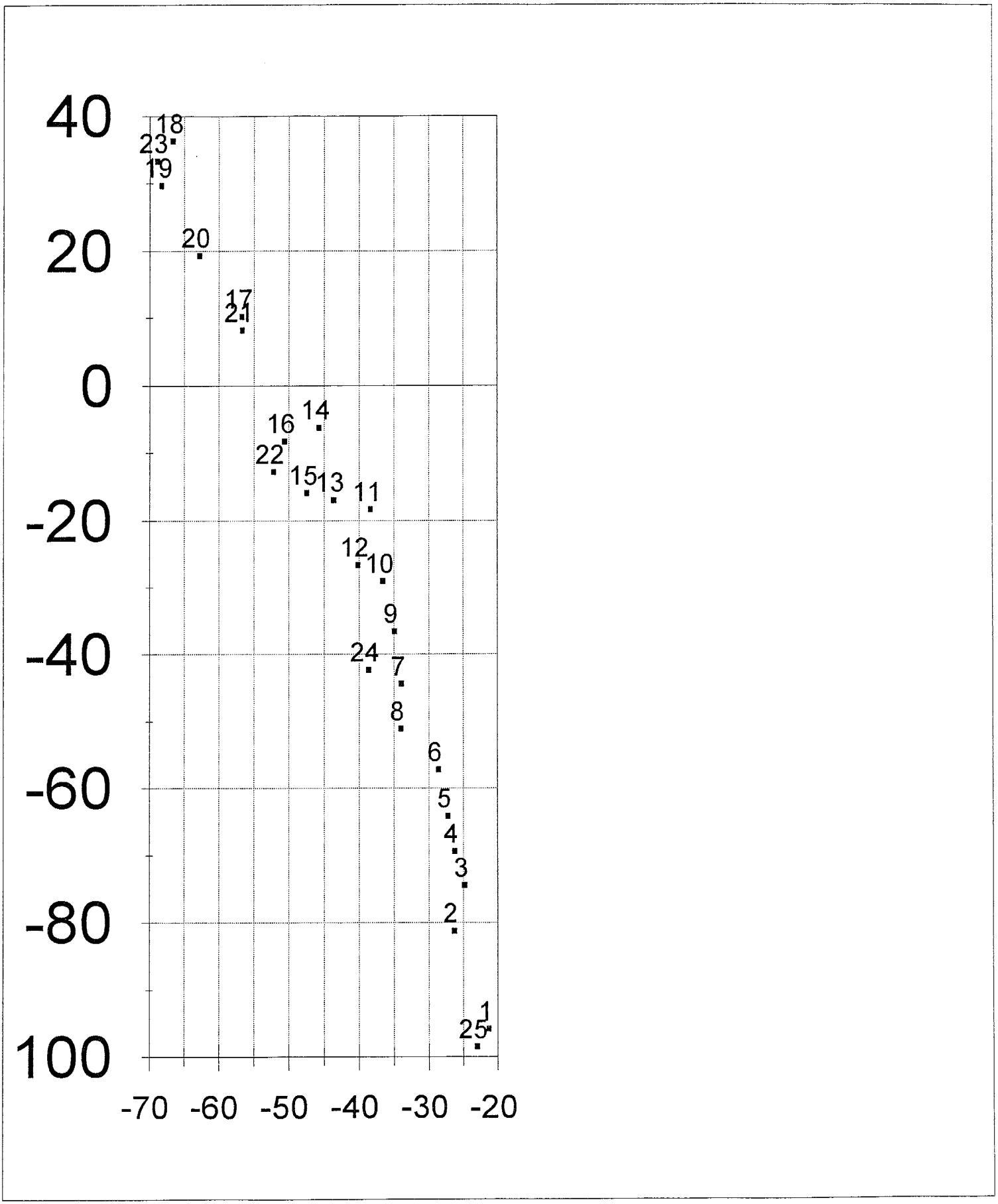

MAGNETIC DECLINATION

Degrees	12
Minutes	30
Declination	EAST
Radians	0.2182

REFERENCE AZIM

Inverse?	0
Degrees	12.5
Radians	0.2182

INSTRUMENT POSITION

North	0.00
East	0.00
Elevation	5270.00
Instrument Height	4.78

BACKSIGHT

North	0.00
East	0.00

	ANGLE RT			ZENITH								
SHOT	D	M	S	D	M	S	STADIA	ROD	DESCRIPTION	N COOD	E COOD	ELV
1	26	38	18	90	17	32	149.32	0	contact:: gvl/sand	115.81	94.25	5274.02
2	30	12	22	90	12	20	144.16	0	contact: sand/sand	105.93	97.77	5274.26
3	31	50	18	89	52	50	141.93	0	contact: gvl/sand	101.51	99.19	5275.08
4	34	49	4	89	36	25	138.22	0	trough base	93.70	101.60	5275.73
5	30	30	11	89	10	30	144.38	0	base of sand above white x-bed	105.57	98.45	5276.86
6	33	23	58	88	52	49	141.03	0	same to SE	98.11	101.24	5277.54
7	38	58	50	89	15	5	134.41	0	base of light x-trough	83.69	105.14	5276.54
8	41	44	26	89	37	40	136.29	0	base of same	79.64	110.59	5275.67
9	46	28	15	89	21	10	142.1	0	same on rising to s	73.24	121.75	5276.39
10	50	19	22	89	1	40	142.11	0	more trough	64.89	126.38	5277.19
11	40	20	42	88	34	16	138.12	0	top of trough	83.37	110.01	5278.22
12	47	13	49	88	17	18	143.99	0	base of gravel	72.52	124.25	5279.08
13	39	44	6	92	16	48	122.12	0	base of outcrop	74.67	96.39	5269.93
14	58	41	5	87	39	2	137.3	0	top of x bed	44.21	129.74	5280.40
15	61	5	0	89	27	55	123.91	0	ditto	35.02	118.85	5275.94
16	64	41	31	87	47	23	124.52	0	ditto	27.56	121.24	5279.58
17	70	34	56	87	3	49	119.82	0	?	14.39	118.64	5280.91
18	77	40	35	87	4	30	122.72	0	?	-0.38	122.40	5281.03
19	78	27	29	89	50	30	115.4	0	base of gvlly sand	-1.93	115.38	5275.10
20	84	4	24	89	52	11	117.59	0	base of x bed	-13.46	116.82	5275.05
21	82	36	8	87	6	2	123.36	0	top of sand\base of clay	-10.94	122.56	5281.01
22	87	2	8	87	43	17	124.04	0	same to right	-20.52	122.13	5279.71
23	90	58	22	87	6	32	124.54	0	same further right	-28.94	120.80	5281.05
24	94	56	50	86	25	42	124.16	0	clay/sand farther south	-37.08	117.99	5282.50
25	85	40	53	85	29	49	129.54	0	top of x beds, base of gvl	-18.32	127.43	5284.92
26	90	33	33	85	35	11	128.86	0	same to south	-28.94	124.78	5284.67
27	82	10	0	84	30	58	133.65	0	base of horiz gvl	-10.77	131.99	5287.49
28	86	29	59	84	15	0	134.56	0	same to south	-20.84	131.57	5288.19
29	90	24	8	84	8	31	134.62	0	ditto	-29.75	129.85	5288.45
30	96	42	15	84	16	12	132.02	0		-42.99	123.43	5287.90
31	88	31	30	83	0	0	137.62	0		-25.93	133.07	5291.43
32	81	16	3	83	13	48	140.66	0		-9.11	138.41	5291.25
33	84	46	42	82	55	37	140.10	0		-17.48	136.86	5291.90
34	101	40	55	84	32	53	129.00	0	place 2" higher, top of gvl	-52.37	116.62	5286.98
35	105	4	42	84	58	40	127.86	0		-58.74	112.46	5285.93
36	110	16	35	84	48	43	128.11	0		-68.79	106.83	5286.32
37	108	13	39	87	32	39	119.80	0	gully	-61.10	102.79	5279.91
38	127	29	22	87	25	45	103.87	0	top of sand in gully	-79.40	66.65	5279.43
39	150	11	33	89	15	58	99.59	0		-95.07	29.62	5276.06
40	155	20	40	90	37	17	105.98	0	x bed sand in alcove	-103.59	22.31	5273.63
41	160	24	0	90	52	13	102.46	0	held target on face	-101.65	12.66	5273.22
42	168	46	3	89	39	24	106.09	0	next to tusk hole-gvl/sand	-106.06	-2.35	5275.42
43	175	49	47	89	33	17	127.79	0	sw of tusk hole	-126.43	-18.51	5275.77
44	149	23	29	88	2	50	103.06	0	gvl/sand, next up	-97.84	32.00	5278.29
45	154	48	13	87	42	45	110.27	0	gvl/sand in alcove	-107.40	24.20	5279.18
46	159	35	48	87	57	0	110.90	0	gvl/sand w in alcove	-109.71	15.23	5278.74
47	163	50	12	88	2	20	109.56	0	same @ corner to west	-109.21	6.99	5278.53
48	172	7	39	87	58	9	117.87	0	same to sw	-117.34	-9.50	5278.95
49	153	35	10	86	10	35	115.61	0	next overlying base of gvl, E alc	-111.72	27.68	5282.47
50	157	42	47	86	32	40	116.75	0	same to S in alcove	-114.63	19.77	5281.80
51	160	35	21	86	35	50	115.65	0	same on corner	-114.41	13.87	5281.63
52	152	36	20	91	50	28	96.38	0	lowest part of outcrop, E alcove	-93.05	24.75	5271.69

Rio Bravo Survey

MAGNETIC DECLINATION		REFERENCE AZIM	
Degrees	12	Inverse?	0
Minutes	30	Degrees	12.5
Declination	EAST	Radians	0.2182
Radians	0.2182		

INSTRUMENT POSITION		BACKSIGHT	
North	0.00	North	0.00
East	0.00	East	0.00
Elevation	5160.00		
Instrument Height	4.92		

DESCRIPTION	N COOD	E COOD	ELV
base of gvl	145.20	-28.50	5165.20
near top of low < x bed	147.36	-24.13	5168.85
base ofgvlly < x beds	131.55	-25.31	5165.30
top of low gvl	121.57	-20.91	5166.28
base of gvl	116.51	-20.14	5165.33
near top of x beds	117.18	-14.54	5169.32
base of upper gvl laxb	105.51	-7.20	5170.59
base of upper gvl @ corner	92.75	-1.41	5170.69
base of gvl trough @ corner	88.92	-1.89	5168.32
base of upper gvle e of corner	89.52	7.41	5169.88
middle of low < x bed east	87.60	14.37	5167.82
base of upper gvl intertongue	92.10	29.43	5169.81
base of gvlly base NW	103.34	-13.84	5165.50
top of lower gvl nr corner	94.59	-9.67	5165.85
base of scour gvl base	91.28	-8.44	5165.29
base of gvl @ corner	84.19	-3.41	5165.21
top of lower gvl @ corner	84.73	-2.49	5165.95
base of lower gvl east	83.72	7.43	5165.23
top of lower gvl tongue	83.37	10.35	5165.68
x bed sand higher to E	131.36	105.39	5177.79
x bed contact	129.50	117.52	5177.75
base of scour fill sand below	130.77	122.91	5179.71
ditto up to left	131.36	111.46	5180.93
sand face at corner	131.11	105.40	5180.57
up there	138.05	102.47	5180.37
top of gvl	141.92	104.00	5183.29
x bed channel	147.97	100.21	5180.10
base of sand over gvl	146.46	103.08	5183.07
xx	150.76	91.63	5176.53
	152.61	98.62	5180.19
top of gvl	155.47	100.39	5182.84
	183.36	99.25	5189.42
base of x bed gvlly sand	211.05	95.58	5192.82
top of x bed gvlly sand	211.42	100.86	5196.35
	211.25	100.82	5198.12
	234.58	96.64	5198.14
	234.21	96.83	5195.85
in strless sand unit	209.40	92.33	5189.02
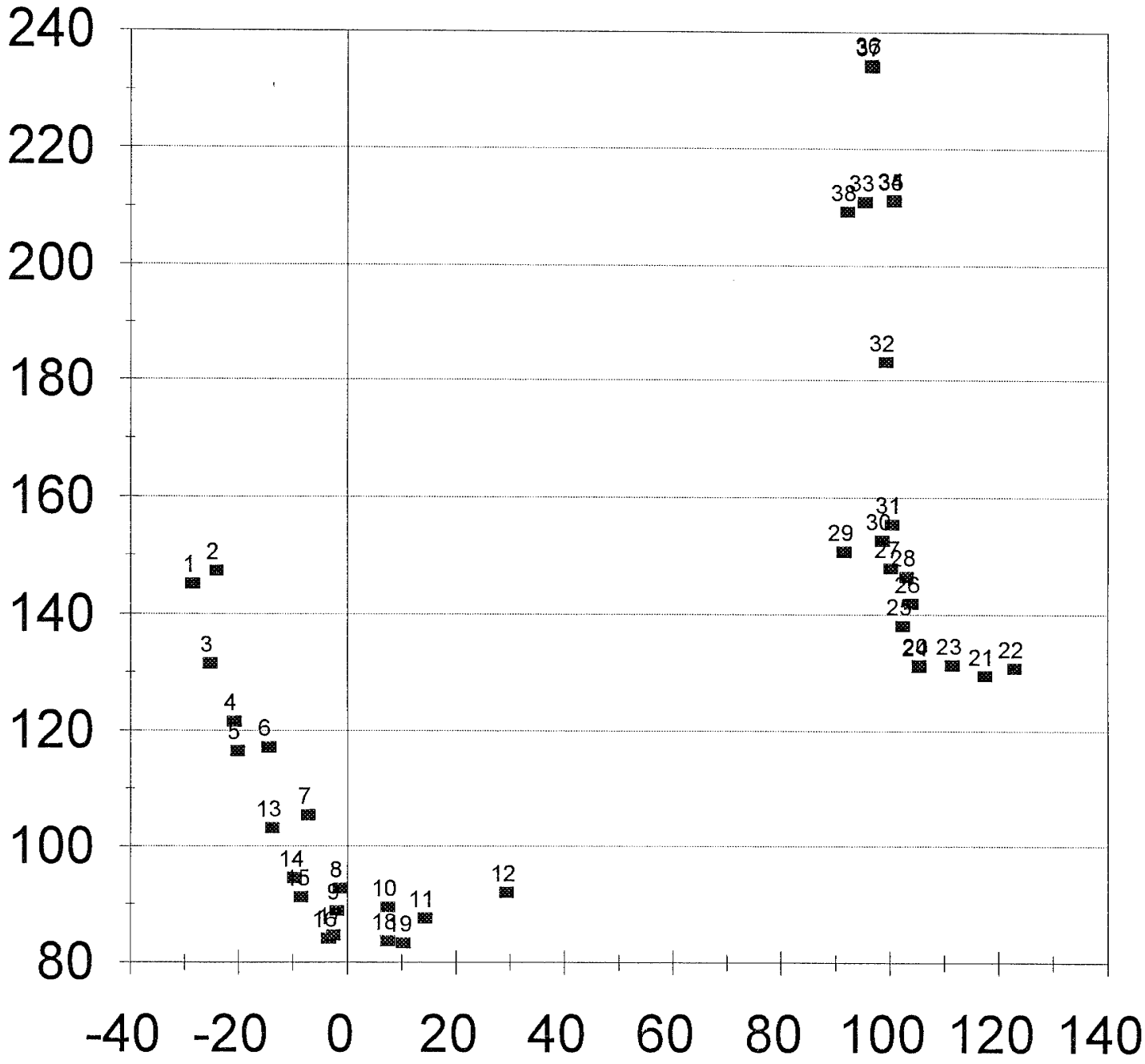
Río Bravo inlet section